Cholesterol metabolism in *t(4;11)* leukemia

Dissertation

der Mathematisch-Naturwissenschaftlichen Fakultät

der Eberhard Karls Universität Tübingen

zur Erlangung des Grades eines

Doktors der Naturwissenschaften

(Dr. rer. nat.)

vorgelegt von

M.Sc. Estelle Erkner

aus Leipzig

Tübingen

2025

Gedruckt mit Genehmigung der Mathematisch-Naturwissenschaftlichen Fakultät der Eberhard Karls Universität Tübingen.

Tag der mündlichen Qualifikation:	25.06.2025
Dekan:	Prof. Dr. Thilo Stehle
1. Berichterstatter:	PD Dr. Corina Schneidawind, Ph.D.
2. Berichterstatter:	Prof. Dr. Thilo Stehle

Abstract

Chromosomal translocations involving the *KMT2A* gene (*KMT2A*r leukemia) occur in nearly 5% to 10% of acute leukemia cases and are associated with an aggressive disease course and poor prognosis. The *AFF1* gene is the most common translocation partner of the *KMT2A* gene, causing *t(4;11)* leukemia. It is well known that cancer cells undergo metabolic reprogramming, including changes in cholesterol homeostasis, which contribute to increased proliferation and survival. Thus, dysregulated cholesterol metabolism not only promotes tumorigenesis and chemotherapy resistance, but also represents an emerging new hallmark of cancer. Research on leukemia suggests that leukemia cells have an abnormal cholesterol metabolism characterized by increased cholesterol synthesis, lipid uptake, and potential effects of oxysterols. Statins, which inhibit 3-hydroxy-3-methylglutaryl-CoA reductase (HMGCR), the rate-limiting enzyme in cholesterol homeostasis, may have anti-leukemic properties by interfering with the cellular cholesterol pathway. Preclinical and early clinical studies have investigated the potential of statins as an adjuvant therapy option for leukemia patients. However, the results are controversial and require a deeper understanding of cholesterol metabolism in subgroups of leukemia patients who may benefit from such therapy. This study was dedicated to the comprehensive investigation of cholesterol homeostasis in *t(4;11)* leukemia cells, including the regulatory activities of two transcription factors, sterol regulatory element-binding protein 2 (SREBP2) and retinoid-related orphan receptor gamma (RORγ). In addition, the effect of inhibition of the cholesterol signaling cascade on cellular cholesterol metabolism and *t(4;11)* tumor growth was examined. The aim was to understand the basis of these signaling pathways in order to identify potential therapeutic targets for the treatment of leukemia patients harboring a *KMT2A-AFF1* chromosomal translocation. The results of this work revealed a significant overexpression of SREBP2 in *t(4;11)* leukemia cells, indicating a dysregulated cholesterol homeostasis. By specifically inhibiting RORγ, a dose-dependent reduction in leukemia cell growth was observed, along with the induction of cell cycle changes and apoptosis. RNA sequencing (RNA-Seq) analysis revealed a significant change in the transcriptome of *t(4;11)* leukemia cells after RORγ inhibition. This included downregulation of SREBP2-dependent key genes involved in cholesterol synthesis and import, as well as modulation of genes associated with intrinsic, mitochondrial involvement in apoptosis. This suggests that RORγ has a regulatory effect on SREBP2. When *t(4;11)* cells were treated with a combination of the RORγ inhibitor and cytarabine, additive effects were observed. Furthermore, when atorvastatin was added, a strong anti-leukemia synergism was observed by circumventing the statin-induced feedback. These findings provide insights into the molecular basis of cholesterol metabolism in *t(4;11)* leukemia cells and suggest that targeted inhibition of these pathways may be a promising therapeutic approach for the treatment of *t(4;11)* leukemia patients.

Zusammenfassung

Chromosomale Translokationen, an denen das *KMT2A*-Gen beteiligt ist, treten bei etwa 5% bis 10% der akuten Leukämien auf und sind mit einem aggressiven Krankheitsverlauf und einer schlechten Prognose assoziiert. Das *AFF1*-Gen ist der häufigste Translokationspartner des *KMT2A*-Gens und führt zu einer *t(4;11)*-Leukämie. Es ist bekannt, dass Krebszellen eine metabolische Reprogrammierung durchlaufen können, zu der auch Veränderungen in der Cholesterinhomöostase gehören, die wiederum zu einer erhöhten Proliferation und Überlebensrate beitragen. Ein gestörter Cholesterinstoffwechsel begünstigt somit nicht nur die Tumorentstehung und die Chemotherapieresistenz, sondern stellt auch ein neues Merkmal von Krebs dar. Die Leukämieforschung weist darauf hin, dass bestimmte Leukämiezellen einen abnormalen Cholesterinstoffwechsel aufweisen, der durch eine erhöhte Cholesterinsynthese, Lipidaufnahme und mögliche Wirkungen von Oxysterolen gekennzeichnet ist. Statine, welche die 3-Hydroxy-3-Methylglutaryl-CoA-Reduktase (HMGCR), das geschwindigkeitsbegrenzende Enzym der Cholesterin-Homöostase, hemmen, könnten durch Beeinflussung des zellulären Cholesterin-Stoffwechsels eine leukämiehemmende Wirkung entfalten. In präklinischen und ersten klinischen Studien wurde das Potenzial von Statinen als adjuvante Therapieoption für Leukämiepatienten untersucht. Die Ergebnisse sind jedoch umstritten und erfordern ein tieferes Verständnis des Cholesterinstoffwechsels in spezifischen Subgruppen von Leukämiepatienten, die von einer solchen Therapie profitieren könnten.

Die vorliegende Studie widmete sich der Untersuchung der Cholesterinhomöostase in *t(4;11)*-Leukämiezellen, einschließlich der regulatorischen Aktivitäten von zwei Transkriptionsfaktoren, dem *sterol regulatory element binding protein 2* (SREBP2) und dem *retinoid-related orphan receptor gamma* (RORγ). Darüber hinaus wurde die Wirkung einer Hemmung der Cholesterin-Signalkaskade auf den zellulären Cholesterinstoffwechsel und das *t(4;11)*-Tumorwachstum untersucht. Ziel war es, die Grundlagen dieser Signalwege zu verstehen, um mögliche therapeutische Ziele für die Behandlung von Leukämiepatienten mit einer *KMT2A-AFF1*-Chromosomentranslokation zu identifizieren. Die Ergebnisse dieser Arbeit zeigten eine signifikante Überexpression von SREBP2 in *t(4;11)*-Leukämiezellen, was auf eine gestörte Cholesterinhomöostase hinweist. Die spezifische Hemmung von RORγ führte zu einer dosisabhängigen Reduktion des Wachstums der Leukämiezellen sowie zur Induktion von Zellzyklusveränderungen und Apoptose. Die Analyse mittels RNA-Sequenzierung zeigte eine signifikante Veränderung des Transkriptoms von *t(4;11)*-Leukämiezellen nach RORγ-Hemmung. Dazu gehörten die Herunterregulation von SREBP2-abhängigen Schlüsselgenen, die an der Cholesterinsynthese und am Cholesterinimport beteiligt sind, sowie die Modulation von Genen, die mit der intrinsischen mitochondrialen Beteiligung an der Apoptose in Verbindung stehen. Diese Ergebnisse deuten darauf hin, dass RORγ eine regulatorische Wirkung auf SREBP2 hat. Bei der Behandlung von *t(4;11)*-Zellen mit einer Kombination aus

RORγ-Inhibitor und Cytarabin wurden additive Effekte beobachtet. Zudem wurde beobachtet, dass die Zugabe von Atorvastatin einen starken Anti-Leukämie-Synergismus bewirkt, ohne dass es zu einer Statin-induzierten Rückkopplung kommt. Diese Ergebnisse liefern Erkenntnisse über die molekularen Grundlagen des Cholesterinstoffwechsels in *t(4;11)*-Leukämiezellen und deuten darauf hin, dass eine gezielte Hemmung dieser Stoffwechselwege ein vielversprechender therapeutischer Ansatz für die Behandlung von *t(4;11)*-Leukämiepatienten sein könnte.

Table of contents

List of figures

List of tables

List of abbreviations

-	missing
+	expression
7-AAD	7-aminoactinomycin
27HC	27-hydroxycholesterol
ABC	ATP-binding cassette
ABCA1/ ABCG1	ABC transporter
ac	acetylation
ACAT1	Acetyl-CoA acetyltransferase 1
acetyl-CoA	acetyl coenzyme A
AFF1	AF4/FMR2 family member 1 (also known as AF4)
ALL	acute lymphocytic/lymphoblastic leukemia
AML	acute myeloid leukemia
ATV	atorvastatin
BCR	breakpoint cluster region
BM	bone marrow
BMI1	BMI1 polycomb ring finger proto-oncogene
BrdU	bromodeoxyuridine
CAR	chimeric antigen receptor
CBMCs	Cord blood mononuclear cells
CBP/p300	CREB-binding protein
CD	cluster of differentiation
cDNA	complementary DNA
CFU	colony-forming units
ChIP-Seq	chromatin immunoprecipitation sequencing
CI	combination index
CLL	chronic lymphocytic leukemia
CML	chronic myeloid leukemia
CREB	cAMP response element–binding protein
CRISPR	clustered regularly interspaced short palindromic repeats
CtBP	C-terminal binding protein
CYP33/PPIE	cyclophilin E
DBD	DNA-binding domain
DEGs	differentially expressed genes
der11	*KMT2A-AFF1*
der4	*AFF1-KMT2A*
DMAPP	dimethylallyl pyrophosphate

DMSO	dimethyl sulfoxide
DOT1L	disruptor of telomeric silencing 1-like
DSB	double-strand break
ER	endoplasmic reticulum
FcR	Fc receptor
FDPS	farnesyl pyrophosphate synthase
FISH	fluorescence *in situ* hybridization
FL	fetal liver
FPP	farnesyl pyrophosphate
FS	fatostatin
GAPDH	Glyceraldehyde-3-phosphate dehydrogenase
GGPP	geranylgeranyl pyrophosphate
GPP	geranyl diphosphate
GRN	gene regulatory network
GTPases	small guanosine triphosphate hydrolases
H	histone
HCF-1	host cell factor-1
HDAC1	histone deacetylase 1
HDL	high-density lipoprotein
HMGCR	3-hydroxy-3-methylglutaryl-CoA reductase
HMGCS	3-hydroxy-3-methylglutaryl-CoA synthase
HOX	homeobox
HPC2	hereditary prostate cancer protein 2
HPCs	hematopoietic progenitor cells
HRP	horseradish peroxidase
HSCs	hematopoietic stem cells
HSCT	hematopoietic stem cell transplantation
HSPCs	hematopoietic stem and progenitor cells
huCB	human umbilical cord blood
IC	inhibitory concentration
INSIG1	insulin induced gene 1 protein
IPA	Ingenuity Pathway Analysis
IPP	isopentenyl pyrophosphate
K	lysine
kd	knockdown
KMT2A	histone-lysine *N*-methyltransferase 2A (also known as MLL)
KMT2A-C	C-terminal fragment of KMT2A
KMT2A-N	N-terminal fragment of KMT2A

*KMT2A*r	*KMT2A*-rearrangement
LBD	ligand-binding domain
LDL	low-density lipoprotein
LDLR	LDL receptor
LEDGF	lens epithelium-derived growth factor
LSC	leukemic stem cell
LXRs	liver X receptors
MACS	magnetic-activated cell sorting
MAT2A	methionine adenosyltransferase 2A
MBM	Menin-binding motif
mCRPC	metastatic castration-resistant prostate cancer
me	methylation
MLL	mixed-lineage leukemia
MPAL	mixed phenotype acute leukemia
mRNA	messenger RNA
MS-5	murine stromal cell line
MSCs	mesenchymal stromal cells
MVK	mevalonate kinase
MYLIP/IDOL	myosin regulatory light chain interacting protein
NCCT	NGS Competence Center Tübingen
NHEJ	non-homologous end joining
NRs	nuclear receptors
P	phosphorylation
PAFc	polymerase associated factor complex
PAM	protospacer adjacent motif
PBMCs	peripheral blood mononuclear cells
PBS	phosphate-buffered saline
PCR	polymerase chain reaction
PHD	plant homeodomains
PI	propidium iodide
P-TEFb	positive transcription elongation factor b
q.s.	quantum satis
RNAi	RNA interference
RNAP II	RNA polymerase II
RNA-Seq	RNA sequencing
RNP	ribonucleoprotein
RORγ	retinoid-related orphan receptor gamma
RORs	Retinoid-related orphan receptors

RT-qPCR	Reverse transcription quantitative PCR
S1P/ S2P	site-1 protease/ site-2 protease
SCAP	SREBP cleavage-activating protein
SD	standard deviation
SDS-PAGE	SDS-polyacrylamide gelektrophoresis
SEC	super elongation complex
sgRNA/shRNA	single guide RNA/short hairpin RNA
SQLE	squalene epoxidase
SQS	squalene synthase
SRE	sterol regulatory elements
SREBF	sterol regulatory element-binding factor
SREBP	sterol regulatory element-binding protein
SSD	sterol-sensing domain
t	translocation
TAD	transactivation domain
TALENs	transcription activator-like kinases
taspase I	threonine aspartase I
TNBC	triple-negative breast cancer
TRC	the RNAi Consortium
Treg	regulatory T cell
TRX	Drosophila trithorax
WHO	World Health Organization

1 Introduction

1.1 Cellular hematopoiesis and acute leukemias

Cellular hematopoiesis is defined as the production of the solid components of human blood and takes place in the red bone marrow (BM). It is a hierarchical process that begins with hematopoietic stem cells (HSCs). HSCs have two main properties: the ability to self-renew and to differentiate into various hematopoietic progenitor cells (HPCs). As differentiation progresses, the lineage potential of the cells to eventually differentiate into mature blood cell types becomes more limited (reviewed by [1]). Cell populations of the hematopoietic system are typically identified by lineage surface markers (clusters of differentiation, CD), and human HSCs have been identified as $Lin^-/CD34^+/CD38^-/CD90^{+/-}/CD45RA^-/CD49f^+/Rho^{low}$ [2]. As a sign of differentiation, hematopoietic stem and progenitor cells (HSPCs) are able to form colony-forming units (CFUs) and differentiate into lymphoid and myeloid cells. Myeloid cells include erythrocytes, platelets, monocytes, macrophages, and granulocytes, which are further subdivided into neutrophils, eosinophils, and basophiles. Cells with lymphoid properties include NK cells, T cells, and B cells (reviewed by [3, 4]).

The term leukemia refers to neoplastic diseases associated with uncontrolled changes in the red BM, leading to a more or less pronounced impairment of hematopoiesis. A common feature of leukemia development is the mutation of a single cell in the BM, followed by mitotic divisions and leading to the development of a monoclonal cell population. These malignant cells can proliferate uncontrollably in the BM and lead to BM failure by displacing normal hematopoiesis (reviewed by [4]). Since the affected cells cannot perform their physiological differentiation function, cytopenia is part of the general symptomatology of the clinical manifestation and includes bleeding (thrombocytopenia), infection (granulocytopenia), and reduced performance (anemia). As the disease progresses, mutated cells migrate from the BM into the peripheral blood and infiltrate lymphatic and non-lymphatic organs [5, 6]. The first classification of leukemia is based on the mutated cell of origin. It can be divided into the acute phase, in which leukemia develops in early HSPCs and is associated with rapid disease progression. Chronic leukemia develops in more mature cells, resulting in a slower progression of the disease [7]. An epidemiologic classification is also based on the occurrence of affected cells and is divided into myeloid and lymphoid leukemias. Acute leukemias have two subcategories, acute myeloid leukemia (AML) and acute lymphocytic/lymphoblastic leukemia (ALL) [5, 6, 8, 9]. If a primary BM disorder is suspected, a comprehensive diagnostic setup is available. These include cytomorphology of peripheral blood (differential blood count) and BM (myelogram), immunophenotyping (flow cytometry), and cytogenetics (polymerase chain reaction (PCR), sequencing, fluorescence *in situ* hybridization (FISH). In particular, cytogenetics and the detection of genetic aberrations have become increasingly important in recent years and provide more precise information about the course of therapy and prognosis [10].

1.2 *t(4;11)* chromosomal translocations

1.2.1 Epidemiology

In 1999, the World Health Organization (WHO) recognized genetic aberrations including leukemias with translocations of the histone-lysine *N*-methyltransferase 2A (*KMT2A)* gene (*KMT2A*-rearrangement, *KMT2A*r) in the classification of hematological diseases [11]. Since then, the importance of genetic aberrations has been steadily increased and the current classification recognizes *KMT2A*r under its specific immune phenotype in AML and ALL with any fusion partner [8, 9]. For example, AML with defined genetic alterations including *KMT2A* fusions is distinguished from AML classification based on morphology and differentiation alone [8]. Rearrangements of *KMT2A* occur in 5% to 10% of acute leukemias and B-ALL and AML are the most frequently diagnosed neoplasms carrying a *KMT2A*r [8, 9, 12, 13].

A key feature of *KMT2A*r leukemias is the diversity of fusion partner genes ([13], reviewed by [14]). The eight most common partner genes of the *KMT2A* gene are *AFF1* (*AF4*), *MLLT3* (*AF9*), *MLLT1* (*ENL*), *MLLT10* (*AF10*), *ELL*, *AFDN* (*AF6*), *EPS15*, and *PTD* and have been found in more than 90% of the patients studied [13]. This was demonstrated in a study by Meyer *et al.* with more than 3000 leukemia patients. In this context, the occurrence of *KMT2A* fusions was also analyzed with regard to the disease phenotype. While the majority of patients with an ALL phenotype (56.5%) were positive for a *KMT2A-AFF1* translocation, the most frequent translocation in AML patients was *KMT2A-MLLT3* (30.4%) [13] (**Figure 1**).The presence of different *KMT2A* fusions was also found to be significantly different in cohorts of infant, pediatric, and adult patients. In infants and adults, most patients had a *KMT2A-AFF1* translocation (40.2% and 48.5%, respectively), whereas in pediatric patients, the *KMT2A-MLLT3* translocation was the most common (25.9%) [13].

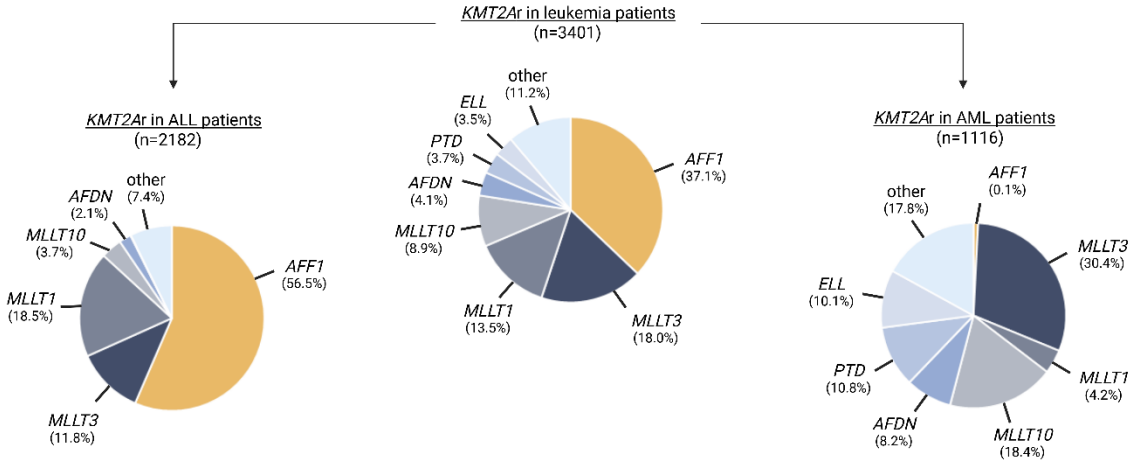

Figure 1: Distribution of *KMT2A*r fusion partner genes.

The frequency of each fusion gene was determined in a study population of 3401 *KMT2A*r acute leukemia patients, including 2182 ALL and 1116 AML patients. The figure is based on data from Meyer *et al.* [13]. Figure generated with BioRender.

1.2.2 Molecular characterization

In the recent years, it has been evaluated that the prognosis of leukemia patients is strongly influenced by cytogenetic parameters and genetic aberrations [7, 10]. Normally, malignant or mutated cells are recognized and eliminated by the immune system. However, in some cases, cells with genetic aberrations remain undetected by immune cells. Genetic aberrations include deletions, inversions, duplications, and translocations. Chromosomal translocations are characterized by the transfer of a chromosomal segment to another chromosome, which may be homologous or non-homologous. A balanced reciprocal chromosomal translocation refers to the transfer of a chromosomal segment to another non-homologous chromosome. In this process, the two non-homologous chromosomal segments are exchanged. The genetic material remains intact and can lead to the appearance of chimeric proteins with new properties and phenotypic changes. In many cases, this event is referred to as the onset of leukemogenesis. The most prominent example of a chromosomal translocation is the Philadelphia chromosome, which is characterized by the *BCR-ABL1* gene, resulting in permanently stimulated tyrosine kinase activity of the ABL protein. The uncontrolled proliferation of granulopoietic cells leads to an imbalance of the hematopoietic system, ultimately resulting in a clinically manifested ALL or chronic myeloid leukemia (CML). The presence of the Philadelphia chromosome is usually associated with other mutations (reviewed by [15, 16]). In contrast to this, translocations of the *KMT2A* gene, also known as mixed-lineage leukemia (*MLL*), are characterized by the presence of a single chimeric KMT2A-X and its reciprocal X-KMT2A protein, which are sufficient to induce leukemia [17].

Physiological protein functions of MLL

The *KMT2A* gene is the most common translocation partner of leukemia-inducing chromosomal translocations and is associated with high-risk potential [13]. The genetic locus on chromosome 11q23 encodes a histone methyltransferase that induces a methylation of histone H3 at lysine 4 (H3K4me) and was found to be a homologue of the Drosophila trithorax (TRX) protein [18, 19]. H3K4me is an epigenetic mark for transcriptional activation of certain promoters and is expressed in all tissues. Post-translational cleavage of threonine aspartase I (taspase I) leads to the formation of N- and C-terminal fragments of the KMT2A protein (KMT2A-N and KMT2A-C), which form a nuclear complex with other proteins [20, 21]. The major functional domains of KMT2A are discussed below as they are important for understanding the functional consequences of *KMT2A*r leukemias. Throughout this thesis, lysine methyltransferase 2A will be referred to as KMT2A.

The KMT2A-N module interacts with Menin through a Menin-binding motif (MBM), which has an adapter function. Both form an interaction surface with lens epithelium-derived growth factor (LEDGF), which has a PWWP domain capable of recognizing H3K36 methylation marks (H3K36me) on active chromatin, thereby recruiting KMT2A to previously transcribed genes

[22-24]. Recruitment of KMT2A to target loci for activating transcription of target genes is also linked to its interaction with the polymerase-associated factor complex (PAFc), which interacts with KMT2A-N. The PAFc-interacting CxxC motif is responsible for the binding of KMT2A to unmethylated CpG sequences [25]. Thus, PAFc recruits the KMT2A protein to its target sites and also mediates the ubiquitination of H2B, which in turn can enhance H3K79 methylation (H3K79me) [26, 27]. The latter plays a role in the transcriptional activity of *t(4;11)* leukemias, which will be discussed in more detail in the following paragraph. Several proteins have been observed to interact with the CxxC domain of KMT2A, which has been defined as a repression domain based on the effects of these interactions on transcription. Binding partners include the polycomb group proteins BMI1 polycomb ring finger proto-oncogene (BMI1) and hereditary prostate cancer protein 2 (HPC2), and the corepressors C-terminal binding protein (CtBP) and histone deacetylase 1 (HDAC1) [28]. In addition, KMT2A-N contains four important chromatin readers known as plant homeodomains (PHDs). PHD3 specifically recognizes H3K4me resulting in a positive feedback loop in which KMT2A can both write and read H3K4me [29]. PHD2 and PHD3 can homodimerize and affect target gene expression via cyclophilin E (CYP33/PPIE) binding [30]. This catalyzes conformational changes in the KMT2A protein and subsequently recruits HDAC1 and other polycomb group proteins, resulting in transcriptional repression [28] (**Figure 2**).

The KMT2A-C fragment is physiologically fused to four conserved factors called WDR5, RBBP5, ASH2L, and DPY30, stimulating the H3K4me epigenetic activity [31, 32]. Mono-, di-, and trimethylation of H3K4 is an important feature of active genes and is generated by the transfer of a methyl group from S-adenosylmethionine to a lysine residue of histone proteins. KMT2A-C also contains a SET domain, which mediates the methyltransferase activity [33], and a transactivation domain (TAD). The latter recruits the histone acetyltransferases cAMP response element–binding protein CREB)-binding protein (CBP)/p300 and MOF, which have been reported to bind to KMT2A as transiently associated factors [34, 35]. Acetylation of H3K9, H3K18, H3K27, and H4K16 enhances transcriptional activation of target genes [36]. In its physiological form, the KMT2A protein complex with its functional domains is able to control the transcription of several target genes. Of particular importance is the activation of homeobox (*HOX*) genes, which is mediated by the direct binding of the KMT2A protein to *HOX* promoters and its methylation [26, 33] (**Figure 2**).

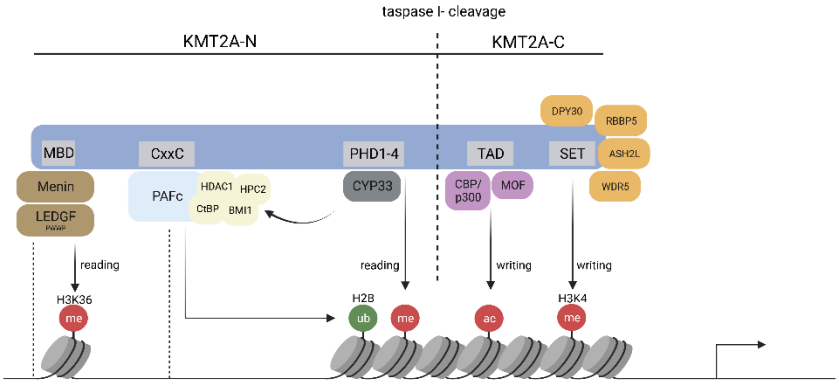

Figure 2: Schematic representation of the KMT2A multi-protein complex.
Proteolytic cleavage of taspase I results in the formation of KMT2A-N and KMT2A-C. The subsequent interaction of the two peptide fragments leads to the stabilization of the KMT2A complex, providing a platform for the formation of a multi-protein complex. Important functional domains of the KMT2A protein are shown in grey with the corresponding interaction partners. The multi-protein complex binds to histones in the promoter region of e.g. *HOX* genes and activates their expression via H3K4me. The figure shows a simplified representation of the KMT2A complex and does not include all known functional domains and interaction partners. Figure generated with BioRender.

Due to its high homology to the TRX protein [18, 19], which plays a crucial role in embryonic development, a similar role has been attributed to the KMT2A protein. It has been shown that KMT2A knockout mice exhibit embryonic lethality, mainly due to the altered *HOX* expression. KMT2A deficiency also led to hematopoietic abnormalities, suggesting an important role of KMT2A in early hematopoiesis [37]. Thus, it was established early on that the KMT2A protein is particularly strongly expressed in organ tissues of the hematopoietic and lymphoid systems [38]. A direct correlation between *HOX* expression and hematopoietic differentiation has also been demonstrated, suggesting that KMT2A is required for hematopoietic differentiation [39-41]. There is also strong evidence that the presence of the KMT2A protein complex is essential for cell proliferation. It has been shown that the KMT2A protein is recruited by host cell factor-1 (HCF-1) during the G1-S transition of the cell cycle and binds to E2F promoters [42]. Further, cell cycle-specific transcriptional activation is induced, and proliferation is promoted. A study by Liu and colleagues demonstrated that biphasic expression of KMT2A during the cell cycle transition periodically activates cyclin transcription during cell proliferation. This includes the need to turn off KMT2A expression in a built-in program to ensure normal regulation of the cell cycle and proliferation [43]. This is achieved in part by the self-regulatory ability of the KMT2A protein to simultaneously activate and read methylation patterns.

Pathophysiological consequences of *KMT2Ar*

Chromosomal translocations require DNA double-strand breaks (DSBs) within the involved chromosomes and are located in breakpoint cluster regions (BCRs) [44]. DNA DSBs can be

caused by a variety of factors, including topoisomerase II, ionized radiation, and cytotoxic agents, or they can occur spontaneously [45]. In the case of the *KMT2A* gene, the regions between intron 7 and exon 13 in the KMT2A-N coding region have been defined as the major BCR [13]. Once chromosomal damage has occurred, it must be repaired by the cell. Since *KMT2A*r occur between non-homologous sequences, homologous repair mechanisms do not play a role. The repair mechanism underlying KMT2A translocations has been traced back to non-homologous end joining (NHEJ) and ultimately leads to the formation of chimeric fusion genes at the fusion sites of both chromosomes [46, 47]. In the case of a *t(4;11)* translocation, the *KMT2A* gene on chromosome 11 fuses with *KMT2A* including AF4/FMR2 family member 1 (*AFF1*), previously known as ALL1-fused gene from chromosome 4 (*AF4*), on chromosome 4, resulting in the development of derivate 11 (der11, *KMT2A-AFF1*) and the reciprocal derivate 4 (der4, *AFF1-KMT2A*) [48, 49] (**Figure 3**). Throughout this thesis, the main translocation partner of *KMT2A* will be referred to as AFF1.

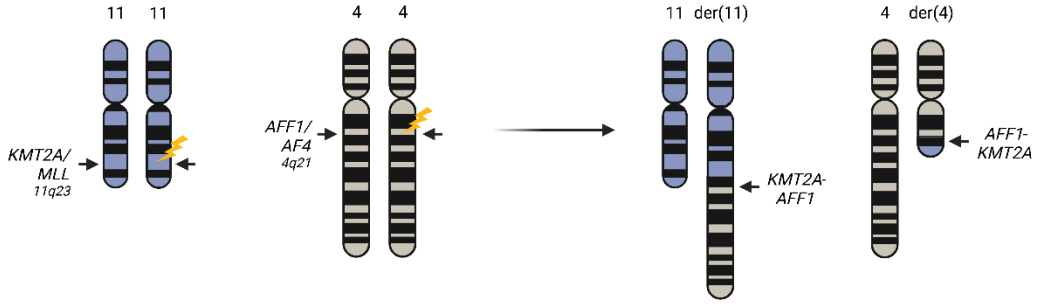

Figure 3: Schematic representation of the *t(4;11)* chromosomal translocation.
A simultaneous double-strand break (DSB) occurs in the *KMT2A* gene on chromosome 11 and in the *AFF1* gene on chromosome 4. Subsequent cellular repair mechanisms rejoin the two chromosome fragments, resulting in two illegitimate recombinations at the fusion sites between the two affected genes and the formation of der11 and der4. Figure generated with BioRender.

Translocation partners of *KMT2A* are genes encoding for nuclear, membrane-associated, or cytoplasmic proteins capable of binding multimeric biochemical complexes. Several common partners (including AFF1, AFF4, MLLT1, MLLT3, and ELL) are part of the super elongation complex (SEC), which is involved in transcriptional elongation, and is formed in the KMT2A-AFF1 protein complex upon fusion of *KMT2A* to *AFF1*. As a result of the translocation, KMT2A-N abnormally stabilizes the localization of SEC at KMT2A target genes, including *HOX* genes and the protooncogene *MYC* [50, 51]. This leads to abnormal phosphorylation of RNA polymerase II (RNAP II) by positive transcription elongation factor b (P-TEFb), the central catalytic component of SEC, and increases transcriptional elongation. By elongating RNAP II, the SEC is also a direct mediator of H3K79me by recruiting disruptor of telomeric silencing 1-like (DOT1L) [50, 52-54]. DOT1L, in turn, is stimulated by PAFc-mediated ubiquitination of H2B [27]. In this formation, the KMT2A-AFF1 protein is still able to bind to promoters via Menin,

LEDGF, and PAFc to cause transcriptional elongation, but without the inhibitory feedback of CYP33. On the other hand, the reciprocal fusion protein AFF1-KMT2A still contains the methyltransferase activity mediating SET domain and CBP recruiting domain. As a result, the methylation pattern changes from H3K4 to H3K79 and the previously moderate expression of key *KMT2A* translocation-specific target genes is upregulated [50, 55]. *KMT2A*r leukemias are characterized by a specific gene expression pattern including the upregulation of several *HOX* genes (*HOXA9*, *HOXA5*, *HOXA10*, *HOXA6*), *MEIS1*, and *PRMT5* and can therefore be distinguished from gene expression in other leukemia subtypes [40, 51, 55, 56]. Finally, affected HSPCs harboring the translocation are characterized by decreased differentiation and uncontrolled proliferation with oncogenic potential (reviewed by [14]) (**Figure 4**).

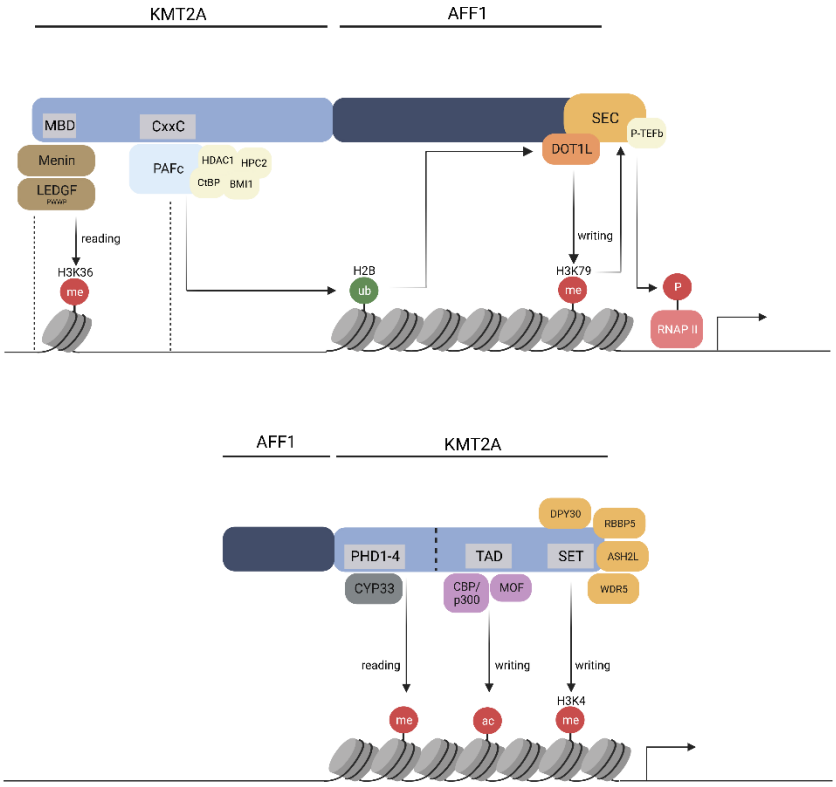

Figure 4: Schematic representation of the KMT2A-AFF1 and AFF1-KMT2A protein complexes. The KMT2A-AFF1 and AFF1-KMT2A fusion protein complexes are shown post-transcriptionally after chromosomal translocation. AFF1 is part of the SEC that is recruited to target genes by the KMT2A fusion protein to increase phosphorylation (P) of RNAP II and enhance transcriptional elongation. AFF1 interacts with DOT1L to cause H3K79me and subsequent activation of the SEC. KMT2A interacts with PAFc and catalyzes the ubiquitination of H2B, further enhancing the activity of DOT1L (top). In the AFF1-KMT2A fusion protein, KMT2A retains the SET domain and thus the H3K4me-writing function. Due to the loss of the CYP33-mediated inhibitory function, it has oncogenic potential (bottom). The figure shows a simplified representation of both protein complexes and does not include all known functional domains and interaction partners. Figure generated with BioRender.

Despite intensive research in this field and extensive knowledge of the complex partners involved, the leukemogenesis of *KMT2A*r leukemia has not been conclusively elucidated until today. It has long been suspected that the KMT2A-AFF1 protein is critical for oncogenic leukemogenesis [57], which has been demonstrated in a conditional knockin mice model. Mice in which KMT2A-AFF1 was expressed under the control of the endogenous promoter showed features of both AML and ALL and the H3K79me pattern was identified as a critical factor [55]. However, in a study by Kowarz *et al.*, the reciprocal AFF1-KMT2A was found in addition to the KMT2A-AFF1 in 80% of the patients studied [58]. In addition, transplantation of either product did not show a disease phenotype in KMT2A-AFF1 transplanted mice, whereas populations receiving AFF1-KMT2A or both transcripts developed a pro-B-ALL [59]. Ultimately, the involvement of each translocation product is still controversial; however, many data suggest that both fusion products are involved in the mechanism of leukemogenesis ([60], reviewed by [14]).

1.2.3 Prognosis and therapeutic options

AML and ALL with *KMT2A*r fusion genes are listed as cytogenetic diagnostic criteria in the latest WHO classification and in the German guidelines [5, 6, 8-10]. There are important differences between the individual subgroups in terms of disease progression, prognosis, and therapeutic interventions. The most frequently described fusion gene is *KMT2A-MLLT3* in AML and *KMT2A-AFF1* in B-ALL [8, 9, 13]. In adult AML, the potential risk on the basis of risk stratification is intermediate [61], whereas the detection of *KMT2A*r in adults with ALL places these patients in the high-risk group with poor prognosis [5]. Pediatric patients with both AML and ALL features and *KMT2A*r are considered to have a poor prognosis [62, 63].

Due to the rapid progression of the disease, *KMT2A*r leukemia patients need an aggressive therapeutic regimen. Both AML and ALL require standard frontline therapy with cytarabine and anthracyclines (daunorubicin, idarubicin) to induce remission. Depending on the patient's condition and the risk of remission, subsequent consolidation and maintenance therapy may be continued [5, 6]. However, *KMT2A*r leukemias are characterized by resistance to chemotherapy and high relapse rates after standard treatment [64, 65]. Treatment options such as allogeneic hematopoietic stem cell transplantation (HSCT) and chimeric antigen receptor (CAR) T-cell therapy have been approved and may offer some benefit to patients. Unfortunately, these are limited by a high risk of adverse late effects and cytotoxicity [66], as well as the risk of lineage switching from ALL to AML [67, 68]. For this reason, efforts are being made to explore alternative therapeutic options, including the development of small molecule drugs. To date, there are current approaches to develop novel treatment strategies for *KMT2A*r acute leukemias. These are focused on molecularly targeted treatment strategies and include the modification at epigenetic transcription level, proteasome and FLT3 inhibition, as well as

inhibition of cell cycle checkpoints and anti-apoptotic mechanisms (reviewed by [69, 70]) (**Figure 5**).

The current results regarding the therapy and prognosis of patients with *KMT2A*r leukemia show that there is an ongoing need to better investigate and understand the underlying cytogenetics in order to develop new therapeutic approaches. Identifying specific signaling pathways and resulting targets that are characteristic of this leukemia subtype may improve the chances of therapy success and long-term patient outcomes.

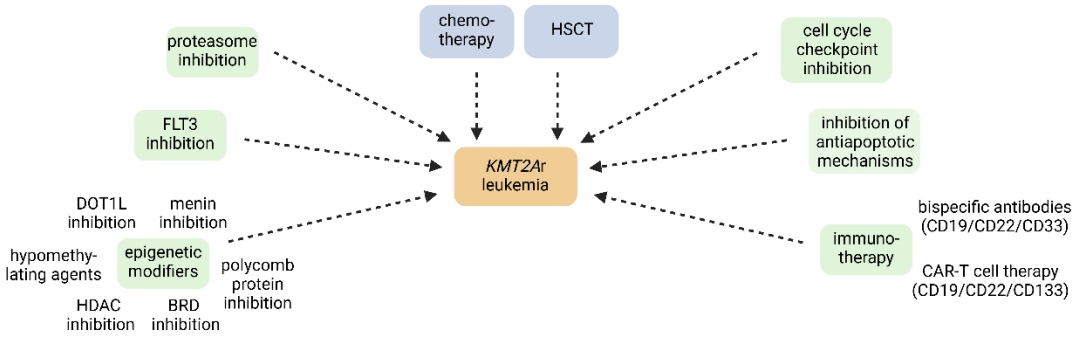

Figure 5: Targeted therapies for *KMT2A*r leukemia.

The rapid progression of *KMT2A*r leukemias requires aggressive therapies such as chemotherapy and HSCT. But outcomes are often poor to suboptimal and not all cases have been shown to benefit. A better understanding of the biology has identified important vulnerabilities that can be targeted and promises new therapeutic approaches to improve patient outcomes. The figure is modified from Winters and Bernt [69], Rice and Roy [70]. Figure generated with BioRender.

1.2.4 Cellular models

Both *in vitro* and *in vivo* cell models are essential for the study of leukemogenesis and the development of new treatment strategies. First and foremost, primary patient material is the non-plus-ultra when it comes to characterizing the properties of leukemia cells. *KMT2A*r leukemias occur relatively frequently (up to 10%) in patients with acute leukemia [12, 13]. However, obtaining sufficient cell material for research purposes is often challenging. In many cases, especially when children are affected or the patients are already in a very poor state of health, the availability of blood and BM samples can be very limited. Furthermore, the stability and viability of primary *ex vivo* patient cells is generally very low and cells rapidly undergo programmed cell death or differentiation within hours to days ([71], reviewed by [72, 73]). However, with appropriate and adapted optimization of culture conditions, primary cells can be used for basic and short-term experiments [74, 75]. Although *KMT2A*r leukemia cells usually have only few additional mutations, however even few mutations can change the outcome of the study and are extremely limiting when studies specifically aim to evaluate *KMT2A*r. Established cell lines have shown some advantages in terms of their ease of culture and similar gene expression signature comparable to primary leukemia cells [76]. Nevertheless, cell lines are often not ideal due to their different biology compared to primary cells. A cell line is

genetically homogeneous and acquires multiple cytogenetic aberrations during prolonged cultivation, making the investigation of a single gene mutation practically impossible [77]. An important focus of preclinical analysis is, of course, on *in vivo* models. In xenograft models, leukemia patient samples are transplanted into immunodeficient mice [78]. This allows the inclusion of patient diversity, but requires a large number of cells, and is influenced by possible other genetic aberrations. Moreover, not all patient samples are capable of sufficient engraftment in mice. Alternative knockin models of *KMT2A-AFF1*, *KMT2A-MLLT3*, and *KMT2A-MLLT1* in embryonic stem cells specifically modified by the Cre-loxP system allow the expression of *KMT2A* fusion genes controlled by the expression of Cre recombinase and mimic the patient situation with one rearranged and one healthy copy [55, 79]. However, murine models have shown important differences between mouse and human (epi-)genetics, and these *in vivo* experiments still require appropriate *ex vivo* preliminary studies. In this context, the Marschalek group has demonstrated the integration of vectors with an inducible Sleeping Beauty backbone to generate stable *KMT2A*r-expressing cell lines [80]. Lentiviral transduction with expression vectors has also provided stable CD34+ HSPCs with *KMT2A*r [81]. Unfortunately, the use of viral vectors mostly induces the overexpression of fusion genes and is not comparable to the situation in patients. Finally, there is a particular need for innovative cell models that can mimic patient gene expression and heterogeneity while focusing on the single *KMT2A*r translocation.

To overcome these challenges, the Schneidawind lab has developed a preclinical model for translational studies of *t(4;11)* and *t(9;11)* leukemia [82]. Since chromosomal translocations arise from DNA DSBs, gene editing has been successfully used to induce *KMT2A*r translocations to mimic patient-like cell models. These techniques allow careful selection of sites for specific introduction of a DSB. Based on the hypothesis that *KMT2A*r serves as a potential oncogenic initiating event, previous studies have used transcription activator-like kinases (TALENs) to induce *KMT2A-MLLT3* and *KMT2A-AFF1* translocations in CD34+ HSPCs [83, 84]. Xenograft transplantation of endogenous *KMT2A-MLLT3* and reciprocal *MLLT3-KMT2A* expressing cells also led to AML in mice after long latencies [84, 85]. However, these studies were limited by their low efficiency to induce a chromosomal translocation, which resulted in a long time period to obtain pure culture systems. This also led to a high variability of observed cell fates [84]. The use of clustered regularly interspaced short palindromic repeats /CRISPR-associated protein 9 (CRISPR/Cas9) for genetic engineering has overcome some of these obstacles. The main advantage of CRISPR/Cas9-generated cells was shown with a significantly higher efficiency of the induced translocation compared to TALENs [86]. Gundry *et al.* have described the successful gene editing of CD34+ HSPCs by ribonucleoprotein (RNP) complexes containing the Cas9 protein and the targeting single guide RNA (sgRNA), followed by nucleofection. The method has been shown to be fast, efficient, and cost-effective for the example of specific genetic knockouts [87]. Derived from this, *t(4;11)* and *t(9;11)* translocations

could be achieved in CD34+ HSPCs from human umbilical cord blood (huCB) and led to the outgrowth of leukemic cells in suspension cell culture [82]. A specific cytokine milieu including FLT3-L, SFC, TPO, IL-3, IL-6, and G-CSF contributed to the proliferative potential of the translocated cells, which exhibit a poorly differentiated, myelomonocytic progenitor blast cell phenotype ($CD14^{low}$, $CD34^{-}$, $CD38^{+}$, $CD15^{+}$, $CD64^{+}$, $CD33^{+}$) with *KMT2A*r-specific marker expression ($CD32^{+}$, $CD9^{+}$) [82, 88]. Specific sgRNAs derived from the most common patient-specific breakpoints were used; with intron 11 for *KMT2A* [48], exon 3 for *AFF1* [49], and intron 4 for *MLLT3* [89]. The *in vitro* model allows the analysis of the *t(4;11)* and *t(9;11)* translocation as a first hit event in human leukemogenesis in different CB donors, resembling the *KMT2A*r-specific gene expression pattern with high *HOX*, *MEIS1*, *PRMT5*, and *MYC* expression [82, 90]. Another major advantage of modern gene editing is the similarity to the occurrence in patients with one rearranged and one healthy copy of *KMT2A*. Furthermore, the presence of the reciprocal fusion gene mimics the molecular features in the majority of the patients [58]. CRISPR/Cas9 as a gene-editing tool has been steadily expanded in the recent years and has moved into focus for the induction of chromosomal translocations, especially for *KMT2A*r. These studies differ mainly in the location of the breakpoint regions, the target cells used, and the culture conditions of the translocated cells, which seems to have a significant impact on the phenotypic characteristics related to AML or ALL [82, 91-94]. Coculture on a murine stromal cell line (MS-5) has forced the maturation of *t(4;11)* cells derived from CD34+ HSPCs from human fetal liver (FL) tissue samples towards a pro-B ALL leukemic phenotype [93]. In contrast, the *t(4;11) in vitro* model from our laboratory has shown a myelocytic phenotype with a high blast count when translocated cells were derived from CD34+ of huCB and cultured with the provision of a specific myeloid cytokine environment [82]. *In vitro* cell culture conditions appear to play an important role even before the selection of appropriate target cells [94]. Furthermore, CRISPR/Cas9-generated *KMT2A*r cells have the potential to lead to engraftment of AML, ALL, and mixed phenotype acute leukemia (MPAL) after transplantation into immunodeficient mice [86].

Regardless of the immunophenotype, various approaches using CRISPR/Cas9 have shown the induction of patient-like models harboring *KMT2A*r translocations with oncogenic potential. Testing new substrates in primary human cell models is essential as a bridge to clinical translation. Especially when these models are combined with approaches using primary *KMT2A*r patient material and established cell lines, the impact of preclinical studies can be increased.

1.3 Cholesterol pathway at different levels and possibilities for inhibition

With cholesterol representing a central role, sterols are essential components of cellular membranes to maintain permeability and fluidity. In addition to its involvement in intracellular transport and signaling, cholesterol also serves as precursor for the biosynthesis of steroid hormones, bile acids, and cholecalciferol. Both dietary intake and *de novo* biosynthesis are important sources of cholesterol in mammalian cells and membrane properties can be significantly influenced by even small changes in the local cholesterol concentration (reviewed by [95]). To ensure cell growth and proliferation, but also to avoid excessive cholesterol accumulation, mammalian cells under normal physiological conditions must carefully regulate the set of molecular pathways involved in cholesterol biosynthesis, uptake, storage, and efflux (reviewed by [96]).

1.3.1 Transcriptional regulation of cholesterol

Cholesterol metabolism is adapted to changes in cell growth and membrane remodeling. This is achieved through transcriptional regulation mediated by sterol regulatory element-binding proteins (SREBPs) and liver X receptors (LXRs).

In humans, there are different isoforms of SREBPs: while SREBP1a and SREBP1c (both encoded by the *SREBF1* gene) control the regulation of genes involved in fatty acid synthesis, SREBP2 (encoded by the *SREBF2* gene) activates genes related to cholesterol metabolism [97]. Since the regulation of cholesterol homeostasis by SREBP2 was elucidated by Brown & Goldstein [98], this mechanism has been extensively studied. In the presence of sterols, the inactive precursor form of SREBP2 binds with high affinity to SREBP cleavage-activating protein (SCAP), which in turn binds to the insulin induced gene 1 protein (INSIG1) in the membrane of the endoplasmic reticulum (ER) [98-100]. In contrast, a decrease in intrinsic sterol concentrations causes SCAP to detach from INSIG and transport SREBP2 to the Golgi apparatus, where it is proteolytically cleaved by site-1 protease (S1P). The N-terminal active form of SREBP2 is released by site-2 protease (S2P) and enters the nucleus to bind to promoters containing the sterol regulatory element (SREs) sequence [99, 101]. This induces the expression of *HMGCR* and *LDLR* target genes and leads to an increased *de novo* biosynthesis and uptake of cholesterol. The mechanism relies on a self-regulatory feedback loop, as activation of downstream SREBP2 genes increases intracellular cholesterol concentration, which in turn inhibits their expression. In the presence of excess intracellular cholesterol, the cell is able to store cholesterol in lipid droplets through esterification by acetyl coenzyme A (acetyl-CoA) acetyltransferase 1 (ACAT1), which contains a sterol-sensing domain (SSD), resulting in allosteric activation of enzymatic activity (reviewed by [102, 103]). In addition, sterol binding causes dissociation of the SSD of INSIG, which also directly inhibits biosynthesis by accelerating the degradation of 3-hydroxy-3-methylglutaryl-CoA reductase (HMGCR) [104] (**Figure 6**).

Oxysterols also serve as ligands for LXRs, so that high sterol levels cause their activation [105, 106]. So far, two isoforms are known, of which LXRα (encoded by the *NR1H3* gene) is mainly expressed in the liver and LXRβ (encoded by the *NR1H2* gene) is ubiquitously expressed [107-110]. Essentially, activation of LXR leads to expression of the cholesterol efflux transporter ATP-binding cassette (ABC) transporters, ABCA1 and ABCG1, and degradation of low-density lipoprotein-receptor (LDLR) by myosin regulatory light chain interacting protein (MYLIP/IDOL) to remove excess cholesterol ([111], reviewed by [112]) (**Figure 6**).

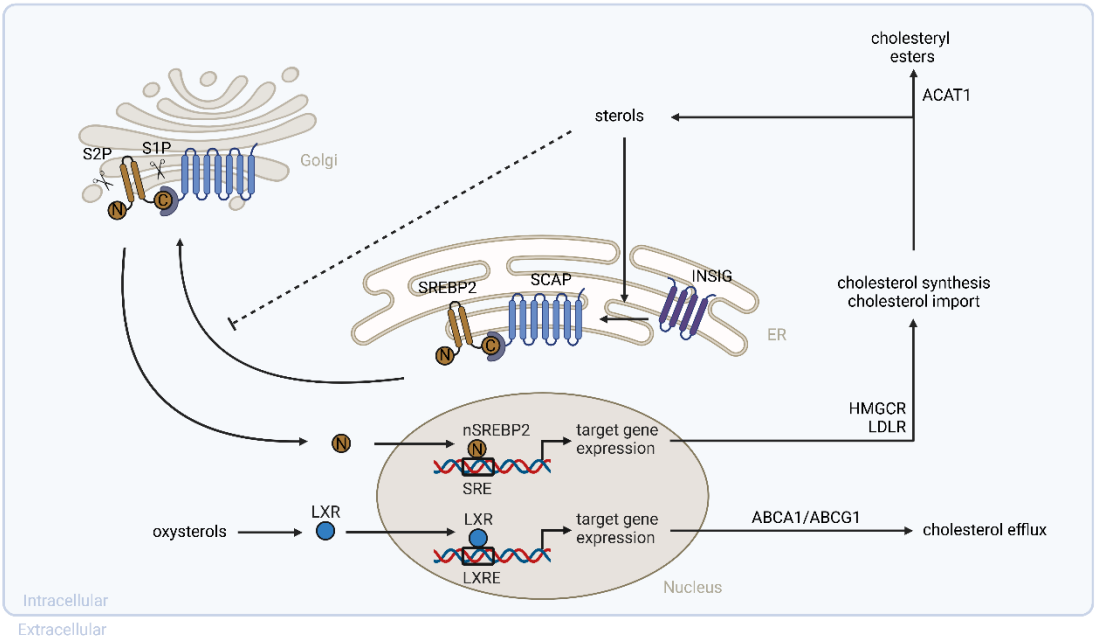

Figure 6: Schematic overview of the transcriptional regulation of cholesterol homeostasis. Cholesterol homeostasis is regulated by the transcription of SREBP2 and LXRs. Depletion of intracellular sterol concentration activates the SREBP2 transcriptional pathway and increases *de novo* cholesterol biosynthesis and cholesterol import. Excessive cholesterol accumulation inhibits SREBP2-processing and activates LXRs, resulting in increased cholesterol efflux. Figure generated with BioRender.

1.3.2 *De novo* cholesterol synthesis

Cholesterol biosynthesis starts with acetyl-CoA, which consists of an acetic acid residue bound to coenzyme A. It is also used for the synthesis of fatty acids and for energy production in the citrate cycle. The first insights into the cholesterol biosynthetic pathway were gained by Lynen and Bloch, who were awarded the Nobel Prize for their discoveries [113, 114]. The initial stage of the mevalonate pathway involves the addition of two acetyl-CoA molecules. Another acetyl-CoA is transferred by 3-hydroxy-3-methylglutaryl-CoA synthase (HMGCS) to form HMG-CoA. The next reaction is the rate-determining step for the entire metabolic pathway, namely the reduction of the thioester group by HMGCR. Now mevalonate is formed, which is phosphorylated twice by mevalonate kinases (MVK) to mevalonate pyrophosphate.

Subsequent decarboxylation produces the isoprenoid structures, isopentenyl pyrophosphate (IPP) and dimethylallyl pyrophosphate (DMAPP), which in turn are in equilibrium with each other via IPP isomerase. The first isoprenoid structures are then bound by the prenyl transferase farnesyl pyrophosphate synthase (FDPS) to create farnesyl pyrophosphate (FPP) via geranyl diphosphate (GPP) [115]. FPP can be used to prenylate proteins and to produce dolichol, heme A, and ubiquinones. In the isoprenylation pathway, FPP can be converted into geranylgeranyl pyrophosphate (GGPP), which is used to isoprenylate small guanosine triphosphate hydrolases (GTPases) like Ras and Rho. These GTPases play a critical role in regulating processes such as proliferation, apoptosis, and signal transduction (reviewed by [116]). Most of the FPP is condensed with two molecules to squalene under the catalysis of squalene synthase (SQS, encoded by the *FDFT1* gene). Oxidation by squalene epoxidase (SQLE) converts squalene to squalene epoxide, and a cyclization reaction produces lanosterol, the first steroid skeleton. This is finally converted to cholesterol by further enzymatic reactions [115] (**Figure 7**).

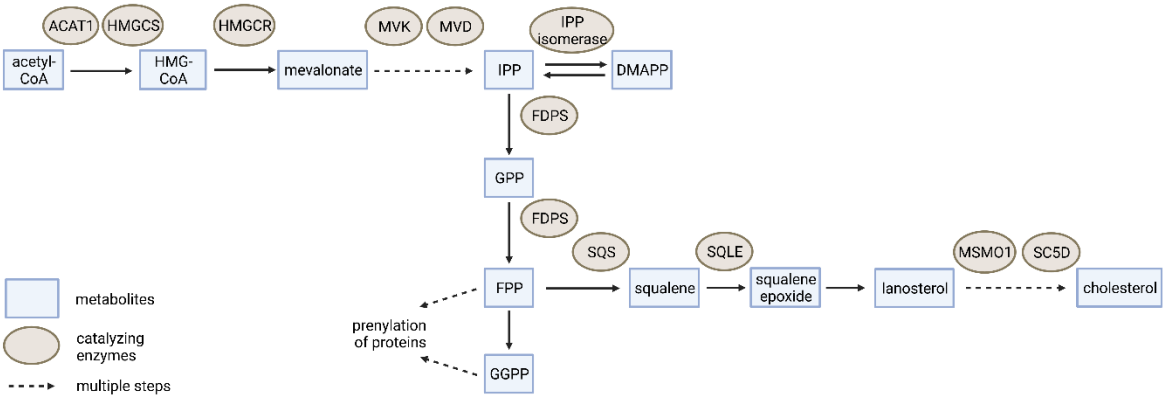

Figure 7: Simplified representation of *de novo* cholesterol synthesis with selected metabolites and enzymes.

Cholesterol biosynthesis from acetyl-CoA to cholesterol with cholesterol synthesis metabolites and catalyzing enzymes. Figure generated with BioRender.

1.3.3 Cholesterol shuffle

In addition to cholesterol synthesis, mammalian cells are also able to take up cholesterol from the extracellular space. This occurs in the form of low-density lipoproteins (LDLs), and receptor-mediated uptake of cholesterol was previously investigated by Goldstein and Brown [117]. Binding of extracellular ligands is followed by receptor-mediated endocytosis of LDL via the LDLR, invagination of the plasma membrane into the cell interior, and constriction of clathrin-coated pits [118]. The clathrin molecules are recycled back to the cell surface along with the receptor. The remaining vesicles containing LDL particles mature into lysosomes, where proteolytic degradation of apoliprotein B-100 takes place. The resulting cholesterol esters are hydrolyzed to cholesterol, which is now used for the synthesis of plasma

membranes, steroid hormones, and bile acids. However, it can be esterified by ACAT1 and stored intracellularly (reviewed by [103]). In the case of intracellular cholesterol excess, unesterified cholesterol and phospholipids are secreted from the cell by the cell membrane-bound transporters ABCA1 and ABCG1 and converted to high-density lipoprotein (HDL) ([119, 120] reviewed by [121, 122]) (**Figure 8**).

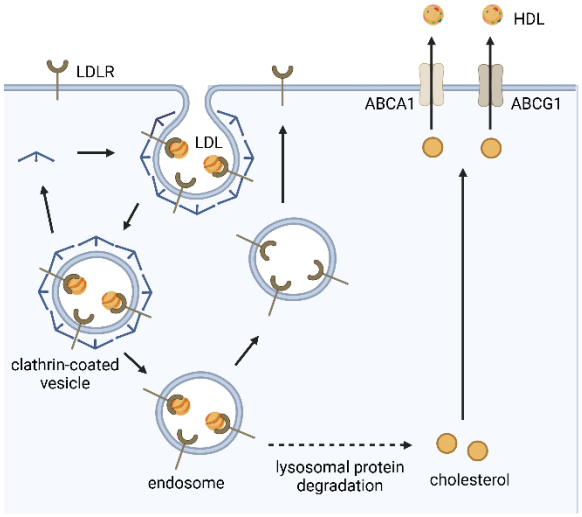

Figure 8: Schematic overview of cholesterol import and efflux.
LDL is internalized via receptor-mediated endocytosis by the LDLR. ABC transporters (ABCA1, ABCG1) ensure the efflux of intracellular free cholesterol and phospholipids across the plasma membrane to bind with apolipoproteins to form HDL particles. Figure generated with BioRender.

1.3.4 Cholesterol metabolism in normal hematopoiesis

The self-renewal potential and differentiation properties of HSPCs suggest that cholesterol as a single metabolite and cholesterol pathway may play a pivotal role in human hematopoiesis. In this regard, studies have indicated a correlation between plasma cholesterol levels and the mobilization of HSPCs in the peripheral blood of mice [123]. Comparable results have been obtained in patients, showing a positive correlation between hypercholesterolemia and the number of CD34+ HSPCs. In addition, the experiments showed an activated IL-17/G-CSF axis outgoing for mobilized HSPCs and their proliferation [124, 125]. Hypercholesterolemia was also shown to affect lymphocytosis and thrombocytosis [123]. These results may be important in deciding whether patients with hypercholesterolemia should discontinue cholesterol-lowering statin therapy during the mobilization period of HSPCs for hematopoietic cell transplantation.

Another focus of stem cell research is the interplay between cholesterol efflux transporters and HSPC proliferation. It has been shown that ABCA1- and ABCG1-deficient mice (*Abca1*$^{-/-}$ *Abcg1*$^{-/-}$) express increased amounts of HSPCs in the BM as well as in peripheral blood, liver, and spleen. Again, stem cell mobilization was associated with IL17/G-CSF signaling leading to an increased cell cycle with respect to synthesis and G2/M phase [126, 127].

1.3.5 Cholesterol metabolism in cancer

Because cancer cells are highly proliferative, they require relatively high levels of cholesterol for their growth. It is therefore not surprising that metabolic reprogramming is considered as a

hallmark of cancer [128]. Accumulating evidence suggests that a variety of malignant cells change their metabolic properties to achieve uncontrolled growth, tumorigenesis, and progression. Cancer cells can maintain high cholesterol requirements through various mechanisms, including a dysregulated transcriptional feedback, increased *de novo* synthesis, or deficient and deregulated uptake, efflux, and esterification.

On the one hand, the role of systemic hypercholesterolemia in the risk of various cancers has been investigated. There are studies showing that an elevated serum cholesterol level is positively correlated with prostate cancer recurrence only in men with dyslipidemia, whereas there was no strong association between serum cholesterol and the risk of cancer recurrence in the entire population ([129], reviewed by [96]). Others have even reported an increased number of NK cells in mice with high serum cholesterol, showing anti-tumor and growth-inhibitory properties against liver tumors [130]. Furthermore, a summarizing review of over 2000 reports and 41 studies found no clear association between serum cholesterol levels and different types of cancer (reviewed by [131]). However, a follow-up study found that high total cholesterol was positively associated with prostate, colon, and breast cancer [132]. It turns out that there are very controversial results on whether high serum cholesterol is associated with cancer growth. In this regard, it may be of decisive advantage to define specific cancer subtypes that would benefit from cholesterol lowering therapy. For example, the cholesterol metabolite 27-hydroxycholesterol (27HC) has not been associated with an increased risk of breast cancer in general, but elevated levels of 27HC have been shown to promote the growth of estrogen receptor-positive (ER+) breast cancer cells [133, 134].
Interestingly, cancer burden may be more influenced by intracellular cholesterol levels than by systemic serum cholesterol levels [135]. However, there exist very different data on this; in research on hematological diseases alone, there is a disagreement as to whether intracellular cholesterol levels in leukemia cells are measurably higher or lower than in healthy cells. On the one hand, there are data indicating that intracellular cholesterol levels are higher in leukemia cells than in healthy peripheral blood mononuclear cells (PBMCs) [136]. However, there are also research articles that have found the opposite [137]. It is understandable that tumor cells, which depend on high amounts of cholesterol, would also have elevated intracellular cholesterol levels. However, since the entire metabolic pathway is highly regulated, it is also not surprising that cancer cells, for their part, have developed mechanisms to inhibit the feedback loop. Of course, there is a need for more cholesterol due to an increased proliferation potential, but on the other hand, the measurable level of intracellular cholesterol must still be kept low enough so that the underlying feedback mechanism does not end up inhibiting intracellular *de novo* cholesterol synthesis. This would explain both the high and low levels of intracellular cholesterol in cancer cells.

The question of whether cancer cells have elevated intracellular cholesterol levels compared to healthy cells has not been conclusively answered. However, it is widely accepted that a variety of malignant cells have an increased consumption and therefore a higher demand for cholesterol is widely accepted. Under physiological conditions, the cholesterol efflux transporter ABCA1 protects cells against damage mediated by accumulated cholesterol in the mitochondria (reviewed by [121]). ABCA1 is also thought to regulate intracellular cholesterol levels in cancer cells and thereby indirectly influencing proliferation and metastasis. Interestingly, as shown by the results of a comparative study, the receptor was highly expressed in normal breast epithelium, while breast cancer cell lines showed ABCA1 differentially expressed. Here, the expression was associated with positive lymph nodes, but not significantly associated with tumor recurrence [138]. Results from others showed a loss of ABCA1-mediated cholesterol export and thus an accumulation of intracellular cholesterol in colon cancer cells. This in turn promoted cancer cell survival and proliferation [139]. There are other data describing ABCA1 as a tumor suppressor, for example in ovarian, skin, and ER+ breast cancer. Experiments with LXR antagonists, among others, increased ABCA1 expression and induced inhibition of tumor cell proliferation and progression [140-142]. In contrast, a strong association between high expression of ABCA1 and the development of other types of human cancers has also been demonstrated. Regarding the observed differential expression in breast cancer cells [138], the results in triple-negative breast cancer (TNBC) tissues suggest that ABCA1 expression is higher compared to healthy tissues [143]. The oncogenic potential of the receptor has also been demonstrated in melanoma and AML cells, where silencing of ABCA1 resulted in increased apoptosis and sensitivity to chemotherapy [144, 145]. However, the underlying mechanism remains controversial and has not been conclusively elucidated.

There is growing evidence that several cancer cells including lymphoma, leukemia, and breast cancer are dependent on exogenous cholesterol supply. This dependence is sometimes more or less pronounced, but these studies highlight the importance of the LDLR in promoting cholesterol-induced tumor growth [146-148]. On the other hand, results from patient samples with aggressive prostate cancer have shown that the more pronounced the cholesterol synthesis, the less dependent the tumors are on LDLR-mediated cholesterol uptake [149].

Regarding to intratumoral cholesterol synthesis, the available studies show a more consistent conclusion. Alterations in cholesterol biosynthesis are strongly associated with tumorigenesis in a large number of tumors, both *in vitro* and *in vivo* (reviewed by [96]). Elevated intracellular cholesterol levels are considered to be more important than elevated systemic cholesterol levels and data also suggest that increased cholesterol synthesis in tumor cells is associated with worse patient prognosis ([150], reviewed by [151]). The alterations may occur at different levels of cholesterol metabolism, for example by upregulation of HMGCR, SQS, or SQLE.

Since most cholesterol biosynthetic genes are regulated by transcription factors, particularly SREBP2, it is not surprising that SREBP2 has become another focus of tumor research. Numerous *in vitro*, *in vivo*, and patient data suggest an increased activity of SREBP2, including prostate cancer [152, 153], breast cancer [135, 154], and hepatocellular carcinoma [155]. Thus, SREBP2, as a master regulator of the entire metabolic pathway, plays a significant role in tumor growth and metastasis. Interestingly, the transcriptional activity of SREBP2 can in turn be regulated in by various signals in oncogenic signaling. Maturation of SREBP2 is altered by p53 status, and mutant p53, known to have tumor-promoting properties in many cancers, interacts with SREBP2 in the promoter region of sterol pathway genes and stimulates their expression [135, 156]. In addition, SREBP2 can regulate c-Myc activation by binding to the 5'-flanking promoter region, thereby inducing stemness, cancer cell growth, and metastasis [153, 157]. In turn, SREBP2 expression can be regulated by the histone acetyltransferase CBP/p300, which acetylates the functional N-terminus of SREBP2 and epigenetically writes an active histone H3K27ac modification [158]. Recent studies have also found that p300 is an activator of RORγ. Inhibition of RORγ decreased p300 and H3K27ac labeling in the promoter region of cholesterol biosynthesis genes, leading to the conclusion that RORγ mediates the transcriptional activity of SREBP2 by recruiting p300 ([159], reviewed by [160]). Since the interaction of SREBP2 with other regulatory proteins is more pronounced in intracellular tumor metabolism than in healthy cells, this has become a promising target for innovative therapeutic strategies.

1.3.6 Targeting cholesterol metabolism as therapeutic approach for leukemia

Statins

Regulation of the cholesterol pathway at multiple levels also provides many opportunities for pharmacological inhibition of cellular metabolism. The most common pharmacological inhibitors of *de novo* cholesterol synthesis are statins, which are approved for the treatment of hypercholesterolemia. By competitively binding to the catalytic domain of HMGCR, statins induce a decrease in intracellular cholesterol levels. This leads to a compensatory increase in LDLR synthesis in hepatocytes, resulting in LDL uptake into the cell, which in turn lowers serum cholesterol levels to prevent cardiovascular disease [161, 162]. Statins can be classified based on their molecular structure. Some statins are derived from fungal fermentation (lovastatin, simvastatin, pravastatin, mevastatin) or occur synthetically (atorvastatin, cerivastatin, fluvastatin, pitavastatin, rosuvastatin). The latter have a fluorophenyl group that gives them the ability to form an additional linkage to the HMGCR. Furthermore, the efficacy of these drugs is strongly influenced by their physicochemical properties. Hydrophilic statins (pravastatin, rosuvastatin) require speciific membrane transporters, whereas lipophilic statins (lovastatin,

simvastatin, atorvastatin, fluvastatin) can cross cell membranes by diffusion ([162], reviewed by [163-165]).

Statins as anti-cancer drugs

With the recognition of HMGCR as a potential oncogene and the possibility of successful inhibition, statins have also gained importance as potential anti-cancer drugs. Aberrant cholesterol metabolism has been implicated as a major contributor to the progression of many types of cancer, making it a potential therapeutic target in cancer therapy. The first anti-cancer trial with lovastatin administration was performed in 1996 [166], followed by a massive interest in its potential to reduce cancer risk. Anti-proliferative effects were observed *in vitro* in various cholesterol-dependent cancer cells, and various statins induced growth inhibitory effects in solid tumors, such as breast cancer, glioblastoma and medulloblastoma brain tumors, colorectal, lung and liver cancer, adenocarcinoma and thyroid cancer (reviewed by [167]). The potential beneficial effects of statin treatment have also been investigated in preclinical studies in hematologic malignancies, including multiple myeloma [168, 169], AML [168, 170-173], ALL [174, 175], CLL [170, 176, 177], and CML [178, 179]. In addition to the knowledge that HMGCR directly promotes cancer transformation [169], there is evidence that cholesterol levels are abnormally high in AML cells which have been exposed to chemotherapy [173, 180]. This has led to the idea that elevated cholesterol levels may serve to protect leukemia cells and that statins may serve as chemotherapy sensitizers when used in combinatorial treatment regimen. *In vitro* studies have shown that the addition of simvastatin and lovastatin sensitizes primary AML cells to chemotherapeutic agents by blocking the increased cholesterol responses [171, 173]. This led to the development of two clinical trials investigating the potential beneficial effects of statins. Kornblau *et al.* reported encouraging results in a phase I study in relapsed AML treated with pravastatin in combination with idarubicin and cytarabine. Clinical responses were observed in eleven of 15 patients and were associated with acceptable toxicity at the statin doses of 40-1680 mg/day for a maximum of eight days [181]. In the subsequent phase II study SWOG0919, Advani *et al.* observed a response rate of 75% in the favorable AML risk group, and a lower response rate (30%) in poor-risk AML patients [182, 183]. Nevertheless, the study was limited by a small patient cohort, an uncontrolled design, and lack of subgroup definition. Randomized phase III trials in AML patients are needed to make a valid statement about the efficacy of pravastatin in combination with existing chemotherapy. These trials would also benefit from the evaluation of other statins with more potent properties and adapted dosing regimens.

Limitations of statin use

Clinical trials investigating the use of statins for the treatment of solid cancers were unsuccessful due to the increased cholesterol metabolism that occurred as a result of the

negative feedback in response to statin therapy [184, 185]. Research involving multiple myeloma and breast cancer cell lines has revealed varying responses in terms of sensitivity to statin-induced apoptosis. The lack of response in insensitive cells was shown to be linked to the inhibition of HMGCR by statins, which initiates a strong homeostatic feedback loop, including the activation of SREBP2. This negative feedback mechanism resulted in an upregulation of mevalonate metabolism, enabling statins to function as cholesterol-lowering agents. Interestingly, statin-sensitive cells did not show the anticipated feedback regarding mevalonate metabolism [162, 169, 186]. With this background, it is not surprising that the efficacy of a statin treatment may be less effective in some cancers. Furthermore, the cytotoxic anti-cancer effects of statins require higher doses of the drug, which can lead to significant side effects. To avoid the feedback activation of SREBP2 and to enhance statin efficacy, it could be of great advantage to simultaneously inhibit cholesterol synthesis and SREBP2 activation [168]. In addition, there is a particular need to define subgroups of cancer patients who would benefit from specially selected cholesterol-modulating treatments. Laboratory markers of tumor biology should be included in the analysis to better understand the pathways that influence clinical response rate and patient outcome.

Alternative inhibitors of cholesterol pathway

For targeting cholesterol synthesis, statins are not the only pharmacological way to inhibit certain cholesterol-related enzymes. Zaragozic acid, a pharmacological inhibitor of SQS, has also been shown to induce anti-tumor effects in AML cells when combined with radiochemotherapy [173]. In addition, the lipid-lowering drug fenofibrate, a PPARα agonist, increased the expression of PPARα, LXRα, and ABCA1, resulting in decreased intracellular cholesterol levels and increased anti-proliferative capacity of non-small cell lung cancer cells [187]. Cholesteryl esters have been shown to enhance the proliferation of glioblastoma cell lines, which could be reduced by avasimibe, an inhibitor of ACAT1, via disruption of cholesteryl ester synthesis [188]. Regulation of the cholesterol pathway by SREBP2 has also been shown to play a significant role in tumor growth, providing another target for manipulation of tumor metabolism. Although direct inhibition of transcription factors is challenging, there are several drugs (fatostatin, betulin, PF-429242) that inhibit SREBP activation by disrupting the translocation from the ER to the Golgi [189]. Fatostatin (FS) displayed anti-tumor activity in prostate cancer, endometrial xenograft mice, and human endometrial cancer cells [190-192]; however, efficacy was limited by toxic effects on control cells [190]. Furthermore, dipyridamole was found to have similar SREBP2 inhibitory activity and, in combination with statins, synergistically induced apoptosis in leukemic cells [168]. Another focus was investigated by Cai *et al.* showing that Retinoid-related orphan receptor gamma (RORγ) selective antagonists decreased the rate of cholesterol synthesis in TNBC cells. In this regard, RORγ shows an

overriding role in SREBP2-mediated cholesterol metabolism and its inhibition caused synergistic anti-tumor effects when combined with statins [159].

1.4 Nuclear receptor RORγ

1.4.1 Retinoid-related orphan receptors

Retinoid-related orphan receptors (RORs) describe a subfamily of nuclear receptors (NRs) and are encoded by different genes, including RORα (*NR1F1* or *RORA*), RORβ (*NR1F2* or *RORB*), and RORγ (*NR1F3* or *RORC*). The alternative use of the promoter and splicing of exons result in the formation of different isoforms of each ROR gene. The most studied RORs are RORγ1/RORγ and its isoform RORγ2/RORγt, which differ by 100 nucleotides at the N-terminus and show a distinct pattern of tissue-specific expression. While RORγ is widely expressed in muscle tissue, prostate, pancreas, heart, liver, and testis, RORγt is exclusively found in lymphatic tissues. Both isoforms differ in their exon structure: exons 1γ and 2γ give rise to RORγ and a single exon 1γt produces the immune-specific isoform RORγt (reviewed by [193]) (**Figure 9A**). In particular, RORγt has been investigated in several studies as a critical regulator of Th17 cell differentiation with connection to inflammatory and autoimmune diseases [194, 195]. RORγ has been shown to play a key role in gluconeogenesis, insulin sensitivity, and lipid/sterol metabolism (reviewed by [193]). All RORs share a typical nuclear receptor domain structure including an N-terminal domain, a DNA-binding domain (DBD), a hinge domain, and a C-terminal ligand-binding domain (LBD) (**Figure 9B**). By binding to specific DNA response elements (ROREs) in the regulatory region of target genes, RORs are involved in the regulation of gene transcription. As a result, RORs influence various physiological processes, including neuronal cell development, immune cell differentiation, circadian rhythms, and cancer development. Binding of ligands leads to conformational changes of the receptor and recruitment of other co-regulatory proteins, resulting in transcriptional activity of the NRs (reviewed by [196]).

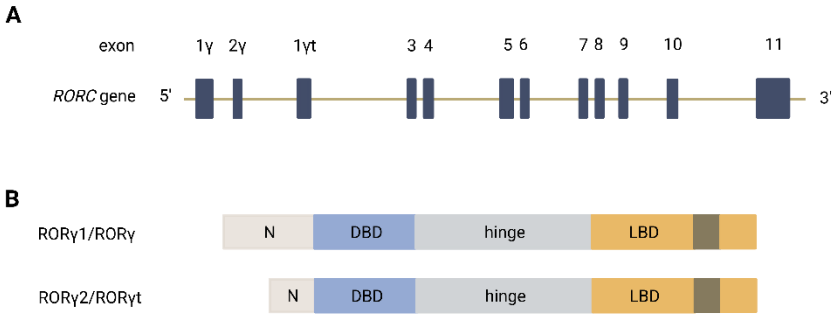

Figure 9: Overview of RORγ and RORγt.

(A) Schematic representation of the *RORC* gene with its eleven exons. Exon 1γ and 2γ produce RORγ and a unique exon 1γt produces the immune-specific isoform RORγt. **(B)** Structure of NRs. RORγ differs

from RORγt with 100 nucleotides at the N-terminus. Adapted from Rutz *et al.* [196]. Figure generated with BioRender.

1.4.2 Function of RORγ in cancer – connection to cholesterol metabolism

In the recent years, intermediates and metabolites of cholesterol metabolism have been suggested to serve as endogenous ligands. In this context, the transcriptional activity of RORγ is dependent on and modified by the cholesterol biosynthesis pathway. On the one hand, endogenous sterol metabolites acting as RORγ agonists control Th17 cell differentiation and can be reduced by statin treatment ([197], reviewed by [96]). Furthermore, in 2016, Wang and colleagues demonstrated a dependence of metastatic castration-resistant prostate cancer (mCRPC) cells on RORγ expression. Here, RORγ was found to be a key regulator of androgen receptor signaling by directly binding to a RORE in the first exon of the androgen receptor gene. Chromatin binding could be successfully decreased by *RORC* gene knockdown (kd) and antagonist treatment [198]. Cai *et al.* revealed that RORγ affects TNBC cell growth through the control of the cholesterol biosynthesis program. The underlying mechanism by which RORγ is able to activate almost the entire cholesterol biosynthesis program has been shown by an interaction of RORγ with SREBP2, where RORγ facilitates the recruitment of SREBP2 to its chromatin target. RORγ mediates transcriptional activation of the cholesterol gene program through recruitment of CBP/p300 in this cancer subtype [159]. Further studies using this approach have observed a unique function of RORγ acting as a repressor to silence LXR genes in mCRPC. In fact, that LXRs play a tumor-suppressive role in prostate cancer this is quite interesting because in this way RORγ modulates not only cholesterol synthesis but also cholesterol efflux to support tumor growth [199]. In contrast to SREBP2, which is expressed in most of healthy and malignant cells, the function of RORγ seems to be restricted to certain cancer types [159, 199]. This has been shown in studies of pancreatic and ER+ breast cancer, where RORγ did not play a significant role in the cholesterol biosynthesis program of healthy cells [159, 200].

1.4.3 Inhibition of RORγ function

The LBD of RORγ/RORγt intrinsically binds small molecules with excellent affinity and selectivity. Because dysfunctions in NRs can lead to various proliferative, metabolic, and inflammatory diseases, the development of synthetic drug targets is of particular research interest. Therefore, the RORγ-specific antagonists SR2211 and GSK805 have been evaluated for the treatment in suppressing Th17-mediated autoimmune diseases [194, 195]. Through structure-based optimization by combining both small molecule structures, Wang *et al.* developed a new compound, named XY018, to selectively inhibit RORγ activity. XY018 can bind to the hydrophobic RORγ LBD through conserved hydrogen bonds and hydrophobic interactions, forming a highly stable complex [198]. XY018 was shown to inhibit tumor cell

growth of both TNBC and mCRPC cells with tissue and genetic selectivity [159, 198, 199, 201]. Interestingly, inhibition of RORγ has been shown to have synergistic cell-killing effects when used in combination with statins [159, 199]. Considering that RORγ may act as an upstream regulator of SREBP2, therapeutic targeting of RORγ may result in a cancer subtype-specific response and better safety than inhibitors targeting SREBP2 or cholesterol synthesis enzymes, which play essential roles in both normal and malignant cells (reviewed by [160]). Nevertheless, future investigations are needed to define other cancer-specific subgroups and effective treatment strategies.

1.5 Aim of the work

The first aim of this study is to evaluate whether and to what extend there is a dysregulation of cholesterol metabolism in leukemic cells. For this purpose, public databases, primary patient samples, cell models and cell lines with a chromosomal translocation of the *KMT2A*r gene will be used.

Subsequently, the extent to which the metabolism differs from that of healthy cells or influences the functional properties of *t(4;11)* leukemia cells will be investigated. The identification of target structures that differ from healthy stem cells should provide a basis for the approach of targeted inhibition of subsequent signaling pathways. Finally, a possible implementation and integration into existing therapeutic regimens of *t(4;11)* leukemia patients will be investigated.

Partial results of this work were published under the title “The RORɣ/SREBP2 pathway is a master regulator of cholesterol metabolism and serves as potential therapeutic target in *t(4;11)* leukemia” at *Oncogene* [202].

2 Materials

2.1 Primary cells, cell lines, bacteria

Table 1: List of primary cells and cell lines.

Name	Characteristics and genetics	Origin
CBMCs	primary cells	huCB from healthy volunteers
PBMCs	primary cells	peripheral blood from healthy volunteers
CRISPR/ Cas9 *t(4;11)*	primary cells, CRISPR/Cas9-generated 46<2n>XY or 46<2n>X? *t(4;11)(q21;q23)*	CD34+ HSPCs from huCB
SKM-1	cell line, myelomonocytic leukemia in myelodysplastic syndrome, AML 43(38-43)<2n>XY, +1, -12, -14, -20, -21, t(1;19)(q21;q13), del(2)(p11), del(9)(q12), add(17)(p1?) - sideline with idem, der(10)t(10;?21)(p11;q11), -21	ATCC, Manassas, Virginia, United States
SEM	cell line, B cell precursor leukemia, ALL 45(40-46)<2n>XX, -13, t(4;11)(q21;q23), del(7)(p14) *t(4;11)(q21;q23)*	ATCC, Manassas, Virginia, United States
RS4;11	cell line, B cell precursor leukemia, ALL 47/48<2n>X/XX, +8, +18, t(4;11)(q21;q23), i(7q) - sideline with +8/18 *t(4;11)(q21;q23)*	ATCC, Manassas, Virginia, United States
HEK293T	cell line, Human embryonic kidney expressing a mutant version of the SV40 large T antigen	DSMZ, Braunschweig, Germany

Table 2: List of bacteria.

Name	Origin
E.coli DH5α Competent Cells	Thermo Fisher Scientific Inc., Waltham, Massachusetts, United States

2.2 Instruments

Table 3: List of instruments.

Product	Model	Manufacturer
Aspiration system	VACUSAFE	INTEGRA Biosciences AG, Zizers, Switzerland
Autoclav	VX-150	Systec GmbH & Co. KG, Linden, Germany
Biological safety cabinet	HERAsafe KS 12	Heraeus Instruments, Heraeus Holding GmbH, Hanau, Germany
	HERAsafe HS 12	Heraeus Instruments, Heraeus Holding GmbH, Hanau, Germany
	HERAsafe 2030i	Thermo Fisher Scientific Inc., Waltham, Massachusetts, United States
Camera	Axiocam 105 colour	Carl Zeiss AG, Oberkochen, Germany

Centrifuge	Microcentrifuge 5415R	Eppendorf AG, Hamburg, Germany
	Centrifuge 5920R	Eppendorf AG, Hamburg, Germany
	Megafuge 1.0R	Heraeus Instruments, Heraeus Holding GmbH, Hanau, Germany
	Micro Star 17R	VWR International, Radnor, Pennsylvania, United States
	Multifuge X3R	Heraeus Instruments, Heraeus Holding GmbH, Hanau, Germany
Chemical fume hood	Scala 1500	WALDNER Laboreinrichtungen GmbH & Co. KG
Chemiluminescence imaging	Fusion FX	Vilber Lourmat, Eberhardzell, Germany
Counting Chamber	Neubauer improved, Bright line	Karl Hecht GmbH & Co. KG, Sondheim von der Rhön, Germany
Flow cytometer	LSRFortessa	BD Biosciences, Franklin Lakes, New Jersey, United States
Freezing container	Mr. Frosty™	Thermo Fisher Scientific Inc., Waltham, Massachusetts, United States
Gel documentation system	E-BOX VX2	PEQLAB Biotechnology by VWR International GmbH, Radnor, Pennsylvania, United States
Gel electrophoresis system	Perfect Blue Horizontal Midi Gel Systems	PEQLAB Biotechnology by VWR International GmbH, Radnor, Pennsylvania, United States
	Mini-PROTEAN Tetra Vertical Electrophoresis Cell	Bio-Rad Laboratories Inc., Hercules, California, United States
Ice machine	AF 100	Scotsman Ice Systems, Milano, Italy
Incubator	HERAcell 150	Heraeus Instruments, Heraeus Holding GmbH, Hanau, Germany
	Binder C170	BINDER GmbH, Tuttlingen, Germany
	HERAcell Vios 160i	Thermo Fisher Scientific Inc., Waltham, Massachusetts, United States
Incubator shaker	New Brunswick Innova 44	Eppendorf AG, Hamburg, Germany
MACS magnet	MidiMACS separator	Miltenyi Biotec, Bergisch Gladbach, Germany
Microscope	Zeiss Primovert	Carl Zeiss AG, Oberkochen, Germany
	Zeiss Axiovert 25	Carl Zeiss AG, Oberkochen, Germany
Microwave	LG MG-3822G	LG Electronics Inc., Seoul, South Korea
Nitrogen tank	Biosafe 420	Cryotherm GmbH & Co. KG, Kirchen, Germany
Nucleofection system	4D-Nucleofector X Unit	Lonza Group AG, Basel, Switzerland
pH-Meter	MP220	Mettler-Toledo, Columbus, Ohio, United States
Photometer	Nanodrop One	Thermo Fisher Scientific Inc., Waltham, Massachusetts, United States

Pipettes	PIPETBOY acu 2	INTEGRA Biosciences AG, Zizers, Switzerland
Plate reader	Pipette Research plus	Eppendorf AG, Hamburg, Germany
	Transferpette S	BRAND GmbH & & Co. KG, Wertheim, Germany
	Sunrise	Tecan Group AG, Männedorf, Switzerland
Power supply system	Infinite M Plex	Tecan Group AG, Männedorf, Switzerland
	EV2310 / E835	Consort bvba, Turnhout, Belgium
Refrigerator	-80°C Green Line	Skadi Refrigeration Equipment, Ho Nan Rd., Taichung, Taiwan
Scale	-20°C	Liebherr, Kirchdorf an der Iller, Germany
	+4°C	Liebherr, Kirchdorf an der Iller, Germany
	M-prove	Sartorius AG, Göttingen, Germany
Shaker	Rocky	Fröbel Labortechnik, Lindau, Germany
Shaking water bath	Phoenix RS-OS	Phönix Laboratorium GmbH, Bondorf, Germany
	GFL-1083	GFL Gesellschaft für Labortechnik mbH, Burgwedel, Germany
Sonication system	Sonoplus HD 3100	BANDELIN electronic GmbH & Co. KG, Berlin, Germany
Thermocycler	T100 Thermal Cycler	Bio-Rad Laboratories Inc., Hercules, California, United States
	Mastercycler	Eppendorf AG, Hamburg, Germany
	LightCycler 480	Roche Holding AG, Basel, Switzerland
Thermoshaker	TS basic	CellMedia GmbH & Co. KG, Zeitz, Germany
Ultrapure water system	Barnstea GenPure Pro	Thermo Fisher Scientific Inc., Waltham, Massachusetts, United States
UV transilluminator	UST-20M-8E	Carl Roth GmbH & Co. KG, Karlsruhe, Germany
Vortex	D-6012	neoLab Migge GmbH, Heidelberg, Germany

2.3 Software and web tools

Table 4: List of software and web tools.

Product	Manufacturer or Reference
ApE version 3.0.5	Open source software by M. Wayne Davis
BD FACSDiva Software	BD Biosciences, Franklin Lakes, New Jersey, United States
Benchling	Benchling Inc., San Francisco, California, United States
BioRender	BioRender / Science Suite Inc., Toronto, Ontario, Canada
CRISPRscan	Giraldez Lab, Yale University, New Haven, Connecticut, United States

Ensembl genome browser 109	European Bioinformatics Institute, Hixton, United Kingdom
Evolution Capt	Vilber Lourmat, Eberhardzell, Germany
FlowJo 10.7.2	FlowJo, LLC, Ashland, Oregon, United States
GraphPad 9.4.1	GraphPad Software Inc., San Diego, California, United States
ImageStudio Lite V5.2	Li-Cor Biosciences Inc., Lincoln, United States
Infinite M200 Reader	Tecan Group AG, Männedorf, Switzerland
LightCycler480	Roche Holding AG, Basel, Switzerland
Microsoft Office	Microsoft, Redmond, Washington, United States
NCBI Primer BLAST	National Centre for Biotechnology Information, Bethesda, Maryland, United States
PrimerExpress 2.0	Applied Biosystems by Thermo Fisher Scientific Inc., Waltham, Massachusetts, United States
ZEN 3.0 blue edition	Carl Zeiss AG, Oberkochen, Germany

2.4 Buffers and cell culture media

Table 5: List of buffers.

Name	Ingredients
Agarose gel (2%)	2% agarose in 1X TAE buffer
Agarose loading buffer (10X)	66.7% sucrose, 1.6 mM EDTA, 0.16% SDS, 0.08% bromphenol blue in H_2O
Blocking Buffer	5% milk powder in 1X TBS-T
$CaCl_2$	2.5 M $CaCl_2$ in H_2O
Erylysis buffer	155 mM NH_4Cl, 10 mM $KHCO_3$, 0.1 mM EDTA in H_2O, pH 7.3
FACS buffer	2% FBS in PBS
HEPES buffer (2X)	280 mM NaCl, 50 mM HEPES, 1.5 mM Na_2HPO_4 in H_2O, pH 7.05
Laemmli buffer (4X)	250 mM tris-acetate, 25% glycerol, 8% SDS, 400 µg/ml bromphenol blue, 5% 2-mercaptoethanol in H_2O, pH 6.8
MACS buffer	2 mM EDTA, 0.5% FBS in PBS
PEG 8000	50% PEG 8000 in PBS
RIPA buffer	80 mM NaCl, 50 mM tris-acetate, 50 mM NaF, 20 mM $Na_4P_2O_7$, 1 mM EDTA, 1mM EGTA, 1% NP40, 0.5% DOC, 0.1% SDS in H_2O
SDS resolving gel (10%)	2 ml H_2O, 1.65 ml acrylamide (Rotiphorese), 1.25 ml tris-acetate (1.5 M, pH 8.8), 50 µl SDS (10%), 52.2 µl APS (10%), 7.5 µl TEMED
SDS running buffer	25 mM tris-acetate, 192 mM glycine, 0.1% SDS in H_2O
SDS stacking gel (6%)	1.6 ml H_2O, 565 µl acrylamide (Rotiphorese), 875 µl tris-acetate (0.5 M, pH 6.8), 35 µl SDS (10%), 35 µl APS (10%), 3.5 µl TEMED
Sorensen's buffer	0.033 M KH_2PO_4 and 0.063 M Na_2HPO_4 in H_2O

Tris-acetate EDTA (TAE) buffer (50X)	2 M tris-acetate, 50 mM EDTA in H_2O
Tris-buffered saline Tween 20 (TBS-T) (10X)	100 mM tris-acetate, 1.5 M NaCl, 0.5% Tween 20 in H_2O, pH 7.6
Western blot transfer buffer	25 mM tris-acetate, 192 mM glycine, 10% methanol in H_2O

Table 6: List of cell culture media.

Name	Ingredients
Lysogeny broth (LB) agar	2% LB Lennox, 1.5% agar agar, 100 µg/ml ampicillin in H_2O
Freezing medium	RPMI Medium 1640 (1X) 20% FBS, 10% DMSO
HEK293T medium	DMEM (1X) 10% FBS, 1% penicillin/streptomycin
LB medium	2% LB Lennox, 100 µg/ml ampicillin in H_2O
RS4;11 medium	RPMI Medium 1640 (1X) + GlutaMAX-I 10% FBS, 1% penicillin/streptomycin
SEM medium	IMDM (1X) 10% FBS, 1% penicillin/streptomycin
SKM-1 medium	RPMI Medium 1640 (1X) + GlutaMAX-I 15% FBS, 1% penicillin/streptomycin
Stem cell medium (SCM)	StemMACS HSC Expansion Medium XF, human 10% FBS, 1% penicillin/streptomycin 50 ng/ml IL-3, IL-6, SCF, FLT3-L, TPO, G-CSF 0.75 µM SR-1, UM729

2.5 Chemicals, reagents and kits

Table 7: List of chemicals and reagents.

Name	Manufacturer
2-propanol	VWR International, Radnor, Pennsylvania, United States
4-(2-Hydroxyethyl)piperazine-1-ethanesulfonic acid (HEPES)	Merck KGaA, Darmstadt, Germany
Acetic acid 100%	Merck KGaA, Darmstadt, Germany
Acrylamide (Rotiphorese, 37, 5:1)	Carl Roth GmbH & Co. KG, Karlsruhe, Germany
Agar agar	Carl Roth GmbH & Co. KG, Karlsruhe, Germany
AlamarBlue Cell Viability Reagent	Invitrogen by Thermo Fisher Scientific Inc., Waltham, Massachusetts, United States
Ammonium chloride (NH_4Cl)	Sigma-Aldrich, St. Louis, Missouri, United States
Ammonium persulfate (APS)	Sigma-Aldrich, St. Louis, Missouri, United States
Ampicillin	Sigma-Aldrich, St. Louis, Missouri, United States
Ampuwa rinsing solution	Fresenius Kabi, Bad Homburg vor der Höhe, Germany
Aqua resist	VWR International, Radnor, Pennsylvania, United States
ARA-cell (cytarabine)	STADA Arzneimittel AG, Bad Vilbel, Germany
Atorvastatin (ATV)	Selleck Chemicals, Houston, Texas, United States

Bambanker Serum-Free Cell Freezing Medium	Nippon Genetics Europe GmbH, Düren, Germany
Bromphenol blue sodium	Sigma-Aldrich, St. Louis, Missouri, United States
Calcium chloride ($CaCl_2$)	Sigma-Aldrich, St. Louis, Missouri, United States
Cas9 protein with NLS, high concentration	PNA Bio Inc., Thousand Oaks, California, United States
Chloroform	Merck KGaA, Darmstadt, Germany
Cholesterol	Selleck Chemicals, Houston, Texas, United States
Dimethyl sulfoxide (DMSO)	Sigma-Aldrich, St. Louis, Missouri, United States
Disodium hydrogen phosphate (Na_2HPO_4)	Carl Roth GmbH & Co. KG, Karlsruhe, Germany
dNTPs	Thermo Fisher Scientific Inc., Waltham, Massachusetts, United States
Dulbecco´s phosphate buffered saline (PBS, 1X)	Gibco by Thermo Fisher Scientific Inc., Waltham, Massachusetts, United States
Dulbecco′s Modified Eagle′s Medium (DMEM)	Gibco by Thermo Fisher Scientific Inc., Waltham, Massachusetts, United States
Ethanol absolute	VWR International, Radnor, Pennsylvania, United States
Ethylenediaminetetraacetic acid (EDTA)	AppliChem GmbH, Darmstadt, Germany
Ethyleneglycoltetraacetic acid (EGTA)	AppliChem GmbH, Darmstadt, Germany
Fatostatin (FS)	MedChemExpress, Monmouth Junction, New Jersey, United States
FcR blocking reagent, human	Miltenyi Biotec, Bergisch Gladbach, Germany
Foetal bovine serum (FBS), qualified	Gibco by Thermo Fisher Scientific Inc., Waltham, Massachusetts, United States
Formaldehyde solution (4%), buffered, pH 6.9	Merck KGaA, Darmstadt, Germany
Gene Ruler low range DNA ladder	Thermo Fisher Scientific Inc., Waltham, Massachusetts, United States
Geranylgeranyl diphosphate (GGPP)	Sigma-Aldrich, St. Louis, Missouri, United States
Giemsa´s azur eosin methylene blue solution	Merck KGaA, Darmstadt, Germany
Glycerol	Merck KGaA, Darmstadt, Germany
Glycine	AppliChem GmbH, Darmstadt, Germany
Human hematopoietic stem cell expansion cytokine package (SCF, FLT3-L, TPO)	PeproTech Inc., Rocky Hill, New Jersey, United States
Hydrochloric acid (HCl), fuming, 37%	Merck KGaA, Darmstadt, Germany
Iscove′s Modified Dulbecco′s Medium (IMDM)	Gibco by Thermo Fisher Scientific Inc., Waltham, Massachusetts, United States
LB Lennox	Carl Roth GmbH & Co. KG, Karlsruhe, Germany
LiChrosolv water for chromatography (LC-MS grade)	Merck KGaA, Darmstadt, Germany
Magnesium chloride ($MgCl_2$)	Carl Roth GmbH & Co. KG, Karlsruhe, Germany

Maxima Probe qPCR Master Mix (2X), no ROX	Thermo Fisher Scientific Inc., Waltham, Massachusetts, United States
Maxima SYBR Green qPCR Master Mix (2X), no ROX	Thermo Fisher Scientific Inc., Waltham, Massachusetts, United States
May Grünwald´s eosine methylene blue solution, modified	Merck KGaA, Darmstadt, Germany
Methanol	Merck KGaA, Darmstadt, Germany
MIDORI Green Advance DNA stain	Nippon Genetics Europe GmbH, Düren, Germany
Milk powder	AppliChem GmbH, Darmstadt, Germany
Neo-Mount anhydrous mounting medium	Sigma-Aldrich, St. Louis, Missouri, United States
Nuclease-Free Water	Thermo Fisher Scientific Inc., Waltham, Massachusetts, United States
OneComp eBeads	Invitrogen by Thermo Fisher Scientific Inc., Waltham, Massachusetts, United States
PAGE Ruler Plus Prestained Protein Ladder	Thermo Fisher Scientific Inc., Waltham, Massachusetts, United States
Pancoll, human, density 1.077 g/mL	PAN-Biotech GmbH, Aidenbach, Germany
Penicillin/streptomycin, 10.000 U/mL	Gibco by Thermo Fisher Scientific Inc., Waltham, Massachusetts, United States
Polyethylene glycol 8000 (PEG 8000)	AppliChem GmbH, Darmstadt, Germany
Potassium bicarbonate ($KHCO_3$)	Carl Roth GmbH & Co. KG, Karlsruhe, Germany
Potassium dihydrogen phosphate (KH_2PO_4)	Carl Roth GmbH & Co. KG, Karlsruhe, Germany
PrimeSTAR Max polymerase	Takara Bio Inc., Kusatsu, Präfektur Shiga, Japan
Puromycin dihydrochloride	Sigma-Aldrich, St. Louis, Missouri, United States
Random hexamer primer	Thermo Fisher Scientific Inc., Waltham, Massachusetts, United States
Recombinant human G-CSF (Granocyte 34, Lenograstim, 34 x 106 I.U./mL)	Chugai Pharma Germany GmbH, Frankfurt/Main, Germany
Recombinant human IL-3	PeproTech Inc., Rocky Hill, New Jersey, United States
Recombinant human IL-6	PeproTech Inc., Rocky Hill, New Jersey, United States
RevertAid H Minus reverse transcriptase	Thermo Fisher Scientific Inc., Waltham, Massachusetts, United States
RiboLock RNase inhibitor	Thermo Fisher Scientific Inc., Waltham, Massachusetts, United States
RNaseZAP	Sigma-Aldrich, St. Louis, Missouri, United States
Roswell Park Memorial Institute (RPMI) Medium 1640 (1X) + GlutaMAX-I	Gibco by Thermo Fisher Scientific Inc., Waltham, Massachusetts, United States
SeaKem LE agarose	Lonza Group AG, Basel, Switzerland
Sodium acetate anhydrous	Merck KGaA, Darmstadt, Germany
Sodium chloride (NaCl)	Merck KGaA, Darmstadt, Germany

Sodium deoxycholate (DOC)	Sigma-Aldrich, St. Louis, Missouri, United States
Sodium diphosphate ($Na_4P_2O_7$)	Sigma-Aldrich, St. Louis, Missouri, United States
Sodium dodecyl sulfate (SDS)	AppliChem GmbH, Darmstadt, Germany
Sodium fluoride (NaF)	Merck KGaA, Darmstadt, Germany
StemMACS HSC Expansion Medium XF, human	Miltenyi Biotec, Bergisch Gladbach, Germany
StemRegenin 1 (SR-1)	STEMCELL Technologies Inc., Vancouver, Canada
Sucrose	Sigma-Aldrich, St. Louis, Missouri, United States
Tetramethylethylenediamine (TEMED)	AppliChem GmbH, Darmstadt, Germany
Tris-acetate	Sigma-Aldrich, St. Louis, Missouri, United States
Trypan blue solution (0.4%)	Sigma-Aldrich, St. Louis, Missouri, United States
Tween 20	AppliChem GmbH, Darmstadt, Germany
UM-729	STEMCELL Technologies Inc., Vancouver, Canada
NP40	Sigma-Aldrich, St. Louis, Missouri, United States
XY018	Tocris Bioscience, Bristol, United Kingdom
Z-VAD-FMK, pan caspase inhibitor	Adooq Bioscience LLC, Irvine, California, United States
ZytoLight SPEC *KMT2A* Dual Color Break Apart Probe	ZytoVision GmbH, Bremerhaven, Germany
2-mercaptoethanol	Sigma-Aldrich, St. Louis, Missouri, United States

Table 8: List of kits.

Name	Manufacturer
Amplex Red Hydrogen Peroxide/Peroxidase Assay Kit	Invitrogen by Thermo Fisher Scientific Inc., Waltham, Massachusetts, United States
Annexin V-FITC Kit	Miltenyi Biotec, Bergisch Gladbach, Germany
BD Pharmingen FITC BrdU Flow Kit	BD Biosciences, Franklin Lakes, New Jersey, United States
CD34 MicroBead Kit UltraPure, human	Miltenyi Biotec, Bergisch Gladbach, Germany
Cytochrome c releasing apoptosis Kit	Enzo Life Sciences Inc. by Enzo Biochem Inc., Farmingdale, New York, United States
DC Protein Assay Kit	Bio-Rad Laboratories Inc., Hercules, California, United States
eBioscience Foxp3 / Transcription Factor Staining Buffer Set	Invitrogen by Thermo Fisher Scientific Inc., Waltham, Massachusetts, United States
HiScribe T7 High Yield RNA Synthesis Kit	New England Biolabs, Ipswich, Massachusetts, United States
KAPA HIFI HotStart ReadyMix PCR Kit	Roche Holding AG, Basel, Switzerland
NextSeq 500 High Output Kit v2.5 75 Cycles	Illumina, San Diego, California, United States
NucleoBondTM Xtra Midi Plus EF Kit	MACHEREY-NAGEL, Düren, Germany

NucleoSpin DNA RapidLyse Kit	MACHEREY-NAGEL, Düren, Germany
NucleoSpin Gel and PCR Clean-up Kit	MACHEREY-NAGEL, Düren, Germany
NucleoSpin RNA Kit	MACHEREY-NAGEL, Düren, Germany
P3 Primary Cell 4D-Nucleofector Kit	Lonza Group AG, Basel, Switzerland
Pierce ECL Western Blotting Substrate Kit	Thermo Fisher Scientific Inc., Waltham, Massachusetts, United States
QuantSeq 3' mRNA-Seq Library Prep Kit FWD	Lexogen GmbH, Vienna, Austria
TruSeq RNA Library Prep Kit v2	Illumina, San Diego, California, United States
TruSeq Stranded Total RNA Kit	Illumina, San Diego, California, United States
RNA Clean and Concentrator-25 Kit	Zymo Research, Irvine, California, United States
ZytoLight FISH-Cytology Implementation Kit	ZytoVision GmbH, Bremerhaven, Germany

2.6 Disposables

Table 9: List of disposables.

Name	Specification	Manufacturer
Bacteria petri dishes	100/20 mm	Greiner Bio-One GmbH, Frickenhausen, Germany
Cell culture dishes	100/20 mm, tissue culture treated	Sarstedt AG & Co. KG, Nümbrecht, Germany Greiner Bio-One GmbH, Frickenhausen, Germany
Cell culture flasks, sterile	25 cm2, tissue culture treated 75 cm2, tissue culture treated	Corning Inc., Corning, New York, United States
Cell culture plates, sterile	24-well, flat bottom 48-well, flat bottom 96-well, flat bottom 96-well U bottom	Corning Inc., Corning, New York, United States
Combi tips	5 ml	Eppendorf AG, Hamburg, Germany
Counting chamber	C-Chip Neubauer improved	Carl Roth GmbH & Co. KG, Karlsruhe, Germany
Cover glasses	20 x 23 x 0.44 mm 24 x 60 x 0.13-0.16 mm	neoLab Migge GmbH, Heidelberg, Germany R. Langenbrinck GmbH, Emmendingen, Germany
Cryo vials, PP with screw cap, sterile	2 ml	Greiner Bio-One GmbH, Frickenhausen, Germany
Disposable bags		BRAND GmbH & Co. KG, Wertheim, Germany

Filter	0.2 µm, 0.45 µm	Sarstedt AG & Co. KG, Nümbrecht, Germany
Filter cards Shandon		Thermo Fisher Scientific Inc., Waltham, Massachusetts, United States
Filter tips	10 µl, 100 µl, 200 µl, 1250 µl	STARLAB International GmbH, Hamburg, Germany nerbe plus GmbH & Co. KG, Winsen (Luhe), Germany Biozym Scientific GmbH, Hessisch Oldendorf, Germany Sarstedt AG & Co. KG, Nümbrecht, Germany
Immobilon-FL PVDF membrane	0.45 µm, 26.5 cm x 3.75 cm	Merck KGaA, Darmstadt, Germany
KIMTECH precision wipes	white	Kimberly-Clark Professional, Roswell, Georgia, United States
MACS columns	LS, MS	Miltenyi Biotec, Bergisch Gladbach, Germany
Microplates	96-well, PS, V-bottom, clear	Greiner Bio-One GmbH, Frickenhausen, Germany
Microplates for LightCycler	96-well, PP	Sarstedt AG & Co. KG, Nümbrecht, Germany
Microscope slides	SuperFrost Plus	R. Langenbrinck GmbH, Emmendingen, Germany
Pasteur capillary pipettes	230 mm	Ulbrich Wilhelm GdbR, Bamberg, Germany
PCR tubes	Multiply Pro Cup 0.2 ml Multiply-µStrip Pro 8-strip	Sarstedt AG & Co. KG, Nümbrecht, Germany
Polypropylene tubes	14 ml	Greiner Bio-One GmbH, Frickenhausen, Germany
Reaction tubes	0.5 ml, 1.5 ml, 2 ml, 5 ml	Eppendorf AG, Hamburg, Germany
Serological pipettes	2 ml, 5 ml, 10 ml, 25 ml, 50 ml	Greiner Bio-One GmbH, Frickenhausen, Germany Corning Inc., Corning, New York, United States
Syringes	2 ml, 5 ml, 20 ml	B. Braun GmbH, Melsungen, Germany
Tubes	15 ml, 50 ml, PP	Greiner Bio-One GmbH, Frickenhausen, Germany
Tubes for flow cytometry	5 ml, PS	Greiner Bio-One GmbH, Frickenhausen, Germany
VIEWSEAL sealer	clear	Greiner Bio-One GmbH, Frickenhausen, Germany
Whatman paper		VWR International, Radnor, Pennsylvania, United States

2.7 Plasmids

Table 10: List of plasmids.

Name	Characteristics or target sequence	Manufacturer
PX458	cloning backbone for sgRNA, Cas9 from S. pyogenes	Addgene Inc., Watertown, United States
pmaxGFP	expression of GFP, positive control for nucleofection efficiency	Lonza Group AG, Basel, Switzerland
psPAX2	2nd generation lentiviral packaging plasmid, empty backbone	Addgene Inc., Watertown, United States
pMD2.G	VSV-G envelope expressing plasmid	Addgene Inc., Watertown, United States
pLKO.1-puro (sh ctrl)	shRNA negative control	Horizon Discovery, Waterbeach, United Kingdom
pLKO.1-TRCN0000020665 (sh1 *SREBF2*)	GCCCTCTATTGGATGATGCAA	Horizon Discovery, Waterbeach, United Kingdom
pLKO.1-TRCN0000020666 (sh2 *SREBF2*)	GCAACAACAGACGGTAATGAT	Horizon Discovery, Waterbeach, United Kingdom
pLKO.1-TRCN0000020668 (sh3 *SREBF2*)	GACCTGAAGATCGAGGACTTT	Horizon Discovery, Waterbeach, United Kingdom

2.8 Primers

Table 11: List of primers used for sgRNA production.

Name	Sequence (5' - 3')
KMT2A fwd	taatacgactcactataGGAGCTCCTTATAGATGAAGgttttagagct agaaATAGC
AFF1 fwd	taatacgactcactataGGCTGCTGTCGATAGTCCTCgttttagagctagaaATAGC
universal rev	AGCACCGACTCGGTGCCACT

Table 12: List of primers used for translocation PCR.

Name	Sequence (5' - 3')
t(4;11) fwd	ATTCCCTGTTTAAACCAGCTAAAGAA
t(4;11) rev	GACATTTTCATCTCAAATCCGTCTTC

Table 13: List of primers used for RT-qPCR.

Name	Sequence (5' - 3')
18s rRNA fwd	CGGCTACCACATCCAAGGAA

18s rRNA rev	GCTGGAATTACCGCGGCT
hu *SREBF2* fwd	CGAATTGAAAGACCTGGTCATG
hu *SREBF2* rev	TCCTCAGAACGCCAGACTTGT
hu *HMGCS1* fwd	ACTTGTGCATTCAAACATAGCAACT
hu *HMGCS1* rev	GCAGGGAGTCTTGGTACTTTCTTG
hu *HMGCR* fwd	GAATGTCTTGTGATTGGAGTTGGTA
hu *HMGCR* rev	CAAAGCAGCACATAATTTCAAGCT
hu *MVK* fwd	TGGTGGCTGTGGCATCAC
hu *MVK* rev	TGGTTTCCAAGCAGTCAAAGC
hu *FDFT1* fwd	GCCAGGTGCTGGAGGACTT
hu *FDFT1* rev	GTATTTCTCAGCCAGATTTCTAAACTC
hu *SQLE* fwd	GCCAGCAAGCTTCCTTCCT
hu *SQLE* rev	GCGTCTCCCAAAAGAAGAACA
hu *MSMO1* fwd	TCATCATGAGTTTCAGGCTCCA
hu *MSMO1* rev	GGATGTGCATATTCAGCTTCCAT
hu *SC5D* fwd	CATGATGACCTAGGAGAGTTTCCA
hu *SC5D* rev	CAGTGAAAAAGAGGAAAGATATTATACTAACG
hu *ABCA1* fwd	CTCCCGGAGTTGTTGGAAAC
hu *ABCA1* rev	CCTCCGAGCATCTGAGAACAG
hu *LDLR* fwd	CACGGTGGAGATAGTGACAATGTC
hu *LDLR* rev	TTTCCTCTGCCAGCAACGT
hu *MEIS1* fwd	TGGCCACACGTCACACAGT
hu *MEIS1* rev	TTTGTCCTTATCAGGGTCATCATC
hu *HOXA9* fwd	ATGAGAGCGGCGGAGACA
hu *HOXA9 rev*	CGCGCATGAAGCCAGTT
hu *HOXA6* fwd	CGGTTTACCCTTGGATGCA
hu *HOXA6 rev*	CCCATGGCTCCCATACACA
hu *MYC* fwd	CCTGGTGCTCCATGAGGAGAC
hu *MYC rev*	CAGACTCTGACCTTTTGCCAGG
hu *PRMT5* fwd	GTGACCCTGAGGCCCAGTTT
hu *PRMT5 rev*	GAAGTTGTGCAGCCGTACCA
hu *CBX5* fwd	GCCGATGACATCAAATCTAAAAAA
hu *CBX5 rev*	CAAAGCCCCGAGCGATATC
hu *MYB* fwd	AAAAACTGAAGAAGCTGGTGGAA
hu *MYB rev*	GCTGGCACTGCACATCTGTT
hu *HMGB3* fwd	CCCTGTCAATTTTGCGGAAT
hu *HMGB3 rev*	GACATCGTCTTCCACCTCTCAGA

2.9 Antibodies

Table 14: List of primary antibodies used for Western blot.

Antigen	Clone	Host	Dilution	Manufacturer	kDa
ABCA1	AB.H10	mouse	1:500	Santa Cruz Biotechnology, Dallas, Texas, United States	220
ACTIN	C-2	mouse	1:500	Santa Cruz Biotechnology, Dallas, Texas, United States	42
cHMGCS	A-6	mouse	1:500	Santa Cruz Biotechnology, Dallas, Texas, United States	65

Cytochrome c	7H8.2C12	mouse	1:200	Enzo Life Sciences Inc. by Enzo Biochem Inc., Farmingdale, New York, United States	12
GAPDH	14C10	rabbit	1:1000	Cell Signaling Technology, Danvers, Massachusetts, United States	37
HMGCR	C-1	mouse	1:500	Santa Cruz Biotechnology, Dallas, Texas, United States	100 & 55
LDLR	polyclonal	rabbit	1:500	ProteinTech Group, Rosemont, Illinois, United States	120
RORγ	AFKJS-9	rat	1:100	Thermo Fisher Scientific Inc., Waltham, Massachusetts, United States	58
SQLE	H-6	mouse	1:500	Santa Cruz Biotechnology, Dallas, Texas, United States	55
SREBP2	polyclonal	rabbit	1:1000	Abcam, Cambridge, United Kingdom	126 & 62
VDAC1	polyclonal	rabbit	1:1000	Abcam, Cambridge, United Kingdom	32

Table 15: List of secondary antibodies used for Western blot.

Antibody	Dilution	Manufacturer
Anti-mouse HRP	1:1000	Cell Signaling Technology, Danvers, Massachusetts, United States
Anti-rabbit HRP	1:1000	Cell Signaling Technology, Danvers, Massachusetts, United States
Anti-rat HRP	1:1000	Cell Signaling Technology, Danvers, Massachusetts, United States

Table 16: List of antibodies and viability dyes used for flow cytometry.

Antigen	Fluorophore	Clone	Dilution	Manufacturer
7-AAD	7-AAD	-	1:50	Becton Dickinson, Franklin Lakes, New Jersey, United States
BrdU	FITC	-	1:400	Becton Dickinson, Franklin Lakes, New Jersey, United States
Fixable viability dye eFluor 506	≈ Amcyan	-	1:1000	eBioscience by Thermo Fisher Scientific Inc., Waltham, Massachusetts, United States
Fixable viability dye eFluor 780	≈ ZombieNIR	-	1:1000	eBioscience by Thermo Fisher Scientific Inc., Waltham, Massachusetts, United States
Isotype control, rat, IgG2a κ	APC	-	1:200	BioLegend, San Diego, California, United States
PI	PI	-	1:100	Miltenyi Biotec, Bergisch Gladbach, Germany

Phosphatidyl-serine	FITC	-	1:100	Miltenyi Biotec, Bergisch Gladbach, Germany
RORγ	APC	AFKJS-9	1:200	Thermo Fisher Scientific Inc., Waltham, Massachusetts, United States

3 Methods

3.1 Cell biological methods

3.1.1 Patient samples

Isolation of PBMCs from patients with *KMT2A*r leukemia was performed by the Department of Pediatrics and Adolescent Medicine, University Hospital Tübingen, Germany, after obtaining written informed consent from the patient. In the case of underage patients, informed consent of their legal guardians was obtained. The study was approved by our Institutional Review Board in accordance with ethical standards and the Declaration of Helsinki of 1975 as revised in 2013 (IRB approval 137/2017BO2).

3.1.2 Isolation of human umbilical cord blood

HuCB was collected only after written informed consent of the patient by the responsible physicians and was anonymized without subsequent identification of the patient (IRB approval 751/2015BO2 and 461/2022BO2). The collection was performed after a cesarean section in collaboration with the Department of Pediatrics IV - Neonatology, Neonatal Intensive Care Medicine of the Department of Pediatrics and Adolescent Medicine, University Hospital Tübingen, Germany. Blood was taken from the freshly collected placenta and 3-5 ml of sodium heparin was added.

3.1.3 Isolation of CBMCs from huCB

Cord blood mononuclear cells (CBMCs) were isolated by density gradient centrifugation according to Boyum [203], for which up to 50 ml of umbilical cord blood was diluted to 175 ml with PBS. Then, 35 ml each of the blood/PBS mixture was carefully layered on 15 ml of the synthetic polymer Biocoll and centrifuged for 18 min at 800 g with reduced brake and acceleration. The mononuclear cells contained in the interphase were removed, diluted to 50 ml with PBS, and centrifuged again (300 g, 5 min, RT). The supernatant was discarded, and the remaining cell pellets were pooled and diluted to 40 ml with PBS. A 10 µl cell suspension was taken as a counting sample, and another washing step (200 g, 10 min, RT) removed the remaining platelets.

3.1.4 Positive magnetic isolation of CD34+ HSPCs

CD34+ HSPCs were obtained using magnetic activated cell sorting (MACS) and the CD34 MicroBead Kit according to the manufacturer's instructions. For this purpose, up to 1 x 10^8 CBMCs were resuspended in 300 µl MACS buffer, mixed with 100 µl Fc receptor (FcR) Blocking Reagent as well as 100 µl CD34 MicroBeads and incubated for 30 min at 4 °C. After washing with 10 ml MACS buffer (300 g, 5 min, RT), the cells were again collected up in MACS

buffer and isolated using an LS MACS column in a magnetic field. After three washes with MACS buffer, the magnetic field was removed, the CD34+ cells were rinsed from the column, and the exact cell number was determined.

3.1.5 Induction of *t(4;11)* using CRISPR/Cas9

Genome editing with RNPs was performed using the P3 Primary Cell 4D Nucleofector Kit. All work surfaces were cleaned with RNaseZap prior to starting work. To induce a *t(4;11)* chromosomal translocation, 1 µg of Cas9 protein and 1 µg of the corresponding *in vitro* transcribed sgRNA (*KMT2A*, *AFF1*) were incubated for 15-30 min at RT. For each nucleofection approach, 3 x 10^5 HSPCs were centrifuged (300 g, 5 min, RT) and resuspended in 17 µl P3 solution. After careful mixing of the cells with the Cas9-sgRNA-RNP complex, the cells were electroporated with the 4D-NucleofectorTM X Unit (program: EO-100) and incubated for 3 min at RT. The reaction was stopped by the addition of SCM. As a control, cells were incubated without RNP complex or with pmaxGFP plasmid. Cells were transferred equally into two 96-wells each (U-bottom) and cultured in SCM at 37 °C and 5% CO_2. After 48 hours, 20 µM of the caspase inhibitor Z-VAD-FMK was added, and the cell population was transferred to a 24-well plate for long-term cultivation when a cell density of at least 1 x 10^6 cells/ml was reached (**Figure 10**).

Identification of a positive translocation was based on the workflow of study and diagnostic centers, including split-signal and PCR [204, 205]. Detection by PCR was performed using genomic DNA and specifically designed primers (see **Section 3.2.2**). A pure CRISPR/Cas9 *t(4;11)* cell population was defined by the presence of at least 90% translocated cells detected by FISH (see **Section 3.2.6**). The presence of leukemic myeloblasts in the cell population was analyzed by Pappenheim staining (see **Section 3.2.7**).

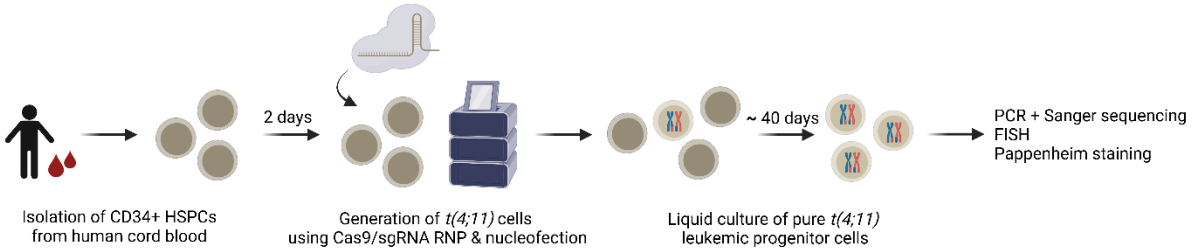

Figure 10: Experimental setup of generation of CRISPR/Cas9 *t(4;11)* cells.
CD34+ isolated HSPCs from huCB were cultured and nucleofected with an RNP complex of Cas9 protein and sgRNAs targeting the *KMTA2* and *AFF1* genes. This resulted in the outgrow of a single clone and a pure culture of *t(4;11)* leukemia cells. Positive translocations were identified using various molecular biological techniques. Figure generated with BioRender.

3.1.6 Cultivation of primary cells and cell lines

CRISPR/Cas9-generated *t(4;11)* cells, CD34+ HSPCs, and commercial cell lines were cultured under constant conditions at 37 °C and 5% CO_2.

CRISPR/Cas9 *t(4;11)* cells and CD34+ HSPCs were cultured in SCM at a cell density of 0.5 to 2.0 x 10^6 cells/mL in 24-well plates (**Table 6**). Cells were passaged or medium changed every two days, depending on cell number.

t(4;11) cell lines and non-*KMT2A*r control cell lines were cultured in T25 cell culture flasks according to the instructions of the German Collection of Microorganisms and Cell Cultures (DSMZ) (**Table 6**).

HEK293T cells were cultured in 10 cm cell culture plates in the appropriate culture medium (**Table 6**). At a maximum confluence of 70-90%, the semi-adherent cells were washed with PBS, rinsed with fresh culture medium from the bottom of the cell culture plate, and seeded onto new plates at a ratio of 1:10.

3.1.7 Freezing and thawing of cells

For freezing, primary cells and cell lines at a constant growth stage were pelleted by centrifugation (300 g, 5 min, RT) and resuspended in freezing medium at a concentration of 5 x 10^6 cells/ml. 1 ml of the cell suspension was transferred to cryotubes and frozen at -80 °C in a freezing container filled with isopropanol (Mr. Frosty™). Long-term storage of the cells was performed in liquid nitrogen.

To re-culture cryopreserved cells, they were thawed at 37 °C in a water bath and rapidly transferred to 50 ml of pre-warmed PBS. Cells were pelleted by centrifugation (300 g, 5 min, RT) and resuspended in the appropriate cell culture medium. After determining the correct number of cells by cell counting, cells were seeded at the appropriate concentration and cultured at 37 °C and 5% CO_2.

3.1.8 Determination of cell growth and viability

The growth of *t(4;11)* and control cells over a period of time was determined by counting the number of cells using a Neubauer counting chamber. For this purpose, cells were seeded at their optimal initial concentration in 96-well cell culture plates and cultured in the appropriate medium (**Table 6**). Every two or three days, 10 µl of the cell suspension was removed, mixed with 0.04% trypan blue at a 1:10 ratio, and the number of cells with intact membrane integrity was determined in four squares of the counting chamber as described below.

$$\text{cells/ml} = \frac{\text{living cells}}{\text{number of counted squares}} \times \text{dilution factor} \times 10^4$$

Cells were divided on each counting day using the appropriate control, and a growth curve could be plotted in terms of absolute cell number.

AlamarBlue cell viability reagent was used to determine the cell viability of the total population. For this purpose, 90 µl of cell suspension was transferred in triplicate to a new 96-well plate and mixed with 10 µl each of alamarBlue. After incubation at 37 °C and 5% CO_2 for 2 h, fluorescence was measured at 560/590 nm (absorbance/emission). The viability of the total cell suspension in each sample was calculated relative to the corresponding control after subtracting the background fluorescence.

3.1.9. Preparation of plasmid DNA from *E. coli*

To generate cells carrying an *SREBF2* knockdown (kd), CRISPR/Cas9 *t(4;11)* cells were transduced with lentiviral short/small hairpin RNA (shRNA) constructs. For this purpose, glycerol stocks of *E. coli* bacteria containing the lentiviral plasmids were obtained from Horizon Discovery. To ensure a pure bacterial culture, a portion of the frozen glycerol stocks was spread with a pipette tip onto an LB agar plate mixed with the selection antibiotic. Incubation was performed overnight at 37 °C. Subsequently, 5 ml of sterile LB medium containing selection antibiotic was inoculated with a single colony from the agar plate and grown at 37 °C and 250 rpm in a shaker incubator. After reaching an optical density (OD600) of 0.2 to 0.5, 100 ml of LB medium with selection antibiotic was again inoculated with 5 ml of bacterial suspension for midi preparation. Incubation was performed overnight at 37 °C and 250 rpm on a shaking incubator.
Plasmid isolation was performed using the NucleoBondTM Xtra Midi Plus EF Kit according to the manufacturer's instructions. Plasmid DNA was eluted in 400-600 µl of nuclease-free H_2O and stored at -20 °C.

3.1.10 ShRNA-mediated kd in *t(4;11)* cells

All subsequent work was performed according to biological safety level 2.
For the preparation of virus supernatant, HEK293T cells with a maximum confluence of 80% were plated at a ratio of 1:8 in the appropriate medium in new cell culture plates one day before transfection. The calcium phosphate method was used for transfection. For this purpose, 450 µl of nuclease-free H_2O was mixed with 50 µl of $CaCl_2$ (2.5 M) per transfection batch and the packaging plasmids pMD2.G (5 µg) and psPAX2 (7.5 µg) and the respective lentiviral shRNA plasmids (10 µg each, pLKO.1 constructs) were added. Next, 500 µl of 2X HeBS buffer was added with moderate mixing and incubated at RT for 10 min. The solution was then added dropwise to HEK293T cells, which were seeded the previous day and incubated at 37 °C and 5% CO_2. After 6 h, the medium was completely removed and replaced with 6 ml DMEM containing 10% FBS and 1% penicillin/streptomycin. After another 48 h, the supernatant, which now contained viral particles, was removed and filtered through a 0.45 µm filter. To each 6 ml of virus supernatant, 3.5 ml of PBS, 325 µl of NaCl (5 M), and 2 ml of PEG 8000 were added,

and the virus supernatant was concentrated overnight at 4 °C under continuous rotation. The solution was then centrifuged (4 000 rpm, 1 h, 4 °C) and resuspended in 300 µl PBS.
For the infection of target cells, 8 x 10^5 CRISPR/Cas9 *t(4;11)* cells were seeded in SCM in 24-well plates and incubated at 37 °C and 5% CO_2 for 6 h. Then, 100 µl of concentrated virus supernatant was added per well and incubated for 72 h at 37 °C and 5% CO2. After being centrifuged three times with PBS (300 g, 5 min, RT), the transduced cells were selected with 0.5 µg/ml puromycin for seven days and used for subsequent analyses (**Figure 11)**.
All materials and solutions that came into contact with lentiviral particles were then disinfected with Perform according to the manufacturer's instructions and under UV light.

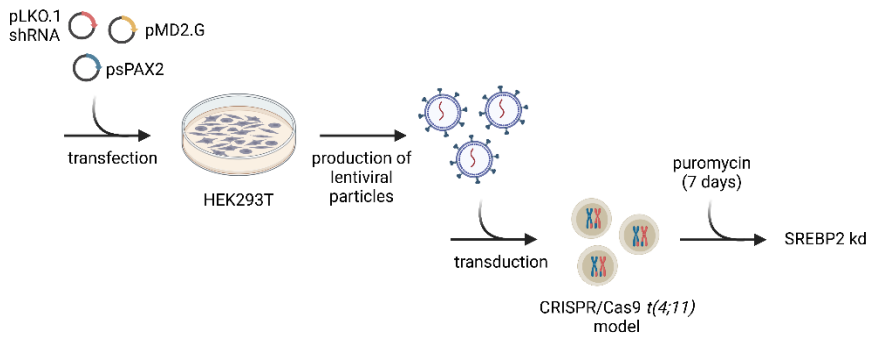

Figure 11: Experimental setup of generation of CRISPR/Cas9 *t(4;11) SREBF2* kd cells.
A pure culture of CRISPR/Cas9 *t(4;11)* cells was transduced with lentiviral supernatant containing shRNAs targeting the *SREBF2* gene. Bacterial selection with puromycin was performed for seven days resulting in *t(4;11) SREBF2* kd cells. Figure generated with BioRender.

3.1.11 Measurement of intracellular cholesterol content

For the determination of intracellular cholesterol concentration, the Amplex™ Red Cholesterol Assay Kit was used according to the manufacturer's instructions. First, lipid extraction was performed according to Bligh and Dyer [206]. with slight modifications. For this, 1 x 10^6 cells were harvested, washed in PBS, mixed with methanol/chloroform [2:1; v/v], and incubated on a shaker (14000 rpm, 15 min, RT). H_2O/chloroform [1:1; v/v] was added to the mixture and incubated again with shaking (14000 rpm, 10 min, RT). For subsequent phase separation, the samples were centrifuged at 800 g for 15 min at RT. The lower organic phase containing lipids was completely removed, evaporated under continuous nitrogen supply and resuspended in 400 µl 1X reaction buffer. In duplicate, 50 µl of each extracted lipid was added to a 96-well plate. Subsequently, 50 µl of the freshly prepared working solution consisting of Amplex Red reagent, horseradish peroxidase (HRP), cholesterol oxidase as well as cholesterol esterase were added and the samples were incubated for 30 min at 37 °C without exposure to light. Subsequent fluorescence measurement was performed at 530/590 nm (absorbance/emission). After subtracting the background fluorescence, the intracellular cholesterol concentration was calculated using a cholesterol standard curve. The final

cholesterol concentration was normalized to the total protein in each sample and specified in ng cholesterol per µg protein.

3.2 Molecular biological methods

3.2.1 SgRNA synthesis

The sgRNAs targeting the *KMT2A* and *AFF1* genes were previously designed by Secker *et al.* [82] using CRISPRscan [207], and sequences with high on-target efficiency and lowest probability of off-target effects were selected. The human reference genome (GRCh38) was selected, and 5'-NGG-3' was chosen as the protospacer adjacent motif (PAM). Synthesis of sgRNAs was performed by PCR and transcribed *in vitro* according to the protocol by Gundry *et al.* [87]. Forward primers for sgRNA production were designed including a T7 promoter (5'-taatacgactcactata-3'), sgRNA target sequence, overlap with plasmid PX458 encoding the sgRNA backbone (5'-gttttagagctagaa-3'), and a 5'-ATAGC-3' modification. Template DNA for sgRNA was prepared using the KAPA HIFI HotStart ReadyMix PCR Kit according to the scheme and the appropriate program.

PCR – pipette scheme	
KAPA HIFI HotStart ReadyMix MM	10 µl
Primer sgRNA fwd (10 µM)	2 µl
Primer universal rev (10 µM)	2 µl
Plasmid PX458 (2-4 ng/µl)	1 µl
RNase free H_2O	5 µl

PCR - program		
Initial denaturation	95 °C, 3 min	
Denaturation	98 °C, 5 sec	30 cycles
Primer annealing	60 °C, 5 sec	
Elongation	72 °C, 10 sec	
Final elongation	72 °C, 1 min	
Cooling	4 °C, 5 min	

The DNA templates were mixed with 10x agarose loading buffer and separated using a 2% agarose gel at 100 V for 45 min using Midori Green (1:10000). *In vitro* transcription of the sgRNAs was performed using the HiScribe T7 High Yield RNA Synthesis Kit according to the scheme and the appropriate program.

In vitro transcription of sgRNAs – pipette scheme	
DNA (400 to 1000 ng)	9 µl
NTPs (ATP, CTP, GTP, UTP)	4x4 µl
T7 reaction buffer (10X)	4 µl
T7 TNA polymerase mix	4 µl
RNase free H_2O	7 µl

In vitro transcription of sgRNAs –program
37 °C, 5 hours

Synthesized sgRNAs were purified using the RNA Clean and Concentrator-25 Kit and diluted in RNase free H2O to a final concentration of 1 µg/µl before being aliquoted and stored at -80 °C until use. To verify successful synthesis, sgRNAs (2 µg) were diluted in RNase free H_2O (7

µl) and 10x agarose loading buffer (1 µl), denatured at 65 °C for 5 min, and separated on a 2% agarose gel at 100 V for 60 min.

3.2.2 Polymerase chain reaction (PCR) and Sanger sequencing

For genotyping of CRISPR/Cas9-generated *t(4;11)* cells, a PCR was performed to amplify the specific DNA segment of the translocation site. For this purpose, cells were harvested and pellets were stored at -20 °C until use. Genomic DNA was isolated using the NucleoSpin DNA Rapid Lysis Kit and translocation PCR was performed using the PrimeSTAR Max according to the scheme and the appropriate program.

PCR – pipette scheme	
2x Primestar Max Mix	12,5 µl
Primer fwd (10 µM)	0,75 µl
Primer rev (10 µM)	0,75 µl
Genomic DNA (100 ng)	q.s.
RNase free H_2O	q.s.

PCR - program		
Initial denaturation	98 °C, 10 sec	
Denaturation	98 °C, 10 sec	40 cycles
Primer annealing	60 °C, 10 sec	
Elongation	72 °C, 10 sec	
Cooling	4 °C, 5 min	

After PCR amplification, samples were mixed with 10x agarose loading buffer and separated using a 2% agarose gel at 100 V for 45 min using Midori Green (1:10000). Images were analyzed using the E-BOX VX2 gel documentation system. For subsequent sequencing, bands could be excised and isolated using the NucleoSpin Gel and PCR Clean-up Kit. To verify the sequence of the fusion gene, the isolated DNA was sent to Microsynth SeqLab using the previously used primers. For sequencing, 18 ng of DNA per 100 bp was diluted in nuclease-free water to a total volume of 12 µl. Subsequently, 3 µl of the previously used forward or reverse primers were added to each DNA sample.

3.2.3 RNA isolation and cDNA synthesis

For the isolation of RNA from cell material, the NucleoSpin RNA Kit was used. For this, up to 3 x 10^6 cells were pelleted (16 000 g, 1 min, 4 °C), washed with PBS, and RNA was isolated according to the manufacturer's instructions. The elution volume was 25 µl. Subsequently, both the concentration and purity of the sample were determined using a nanodrop. The samples were be stored at -80 °C until further analysis.

Reverse transcription was used to synthesize the complementary DNA (cDNA) of the previously isolated messenger RNA (mRNA). For denaturation, 1 µg of RNA was diluted with RNase free water to 11.5 µl total volume. The solution was first heated with 1 µl Random Hexamers for 5 min at 65 °C and after subsequent cooling, 5x Reaction Buffer, RevertAid H Minus Reverse Transcriptase, RiboLock RNase Inhibitor and dNTP Mix were added according

to the scheme and the cDNA was synthesized using the appropriate program. The cDNA was then stored at -20 °C.

cDNA synthesis – pipette scheme	
5x RT buffer	4 µl
Reverse transcriptase	1 µl
Ribolock	0,5 µl
dNTPs	1 µl

cDNA synthesis - program	
Primer annealing	25 °C, 5 min
Reverse transcription	42 °C, 60 min
Inactivation RT	70 °C, 5 min

3.2.4 Reverse transcription quantitative PCR (RT-qPCR)

To quantify a specific mRNA expression level, RT-qPCR was performed using the Roche LightCycler® 480 System. For amplification of cDNA, Maxima SYBR Green qPCR Master Mix containing Maxima Hot Start Taq DNA Polymerase and dNTPs was mixed with forward and reverse primers and the cDNA according to the scheme.

RT-qPCR – pipette scheme	
Maxima SYBR Green qPCR MM	10 µl
Primer fwd (2 µM)	3 µl
Primer rev (2 µM)	3 µl
cDNA (50 ng)	2 µl
RNase free H_2O	2 µl

RT-qPCR – program		
Initial denaturation	95 °C, 10 min	
Denaturation	95 °C, 14 sec	45 cycles
Primer annealing	60 °C, 1 min	
Melting curve	65 °C - 95 °C	
	+ 0.06 °C / 1 sec	
Cooling	37 °C, 5 min	

18S rRNA was used as the reference gene using an 18S probe and the Maxima Probe qPCR Master Mix.

RT-qPCR – pipette scheme	
Maxima Probe qPCR MM	10 µl
Primer fwd (2 µM)	3 µl
Primer rev (2 µM)	3 µl
cDNA (50 ng)	2 µl
RNase free H_2O	1 µl
18S rRNA probe (4 µM)	1 µl

RT-qPCR - program		
Initial denaturation	95 °C, 10 min	
Denaturation	95 °C, 14 sec	45 cycles
Primer annealing	60 °C, 1 min	
Melting curve	65 °C - 95 °C	
	+ 0.06 °C / 1 sec	
Cooling	37 °C, 5 min	

Samples were measured in duplicates according to the indicated PCR program and subsequently analyzed using the Roche LightCycler software. The obtained CT values were normalized to the CT values of the reference gene (*18S*) using the ΔΔCT method.

3.2.5 RNA sequencing (RNA-Seq)

Total RNA was isolated using NucleoSpin RNA Kit according to the manufacturer's instructions. All samples were examined for quality assessment using Nanodrop One and

Bioanalyzer. Only samples with an RNA integrity number of 7 and higher were used for sequencing library preparation which was performed in the NGS Competence Center Tübingen (NCCT) in randomized batches. Raw data analysis including alignment, differential gene expression analysis, and Ingenuity Pathway Analysis was performed in collaboration with Dr. Thomas Hentrich.

Libraries for 3′ RNA-Seq were prepared using the TruSeq Stranded Total RNA Kit according to the manufacturer's instructions. Sequencing was performed according to the paired-end RNA sequencing protocols from Illumina on a NextSeq 500 platform. First-strand synthesis of polyA-tailed RNA from total RNA using oligo-dT primers was followed by RNA template degradation. This was then followed by second-strand synthesis using random primers with 5′ Illumina-compatible linker sequences, and amplification using random primers with added barcodes and cluster generation sequences [208]. The libraries were sequenced on the NCCT Nova sequencing platform to a depth of approximately 10 million reads of 100 bp in length. Read preprocessing was performed using the Lexogen pipeline [209], which uses *bbduk* of the *BBTools* suite (*https://sourceforge.net/projects/bbmap/*, accessed 07/2021) for quality trimming. Cleaned reads were aligned with *STAR* [210] to the human reference genome GRCh38.104. Only reads that mapped to a single unique location were considered for further analysis and differential gene expression analysis was determined with *DESeq2* [211] on genes with at least 50 normalized read counts [212]. Significance thresholds were set at Benjamini-Hochberg adjusted $p_{FDR} < 0.05$ and $|\log_2 \text{fold-change}| > 0.5$. Enrichment of affected biological pathways and possible upstream regulators was determined in *Ingenuity Pathway Analysis* (July 2021 version).

3.2.6 Fluorescence *in situ* hybridization (FISH)

To determine the percentage of translocated cells in the culture, FISH was performed with a *KMT2A*-specific two-color Breakapart probe (ZytoLight SPEC *KMT2A* Dual Color Break Apart Probe) in collaboration with the Institute of Pathology and Neuropathology at the University Hospital Tübingen under the direction of Prof. Dr. Falko Fend and in cooperation with Barbara Mankel.

For this, 1.5 x 10^6 cells per sample were taken from the culture, centrifuged (300 g, 5 min, RT) and washed in 1 ml PBS. After the cells were fixed in 250 µl formaldehyde (4%) on ice for 30 min, 10 µl of the cell suspension was applied to a silanized SuperFrost Plus slide. After drying, the slide was incubated in sodium citrate buffer for 40 min at 95 °C. The samples were then demineralized in water and 0.25 mg/ml pepsin working solution was applied dropwise to the slide and incubated for 4 min at 37 °C. The slides were rehydrated in an ascending ethanol series (70% and 100%) before being dried again. Both the slide and the *KMT2A*-Breakapart probe were heated to 37 °C for 5 min, and 4 µl of the probe was applied to the slide. Samples were covered with coverslips, sealed with Fixogum, and denatured in the HYBrite hybridization

system at 75 °C for 10 min. Incubation was performed overnight at 37 °C. The next day, coverslips and Fixogum were carefully removed and samples were treated with the ZytoLight FISH-Cytology Implementation Kit according to the manufacturer's instructions. After washing three times with pre-warmed Cytology Stringency Wash Buffer SSC for 30 min, 1 min, and 5 min, respectively, the samples were dehydrated in ascending ethanol series (70%, 85%, and 100%) for 1 min each. Finally, 3.2 µl of DAPI/DuraTect solution was applied to the slide and sealed with a coverslip.
The slides were analyzed using an Axio Imager M2 and 100 cells per sample were counted to determine the percentage of *KMT2A*r cells in the culture.

3.2.7 Pappenheim staining

For the preparation of cytospins, 2 x 10^5 cells per sample were centrifuged (300 g, 5 min, RT) and resuspended in 500 µl PBS. First, a filter card and cytology funnel were placed on a microscopy slide, loaded in the cytocentrifuge and fixed with a slide clip. The samples were centrifuged at 700 rpm for 4 min with medium acceleration and dried for 10 min under the fume hood. Next, the slides were incubated in May-Grünwald-solution for 5 min, before rinsed in distilled water. Directly afterwards, the staining was performed for 10 min in Giemsa solution, diluted with Sorensen's buffer (1:50), after again washed with distilled water. The samples were dried and covered with Neo-Mount anhydrous mounting medium. Subsequently, samples were analyzed with the Zeiss Primovert microscope using the 40x objective and ZEN 2.3 lite blue software. Pictures were taken with the Axiocam 105 colour.

3.3 Protein biochemical methods

3.3.1 Preparation of total protein lysate

Pelleted cells were used as starting material for the preparation of total cell extracts. For this purpose, up to 5 x 10^6 cells were washed with ice-cold PBS and centrifuged (300 g, 5 min, 4 °C). For all subsequent steps, samples were chilled on ice. Cells were resuspended in 50-100 µl RIPA buffer depending on cell number and lysed for 1 h followed by sonication. Subsequent centrifugation (16000 g, 20 min, 4 °C) separated all cellular components and RNA and DNA molecules from the total protein in the supernatant. The protein lysate contained in the supernatant was then quantified and could be stored at -20 °C until further analysis.

3.3.2 Determination of total protein using DC Assay

To determine the protein concentration in the total cell lysate, the method of Lowry *et al.* [213] was used using DC Protein Assay Kit according to the manufacturer's instructions. For analysis, 5 µl each of a bovine serum albumin standard series and 5 µl of the protein lysate were pipetted in duplicates into a 96-well flat-bottomed plate. Per well, 25 µl of Lowry reagent,

consisting of 50 parts reagent A (alkaline copper tartrate solution) and one part reagent S (surfactant solution), was added. To the samples, 200 µl of reagent B (diluted Folin-Ciocalteu solution) was added and incubated at RT for 15 min in the absence of light. Subsequently, the resulting color change was detected by photometry at 650 nm and the protein concentration was calculated using the standard series.

3.3.3 SDS-polyacrylamide gelektrophoresis (SDS-PAGE)

Proteins in the cell lysates were separated based on their molecular weight using an SDS-polyacrylamide gel consisting of 10% resolving gel and 6% stacking gel (**Table 5**). To do this, 20-50 µg of protein were mixed with 4X sample buffer (Lämmli) and heated at 95 °C for 5 min. Samples were then loaded onto the gel and separated for 1 h 15 min at 140 V using the PageRuler Plus Prestained Protein Ladder as a reference.

3.3.4 Western blot

For detection, the separated proteins were transferred from the SDS gel to an Immobilon-FL polyvinylidene fluoride (PVDF) membrane using the wet blot method. For this, the membrane was first equilibrated for 1 min in methanol as well as in transfer buffer. The membrane and gel were placed together, free of air bubbles, between Whatman filter paper in the Mini Trans Blot Cell System and the proteins were transferred to the membrane under constant cooling and 100 V for 1 h 20 min. To avoid nonspecific bands, the membrane was blocked with 5% milk powder in TBS-T for 1 h at RT and incubated with the appropriate primary antibody (in 5% milk powder in TBS-T) at 4 °C overnight. After washing three times for 10 min with TBS-T, the membrane was incubated in the absence of light for 1 h at RT with a corresponding species-specific HRP-linked secondary antibody. After washing the membrane three times again, detection was performed by chemiluminescence. For this purpose, the Pierce ECL Western Blotting Substrate Kit was used according to the manufacturer's instructions and the localization of the antibody bound to the target protein was detected with the Vilber Fusion FX detection device.

3.3.5 Cytochrome c release

During intrinsic apoptosis, mitochondrial cytochrome c is released into the cytosol leading to caspase activation and ultimately to apoptotic cell dismantling [214]. To analyze a mitochondrial involvement in apoptotic processes, the release of mitochondrial cytochrome c into the cytosol was investigated using the Cytochrome c releasing apoptosis Kit. For this purpose, cells were treated with indicated inhibitor concentrations and controls. 5 x 10^6 cells were centrifuged (600 g, 5 min, 4 °C) and washed with 10 ml of ice-cold PBS. Cytosolic and mitochondrial fractions were isolated according to the manufacturer's instructions. 20 µg of

cytosolic and mitochondrial proteins were separated on a 12% SDS-polyacrylamide gel (**Table 5**), transferred to a PVDF membrane, and Western blot was performed as previously described (see **Section 3.3.4**). Both cytosolic and mitochondrial fractions were probed for cytochrome c. Anti-GAPDH was used as cytosol fraction loading control and anti-VDAC1 as mitochondrial fraction loading control.

3.3.6 Flow cytometry

3.3.6.1 Intracellular staining

To examine RORγ expression, the FoxP3/transcription factor staining buffer set was used and intranuclear staining was performed according to the manufacturer's instructions with slight modifications. For this purpose, approximately 0.5 - 1.0 x 10^6 cells were washed with 500 µl FACS buffer and incubated with FcR blocking reagent (1:100 in FACS buffer) for 5 min at RT. Then, for live cell analysis only, cells were incubated with eFluor506 viability dye for 20 min at 4 °C in the absence of light and washed again. Cells were then fixed with 500 µl of a freshly prepared FoxP3 fixation/permeabilization solution for 1 h at 4 °C. Samples were washed twice with 500 µl of 1x Perm buffer and the RORγ antibody, diluted in 1x Perm buffer (1:200), was added to the cells. To exclude the presence and extent of non-specific antibody binding, an isotype was used as control. After another incubation under light exclusion for 1 h at 4 °C, the cells were washed, resuspended in 100 µl FACS buffer and measured on the flow cytometer.

3.3.6.2 Cell cycle analysis

Cell cycle analysis was performed using the FITC BrdU Flow Kit according to the manufacturer's instructions with slight modifications. Here, bromodeoxyuridine (BrdU) is integrated into the newly synthesized DNA in the synthesis phase instead of thymidine and detected by antibody binding. In addition, the analysis includes staining with 7-aminoactinomycin (7-AAD), which in turn intercalates with the double-stranded DNA (**Figure 12**).

For this, approximately 5 x 10^5 of the cells to be analyzed were incubated with 10 µM BrdU for 1 h at 37 °C and 5% CO_2. The samples were then washed with FACS buffer and fixed with 100 µl Cytofix/Cytoperm Wash Buffer for 20 min at RT. This was followed by a permeabilization step with 100 µl Cytoperm Permeabilization Buffer Plus for 10 min at 4 °C and another 5-min incubation with Cytofix/Cytoperm Wash Buffer. Subsequent DNase digestion with 15 µg DNase per sample was performed for 1 h at 37 °C and 5% CO_2. The DNase was removed in a wash step and the incorporated BrdU was labeled with an anti-BrdU antibody (1:400) for 20 min at RT. After a final wash step, cells were suspended in 200 µl FACS buffer, and 4 µl 7-AAD was added.

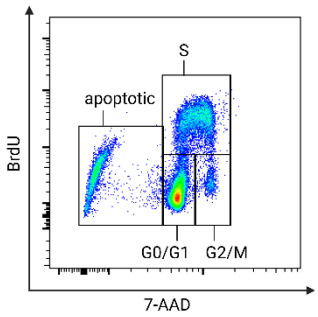

Figure 12: Schematic representation of cell cycle analysis using the FITC BrdU Flow Kit.
The histogram shows the analysis strategy for different stages of the cell cycle. BrdU incorporation and antibody staining are used to detect the synthetic (S) phase, and 7-AAD DNA intercalation is used to detect cells in apoptotic, G0/G1, and G2/M phases.

3.3.6.3 Annexin V staining

For the quantification of apoptotic cells, the Annexin V-FITC Kit was used to detect phosphatidylserine. This is located on the inner side of the cell membrane in living cells and is translocated to the outer cell membrane upon apoptosis induction, whereas propidium iodide (PI) can only enter necrotic cells where it binds double-stranded DNA. Based on this, a distinction can be made between viable (Annexin V-, PI-), early apoptotic (Annexin V+, PI-), and late apoptotic (Annexin V+, PI+) cells (**Figure 13**).
For this purpose, approximately 0.5 - 1.0 x 10^6 of the cells to be analyzed were washed with 500 µl Binding Buffer. Annexin V-FITC antibody was then added to the cells in Binding Buffer at a suitable dilution (1:100) and incubated for 20 min at 4 °C in the absence of light. After another washing step, the cells were added to the dye PI in Binding Buffer (1:100) and measured on the flow cytometer.

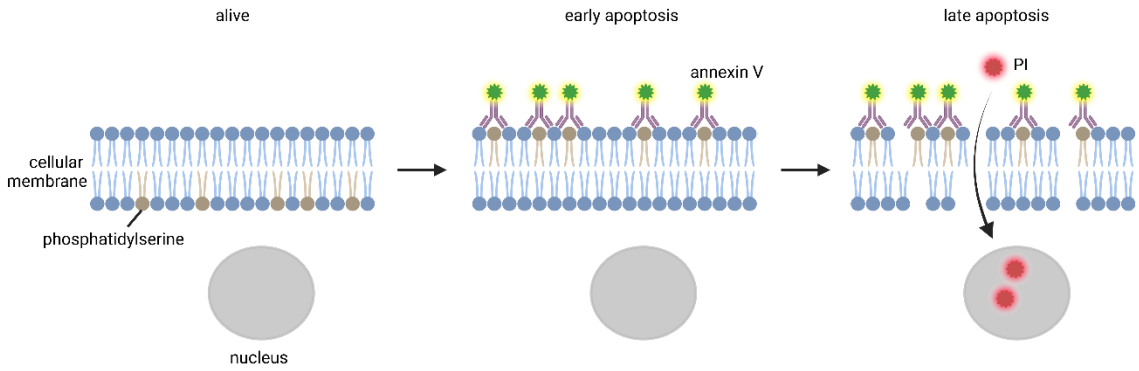

Figure 13: Schematic representation of the Annexin V-FITC Kit.
In healthy cells, phosphatidylserine is located on the cytoplasmic surface he plasma membrane (alive). During apoptosis, the plasma membrane undergoes structural changes, including the translocation of phosphatidylserine from the inner to the extracellular side. Human Annexin V has a high affinity for phosphatidylserine and is therefore used to detect apoptotic cells (early apoptosis). Necrotic or dead cells no longer have an intact cell membrane allowing PI to penetrate and bind to DNA (late apoptosis). Figure generated with BioRender.

3.4 Statistics

3.4.1 Statistical Analysis

Data are presented as arithmetic mean ± standard deviation (SD). Statistical analysis of the data was performed using GraphPad Prism software. Unless otherwise indicated in the figure caption, all experiments were performed in technical duplicates or triplicates and repeated in at least three independent experiments. Results from primary cells or our CRISPR/Cas9 model are based from data from at least three independent donors. The Shapiro-Wilk test was used to test for normal distribution. Significance of differences between individual groups was determined by either a one-way ANOVA or a two-sided unpaired Student's t test. Differences were considered significant when *p<0.05, **p<0.01, ***p<0.001, and ****p<0.0001.

3.4.2 Determination of synergy

For combinatorial treatment studies, cells were treated with various concentrations of the respective compounds alone or in combination for a total of seven days. The data are presented as percentage of viable cells (defined as PI and Annexin V negative), with DMSO-treated cells set as 100%. The estimated *in vitro* half maximal inhibitory concentrations (IC_{50}) were calculated using GraphPad Prism 9 software [202]. Combination index (CI) was analyzed according to the Chou-Talalay method [215] and used to define synergy (CI<1), additivity (CI=1), and antagonism (CI>1) [216] (**Figure 14**).

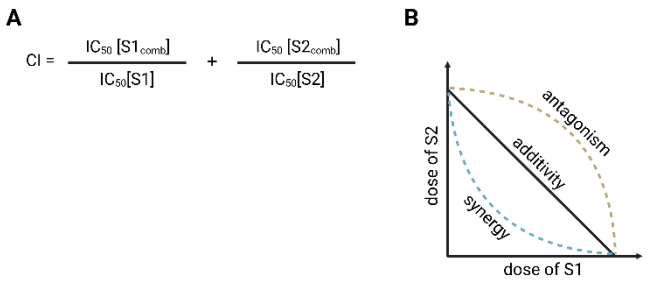

Figure 14: Calculation of the combination index and determination of synergy.
IC_{50} values of combinatorial treatment (comb) of two substances (S1, S2) were used for combination index analysis **(A)** and synergy quantification using the Chou-Talalay method **(B)** [215, 216].

4 Results

Partial results of this work were published under the title “The RORɣ/SREBP2 pathway is a master regulator of cholesterol metabolism and serves as potential therapeutic target in *t(4;11)* leukemia” at *Oncogene* [202].

4.1 Upregulated cholesterol metabolism in *t(4;11)* leukemia

4.1.1 Upregulated *SREBF2* mRNA expression *KMT2A*r leukemia of public patient data

Cholesterol homeostasis is now considered as a hallmark of cancer. To further assess the clinical relevance, AML cases from The Cancer Genome Atlas were divided into *SREBF2*^{low} and *SREBF2*^{high} groups. The overall survival rates of patients in the *SREBF2*^{high} group were significantly lower than those in the *SREBF2*^{low} group, highlighting the important role of this transcription factor in the clinical outcome of AML patients [202] (**Figure 15A**).

As a first step to define the molecular function of cholesterol metabolism in leukemia, publicly available patient databases were used to analyze *SREBF2* mRNA expression. The gent2 database (which contains a large number of independent patient records; **Supplementary Table 1**) showed a significantly upregulated *SREBF2* gene expression in patients with various blood cancers (8.5±0.70) compared to healthy individuals (7.9±0.55) (**Figure 15B**). The analysis using gent2 database was performed in collaboration with Dr. Johan Jeong. As leukemia is defined as a heterogeneous group of hematologic malignancies with different characteristics regarding morphology, immunology, cytogenetics and various molecular features, it is important to classify the disease. An overview from Bloodspot showed the analysis of different acute leukemia subtypes with cytogenetic abnormalities using data from GSE13159 of the Leukemia MILE study. This international multicenter study was initiated in 2005 to define a microarray-based gene expression profile in the diagnosis and subclassification of leukemia. The highest *SREBF2* mRNA expression was found in T-lineage ALL, followed by AML patients with *KMT2A*r leukemia. Additionally, the *SREBF2* expression of these patients was significantly higher than the mRNA level of healthy BM samples, AML patients with normal karyotype as well as *KMT2A*r in pro-B-ALL patients [202] (**Figure 15C**). It has been shown that normal stem cells and cancer cells share similarities, such as the ability to self-renew, and that molecular pathways that classically regulate malignant cells also control the stem cell development (reviewed by [217]). For that reason, it was of particular interest to additionally analyze the *SREBF2* mRNA expression during stem cell development and differentiation. Bloodspot provides data from GSE42519 and GSE13159 of normal human hematopoietic and AML cells. Since cell material from AML patients with *KMT2A*r showed very high *SREBF2* expression levels, healthy cells were compared with this leukemia subtype. Interestingly, healthy HSPCs, which are defined as CD34+ cells, also had high *SREBF2*

expression at baseline, but this decreased with differentiation into CD34- cells (**Supplementary Figure 1**).

These preliminary data suggest a possible overriding role of the *SREBF2* gene expression in different leukemia subtypes, particularly in AML patients with *KMT2A*r.

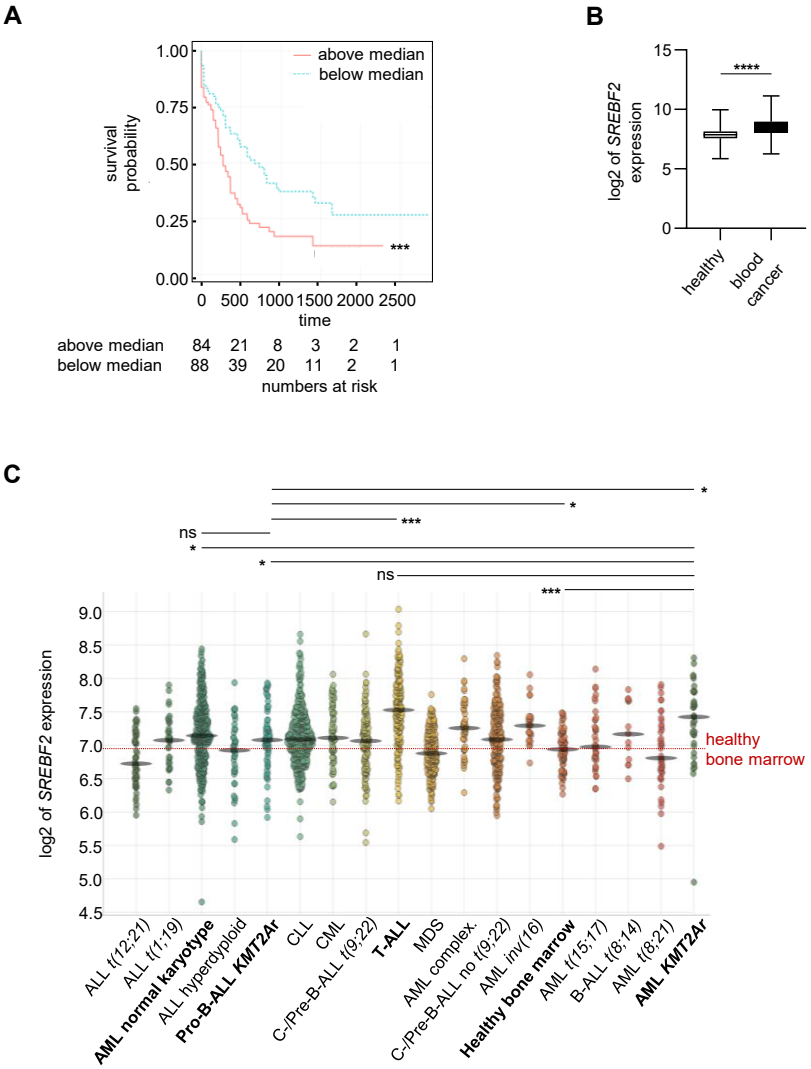

Figure 15: Validation of *SREBF2* level in different types of leukemia using public patient data.

(A) Using data from AML patients from The Cancer Genome Atlas (*https://tcga-data.nci.nih.gov/tcga,* accessed 05/2023), the overall survival of AML patients, divided into *SREBF2*^{low} (blue line) and *SREBF2*^{high} group (red line) according to the median value of *SREBF2* were compared with Kaplan-Meier analysis (data obtained from *https://servers.binf.ku.dk/bloodspot/,* accessed 05/2023). Student's *t* test. ****p*<0.001. **(B)** log2 of *SREBF2* expression level of PBMCs from healthy individuals (n=915) and PBMCs from patients with blood cancer (n=2082) analyzed with gent2 database (*http://gent2.appex.kr,* accessed 04/2021) using patient data from different data sets which contains a wide range of independent patient records (**Supplementary Table 1**). Bars represent the mean ± SD. Student's *t* test. *****p*<0.0001. **(C)** *SREBF2* expression (in log2) in healthy and leukemic patient samples (GSE13159, data obtained from *https://servers.binf.ku.dk/bloodspot/,* accessed 05/2023). Student's *t* test. **p*<0.05. ****p*<0.001. ns=not significant. Modified from Erkner *et al.* [202].

4.1.2 Cells harboring *t(4;11)* express the highest *SREBF2* mRNA level

It was of great interest to validate these initial results in an *in vitro* setting. For this purpose, RT-qPCR experiments with primers specific for the *SREBF2* gene were performed and tested with different cell types derived from primary cell material. The ΔΔCT method was used to calculate the relative *SREBF2* expression, with normalization to the reference gene *18S*. Here, PBMCs isolated from AML patients with normal karyotype and with *KMT2A*r leukemia were compared with PBMCs from healthy individuals and showed an upregulation of *SREBF2* in both groups (fold change of *SREBF2* expression in non-*KMT2A*r: 2.4±1.29; *KMT2A*r: 6.0±4.71), interestingly with the highest trend in *KMT2A*r leukemia patients (**Figure 16A**). Although patients with *KMT2A*r occur in nearly 5% to 10% of acute leukemias, patient material is very rare and there are several limitations for *in vitro* testing regarding the culture and growth potential of these cells. Therefore, a former PhD student of our laboratory established a CRISPR/Cas9-based patient-like *in vitro* model harboring *t(4;11)* or *t(9;11)* chromosomal translocations (**Supplementary Figure 2**). Increased *SREBF2* mRNA expression was confirmed in both cell models (fold change of *SREBF2* expression in *t(4;11)*: 14.7±2.90; *t(9;11)*: 9.9±4.49) compared to healthy PBMCs and huCB-derived HSPCs [202] (**Figure 16B**).

Additional analysis also showed that *SREBF2* gene expression varied greatly depending on the degree of differentiation of the myeloid (stem) cells. For example, undifferentiated CD34+ cells showed relatively high *SREBF2* gene expression. Furthermore, a decrease in this trend could be expected with increasing differentiation of the cells (**Supplementary Figure 1**). Whether this assumption can be confirmed was also investigated in this study. For this purpose, both freshly isolated CD34+ HSPCs and HSPCs cultured for three weeks under myeloid conditions were included in the analysis. The latter showed only low CD34 expression after this time (data not shown) and will be referred to as CD34- in the following. Interestingly, and in accordance with the results from public patient data, the *SREBF2* expression was strongly decreased when CD34+ HSPCs (5.5±1.14) were expanded for three weeks in myeloid culture to CD34- differentiated cells (1.7±0.62) (**Figure 16B**). The results become even more evident when a panel of different leukemia cell lines was tested. All tested cell lines showed an increased *SREBF2* expression level compared to healthy PBMCs (SKM-1: 12.0±3.43; NALM-6: 17.8±0.55; Jurkat: 7.6±0.46; SEM: 36.2±4.57; RS4;11: 24.7±10.69; MOLM-13: 7.1±1.39; THP-1: 11.1±5.47; MONO-MAC-6: 12.7±0.71), whereas SEM and RS4;11 cells harboring a *t(4;11)* translocation, were at highest [202] (**Figure 16C**).

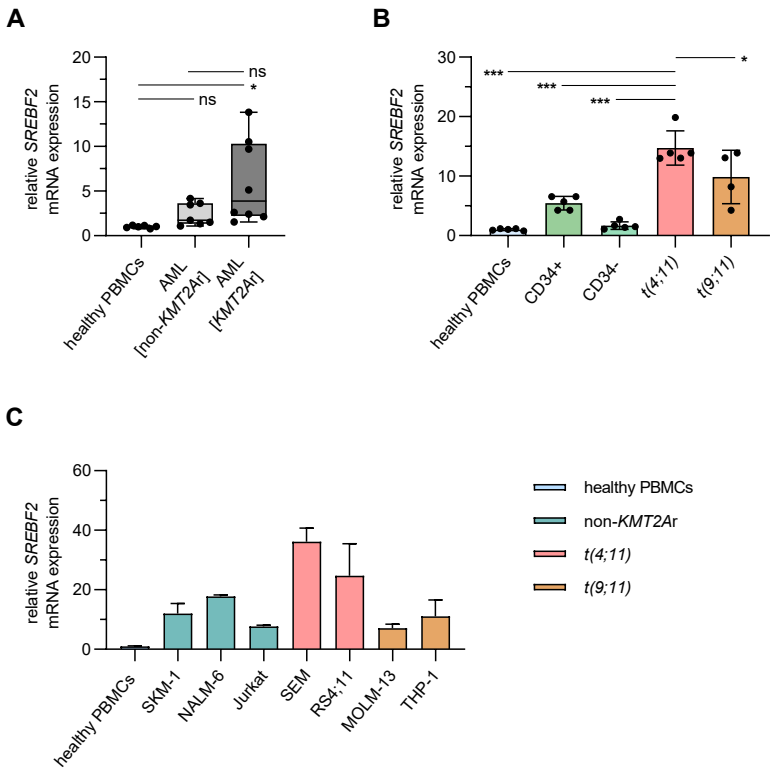

Figure 16: *SREBF2* mRNA expression in different cell types.

(A) Validation of *SREBF2* expression analyzed by RT-qPCR in PBMCs from leukemia patients with normal karyotype (n=7) and patients with *KMT2A*r leukemia (n=8) compared to PBMCs from healthy donors (n=6) which were set as 1. Bars represent the mean ± SD. One-way ANOVA. *p<0.05. ns=not significant. **(B)** *SREBF2* gene expression from RT-qPCR experiments. CD34+ HSPCs from huCB, CD34- cells differentiated over three weeks in myeloid culture from huCB-derived HSPCs and CRISPR/Cas9 *t(4;11)* and *t(9;11)* cells were compared to PBMCs from healthy donors. Experiment was performed with n=5 independent donors in technical duplicates with bars representing the mean ± SD. One-way ANOVA. *p<0.05. ***p<0.001. ns=not significant. **(C)** *SREBF2* mRNA expression was analyzed with RT-qPCR. huCB-derived CD34+ HSPCs and PBMCs from healthy donors were compared to SKM-1 and *t(4;11)* as well as *t(9;11)* cell lines whereas PBMCs were set as 1. Data are shown as mean ± SD. n=3. Modified from Erkner *et al.* [202].

4.1.3 A high *SREBF2* mRNA expression leads to specific upregulation of downstream key regulators of cholesterol metabolism in *t(4;11)* leukemia

Since the initial analyses clearly showed that cells with a *t(4;11)* translocation had the highest *SREBF2* mRNA expression, the subsequent experiments were performed with these cells. To confirm the differential expression of SREBP2 at the protein level, Western blot analysis was performed. A specific antibody was used to detect the 125 kDa precursor form and the active, N-terminal domain of the SREBP2 protein relative to Glyceraldehyde-3-phosphate dehydrogenase (GAPDH) as an internal reference. Importantly, *t(4;11)* cells of our CRISPR/Cas9 model showed predominantly a high expression of the active, N-terminal form of SREBP2 [202] (**Figure 17A**). As a central transcription factor, SREBP2 is able to activate

several downstream rate-limiting enzymes of cholesterol metabolism. For this purpose, the basal expression of cholesterol synthesis (**Figure 17B**) as well as cholesterol import and efflux proteins were evaluated (**Figure 17C**). *t(4;11)* cells especially showed a high expression of mevalonate/sterol synthesis proteins (HMGCS, SQLE) and cholesterol import receptors (LDLR). In contrast, cholesterol efflux, which is regulated by ABCA1 expression, was barely increased.

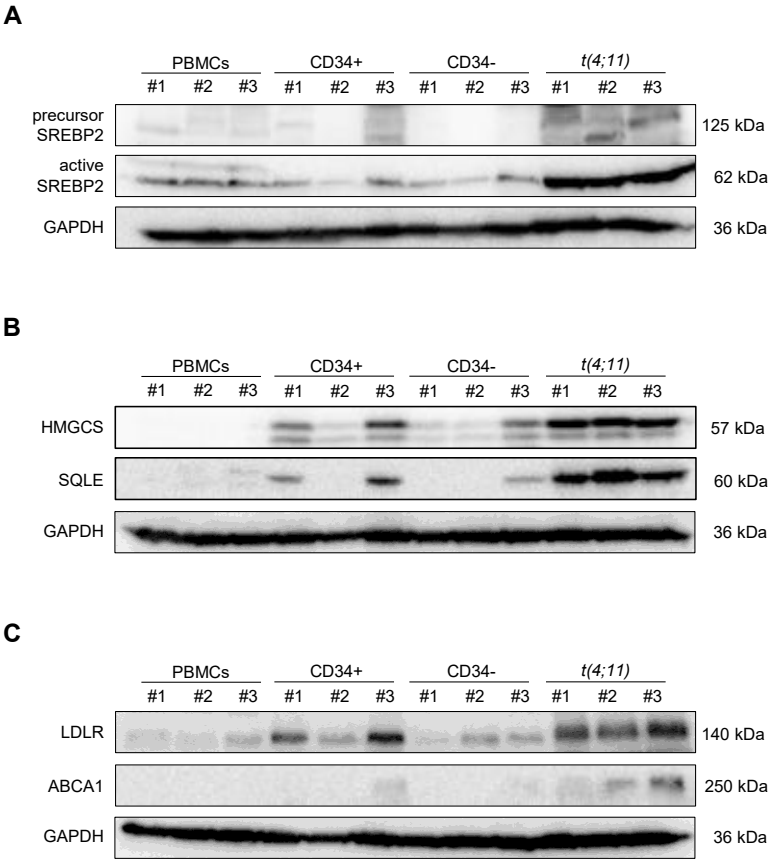

Figure 17: Protein expression pattern of SREBP2 and its downstream targets of cholesterol synthesis, import, and efflux.

Representative Western blot analysis of full length and N-terminal SREBP2 **(A)**, HMGCS and SQLE **(B)**, LDLR and ABCA1 **(C)** in PBMCs from healthy donors, CD34+ HSPCs from huCB, CD34- cells differentiated over three weeks in myeloid culture from huCB-derived HSPCs, and CRISPR/Cas9 *t(4;11)* cells. For each sample, 50 µg of total cell lysate was used, and Glyceraldehyde-3-phosphate dehydrogenase (GAPDH) served as loading control. # describes independent donors. Modified from Erkner *et al.* [202].

In conclusion, these data indicate that SREBP2, a key regulator of cholesterol metabolism, is overexpressed in *KMT2A*r leukemia and correlates with poor patient prognosis. In particular, cells with a *t(4;11)* translocation appear to be dependent on SREBP2-mediated cholesterol metabolism [202].

4.2 Independency of endogenous and exogenous cholesterol supply

4.2.1 Total intracellular cholesterol content in *t(4;11)* leukemia does not differ from healthy HSPCs

There are conflicting studies regarding the intracellular cholesterol concentration of leukemic cells [135-137]. They do not allow a definitive statement on the dependence of the available free cholesterol in degenerated cells of the hematopoietic system. Since SREBP2 serves as a master regulator of cholesterol metabolism and has intracellular cholesterol-regulating properties, the total intracellular cholesterol content was measured using the Amplex Red Cholesterol Assay kit. The measurement consists of several enzyme-coupled reactions and involves the catalyzed oxidation of cholesterol. The released hydrogen peroxide reacts with the contained Amplex Red reagent to form the fluorescent resorufin. By prior addition of cholesterol esterase, stored cholesterol in the form of cholesteryl esters was also included in the analysis (**Figure 18A**).

As a result, no difference in intracellular cholesterol levels was detected between CD34+ HSPCs (10.9±2.25 ng/µg) and CRISPR/Cas9 *t(4;11)* cells (11.4±0.97 ng/µg) (**Figure 18B**). It is assumed that *t(4;11)* cells immediately consume excess of cholesterol to promote proliferation and to avoid an SREBP2-mediated negative feedback of sterol metabolism [202].

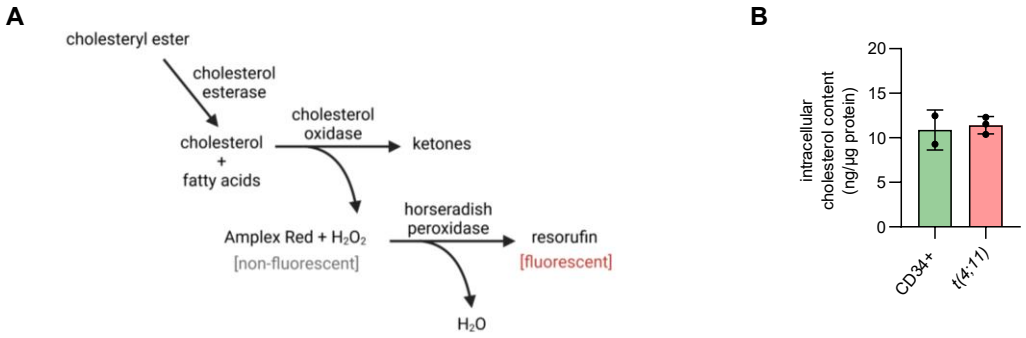

Figure 18: Intracellular cholesterol level in *t(4;11)* leukemia cells.

(A) Amplex Red Cholesterol Assay as enzymatic method used for the quantification of cholesterol based on cholesterol oxidase-peroxidase coupled reaction. **(B)** Total intracellular cholesterol contents in CD34+ HSPCs huCB (n=2) and CRISPR/Cas9 *t(4;11)* cells (n=3) were analyzed with Amplex Red Assay and normalized to protein concentration. Data are shown as mean ± SD. Modified from Erkner *et al.* [202].

4.2.2 The growth of *t(4;11)* leukemia cells is independent of exogenous cholesterol and GGPP supply

The results so far indicate that *t(4;11)* leukemia cells increase their cholesterol requirements by *de novo* SREBP2-mediated synthesis. Another important question is whether these highly proliferating cells also use exogenous cholesterol for their growth. To analyze this, two different metabolites of the cellular cholesterol synthesis program were used. First, cholesterol as the main product of the sterol pathway and second, GGPP from the isoprenylation pathway, were added to the cell culture medium.

The total number of viable cells after four days in culture was determined by excluding trypan blue-positive cells under normal culture conditions of CRISPR/Cas9 *t(4;11)* cells and also by starving the cells without addition of the appropriate cytokines. As an internal control, cells were also treated with the highest concentration of solvent. Since an overdose of exogenous cholesterol can lead to toxic side effects, the optimal concentration range without cytotoxicity was previously determined (data not shown). In this context, cell growth was significantly inhibited without the cytokines, but no proliferative advantage of the cells was observed when cholesterol was added (**Figure 19A**). Since avoidance of apoptosis is considered to be a key mechanism of leukemic cells, cholesterol supplementation was an important point to investigate in terms of the occurrence of apoptotic cells. The percentage of cells entering early and late apoptotic stages was investigated using PI as a viability dye and Annexin V staining of phosphatidylserine. Under normal culture conditions, 13.5%±2.61% of the cells were early apoptotic and 6.3%±2.09% were late apoptotic. Starvation of the cells increased the percentages to 23.1%±7.73% early apoptosis and 49.1%±8.18% late apoptosis (**Figure 19B**). Again, the addition of cholesterol had no effect on this distribution. Almost identical results were observed when GGPP, the major metabolite for isoprenylation of proteins, was added to the cells (**Figure 20**).

These data thus confirm that *t(4;11)* leukemia cells regulate their growth potential independently of external cholesterol metabolites and use only their own *de novo* synthesis for this purpose.

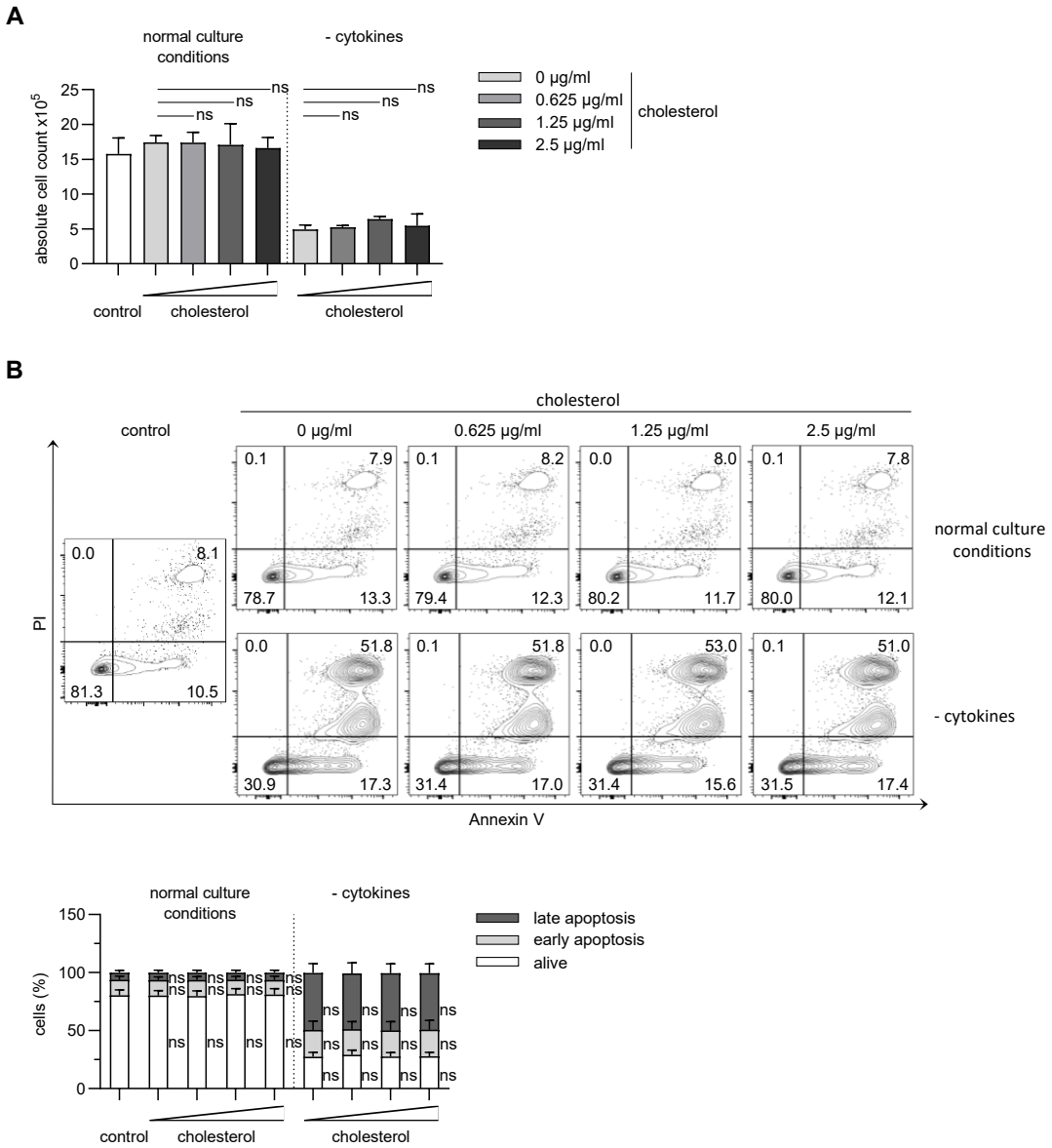

Figure 19: The effect of exogenous cholesterol on growth potential and apoptosis of *t(4;11)* cells. CRISPR/Cas9 *t(4;11)* cells were seeded at their optimal density at 7.5 x 10^5 cells/ml and supplemented with indicated concentrations of cholesterol for 24 hours. Cells were cultured under normal culture conditions as previously described and starved without addition of cytokines. **(A)** Cells were counted with trypan blue and absolute cell number was determined. **(B)** Representative dot plots and pooled data showing living (Annexin V-, PI-), early apoptotic (Annexin V+, PI-) and late apoptotic cells (Annexin V+, PI+). Experiments were performed with n=3 independent donors in technical duplicates with bars representing the mean ± SD. One-way ANOVA. ns=not significant.

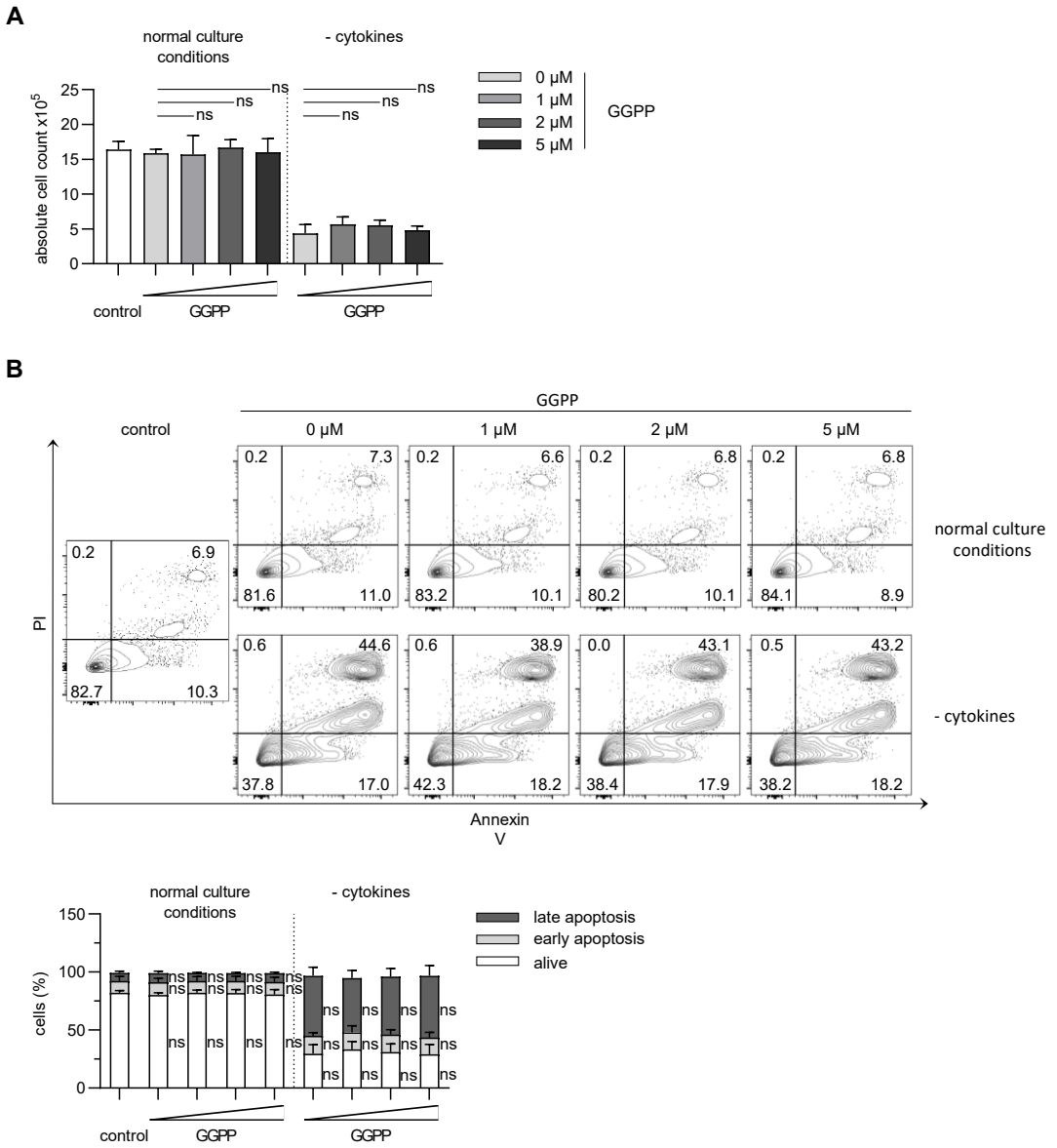

Figure 20: The effect of exogenous GGPP on growth potential and apoptosis of *t(4;11)* cells.
CRISPR/Cas9 *t(4;11)* cells were seeded at their optimal density at 7.5 x 10^5 cells/ml and supplemented with indicated concentrations of GGPP for 24 hours. Cells were cultured under normal culture conditions as previously described and starved without addition of cytokines. **(A)** Cells were counted with trypan blue and absolute cell number was determined. **(B)** Representative dot plots and pooled data showing living (Annexin V-, PI-), early apoptotic (Annexin V+, PI-) and late apoptotic cells (Annexin V+, PI+). Experiments were performed with n=3 independent donors in technical duplicates with bars representing the mean ± SD. One-way ANOVA. ns=not significant.

4.3 shRNA-mediated *SREBF2* kd in *t(4;11)* cells

4.3.1 Establishment of a lentiviral shRNA-mediated *SREBF2* kd in CRISPR/Cas9 *t(4;11)* leukemia cells

Due to the increased expression of SREBP2 in *t(4;11)* leukemia, a special aim of this project was to identify its functional relevance in this type of leukemia. Initial results indicate that leukemia cells are highly dependent on this transcription factor to maintain cell proliferation.
To confirm this, the functional influence of an SREBP2 kd in *t(4;11)* cells was investigated with regard to possible anti-leukemic effects. A pure culture of CRISPR/Cas9 *t(4;11)* cells was transduced with lentiviral particles containing three different shRNAs targeting *SREBF2*. For this purpose, Horizon Discovery offers shRNAs in the pLKO.1 lentiviral vector system, which have been designed and tested by the RNAi Consortium (TRC). The shRNA sequences against *SREBF2* used in this work are shown in **Figure 21A**. A TRC lentiviral non-targeting control shRNA with puromycin resistance was used as a control. A subsequent seven-day selection of the shRNA-expressing cells (sh *SREBF2* and sh control) with puromycin ensured the exclusion of non-transduced cells. Samples were collected and checked throughout the cultivation period of the cells, and kd stability was ensured throughout the experimental period (data not shown).
The successful downregulation of *SREBF2* in *t(4;11)* cells was analyzed by RT-qPCR and Western blot. RT-qPCR showed that the relative mRNA expression was reduced by at least 50% to 75% in the transduced and selected sh*SREBF2* expressing cells (**Figure 21B**). Western blot analysis confirmed the results at the mRNA level, showing the strongest downregulation of SREBP2 with shRNA #688 for both the precursor and the active protein form (**Figure 21C**). Since SREBP2 is a transcription factor with multiple downstream targets, a further RT-qPCR was performed to detect the impaired transcriptional activity of SREBP2. Selected genes involved in cholesterol synthesis (*HMGCR*, *HMGCS1*, *SQLE*, *MSMO1*, *FDFT1*, *SC5D*) showed a significant reduction in mRNA expression. In addition, genes encoding for membrane receptors for cholesterol import (*LDLR*) and efflux (*ABCA1*) were restricted in their expression. These results were confirmed with shRNA #668 as the most effective shRNA with the highest downstream effects (**Figure 21D**).

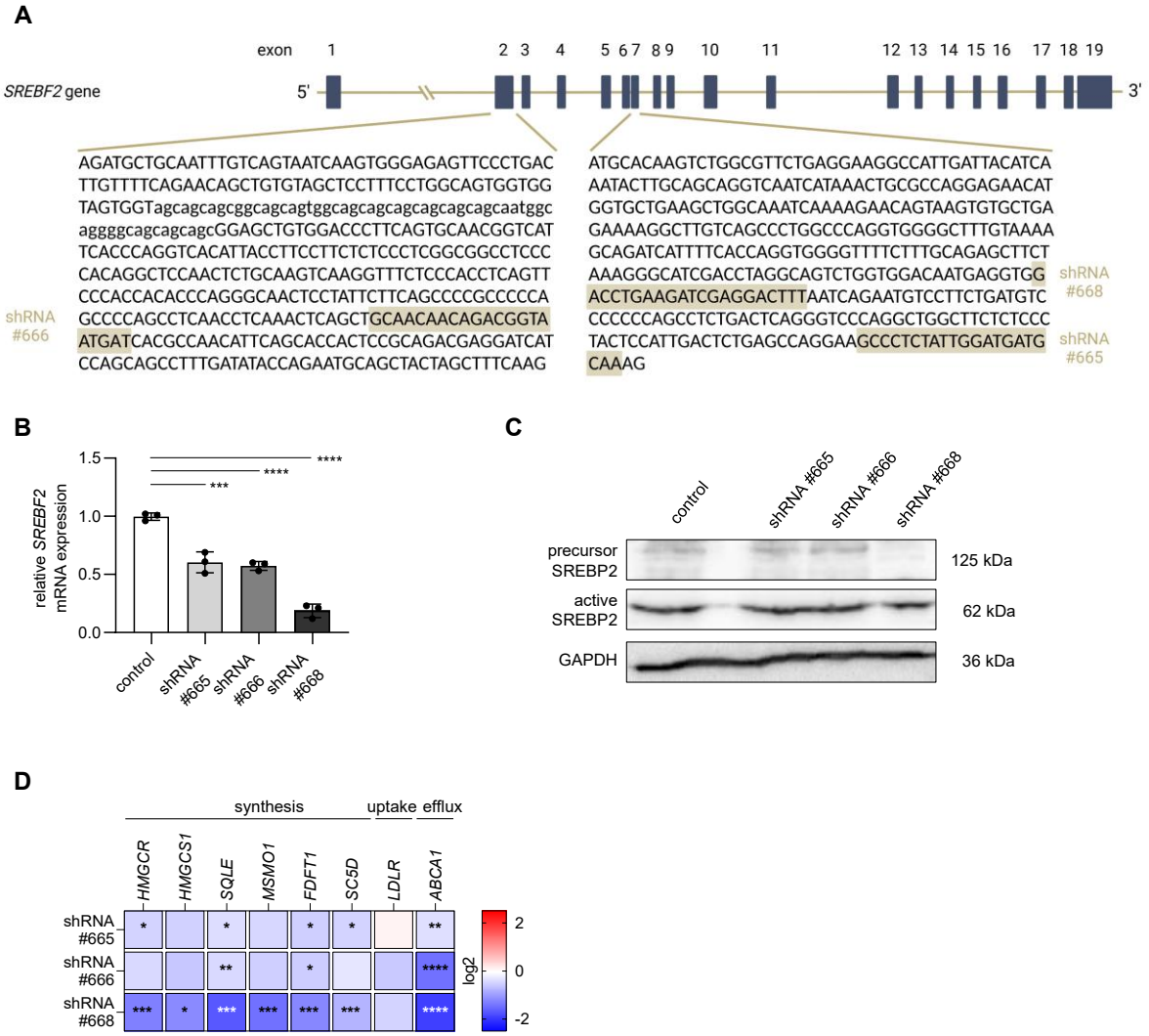

Figure 21: Gene editing by shRNA-mediated kd to reduce SREBP2 expression in CRISPR/Cas9 *t(4;11)* cells.

(A) Illustration of the *SREBF2* gene with its 19 exons and sequences of exon 2 and exon 7 with the selected shRNAs. Figure generated with BioRender. Analysis of relative *SREBF2* mRNA expression from RT-qPCR experiments **(B)** and SREBP2 protein expression **(C)** following lentiviral transduction with shRNA-containing constructs and puromycin selection for seven days. A non-targeting shRNA was used as control. Experiment was performed with n=3 independent donors with bars representing the mean ± SD. One-way ANOVA. ***p<0.001. ****p<0.0001. For representative Western blot analysis, 30 µg of total cell lysate was used, and GAPDH served as loading control. **(D)** Heat map display of fold changes (in log2) of cholesterol pathway-related target gene expression in CRISPR/Cas9 *t(4;11)* cells, which were transduced with shRNA-containing plasmids and analyzed with RT-qPCR. Each square represents the mean of three independent donors (n=3) ± SD compared with cells transduced with a non-targeting shRNA. One-way ANOVA. *p<0.05. **p<0.01. ***p<0.001. ****p<0.0001.

4.3.2 A stable *SREBF2* kd is not sufficient to induce significant anti-leukemic effects in *t(4;11)* leukemia cells

After successful transduction and detection of SREBP2 kd, shRNA-expressing control and low *SREBF2*-expressing *t(4;11)* cells were then examined for their proliferative capacity over a period of one week. The number of viable cells was determined two, four and seven days after cell seeding by staining and counting cells with trypan blue. After determination of the absolute cell count, the cells were returned to their original density (0.75 x 10^6/ml) and fresh medium was added. All populations showed a similar cell growth pattern, with the *SREBF2*-deficient cells tending to have slightly lower cell numbers. However, these effects were not significant (**Figure 22A**).

Although the number of apoptotic cells isolated from the circulation of leukemic patients varies, the results agree that the number of leukemic cells undergoing spontaneous apoptosis is relatively low compared to healthy cells. Furthermore, the dysregulation of apoptosis in leukemia is due to an abnormal expression or mutation of genes. For this purpose, the determination of apoptosis in *SREBF2*-deficient cells was be investigated. *t(4;11)* cells were analyzed for the occurrence of Annexin V+ and PI+ cell populations to detect cells in early and late apoptotic stages. The results showed a high percentage of viable cells in the control cell population (81.6%±1.91%) with equal numbers of *SREBF2*-deficient cells of shRNA #665 (82.6%±1.95%) and shRNA #666 (79.2%±1.93%), whereas cells expressing shRNA #668 (70.4%±3.27%) showed a significant decrease in viable cells and an increase in early and late apoptotic cells (**Figure 22B**).

In addition to the aberrant control of apoptosis, deregulation of cell cycle control has been shown to contribute to an increased proliferation of leukemic cells. In particular, AML with chromosomal aberrations are associated with alterations that promote a more rapid entry into S-phase without a stable G1 phase or a skipping of the DNA damage response, resulting in uncontrolled expansion. Several studies describe that overexpression of PLK1, FOXM1, SET or loss of p53 function allows cells with damaged DNA to enter mitosis without G2 checkpoint inhibition [218]. Pharmacological blockade of SREBP2 in solid tumors disrupted the cell cycle through G2 phase arrest and induced apoptosis [190]. However, the fundamental molecular link between SREBP2 and the cell cycle is still not fully understood. Therefore, a cell cycle analysis of the transduced *t(4;11)* cells should be performed. Although the effects were again marginal, BrdU incorporation into the DNA strand was significantly diminished in *SREBF2*-deficient *t(4;11)* cells, indicating a reduced cell population in the replication phase (control: 20.9%±1.30%; shRNA #665: 19.5%±0.69%; shRNA #666: 18.8%±1.88%; shRNA #668: 14.6%±4.10%). DNA content analysis with 7-AAD confirmed that *SREBF2* kd cells showed an increased occurrence of apoptotic cells compared to the non-targeting shRNA control (control: 9.2%±2.51%; shRNA #665: 9.0%±1.85%; shRNA #666: 13.0%±2.83%; shRNA #668: 13.1%±1.37%) (**Figure 22C**).

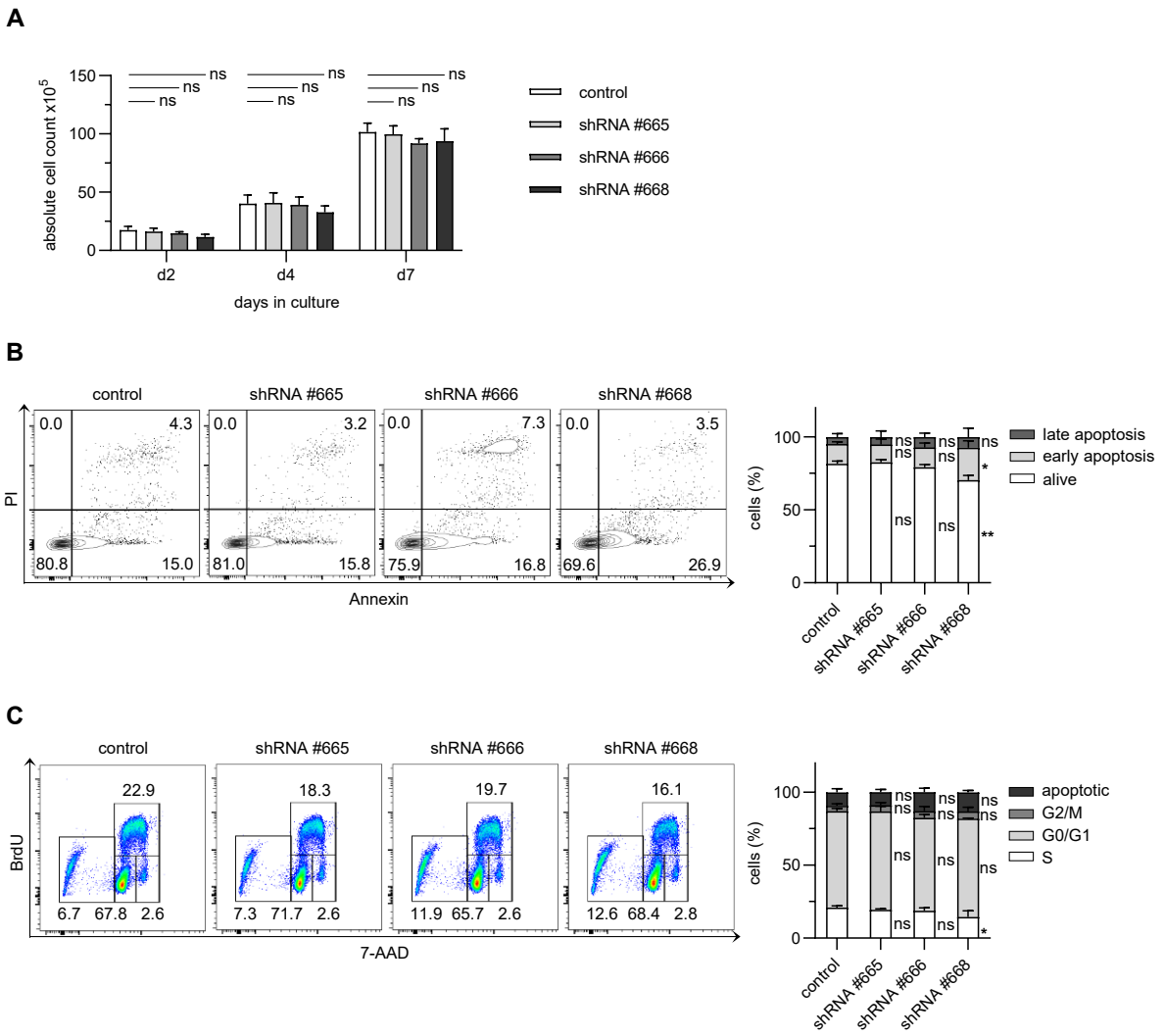

Figure 22: Analysis of CRISPR/Cas9 *t(4;11)* SREBP2 kd cells regarding their leukemic properties. **(A)** Control and *SREBF2*-deficient CRISPR/Cas9 *t(4;11)* cells were seeded at their optimal density at 7.5 x 10^5 cells/ml. Cells were counted with trypan blue on day two, four and seven and reseeded at their original density. To determine apoptosis **(B)** and cell cycle stages **(C)**, cells were cultured for two days under equal growing conditions and analyzed by flow cytometry. A non-targeting shRNA was used as control. Experiments were performed with n=3 independent donors in technical duplicates with bars representing the mean ± SD. One-way ANOVA. **p*<0.05. ***p*<0.01. ns=not significant.

In summary, all selected shRNAs against *SREBF2* were validated for sufficient gene kd with functional downstream effects. shRNA #668 had both the highest kd efficiency and the strongest anti-leukemic effects in terms of cell growth, apoptosis, and cell cycle changes. Nevertheless, the effects were marginal and in general all cell populations showed comparable characteristics.

4.4 Pharmacological inhibition of cholesterol metabolism

4.4.1 Small molecules for the inhibition of cholesterol pathway

The results so far had been shown a strong expression of SREBP2 in *t(4;11)* leukemia cells in the context of the pathophysiology of these cells, but the functional kd of SREBP2 did not seem to have strong anti-leukemic effects. The next step was to identify potential small molecules that could inhibit downstream sterol homeostasis. Three small molecules with different mechanisms of action were selected [202]. We used XY018, a RORγ selective antagonist, which has been shown to act upstream of SREBP2, serving as a master regulator of cholesterol metabolism [159, 198]. We also selected fatostatin (FS), which directly blocks SREBP2 by preventing its translocation to the Golgi apparatus [189], and atorvastatin (ATV), a widely used inhibitor of HMGCR to block cholesterol synthesis [161, 202] (**Figure 23**).

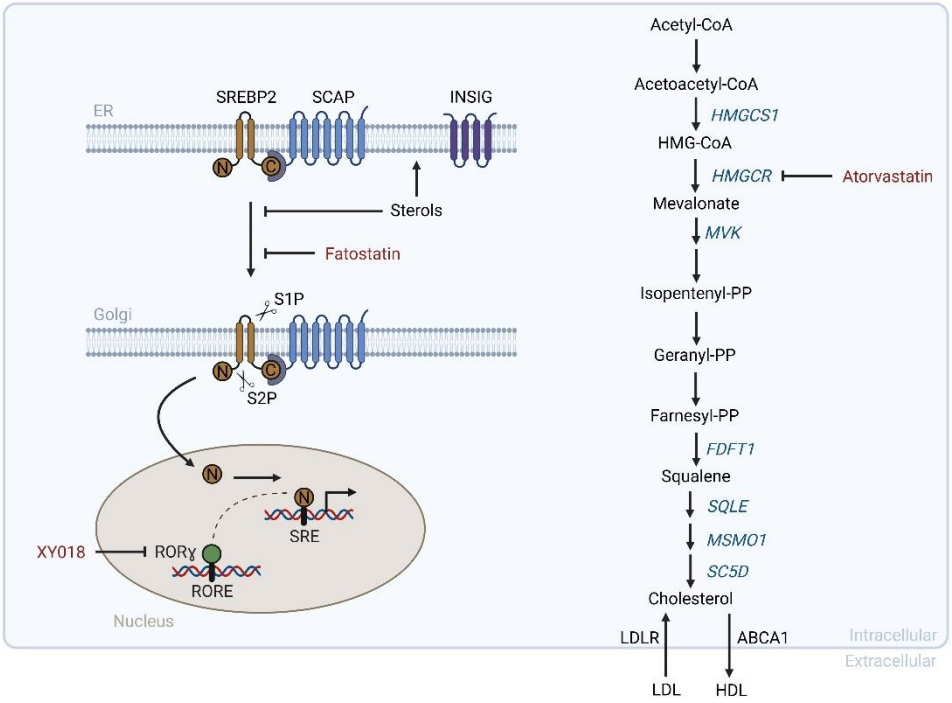

Figure 23: Scheme representing the inhibition of cholesterol metabolism with different compounds.

Fatostatin, which directly blocks SREBP2 by preventing its translocation to the Golgi apparatus [189]; atorvastatin, a widely used inhibitor of HMGCR to block cholesterol synthesis [161]; and XY018, a RORγ selective antagonist [198], were used for the inhibition of cholesterol pathway at different levels [98, 115]. Figure generated with Biorender. Modified from Erkner *et al.* [202].

To define the cytotoxic profile and potential treatment side effects, CD34+ cells were used as control cells due to their also high basal SREBP2 expression. CD34+ cells were freshly isolated from huCB and expanded in culture for a maximum of seven days, while CRISPR/Cas9 *t(4;11)* cells were selected for treatment experiments once a pure culture of translocated cells was achieved. Furthermore, CD34- cells derived from HSPCs and cultured

in myeloid culture for several weeks were selected as a control, expressing low levels of *SREBF2* mRNA. All cell populations were treated with the same inhibitor concentrations *in vitro* for seven days. Cell counts were assessed on days two, four and seven. On each counting day, the cells reseeded to their optimal density using the appropriate control (0 µM) and treated again with the small molecules.

4.4.2 The inhibition of cholesterol metabolism with different small molecules decreases cell growth of *t(4;11)* cells in a dose- and time-dependent manner

First, dose-response profiles of CRISPR/Cas9 *t(4;11)*, CD34+ and CD34- control cells were generated by increasing concentrations of XY018 for seven days, for which Annexin V- and PI- cells were defined as alive. The IC_{50} values of both groups were calculated and compared. For both populations, a dose-dependent decrease in living cells was observed after seven days of treatment. However, CRISPR/Cas9 *t(4;11)* cells showed a significantly lower IC_{50} value (14.6 µM±1.50 µM), while CD34+ HSPCs were more robust (26.7 µM±4.04 µM). Interestingly, CD34- cells, which also showed a low *SREBF2* mRNA expression, had the highest IC50 value (55.1 µM±21.57 µM) (**Figure 24A**). To analyze the effect of the inhibitor in a therapeutic window, cell growth was additionally examined over seven days using trypan blue with selected concentrations of XY018 (**Figure 24B**). The proliferative capacity of *t(4;11)* cells was significantly affected after two days of treatment (0 µM: 30.0±1.52; 10 µM: 26.6±3.92; 15 µM: 21.8±3.68; numbers refer to absolute cell count x 10^5). The effect was evident at day seven after treatment, showing a strong growth inhibition in CRISPR/Cas9 *t(4;11)* cells (0 µM: 59.2±10.77; 10 µM: 37.7±10.89; 15 µM: 15.7±1.61; numbers refer to absolute cell count x 10^5), while CD34+ and CD34- control cells were not significantly affected [202].

So far, the inhibitory effects of XY018 suggest a possible therapeutic window between leukemic and healthy cells. Therefore, the sensitivity of *t(4;11)* cells should be compared to another cell line without the translocation. As mentioned above, cell lines usually carry other genetic aberrations and therefore appear to be more sensitive to anti-proliferative agents. For this reason, the treatment period was shortened and XY018 was added twice to the cell culture on day 0 and day 2 before the percentage of viable cells and the absolute cell count were determined on day 4. A specific sensitivity of the *t(4;11)* cell lines (SEM and RS4;11) was observed in terms of IC_{50} values of the percentage of viable cells compared to the non-translocated cell line SKM-1 (SEM: 3.7 µM±0.81 µM; RS4;11: 6.2 µM±0.37 µM; SKM-1: 10.8 µM±1.10 µM) [202] (**Figure 24C,D**).

SEM and RS4;11 cells are derived from a 5-year-old child and a 32-year-old adult, respectively, and show a B-cell precursor ALL phenotype, whereas the CRISPR/Cas9 *t(4;11)* cells of the translocation model show a more myeloid phenotype. Since the inhibitory effects of XY018 were observed in all *t(4;11)* cells, RORγ appears to play an important role in both *t(4;11)* AML and ALL.

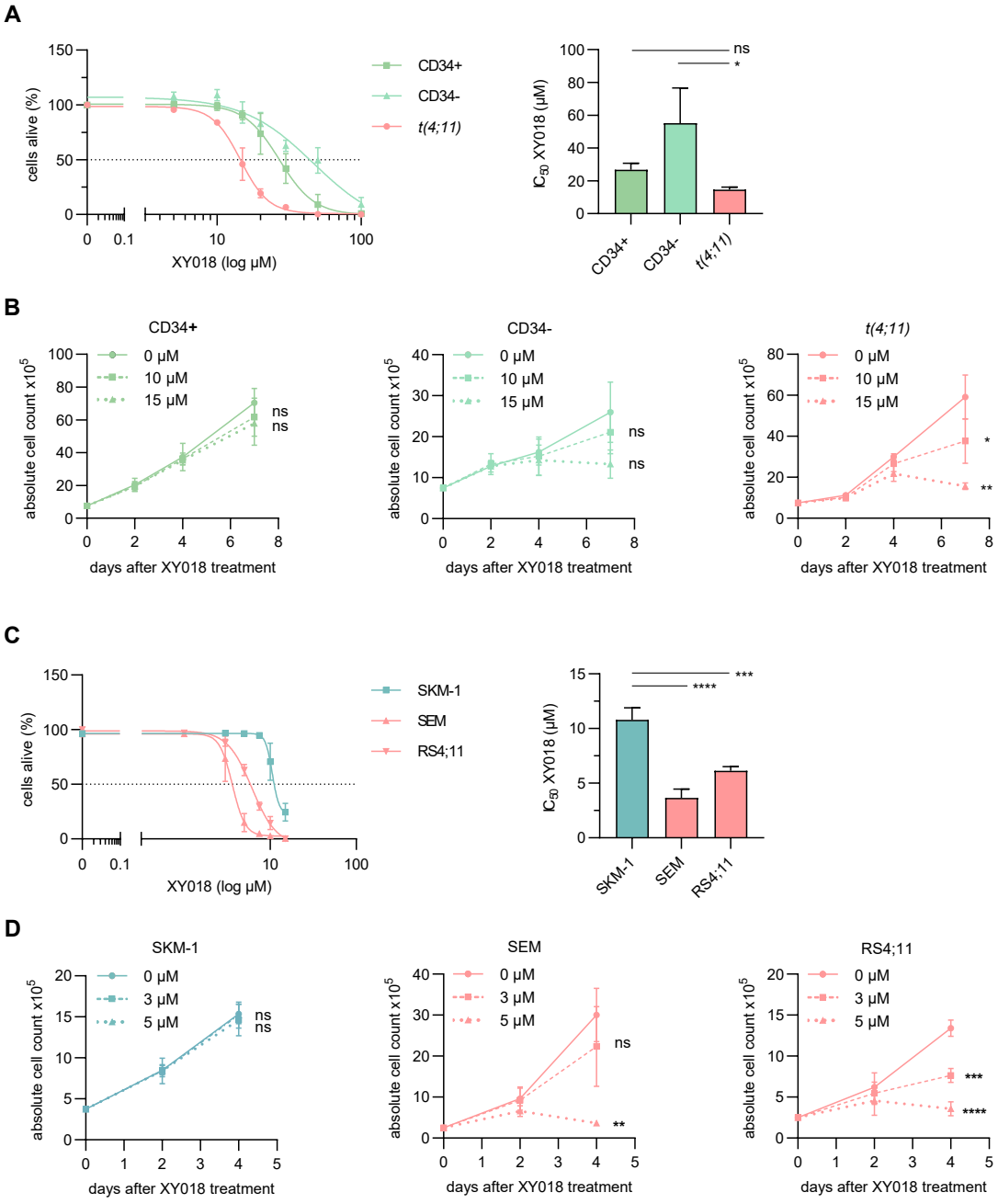

Figure 24: The inhibition of cholesterol metabolism with XY018.

(A) CRISPR/Cas9 *t(4;11)* cells, CD34+ and CD34- control cells were treated with DMSO (0 µM) or increasing concentrations of the RORγ antagonist XY018 for seven days. The percentage of living cells (Annexin V-, PI-) was evaluated with flow cytometry and IC_{50} values were interpolated from a four-parameter logistic model constrained to 0 and 1 in GrapdhPad Prism. **(B)** Cells were counted with trypan blue and absolute cell count was evaluated for different inhibitor concentrations (0 µM, 10 µM, 15 µM) for a total of seven days. Experiments were performed with three independent donors (n=3) in technical triplicates representing the mean ± SD. One-way ANOVA. *p<0.05. **p<0.01. ns=not significant. **(C)** Selected cell lines were treated with increasing concentrations of XY018 for four days. On the fourth day, cells were analyzed for being Annexin V- and PI- and IC_{50} values were determined as described in (A). **(D)** Cell lines were counted with trypan blue and absolute cell count was evaluated for different inhibitor concentrations (0 µM, 3 µM, 5 µM) for a total of four days. Data are shown as mean ± SD. n=3.

One-way ANOVA. **p<0.01. ***p<0.001. ****p<0.0001. ns=not significant. Modified from Erkner *et al.* [202].

Direct inhibition of SREBP2 by FS-induced disruption of SREBP2 processing was also examined in CRISPR/Cas9 *t(4;11)* cells and CD34+ and CD34- healthy cells. In contrast to treatment with the RORγ antagonist, leukemic *t(4;11)* cells had the lowest IC_{50} value (11.9 µM±1.90 µM), but did not show a significant sensitivity to direct SREBP2 inhibition compared to healthy cells (CD34+: 22.6 µM±10.04 µM; CD34-: 18.6 µM±14.22 µM) [202] (**Figure 25**).

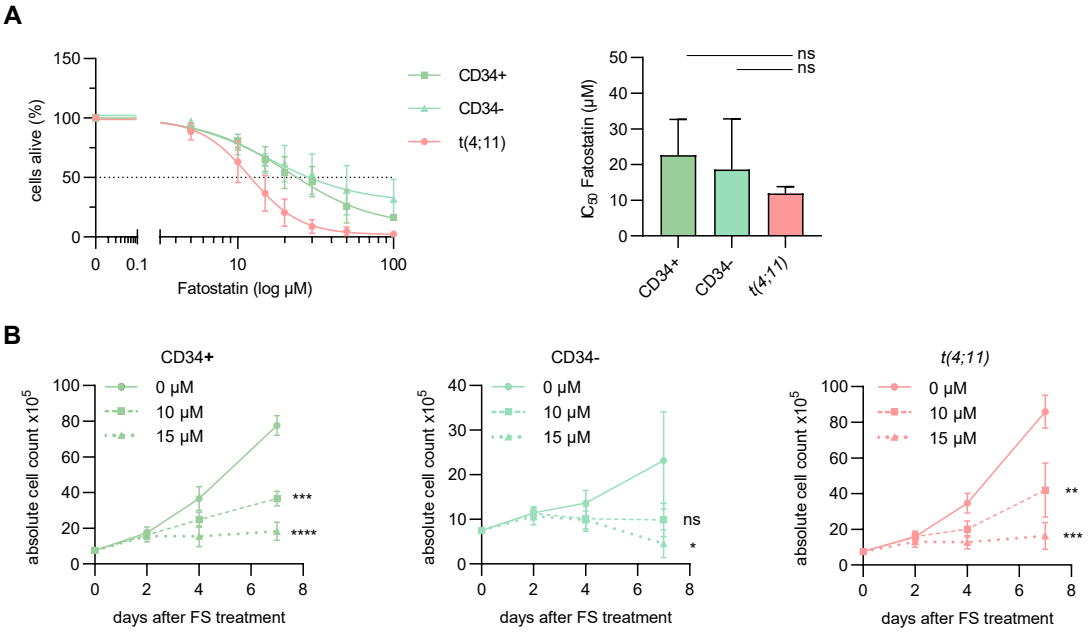

Figure 25: The inhibition of cholesterol metabolism with FS.

(A) CRISPR/Cas9 *t(4;11)* cells, CD34+ and CD34- control cells were treated with DMSO (0 µM) or increasing concentrations of fatostatin for seven days. The percentage of living cells (Annexin V-, PI-) was evaluated with flow cytometry and IC_{50} values were interpolated from a four-parameter logistic model constrained to 0 and 1 in GrapdhPad Prism. **(B)** Cells were counted with trypan blue and absolute cell count was evaluated for different inhibitor concentrations (0 µM, 10 µM, 15 µM) for a total of seven days. Experiments were performed with three independent donors (n=3) in technical triplicates representing the mean ± SD. One-way ANOVA. *p<0.05. **p<0.01. ***p<0.001. ****p<0.0001. ns=not significant. Modified from Erkner *et al.* [202].

In addition, statins have demonstrated efficacy in clinical trials, including several hematologic malignancies [181-183], and have shown anti-proliferative effects in acute leukemia cells in preclinical studies [170-175]. In the *in vitro* setting of this study, ATV was chosen to inhibit cholesterol synthesis because for several reasons. The lipophilic nature allows diffusion-mediated membrane crossing and the addition of a fluorophenyl group provides efficient binding to HMGCR, reflecting some advantages of ATV over other statins (reviewed by [219]). In addition, the longer half-life of ATV has been shown to allow for higher dosing [220].

Compared to XY018 and FS, the half maximal inhibitory concentration of ATV in CRISPR/Cas9 *t(4;11)* cells was almost twice as high (24.6 µM±6.81 µM). In healthy control cells, ATV showed cytotoxic potential in CD34+ and CD34- cells with rather similar IC_{50} values (CD34+: 32.7 µM±8.03 µM; CD34-: 23.2 µM±7.59 µM). Cell growth was significantly affected in both leukemic and healthy cells [202] (**Figure 26**).

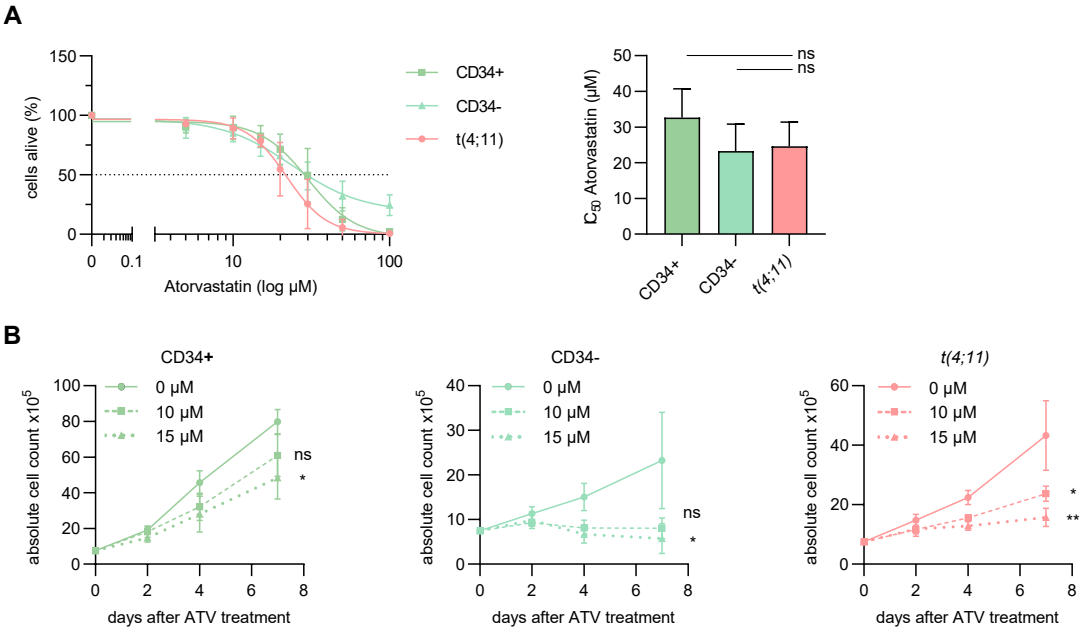

Figure 26: The inhibition of cholesterol metabolism with ATV.

(A) CRISPR/Cas9 *t(4;11)* cells, CD34+ and CD34- control cells were treated with DMSO (0 µM) or increasing concentrations of atorvastatin for seven days. The percentage of living cells (Annexin V-, PI-) was evaluated with flow cytometry and IC_{50} values were interpolated from a four-parameter logistic model constrained to 0 and 1 in GrapdhPad Prism. **(B)** Cells were counted with trypan blue and absolute cell count was evaluated for different inhibitor concentrations (0 µM, 10 µM, 15 µM) for a total of seven days. Experiments were performed with three independent donors (n=3) in technical triplicates representing the mean ± SD. One-way ANOVA. *p<0.05. **p<0.01. ns=not significant. Modified from Erkner *et al.* [202].

4.4.3 Pharmacological inhibition of cholesterol pathway has several downstream effects on the cholesterol-related mRNA expression pattern

Due to the controversial results of the different small molecules, the underlying molecular mechanisms on key cholesterol biosynthesis genes in *t(4;11)* leukemia should be investigated. Therefore, mRNA expression levels of cholesterol-related target genes were measured by RT-qPCR seven days after treatment with the respective inhibitors. As expected, treatment with FS clearly reduced the mRNA expression of cholesterol synthesis genes and increased cholesterol efflux through *ABCA1* transcription. Consistent with previous studies in solid tumors [185, 199], the addition of ATV strongly increased cholesterol biosynthetic genes while

decreasing *ABCA1* due to the known statin-induced feedback of statin-sensitive cells [169, 186]. Interestingly, the effects of the RORγ inhibitor on cholesterol-related target genes were comparable to those of the direct SREBP2 inhibitor FS, but much more pronounced. Regarding the mRNA expression of relevant genes, cholesterol synthesis and uptake were significantly reduced with a concomitant increase in cholesterol efflux [202] (**Figure 27**).

It was also asked whether the gene expression pattern characteristic for of *t(4;11)* and *KMT2A*r leukemia changes with treatment with the different cholesterol-modulating agents. The expression of genes of the *KMT2A*r signature (*MEIS1*, *HOXA9*, *HOXA6*, *MYC*, *PRMT5*) [40, 55, 56] was analyzed by RT-qPCR and showed no significant differences in the treated CRISPR/Cas9 *t(4;11)* cells. In addition, the expression of the leukemic stem cell (LSC) signature genes *CBX5*, *MYB*, and *HMGB3* [221] was not altered (**Supplementary Figure 3**).

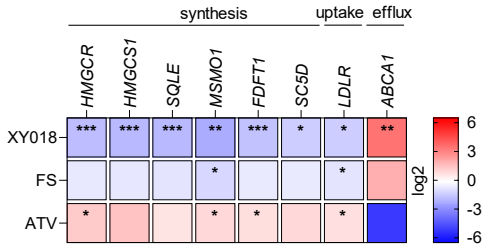

Figure 27: Effect of cholesterol pathway inhibition on the mRNA expression pattern of SREBP2 downstream genes.

Heat map display of fold changes (in log2) in genes of cholesterol homeostasis in CRISPR/Cas9 *t(4;11)* cells treated with 15 µM of each small molecule or 5 nM cytarabine for seven days. The expression of indicated genes was measured by RT-qPCR for which DMSO-treated cells were set as 1. Experiments were performed with three independent donors (n=3) in technical duplicates. One-way ANOVA. **p*<0.05. ***p*<0.01. ****p*<0.001. Modified from Erkner *et al.* [202].

4.4.4 Exogenous cholesterol and GGPP supply does not rescue *t(4;11)* leukemia cell death induced by small molecules

Given that *t(4;11)* cells exhibit enhanced cholesterol homeostasis and are independent of exogenous cholesterol metabolites under normal culture conditions, the question arose whether the anti-leukemic effects mediated by inhibition of cholesterol pathway could be prevented by the addition of exogenous cholesterol or GGPP. To investigate this, CRISPR/Cas9 *t(4;11)* cells were treated with the appropriate inhibitors at a concentration that caused a significant decrease in the viable cell number, but still left the population viable enough to regenerate. Inhibitors were added in combination with increasing concentrations of cholesterol or GGPP for a total of four days, and the percentage of viable cells was examined as the Annexin V- and PI- cell population. No significant proliferative advantage of the cells was observed when cholesterol or GGPP was added to the medium. This may confirm the

previous findings that *t(4;11)* cells are completely independent of exogenous cholesterol metabolites. Surprisingly, double supplementation with fatostatin and cholesterol significantly reduced cell viability (**Figure 28A**). Studies have shown that statin-induced apoptosis in leukemia and multiple myeloma cells can be rescued by exogenous GGPP [170, 222, 223]. Such an effect was also suggested in the *t(4;11)* cells, which showed a slight increase in cell viability when GGPP was added to ATV-treated cells, although this was not significant (**Figure 28B**). Supplementation of XY018-treated cells with cholesterol and GGPP did not alter cell viability, again suggesting that even when cholesterol metabolism is inhibited in *t(4;11)* leukemia cells, these cells are independent of exogenous cholesterol metabolites.

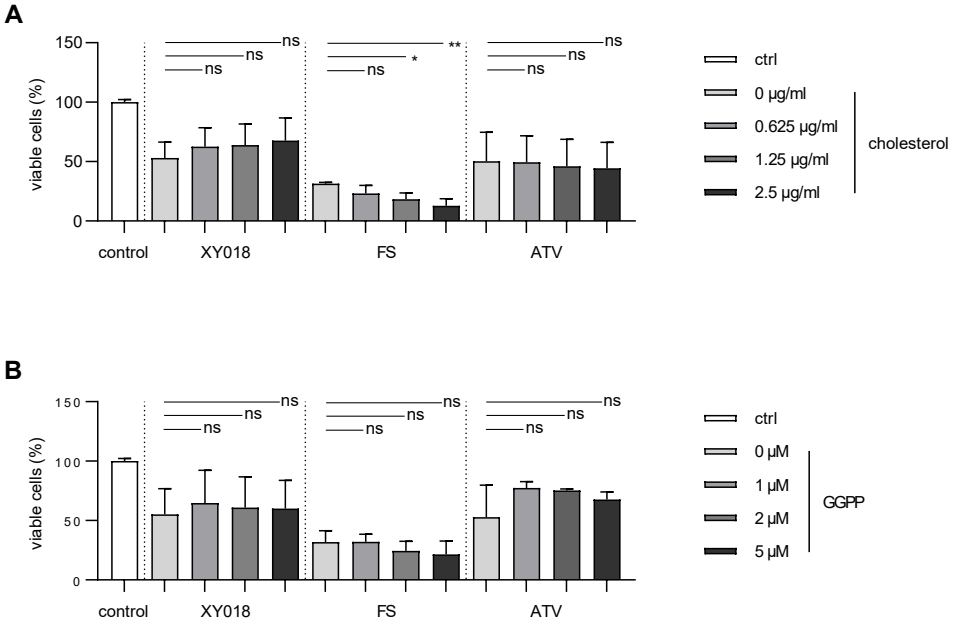

Figure 28: Effects of exogenous cholesterol and GGPP supplementation on the growth of *t(4;11)* cells treated with cholesterol-modulating agents.

CRISPR/Cas9 *t(4;11)* cells were seeded at their optimal density at 7.5 x 10^5 cells/ml and supplemented with indicated concentrations of cholesterol **(A)** or GGPP **(B)**. Simultaneously, cells were treated with XY018, FS or ATV (20 µM each) for 48 hours. Counting was performed with trypan blue and absolute cell number was determined. Experiments were performed with n=3 independent donors in technical duplicates with bars representing the mean ± SD. One-way ANOVA. **p*<0.05. ***p*<0.01. ns=not significant.

These data suggest that inhibition of cholesterol metabolism leads to specific anti-leukemic effects in CRISPR/Cas9 *t(4;11)* cells and *t(4;11)* cell lines [202]. Notably, only the RORγ selective antagonist XY018 induced leukemic cell death without affecting healthy control cells. Endogenous cholesterol metabolism correlated with cell growth and promoted *t(4;11)* leukemogenesis.

4.5 Pharmacological inhibition of RORγ induces anti-leukemic effects in *t(4;11)* leukemia

4.5.1 Basal expression of intranuclear RORγ

As previously reported, RORγ may act as a possible upstream regulator of SREBP2 [159, 160]. Since XY018 is a RORγ selective antagonist and has shown efficacy in inhibiting cholesterol metabolism in *t(4;11)* leukemia, it was of interest to analyze the RORγ expression in different cells. An unconjugated and APC-conjugated anti-RORγ antibody that reacts with human RORγ and the RORγ(t) isoform was used for Western blot and flow cytometric analysis. To analyze intranuclear RORγ expression, cells were fixed and permeabilized, stained with an APC-labelled antibody, and then analyzed by flow cytometry. Among primary cells, the frequency of RORγ+ cells was highest in CD34+ HSPCs (91.3%±4.57%) and CRISPR/Cas9 *t(4;11)* leukemia cells (85.1%±10.00%) compared to healthy PBMCs (4.3%±1.92%) and CD34- differentiated HSPCs (51.0%±5.35%). Analysis of previously used leukemic cell lines showed no difference in intranuclear RORγ expression between non-*t(4;11)* and *t(4;11)* cell lines. All cell lines showed the presence of up to 90% RORγ+ cells (**Figure 29A**). To validate the results, whole cell lysates were examined for semi-quantitative analysis of total RORγ protein by Western blot. The results showed a significant accordance of RORγ in PBMCs from healthy donors, CRISPR/Cas9 *t(4;11)* cells, and *t(4;11)* cell lines. It can be assumed that PBMCs, which also contain immature CD4+ and CD8+ lymphocytes and subpopulations, express RORγ(t), whereas *t(4;11)* leukemia cells express RORγ [202] (**Figure 29B**).
Comparison of the results with public databases again showed, as previously with *SREBF2*, a higher *RORC* mRNA expression, the gene encoding for RORγ, in AML patients with *t(4;11)* leukemia compared to healthy BM samples, AML patients with normal karyotype as well as *KMT2A*r in pro-B-ALL patients. Although the results showed statistical significance, the differences in gene expression were clearly smaller than the previously studied *SREBF2* mRNA expression. Indeed, increased *RORC* expression did not correlate with poor survival of AML patients, suggesting a SREBP2-specific role in leukemia development [202] (**Supplementary Figure 4A,B**). To further distinguish between RORγ and RORγ(t), primers for RT-qPCR were designed to detect both *RORC* and *RORC(t)* in the previously analyzed cell types. Primer efficiency was tested in cell lines already known to be positive for the respective isotype (HepG2 for *RORC*, Jurkat for *RORC(t)*). Both healthy PBMCs and CD34- cells showed a high mRNA expression of *RORC(t)*. Surprisingly, the mRNA expression of the other cell types was very low. This suggests that in the case of RORγ and RORγ(t), mRNA and protein expression may not be concordant (**Supplementary Figure 4C**).

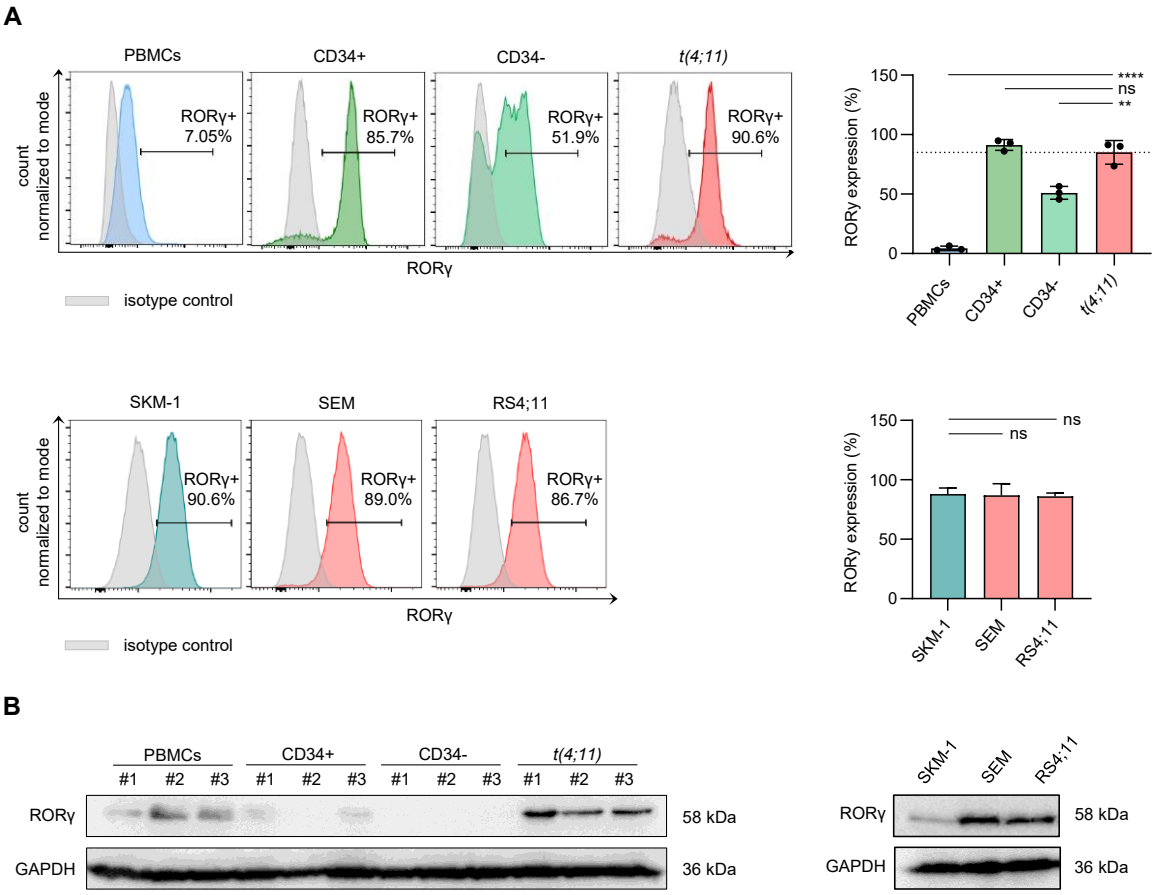

Figure 29: Basal expression pattern of intranuclear RORγ+ cells and amount of RORγ total protein.

(A) Representative flow cytometry histograms of intranuclear RORγ expression and pooled data from independent donors (n=3) for primary cells and independent experiments (n=3) for cell lines performed in technical duplicates are shown. Bars representing the mean ± SD. One-way ANOVA. ***p*<0.01. *****p*<0.0001. ns=not significant. **(B)** Representative Western blot analysis of RORγ total protein in primary cells and cell lines. For each sample, 50 µg of total cell lysate was used, and GAPDH served as loading control. # describes independent donors. Modified from Erkner *et al.* [202].

4.5.2 XY018 induces apoptosis and changes cell cycle in *t(4;11)* leukemia

Given the previous findings in this work that the RORγ antagonist XY018 had an inhibitory effect on the proliferation of KMT2Ar cells without affecting control cells, the consequences of cholesterol pathway inhibition on apoptosis and cell cycle were investigated.

For this purpose, CRISPR/Cas9 *t(4;11)* and culture-expanded CD34+ control cells were treated with increasing concentrations of XY018 and the externalization of phosphatidylserine during apoptosis was analyzed after seven days of treatment. After XY018 treatment, *t(4;11)* cells showed a significant dose-dependent decrease in the percentage of viable cells (0 µM: 84.1%±0.46%; 10 µM: 70.6%±1.57%; 15 µM: 38.6%±12.36%) and an increase of early apoptotic (0 µM: 6.1%±1.00%; 10 µM: 13.7%±3.75%; 15 µM: 16.8%±5.09%) and late apoptotic cells (0 µM: 9.6%±1.10%; 10 µM: 15.6%±5.31%; 15 µM: 44.6%±16.35%). At the same concentrations, healthy HSPCs were not affected [202] (**Figure 30A**).

To verify the results in the context of *KMT2A*r and non-*KMT2A*r cells, cell lines with different molecular subtypes were subjected to drug sensitivity tests with XY018. In agreement with the previously calculated IC_{50} values, the *t(4;11)* cell lines were more sensitive to the treatment than the non-*KMT2A*r cell line SKM-1. SEM and RS4;11 cells showed a significant increase in Annexin V+ cells, indicating that the inhibitory effect of XY018 is due to programmed cell death among other possible pathways. Under the same conditions, XY018 treatment did not induce apoptosis in the SREBP2 low expressing SKM-1 cell line [202] (**Figure 30B**).

Many anti-cancer drugs inhibit DNA repair or directly induce DNA damage in malignant cells. A key property of normal/healthy cells is their ability to prevent the replication of damaged DNA by activating a complex signaling network, whereas cancer cells often exhibit defects in these cell cycle checkpoints ([128], reviewed by [224]). However, cancer cells respond differently to treatment, with some of the defects increasing their sensitivity to drugs and others increasing their resistance to chemotherapy.

To analyze the mechanism for the XY018-induced anti-proliferative effect in *t(4;11)* cells, the cell cycle distribution was investigated. RORγ inhibition concentration-dependently increased the frequency of arrested *t(4;11)* cells in the G2/M phase and simultaneously decreased the number of cells in the G0/G1 phase. At the same time, a significant increase in the number of cells in the apoptotic phase was observed with increasing XY018 concentration. In addition, XY018 reduced the incorporation of BrdU into the replication phase of nuclear DNA, indicating a reduced S phase of the cells. These effects were observed in CRISPR/Cas9 *t(4;11)* cells as well as in all *t(4;11)* cell lines. The cell cycle in healthy CD34+ and SKM-1 cells was less affected at constant concentrations [202] (**Figure 31**).

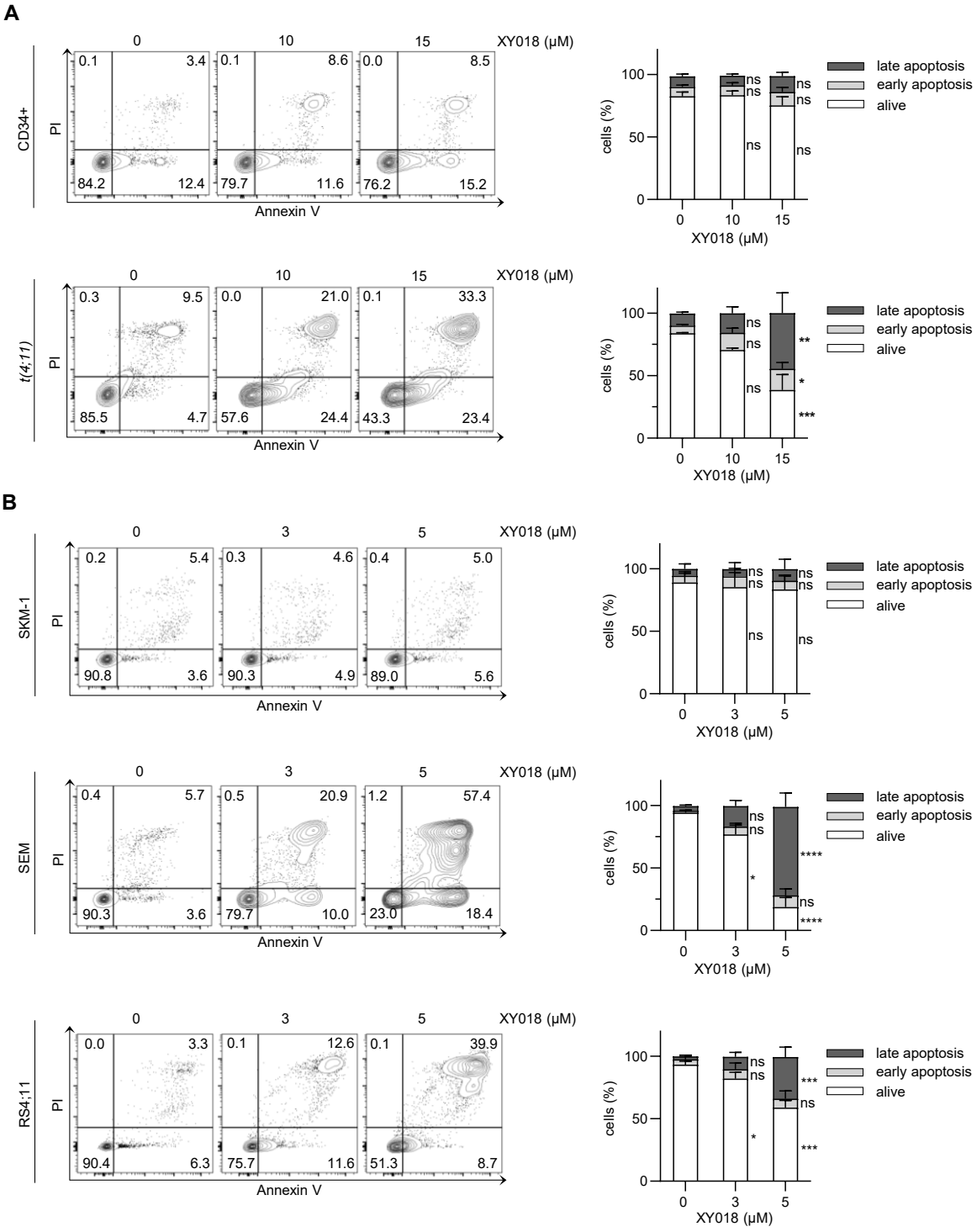

Figure 30: Inhibition of RORγ induces apoptosis in *t(4;11)* cells.

Representative dot plots and pooled data showing living (Annexin V-, PI-), early apoptotic (Annexin V+, PI-) and late apoptotic cells (Annexin V+, PI+). **(A)** CD34+ control and CRISPR/Cas9 *t(4;11)* cells were treated for seven days; **(B)** SKM-1, SEM and RS4;11 cells were treated for four days with indicated concentrations of XY018. Histograms show the mean of three independent donors (n=3) ± SD for primary cells and independent experiments (n=3) for cell lines. One-way ANOVA. *p<0.05. **p<0.01. ***p<0.001. ****p<0.0001. ns=not significant. Modified from Erkner *et al.* [202].

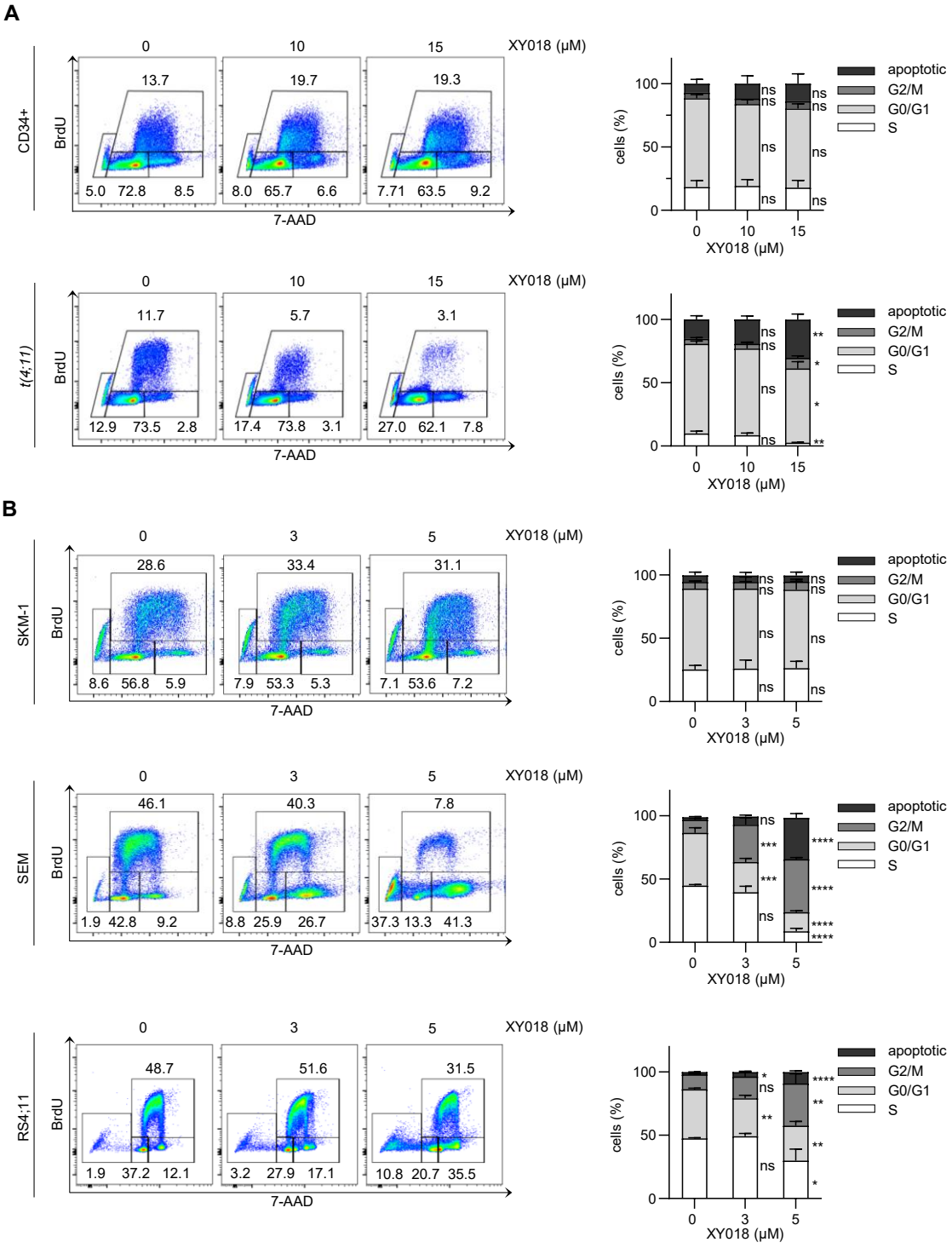

Figure 31: Inhibition of RORγ changes the cell cycle in *t(4;11)* cells.

Representative dot plots and pooled data of cells analyzed for cell cycle distribution using BrdU staining and flow cytometry. **(A)** CD34+ control and CRISPR/Cas9 *t(4;11)* cells were treated for seven days; **(B)** SKM-1, SEM and RS4;11 cells were treated for four days with indicated concentrations of XY018. Histograms show the mean of three independent donors (n=3) ± SD for primary cells and independent experiments (n=3) for cell lines. One-way ANOVA. *p<0.05. **p<0.01. ***p<0.001. ****p<0.0001. ns=not significant. Modified from Erkner *et al.* [202].

4.5.3 XY018 reduced cell viability and metabolic activity in *t(4;11)* leukemia

Since inhibition of the cholesterol pathway is necessarily associated with cellular metabolic activity, the alamarBlue assay was used to measure the metabolic response of the cells exposed to XY018. Similar to the Amplex Red Assay, the alamarBlue assay uses the fluorescent properties of resorufin. The reagent serves as an indicator of cell viability by utilizing the natural reducing ability of viable cells to convert resazurin to the fluorescent resorufin. In conclusion, the reduction of resazurin in the growth media is directly correlated with the proliferative capacity of mammalian cells [225].

CRISPR/Cas9 *t(4;11)* cells showed a reduced relative cell viability after seven days and *t(4;11)* cell lines after four days of treatment with the RORγ antagonist. In contrast, XY018 did not significantly affect cell viability in healthy cells and normal cell lines, including CD34+ HSPCs and SKM-1 cells [202] (**Figure 32**).

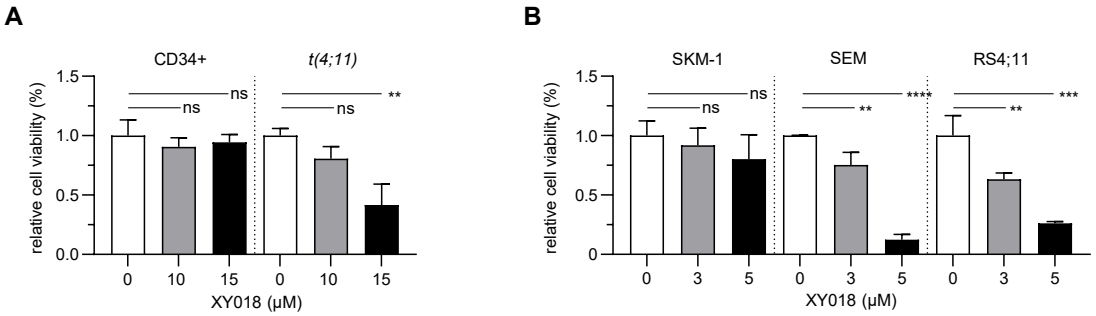

Figure 32: Inhibition of RORγ decreases cell viability of *t(4;11)* cells.

Cells treated with indicated concentrations of XY018 or DMSO (0 µM) were analyzed for cell viability on day seven **(A)** or day four **(B)** of treatment using alamarBlue assay. Changes in viability were analyzed relative to the respective control (0 µM) in each experiment. Bars represent the mean of three independent donors (n=3) ± SD for primary cells and independent experiments (n=3) for cell lines. One-way ANOVA. ***p*<0.01. ****p*<0.001. *****p*<0.0001. ns=not significant. Modified from Erkner *et al.* [202].

These data suggest that the inhibition of RORγ leads to the induction of cell cycle changes and ultimately apoptosis in *KMT2A*r fusion-driven leukemia without negative effects on control cells [202]. A significantly higher expression level of SREBP2 in *t(4;11)* leukemia compared to other acute leukemias and healthy control cells offers a high potential for its inhibition. In summary, the role of cholesterol metabolism in the survival of *KMT2A*r cells was confirmed and can be considered as a targetable pathway for *KMT2A*r cells. Modified from Erkner *et al.* [202].

4.6 RORγ as master regulator of cholesterol metabolism

4.6.1 Reduction of RORγ decreases cholesterol metabolism restricted to *t(4;11)* leukemia cells

Cytotoxic and viability assays with XY018 showed increased sensitivity of CRISPR/Cas9 *t(4;11)* and *t(4;11)* cell lines to the RORγ antagonist compared to control cells. A significantly altered mRNA expression pattern of cholesterol-related target genes in *t(4;11)* cells further supported that the effects were due to inhibition of the cholesterol pathway. As the results regarding a basal intranuclear RORγ expression in *t(4;11)* and non-*KMT2A*r cells were quite controversial, the molecular biological effects after treatment with XY018 were be analyzed in the different cells.

For this set of experiments, primary cells were treated with a DMSO control or 15 µM XY018 for seven days. Cell lines were selected for use at 5 µM and a four day treatment. RT-qPCR was performed and the results are shown as a heat map representation of fold changes (in log2) compared to the DMSO control, respectively. A significant decrease in the mRNA expression of genes involved in cholesterol synthesis and import was observed in CRISPR/Cas9 *t(4;11)* cells, while CD34+ control cells showed only a marginal change in their gene expression pattern. Only the expression of *ABCA1* was upregulated (**Figure 33A**). The mRNA expression pattern of the selected cell lines reflected similar results. While non-*KMT2A*r SKM-1 cells showed no significant changes, gene expression in both *t(4;11)* ALL cell lines was significantly altered at different levels of cholesterol metabolism, suggesting anti-leukemic effects [202] (**Figure 33B**).

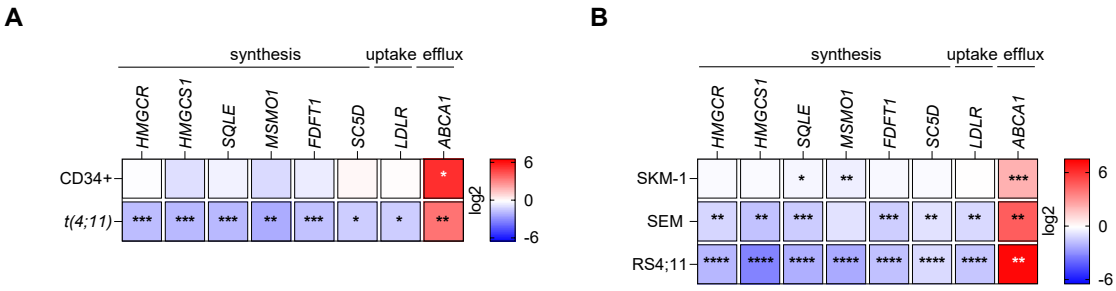

Figure 33: Comparison of the expression pattern of *SREBF2* downstream genes after inhibition of RORγ in different cell types.

(A) Heat map display of fold changes (in log2) of cholesterol pathway-related target gene expression after XY018 treatment in CD34+ control and CRISPR/Cas9 *t(4;11)* cells. Cells were treated with 15 µM XY018 or DMSO for seven days and analyzed with RT-qPCR. **(B)** Heat map display of fold changes (in log2) of cholesterol pathway-related target gene mRNA after XY018 treatment. Cell lines were treated with 3 µM XY018 or DMSO for four days and analyzed with RT-qPCR. Each square represents the mean of three independent donors (n=3) ± SD for primary cells and independent experiments (n=3) for cell lines compared to the respective DMSO control. Student's *t* test. **p*<0.05. ***p*<0.01. ****p*<0.001. *****p*<0.0001. Modified from Erkner *et al.* [202].

Although the results of the inhibitory effect of XY018 on mRNA expression were meaningful, the translation into functional protein synthesis should not be neglected. CRISPR/Cas9 *t(4;11)* cells were incubated with increasing inhibitor concentrations over a period of seven days and total protein expression was analyzed by Western blot from whole cell lysates at different transcription levels. Unexpectedly, measurement of the transcription factor SREBP2 showed only a dose-dependent reduction of the precursor form with marginal effects on the active, N-terminal domain. However, inactivation of the transcriptional activity of SREBP2 was demonstrated in a different way by downregulation of several key factors of the cholesterol regulatory machinery. A clear dose-dependent decrease of HMGCS, SQLE and HMGCR was observed. In addition, the expression of the membrane-bound LDLR with an extracellular ligand-binding domain was reduced. Under normal conditions, the expression of the cholesterol efflux transporter ABCA1 was very low in *t(4;11)* leukemia, but was impressively stimulated by XY018 in a dose-dependent manner [202] (**Figure 34A-D**).

Wang and colleagues have shown that XY018 binds to the hydrophobic RORγ LBD via multiple conserved hydrogen bonds and hydrophobic interactions [198]. Molecular dynamics stimulation studies have also shown that the RORγ-XY018 complex is very stable due to these interactions, and that the total amount of RORγ protein available to the cell decreases with increasing concentrations of the antagonist [198]. To confirm the inhibitory effect of XY018 in *t(4;11)* leukemia, intranuclear RORγ protein expression was again measured by intracellular flow cytometry after CRISPR/Cas9 *t(4;11)* cells were treated with increasing concentrations of XY018. An analogous significant dose-dependent decrease in the RORγ+ cell population was observed (0 µM: 80.8%±3.14%; 10 µM: 75.4%±3.30%; 15 µM: 71.3%±1.65%; 20 µM: 47.0%±20.34%) [202] (**Figure 34E**).

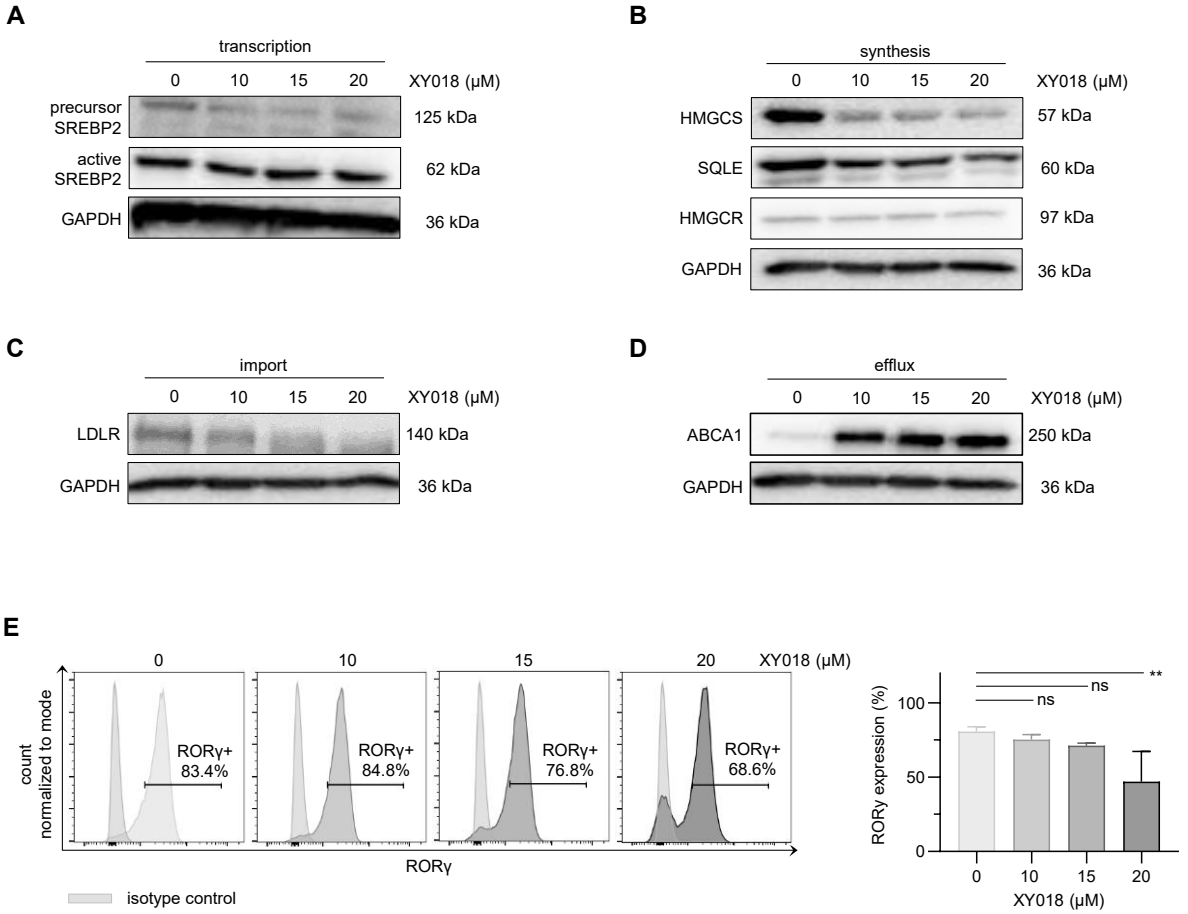

Figure 34: Inhibition of RORγ changes the expression of cholesterol-related proteins in CRISPR/Cas9 *t(4;11)* leukemia cells.

Representative Western blot analysis of full length and N-terminal SREBP2 **(A)**, HMGCS, SQLE, and HMGCS **(B)**, LDLR **(C)** and ABCA1 **(D)** in CRISPR/Cas9 *t(4;11)* cells treated with indicated concentrations of XY018 or DMSO (0 µM) for seven days. For each sample, 50 µg of total cell lysate was used, and GAPDH served as loading control. **(E)** Representative histograms and pooled data show the percentage of intranuclear RORγ+ cells analyzed with flow cytometry. CRISPR/Cas9 *t(4;11)* cells were treated with DMSO (0 µM) or indicated concentrations of XY018 (10 µM, 15 µM and 20 µM) for seven days. Bars represent the mean of three independent donors (n=3) ± SD. One-way ANOVA. ***p*<0.01. ns=not significant. Modified from Erkner *et al.* [202].

Although it was demonstrated that *t(4;11)* leukemia cells do not express higher intracellular cholesterol contents compared to healthy cells, we were interested in analyzing the effects of RORγ inhibition on the intracellular level of total cholesterol. The Amplex Red Assay showed that treatment with XY018 led to a reduction in the amount of total cholesterol content in *t(4;11)* leukemia [202] (**Figure 35**).

This confirmed the previous results that a pharmacological RORγ inhibition reduces functional *de novo* cholesterol synthesis and limits the ability of the cells to proliferate by reducing available intracellular cholesterol.

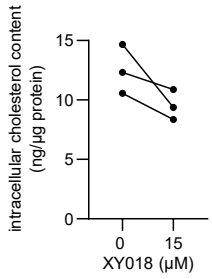

Figure 35: Reduced intracellular cholesterol content after RORγ inhibition.
CRISPR/Cas9 *t(4;11)* cells were treated with DMSO (0 µM) or 15 µM XY018 for seven days and were measured with the Amplex Red Cholesterol Assay Kit after organic extraction and normalized to protein concentration. Each dot represents independent donors. Modified from Erkner *et al.* [202].

4.6.2 RNA-Seq revealed RORγ as molecular driver of SREBP2-mediated cholesterol pathway in *t(4;11)* leukemia

The previous results indicate that RORγ may act as possible upstream regulator of cholesterol metabolism in *t(4;11)* leukemia, as reported by others for solid cancers [159, 199]. Finally, to identify the core transcriptional program that is controlled by RORγ leading to cell growth inhibition, apoptosis, and cell cycle changes, genome-wide RNA-Seq data of XY018-treated CRISPR/Cas9 *t(4;11)* cells were compared to DMSO-treated cells.

For this purpose, CRISPR/Cas9 *t(4;11)* cells were treated with DMSO or 15 µM XY018 for a total of seven days as described above. Library preparation, sequencing, and data quality control were performed by the Genomics Core Facility c.ATG / NCCT of the University Hospital Tübingen. Raw data analysis including alignment, differential gene expression analysis, and Ingenuity Pathway Analysis was performed in collaboration with Dr. Thomas Hentrich. Principle Component Analysis revealed a predominant genotype effect, whereas the treatment effect was comparatively small. However, the genotypic differences between the three donors included in the analysis were also rather small (**Supplementary Figure 5**). After setting significance thresholds, the results showed 189 differentially expressed genes (DEGs), with 91 genes downregulated and 98 genes upregulated in XY018-treated cells compared to controls (**Figure 36A**,

Supplementary Table 2, **Supplementary Table 3**). The top ranked downregulated genes were mainly associated with cholesterol uptake and efflux (*LDLR*, *MSMO1*, *SQLE*, *TMEM97*, *FDFT1*, *HMGCS1*, *HMGCR*, *SC5D*) and confirmed the previously performed RT-qPCR experiments. In contrast, the most highly expressed genes after RORγ inhibition were related to cholesterol efflux (*ABCA1*, *ABCG1*), as previously shown at mRNA and protein level in cells treated with the RORγ antagonist [202] (**Figure 36B**).

Ingenuity Pathway Analysis (IPA) enables the interactive construction of networks representing the biological systems of all DEGs, based on current knowledge of the expected effects between transcription factors and their target genes. The analysis was very clear on this point, showing that RORγ inhibition led to the downregulation of genes which are associated with several sub-pathways of cholesterol metabolism. In particular, the mevalonate and sterol

synthesis pathways were mainly identified, as well as *LXR*/*RXR* activation leading to the transcription of genes encoding for ABC transporters. Upstream transcription factor analysis predicted that the transcriptional function of *SREBF2* in particular significantly decreased in response to treatment with the antagonist. In addition, the function of *SCAP*, *INSIG1* and cholesterol as a metabolite itself were also identified as upstream regulators of the inhibitory effects. MAP2K5 and MAPK7, two protein-coding genes of the MAPK pathway with important functions in cancer-related signaling and apoptosis, were also predicted to be master transcriptional regulators [202] (**Figure 36C,D**).

There was also an increased expression of genes encoding for ribosomal 16S, which we understand to be a compensation mechanism of the cells for the lack of cholesterol. In addition, some mitochondrial genes were upregulated after RORγ inhibition, consistent with the apoptotic phenotype observed [202]. To clarify the upregulation of mitochondrial genes, a cytochrome c release assay was performed on *t(4;11)* cells after treatment with XY018. Cytochrome c is often released from mitochondria into the cytoplasm during the early stages of apoptosis, leading to caspase activation and ultimately apoptotic cell degradation. At all concentrations of XY018 used, more cytochrome c was detected in the mitochondrial fraction compared to control cells. The results confirm an intrinsic activation of the apoptotic pathway with mitochondrial involvement and explain the observed mitochondrial activation with upregulation of genes and pseudogenes in the RNA-Seq. Interestingly, cytochrome c release decreased at the highest inhibitor concentration. To explain this effect, we compared the results with our results from the Annexin V assay and found that at the highest XY018 concentration, a decrease in the early apoptotic cell population (Annexin V+/PI-) was also observed in this assay (**Supplementary Figure 6**).

The results indicate that *t(4;11)* leukemia cells undergo secondary necrosis at certain inhibitor concentrations when treated with XY018 *in vitro*. In addition, the results show that XY018 leads to specific alteration of cholesterol biosynthesis genes and demonstrate the prominent role of RORγ in SREBP2 function in *t(4;11)* leukemia [202].

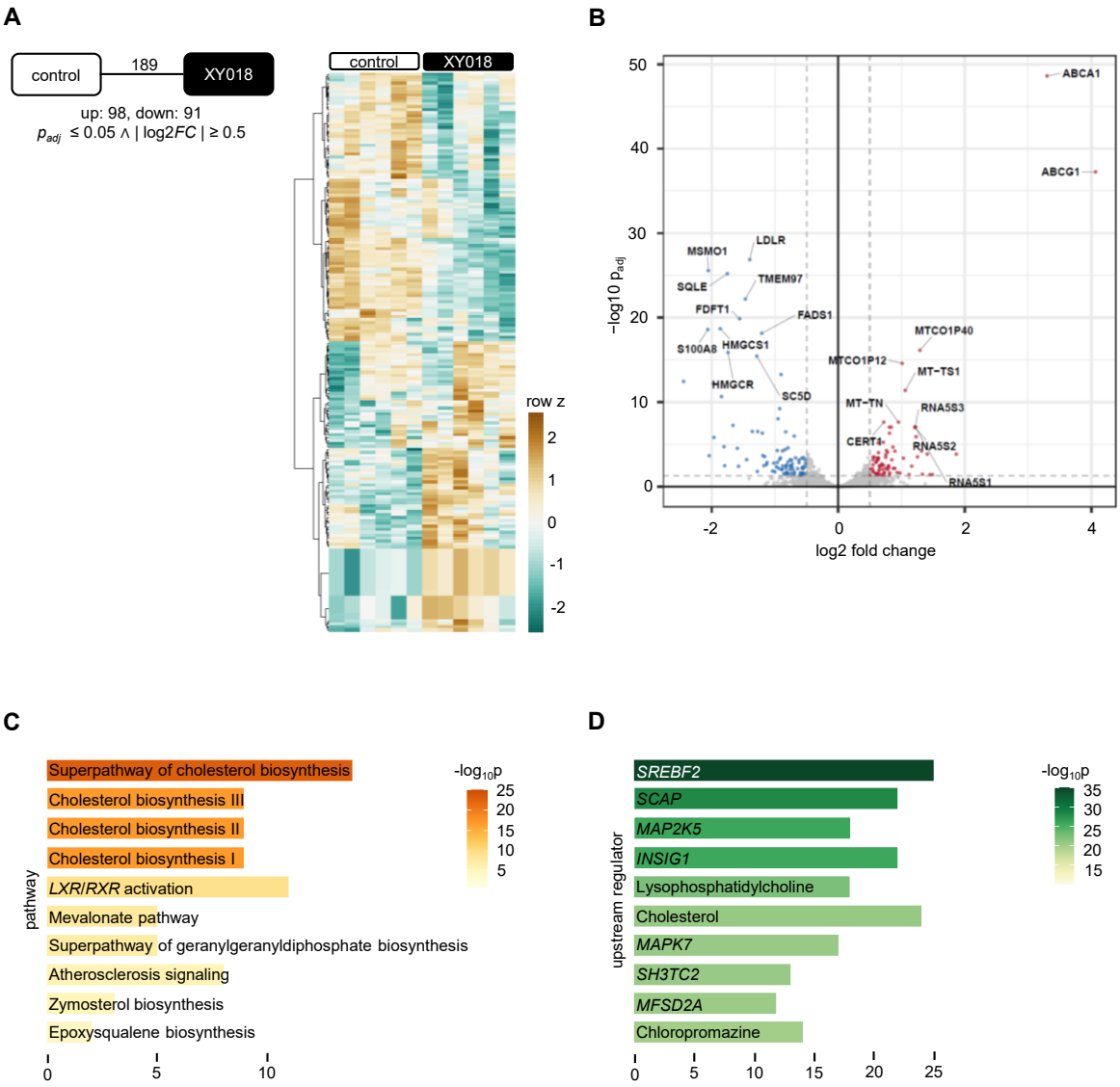

Figure 36: RORγ controls the cholesterol-dependent gene program and is an upstream regulator of SREBP2 in *t(4;11)* cells.

CRISPR/Cas9 *t(4;11)* cells were treated with DMSO (control) or 15 µM XY018 for seven days. Three independent donors (n=3) with biological duplicates were used for RNA-Seq. **(A)** The analysis revealed 189 differentially expressed genes (DEGs). Their expression profile across all samples is shown as z-score. **(B)** Volcano plot highlighting 91 downregulated (blue) and 98 upregulated (red) DEGs. Dotted lines indicate significance thresholds (p_{FDR}≤0.05, |$\log_2$(fold-change)|≥0.5). Top ten overrepresented pathways **(C)** and predicted upstream regulators **(D)** among all DEGs according to Ingenuity Pathway Analysis (IPA) with gene count and significance values in bar graphs. Raw data analysis including alignment, differential gene expression analysis, and Ingenuity Pathway Analysis was performed in collaboration with Dr. Thomas Hentrich. Modified from Erkner *et al.* [202].

4.7 Combinatorial treatment of *t(4;11)* leukemia

4.7.1 RORγ inhibition in combination with chemotherapy

The results so far show the extent to which *t(4;11)* leukemia cells undergo molecular changes induced by inhibition of RORγ and subsequent alterations in cholesterol metabolism. These changes have multiple anti-leukemic effects. However, any targeted therapy should of course be translated into clinical application. It remains to be clarified to what extent the *in vitro* behavior of the cells would change after treatment in the patient. Cytarabine is widely used as a chemotherapeutic agent in the first-line treatment of *KMT2A*r AML and ALL patients [5, 6]. Furthermore, AML cell lines have been reported to respond to chemotherapeutic agents by increasing their intracellular cholesterol levels, and in turn, primary AML cell samples could be sensitized to cytarabine by mevastatin [173, 180]. In our setting, CRISPR/Cas9 *t(4;11)* cells did not respond to chemotherapy exposure with an upregulated cholesterol target gene expression [202] (**Supplementary Figure 7**).

Accordingly, combinatorial treatment with chemotherapeutics and RORγ inhibitors may provide initial insights into potential clinical applicability. Therefore, the aim of this work was to evaluate the potential of RORγ inhibition to improve the efficacy of chemotherapy in CRISPR/Cas9 *t(4;11)* leukemia cells in a co-treatment approach. To define the drug combination according to Chou-Talalay [215], dose-response curves of the inhibitors alone or in combination were generated after seven days of treatment. In this setting, living cells were defined as Annexin V- and PI-. Curves were interpolated from the data according to a four-parameter logarithmic model, and the IC_{50} values were determined and plotted in isobolograms. As the data point for the combination therapy was close to the association line of the single treatments and the corresponding combination index was close to 1 (CI=0.89), an additive effect on decreased cell survival can be assumed (**Figure 37A**). Since the induction of apoptosis has already been shown for the single treatment with the RORγ antagonist, the occurrence of apoptotic cells was also investigated after the combination of selected concentrations of XY018 and cytarabine. Co-treated CRISPR/Cas9 *t(4;11)* cells showed an increased amount of apoptotic cells (Annexin V+, PI+) compared to single treatments, confirming the additive effect [202] (**Figure 37B**).

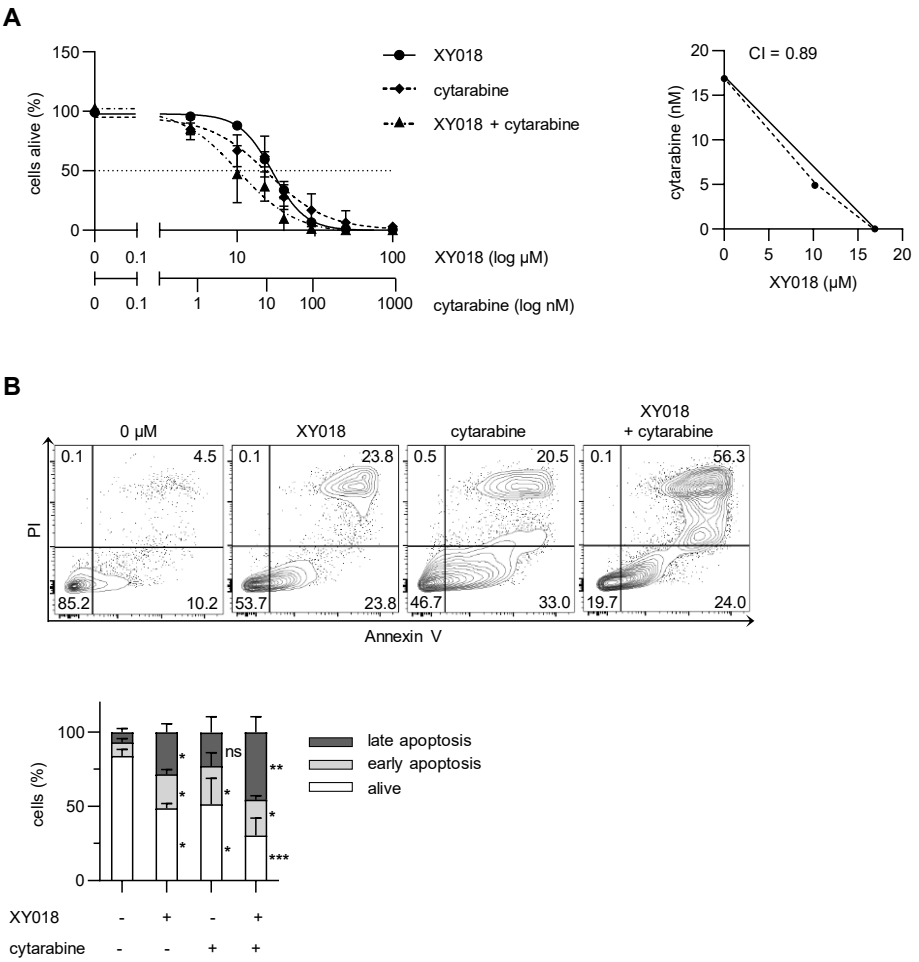

Figure 37: Combination of XY018 and cytarabine induces additive effects in CRISPR/Cas9 *t(4;11)* cells.

(A) CRISPR/Cas9 *t(4;11)* cells were simultaneously treated with increasing concentrations of XY018 alone or in combination with cytarabine for seven days. The percentage of living cells (Annexin V-, PI-) was evaluated with flow cytometry. IC_{50} values were mapped as isobologram and the Chou-Talalay method was used to measure the CI for identification of synergistic, additive or antagonistic effects. **(B)** For measurement of apoptosis, CRISPR/Cas9 *t(4;11)* cells were treated with 15 µM XY018 alone or in combination with 10 nM cytarabine. DMSO-treated or single-treated cells were used as control, respectively. Representative dot plots (top) and pooled data (bottom) show different apoptotic stages of three independent donors (n=3) measured in technical duplicates. Bars represent the mean ± SD. One-way ANOVA. **p*<0.05. ***p*<0.01. ****p*<0.001. ns=not significant. Modified from Erkner *et al.* [202].

One of the major problems with cancer chemotherapy is toxicity to the hematopoietic system. Finally, combinatorial treatment approaches offer the possibility of increasing anti-cancer effects with reduced drug doses. However, toxic side effects on healthy hematological cells should be carefully validated to determine the therapeutic window. To evaluate the toxicity potential of a combined therapy of XY018 and cytarabine, CRISPR/Cas9 *t(4;11)* cells as well as healthy CD34+ and CD34- control cells were treated with selected concentrations of both compounds for a total of 96 hours. Viable cells were defined as Annexin V+ and PI+ and

measured by flow cytometry. A beneficial effect of the combination was only observed when 20 µM XY018 and 50 nM cytarabine were combined, showing a dose-dependent significant decrease in viable *t(4;11)* cells. Unfortunately, the viability of rapidly proliferating CD34+ cells was also affected, although the effect was less pronounced than in leukemia cells. As chemotherapeutic agents show activity in rapidly proliferating cells, these effects were not surprising and reflect the situation in patients. Under the same conditions, differentiated CD34- cells were not affected [202] (**Figure 38**).

To validate the results, the effect of a combination treatment on the previously selected cell lines was also investigated. The combination of cytarabine and XY018 showed little benefit in terms of anti-leukemic effects in SEM and RS4;11 cells after 48 hours. In contrast, the non-translocated SKM-1 cell line was only affected by single treatment with cytarabine, but the combination of the two agents did not lead to an additive reduction in cell viability [202] (**Supplementary Figure 8**).

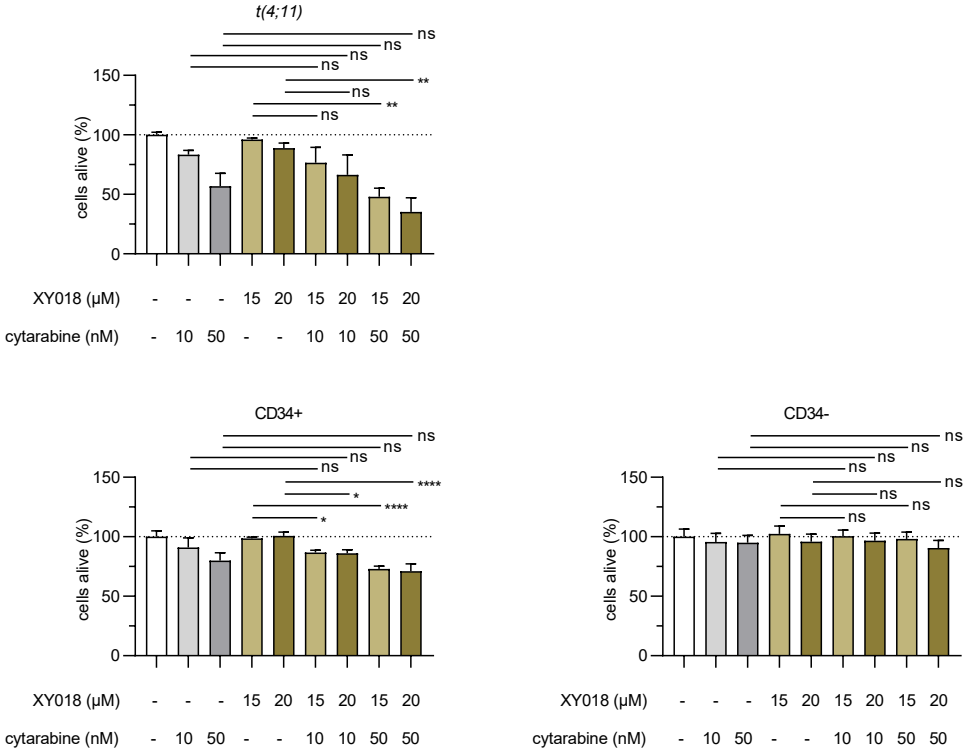

Figure 38: Combinatorial treatment effect of XY018 and cytarabine in CRISPR/Cas9 *t(4;11)* and healthy control cells.

CRISPR/Cas9 *t(4;11)*, CD34+, and CD34- control cells were treated with 15 µM or 20 µM XY018 alone or in combination with 10 nM and 50 nM cytarabine for a total of 96 hours. The percentage of living cells (Annexin V-, PI-) was evaluated with flow cytometry, and vehicle-treated cells were set to 100 as an internal control. Bars represent the mean of three independent donors (n=3) ± SD. One-way ANOVA. **p*<0.05. ***p*<0.01. *****p*<0.0001. ns=not significant. Modified from Erkner *et al.* [202].

4.7.2 RORγ inhibition in combination with cholesterol-modulating agents

All of the cholesterol-modulating compounds used in this study showed effects on reducing the viability and inhibiting the growth of *t(4;11)* leukemia cells. As described above, statins have shown promising therapeutic effects in hematological malignancies *in vitro* [168-179], but overall efficacy failed in clinical trials [181-183]. The combination of anti-cancer drugs can increase their efficacy and optimize the administered dose with tolerable side effects. Therefore, the therapeutic potential of the RORγ antagonist XY018 in combination with FS and ATV was investigated.

CRISPR/Cas9 *t(4;11)* cells were treated with increasing concentrations of FS and ATV alone or in combination with XY018 for seven days. In the case of combining XY018 with FS, a clear antagonistic effect on the percentage of living cells was observed (CI=1.60) (**Figure 39A**). In contrast, the combination of XY018 and ATV had a strong synergistic effect in reducing cell survival (CI=0.44) (**Figure 39B**). Examination of the induction of apoptosis by the combination of RORγ inhibition and inhibition of cholesterol synthesis confirmed these results. The percentage of cells in early and late apoptosis was significantly increased, while the combination of XY018 and FS showed no benefit [202] (**Figure 39C**).

In addition, direct comparison of healthy and leukemia cells confirmed the effect of XY018 in combination with FS, which showed no benefit after 48 hours of treatment (**Figure 40A**, **Supplementary Figure 9A**). When XY018 and ATV were combined, synergistic effects of the two drugs were seen in all cells tested. But the effects were most pronounced in the CRISPR/Cas *t(4;11)* cells and *t(4;11)* cell lines, suggesting a potential therapeutic window for the treatment of *t(4;11)* leukemia (**Figure 40B**, **Supplementary Figure 9B**). Interestingly, the synergistic reduction in live cells was already observed at concentrations of the two compounds that did not yet show individual effects. Accordingly, the efficacy of ATV could be enhanced by the combination, further illustrating the advantage of a synergistic effect over an additive effect in terms of an efficient targeted therapy [202].

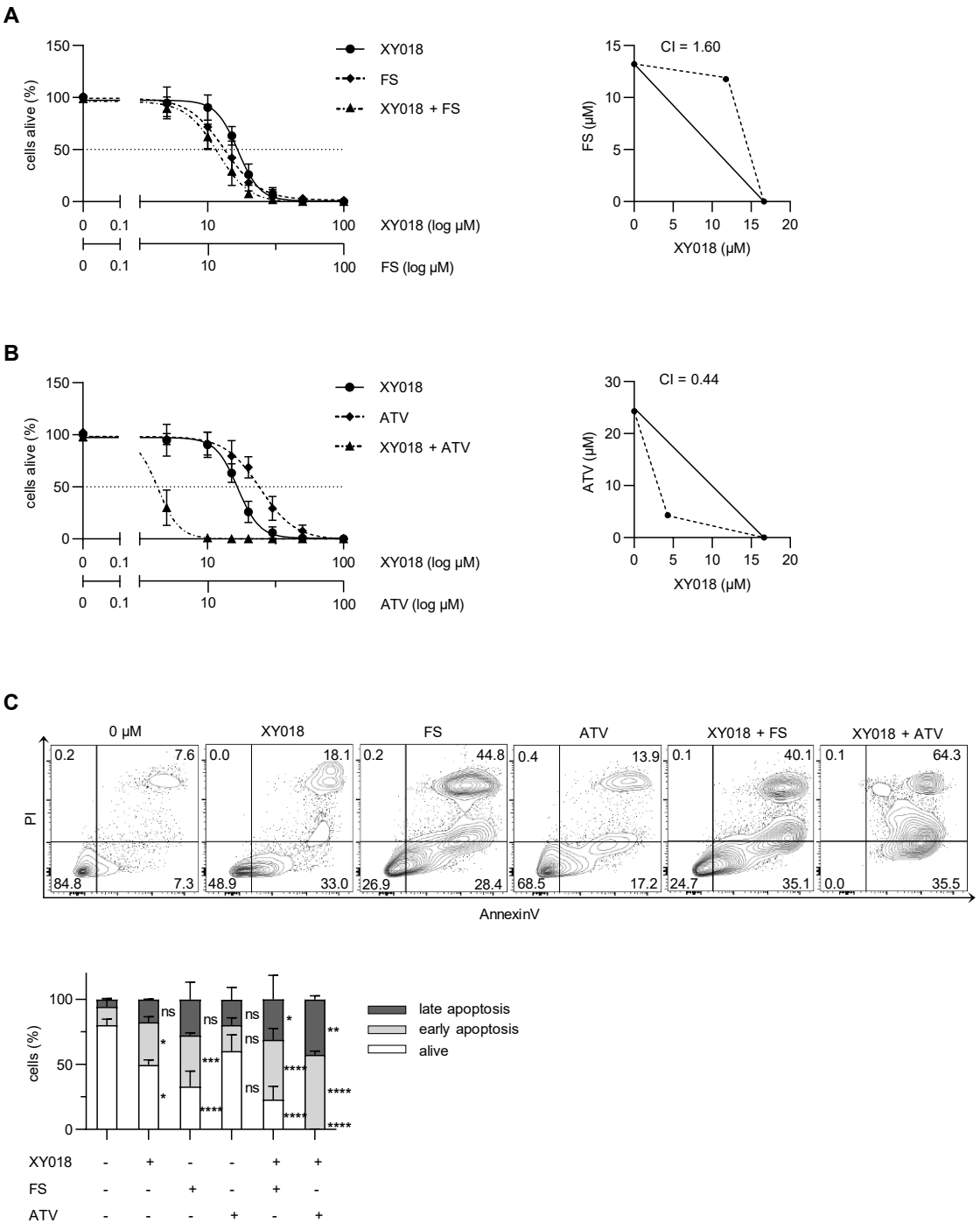

Figure 39: XY018 treatment induces antagonistic effects in combination with FS and synergistic effects with ATV in CRISPR/Cas9 *t(4;11)* cells.

CRISPR/Cas9 *t(4;11)* cells were simultaneously treated with increasing concentrations of XY018 alone or in combination with FS **(A)** or ATV **(B)** for seven days. The percentage of living cells (Annexin V-, PI-) was evaluated with flow cytometry. IC_{50} values were mapped as isobologram and the Chou-Talalay method was used to measure the CI for identification of synergistic, additive or antagonistic effects. **(C)** Apoptosis was measured in CRISPR/Cas9 *t(4;11)* cells treated with 15 µM XY018 alone or in combination with 15 µM FS or ATV. DMSO-treated or single-treated cells were used as control, respectively. Representative dot plots (top) and pooled data (bottom) show different apoptotic stages of three independent donors (n=3) measured in technical duplicates. Bars represent the mean ± SD. One-

way ANOVA. *p<0.05. **p<0.01. ***p<0.001. ****p<0.0001. ns=not significant. Modified from Erkner *et al.* [202].

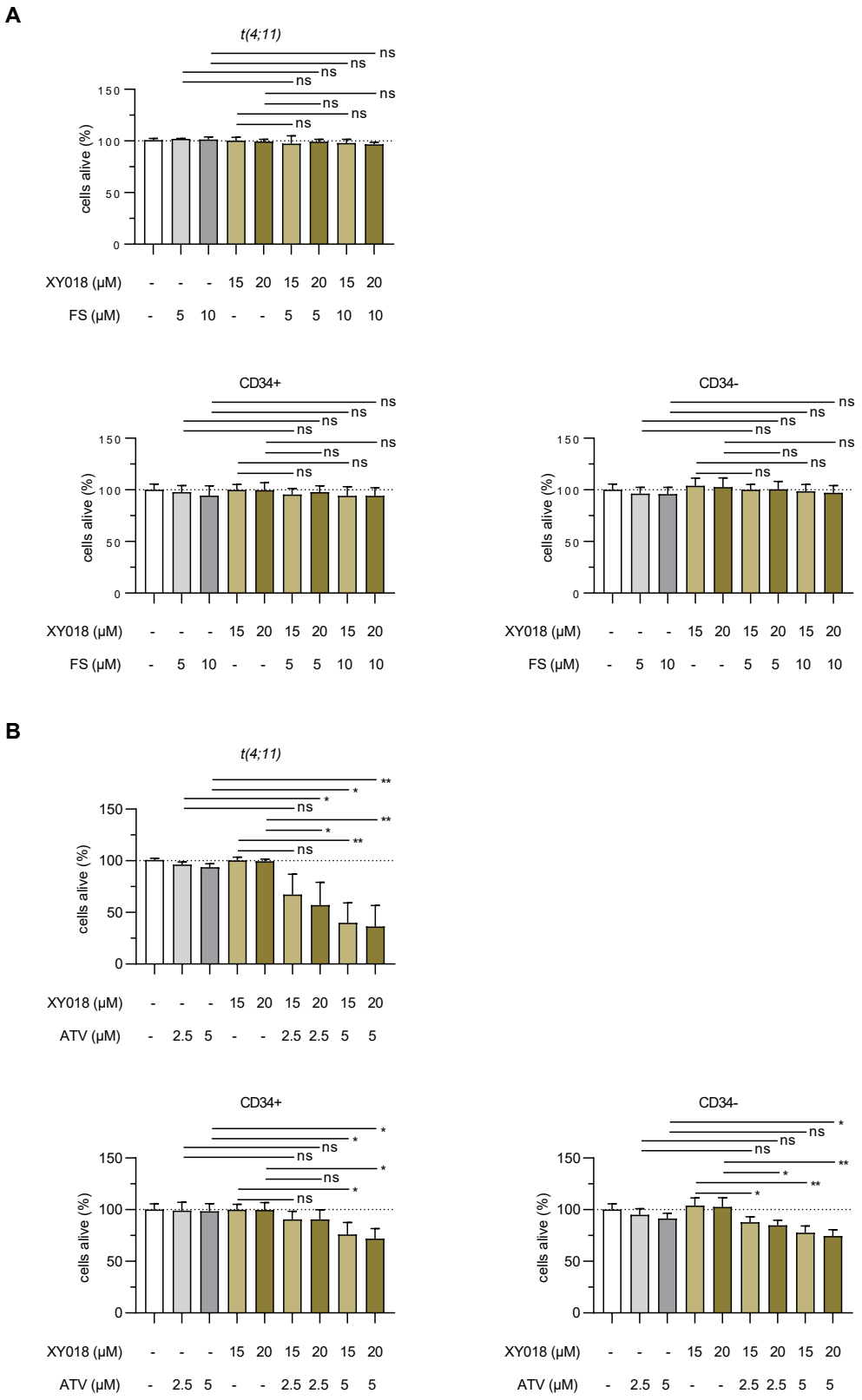

Figure 40: Combinatorial treatment effect of XY018 and cholesterol-modulating agents in CRISPR/Cas9 *t(4;11)* and healthy control cells.

CRISPR/Cas9 *t(4;11)*, CD34+, and CD34- control cells were treated with indicated concentrations of XY018 alone or in combination with FS **(A)** and ATV **(B)** for a total of 48 hours. The percentage of living cells (Annexin V-, PI-) was evaluated with flow cytometry, and vehicle-treated cells were set to 100 as an internal control. Bars represent the mean of three independent donors (n=3) ± SD. One-way ANOVA. **p*<0.05. ***p*<0.01. ns=not significant. Modified from Erkner *et al.* [202].

4.7.3 Effects on mRNA expression of combinatorial treatments

The previous results showed that RORγ blockade, and thus inhibition of the transcriptional regulation of the cholesterol pathway, and inhibition of cholesterol synthesis can be beneficially combined in the treatment of *t(4;11)* leukemia. As clinical trials focusing on the administration of statins in the context of acute leukemias failed due to the already known statin-induced feedback regulation, investigations regarding at the molecular level of the cholesterol pathway came into focus.

We further investigated the effects of RORγ inhibition and cholesterol-modulating agents on *SREBF2* gene expression in CRISPR/Cas9 *t(4;11)* cells after seven days of treatment. The results of single treatments showed a significantly increased *SREBF2* gene expression in ATV-treated cells, while gene expression was not significantly changed when XY018 and FS were added. Interestingly, the combination of XY018 and ATV, significantly decreased the *SREBF2* mRNA expression in *t(4;11)* cells (**Figure 41A**). The results were confirmed by RT-qPCR of cholesterol-related target genes, where combination of XY018 and FS showed no difference in gene expression compared to the single treatments. In fact, similar treatment with the RORγ antagonist reversed the statin-induced upregulation of cholesterol biosynthesis and uptake genes, resulting in a superior inhibition of these key genes [202] (**Figure 41B**).

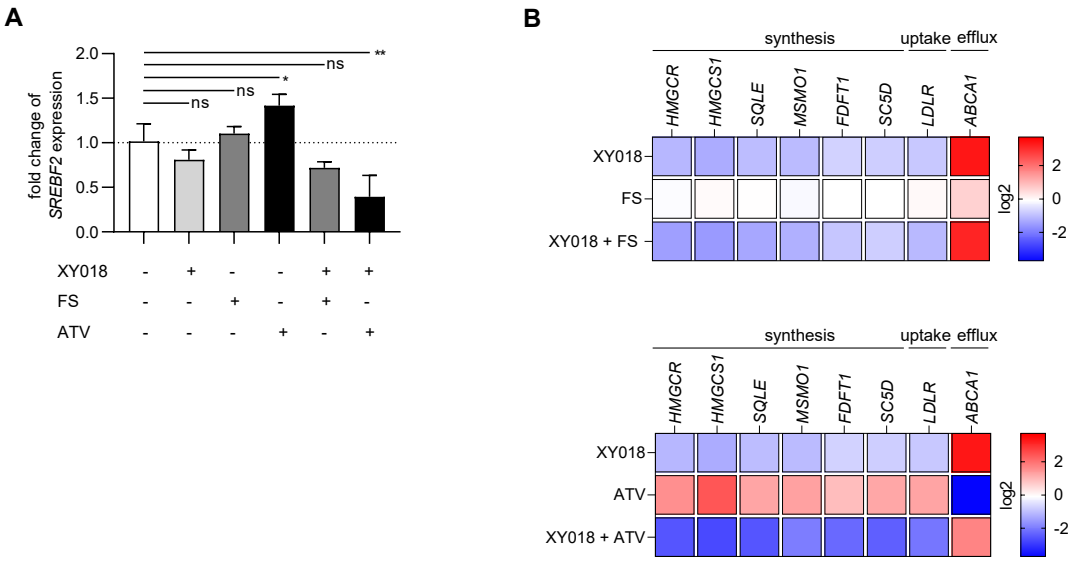

Figure 41: Gene expression profile of combined treatment with XY018 and cholesterol-modulating agents in CRISPR/Cas9 *t(4;11)* cells.

(A) RT-qPCR analysis of *SREBF2* gene expression in the CRISPR/Cas9 *t(4;11)* cells treated with 15 µM XY018, 15 µM FS or 15 µM ATV alone or in combination for 72 hours. Bars represent the mean of three independent donors (n=3) ± SD. One-way ANOVA. **p*<0.05. ***p*<0.01. ns=not significant. **(B)** Heat map display of fold changes (in log2) in genes of cholesterol homeostasis in CRISPR/Cas9 *t(4;11)* cells treated as described in (A). The expression of indicated genes was measured by RT-qPCR for which DMSO-treated cells were set to 1. Experiments were performed with three independent donors (n=3) in technical duplicates. Modified from Erkner *et al.* [202].

Taken together, these data provide evidence that XY018 can be beneficially combined with both chemotherapy and statins [202]. In particular, the use of XY018 in combination with the widely used ATV synergistically increased the anti-leukemic effect in *t(4;11)* leukemia. By combining similar inhibition of transcriptional regulation and cholesterol synthesis, the statin-induced feedback on upregulated cholesterol-related target genes can be circumvented. In addition, the concentration of statin required to induce anti-leukemic effects can be reduced, offering improved safety for patient administration.

5 Discussion

5.1 Classification of upregulated SREBP2-mediated cholesterol metabolism in *t(4;11)* cells

Early observations by Vitols *et al.* showed that AML cells exhibit high rates of cholesterol import and synthesis [226]. In this context, *HMGCR* has been well characterized as a fundamental metabolic gene. Although there are conflicting results on intracellular cholesterol levels [136, 137], it is generally accepted that cholesterol biosynthesis is enhanced in leukemia and that the rate of cholesterol uptake is faster [180, 227]. These studies are also consistent with the general understanding that elevated cholesterol levels may serve to protect leukemic cells. Leukemias with *KMT2A*r, including *t(4;11)* chromosomal translocations, have a poor prognosis and are known to have an unfavorable response to treatment (reviewed by [228]). It is therefore particularly important to identify the molecular characteristics of these cells in order to develop approaches that can serve as the basis for new therapeutic options [202].

This work provides data that *t(4;11)* leukemia cells upregulate their metabolism at a very early time point, at the transcriptional level, and not only during cholesterol synthesis [202]. Studies with malignant solid tumor cells have already shown that an efficient upregulation of cholesterol homeostasis can occur via transcriptional regulation mediated by SREBP2 [135, 152-155]. In addition to the CRISPR/Cas9 *t(4;11)* leukemia model of the Schneidawind lab, an increased SREBP2 activity was confirmed in *t(4;11)* cell lines, primary cells, and publicly available patient data [202]. *SREBF2* gene expression was found to be highly expressed in acute leukemia patients and was negatively correlated with patient survival, suggesting an important role for this transcription factor in this disease. In addition to the comparison with healthy HSPCs and PBMCs, *KMT2A*r leukemia cells should be analyzed in the context of the *KMT2A* fusion partner. For this purpose, the two most frequent translocation partners of *KMT2A*, *AFF1* and *MLLT3* [13], were analyzed. Interestingly, in the CRISPR/Cas9 translocation model and in cell lines harboring both translocations, cells with *t(4;11)* expressed the highest *SREBF2* mRNA levels, which could be confirmed at the SREBP2 protein level. This leads to the hypothesis that the potential oncogenic effect from cholesterol metabolism is not only due to the KMT2A protein, but also to the structural properties of the translocation partner. In this context, Harman and colleagues have generated a gene regulatory network (GRN) for KMT2A-AFF1-expressing leukemias [229]. By including RNA-Seq, chromatin immunoprecipitation sequencing (ChIP-Seq), and CRISPR screens, the authors used SEM and RS4;11 cells to create a GRN that includes both direct targets of KMT2A-AFF1 and a broader network of indirect targets to construct testable hypotheses. *SREBF2* was shown to have a reduced fold change when a KMT2A-AFF1 siRNA was used, and GRN nodes predicted a regulatory interaction of *SREBF2* with KMT2A, among others [229]. Both the SREBP2 and KMT2A protein

share a common binding partner, CBP/p300, which is recruited to the C-terminus of the KMT2A protein [34, 36] and is also able to mediate the transcriptional activity of SREBP2 [230]. The underlying mechanism for a possible relationship between KMT2A-AFF1 and the downstream transcriptional network of SREBP2 remains unclear. However, the results suggest that the KMT2A-AFF1 and AFF1-KMT2A protein complex may involve many more complex partners than previously described. Finally, a more detailed study of the reciprocal fusion product could also shed light on the extent of the association with SREBP2. Since both the CRISPR/Cas9 *t(4;11)* model and the *t(4;11)* cell lines analyzed express both fusion products, no conclusions could be drawn in this regard. Most studies have focused on the expression of KMT2A-AFF1 (reviewed by [231]), but it has also been shown that the single expression of AFF1-KMT2A can induce leukemia [59]. Further experiments with specific siRNAs or expression vectors of the two fusion products might therefore be helpful to investigate a molecular link between the KMT2A-AFF1 or the reciprocal AFF1-KMT2A fusion product and SREBP2 activity. Interestingly, the established GRN has shown that key targets of KMT2A-AFF1 that are critical for leukemogenesis, such as MYC and BCL2, are regulated by many different transcription factors along with KMT2A-AFF1 [229]. In this context, others have found a positive correlation between SREBP2 and MYC in prostate cancer. In this type of cancer, overexpression of SREBP2 and its direct interaction with the promoter region allows MYC to exert its full effect as a protooncogene [153]. In addition, another study has demonstrated an overexpression of SREBP2 in esophageal squamous cell carcinoma, with MYC serving as binding partner of SREBP2 and the cooperation of both proteins enhancing HMGCR expression [157]. A direct link between SREBP2 and MYC has not yet been investigated in KMT2A-AFF1 leukemias, but results from our group have also shown a high expression of MYC in *KMT2A*r leukemias [90]. Further experiments are needed to elucidate the underlying mechanism, but taken together, the data from this thesis and previously published data suggest the possibility of a direct interaction between these proteins.

Since the previous results indicated that SREBP2-mediated cholesterol metabolism seems to play a role especially in KMT2A-AFF1-expressing leukemias, the present work focused on *t(4;11)* translocations. By examining key cholesterol biosynthetic enzymes such as HMGCS and SQLE, the CRISPR/Cas9 *t(4;11)* leukemia model showed increased sterol synthesis, but normal intracellular cholesterol levels compared to healthy HSPCs. Up to this point, the results were in line with very early studies showing that leukemia blasts have an enhanced cholesterol synthesis program [226]. In this context, it seems logical that some study results have shown that the intracellular cholesterol level in leukemia cells is higher than in healthy PBMCs [136]. Nevertheless, other studies have concluded that the intracellular cholesterol content in leukemia cells is not significantly higher, and in some cases even lower, than in normal PBMCs [137, 232]. The different results again underline the importance of analyzing cancers in

different subtypes to get a more valid statement. Based on the results of this work, it can be assumed that *t(4;11)* leukemia cells either directly metabolize or export excess cholesterol. Western blot experiments showed the expression of the cholesterol efflux transporter ABCA1 in leukemic cells, supporting this hypothesis. By maintaining stable intracellular cholesterol levels, the SREBP2-mediated feedback leading to the inhibition of *de novo* cholesterol synthesis [98] can be prevented.

In addition, increased expression of LDLR, the major cholesterol import receptor [117, 118], was observed in *t(4;11)* leukemia cells. On the other hand, the cells did not benefit from growth advantages when exogenous cholesterol and GGPP were supplemented, suggesting that the occurrence of *t(4;11)* leukemia is independent of exogenous cholesterol. These results are interesting in terms of the relevance of plasma cholesterol levels in patients and their association with the possible occurrence of leukemia. There are already studies showing that patients with AML tend to have low plasma cholesterol levels [233], which may be associated with increased LDLR-mediated cholesterol uptake [227, 234]. Similar findings have been reported in ALL patients, in whom increased intracellular cholesterol levels could be measured in primary leukemic lymphocytes despite low serum cholesterol levels [235]. Unfortunately, none of these studies differentiated between molecular characteristics of leukemia subtypes. Nevertheless, the data collected in this thesis suggest that *t(4;11)* leukemia cells obtain their cholesterol requirements for plasma membrane synthesis mainly by *de novo* cholesterol biosynthesis and are not dependent on exogenous cholesterol supply. However, this question cannot be answered conclusively with the available data. Therefore, it would be useful to investigate both the plasma cholesterol levels of *t(4;11)* leukemia patients and the amount of intracellular cholesterol in leukemic blasts. Gomes and colleagues have also shown that elevated plasma cholesterol levels favor BM cell proliferation [123]. Others have reported an increased number of NK cells in mice with high serum cholesterol, which have anti-tumor and growth-inhibitory properties against liver tumors [130]. As numerous studies support a role of the microenvironment in the maintenance of leukemic cells ([236, 237], reviewed by [238, 239]), these findings regarding plasma cholesterol levels on cellular components of the leukemic microenvironment should not be neglected.

So far, the results suggest that leukemia cells expressing KMT2A-AFF1 fusions achieve an activated SREBP2-mediated cholesterol synthesis program. At the same time, there was no evidence that the *t(4;11)* leukemia cells have an increased LDLR-mediated uptake of cholesterol. Nevertheless, it can be argued that *t(4;11)* cells are able to directly consume excess of cholesterol for cell growth or promote increased export from the cell, respectively, thus preventing the feedback response of reduced SREBP2 activity [202].

The next step was to investigate the dependence of *t(4;11)* leukemia cells on *SREBF2* expression. One way to study the dependence of cell phenotypes on a specific transcription

factor is to disrupt gene function. There are several ways to perform this, including RNA interference (RNAi) and the CRISPR/Cas9 system. While CRISPR silences the gene of interest completely and permanently (knockout), RNAi reduces gene expression (knockdown, kd). Due to its key role in overall cholesterol metabolism, it was assumed that a complete knockout of *SREBF2* would have been lethal for the cells. For this reason, an incomplete gene kd was chosen. The use of shRNA constructs has the advantage of producing a stable kd, whereas the introduction of siRNAs allows only short-term experiments.

To exclude off-target effects, three different shRNAs targeting the *SREBF2* gene and a non-targeting shRNA were used. Cells were transduced with lentiviral shRNA-containing particles and transduction efficiency was demonstrated by 50% to 80% reduction of *SREBF2* mRNA. Successful knockdown was also shown by a reduced expression of *SREBF2* target genes involved in cholesterol synthesis, uptake, and efflux. These data clearly demonstrate that SREBP2 also plays an important role in the leukemic metabolism of *t(4;11)* cells and that its activity is closely linked to key enzymes of cholesterol homeostasis. Although slight changes in apoptosis and cell cycle were observed with the most efficient shRNA, kd of *SREBF2* did not result in notable anti-leukemic effects. Reduced *SREBF2* expression was ensured throughout the experimental period, but some methodological limitations should not be overlooked. It should be noted that despite puromycin selection, it was not possible to achieve a high kd efficiency with all of the used shRNAs. Furthermore, although an shRNA-induced *SREBF2* kd can be used to generate stable kd cells [240], a less effective kd efficiency was observed when transduced cells were cultured for several days. A possible reason for this could be that cells with reduced *SREBF2* expression are unable to carry out adequate cholesterol biosynthesis due to the lack of key enzymes and are therefore severely restricted in their growth capacity, as cholesterol as an important building component of the cell membrane is only available in a very reduced form. Since the kd efficiency was less than 100%, it is likely that cells that were not successfully transduced still had a growth advantage and were able to overgrow *SREBF2* kd cells. Although the results obtained should be treated with caution, cells transduced with the most efficient shRNA to reduce *SREBF2* mRNA expression to 20% showed a significant increase in apoptotic cells and a decrease in cells in the synthetic phase of the cell cycle.

These results suggest that SREBP2-driven cholesterol metabolism in these cells contributes to the high proliferative potential of *t(4;11)* leukemias. However, further experiments and the use of an N-terminal SREBP2 overexpression vector would strengthen this statement. In addition, the established *SREBF2* kd can be used to evaluate a potential link between SREBP2 and MYC in *t(4;11)* leukemia.

5.2 Targeting cholesterol metabolism with different small molecules

Since the results so far showed an increased *SREBF2* expression in *t(4;11)* leukemia, but the dependence of the leukemia cells on *SREBF2* could not be conclusively confirmed by a partial kd, the next step was to pharmacologically inhibit the metabolic activity of *t(4;11)* cells. There are several ways to inhibit this complex signaling pathway, as intracellular cholesterol metabolism is a multi-step process. Direct inhibition of SREBPs can be achieved with FS, which aims the function of sterols by blocking the ER-to-Golgi translocation of the SREBP-SCAP complex, thereby reducing transcriptional activity [189, 241]. Preclinical studies have demonstrated anti-tumor effects of FS in prostate, endometrial, colon, and ER+ breast cancer [190, 192, 242, 243]. Consistent with these results, also the percentage of viable CRISPR/Cas9 *t(4;11)* cells decreased in a concentration- and time-dependent manner when FS was added to the culture medium. The negative effect of the inhibitor was shown by an increase in Annexin V+/PI+ and trypan blue stained cells. An expression analysis of selected SREBP2 target genes was performed to demonstrate efficacy and specific anti-metabolic effects with respect to key enzymes of cholesterol metabolism. As expected from the results of others [243], treatment of *t(4;11)* cells with 15 µM FS for seven days resulted in a decrease of cholesterol synthesis genes (*HMGCR*, *HMGCS*, *SQLE*, *MSMO1*, *FDFT1*, *SC5D*) and a reduction of the LDLR-encoding gene. In contrast, mRNA expression of the cholesterol efflux transporter ABCA1 was increased compared to DMSO-treated cells. This demonstrates the functionality of FS by preventing the translocation of the N-terminal SREBP2 to the nucleus, thereby triggering the inhibitory (cholesterol synthesis and import) or activating (cholesterol efflux) effect on several key enzymes that occur under normal physiological conditions in the presence of sterols. The effect was confirmed by the finding that supplementation of exogenous cholesterol significantly reinforced the cell-killing efficacy of FS on leukemia cells. Since SREBP2 processing also occurs in normal cells, the effect of FS treatment was analyzed in CD34+ HSPCs and differentiated CD34- cells. Although *t(4;11)* cells showed the highest sensitivity to FS, the resulting IC_{50} value was not significantly different from that of healthy cells, suggesting no selective anti-proliferative effects of FS.

As described above, HMGCR has been first investigated for its potential proliferative function in leukemia cells in 1994 [226]. With the discovery of statins and their inhibitory effect on cholesterol synthesis, numerous preclinical studies were conducted to investigate the anti-proliferative effect of statins on AML and ALL cells [168, 170-175]. The *in vitro* and *in vivo* results were promising, and based on the previously observed effect of statin supplementation on the sensitization of AML cells to chemotherapy [171, 173], two large clinical trials were conducted [181-183]. Pravastatin in combination with standard induction of chemotherapy has shown encouraging results in AML patients [181], increased complete response rate in favorable-risk AML [182], but less clear effects with improved outcome only in patients with unfavorable prognosis [183]. A major problem with statin use is that tumor cells vary widely in

their sensitivity to statin-induced cell death. Clinical trials of statins in solid cancer therapy have failed due to an elevated cholesterol metabolism as a negative feedback-loop in response to statin therapy [184, 185]. Similarly, studies with multiple myeloma cell lines have shown a differential response in terms of sensitivity and insensitivity to lovastatin-induced apoptosis [169]. The lack of response in insensitive cells has been explained by a statin-induced inhibition of HMGCR, which triggers a robust homeostatic feedback response including the activation of SREBP2. Here, this naturally occurring negative feedback response has led to an upregulation of the mevalonate pathway, allowing statins to act as cholesterol-lowering agents. Importantly, statin-sensitive cells did not exhibit the expected feedback of mevalonate metabolism [169, 186]. As evidenced by the presence of HMGCS and SQLE overexpression in Western blot experiments, the KMT2A-AFF1-expressing cells of the CRISPR/Cas9 model exhibited increased cholesterol synthesis compared to healthy cells [202]. In this context, it was of particular interest how these cells behave when treated with a common statin. The statin to be tested was selected based on several parameters: First, the statin should be of synthetic origin and have lipophilic properties to maximize efficacy. Finally, ATV was chosen because it allows high doses (up to 80 mg), has low renal excretion (2%), and a relatively long half-life (14 hours) compared to other statins (reviewed by [163-165]). Finally, according to calculations of drug prescription data in the second quarter of 2018, ATV was the most prescribed statin in Germany after simvastatin, facilitating its potential use in the clinic as an anti-cancer agent [244]. After treatment with ATV in CRISPR/Cas9 *t(4;11)* cells, an upregulation of *SREBF2* at the transcriptional level and consequently of target genes such as for cholesterol synthesis and *LDLR* was observed. In contrast, the expression of *ABCA1* mRNA was decreased [202]. This observed feedback leads to the conclusion that *t(4;11)* cells show properties of the previously described statin-insensitive cells [169]. Surprisingly and contrary to the results showing an upregulated cholesterol pathway at the mRNA level, both *t(4;11)* and healthy control cells exhibited a reduction in cell growth. This result can be explained by the observation of another group showing that statins are also able to induce intrinsic apoptotic pathways in many cancer cells by directly disrupting the isoprenylation of geranylgeranylated Rho family and other key regulatory proteins [245-247]. Therefore, it is likely that the anti-proliferative effects of statins on *t(4;11)* cells are also due to not only inhibition of cholesterol metabolism but also to activation of pro-apoptotic pathway proteins. This theory should be tested by adding GGPP to ATV-treated cells, as several *in vitro* studies have shown that statin-induced apoptosis can be consistently rescued by exogenous mevalonate-derived GGPP [222, 223, 247]. When GGPP was added to ATV-treated CRISPR/Cas9 *t(4;11)* cells, the cell population showed a slight increase in viability, concluding that the described statin effect also applies to this type of leukemia. However, donor viability was high in this experiment and the timing of the 48-hour treatment may not have been optimal. To confirm the effect with certainty, the experiments should be repeated with adjusted conditions. Although it is generally safe to

use statins at doses for the treatment of hypercholesterolemia, their efficacy as a potential anti-cancer treatment in clinical studies is limited and less encouraging. An explanation is, comparable to our findings, that statin-induced inhibition of HMGCR leads to feedback activation of SREBP2 and subsequently to increased LDLR-mediated cholesterol uptake and synthesis. This makes cancer therapy less effective. Therefore, therapeutic strategies that avoid this negative feedback are needed. In addition, our results and other *in vitro* studies have demonstrated that statins are also known to induce effects in non-malignant cells ([202], reviewed by [248]).

The results so far indicate that the key regulator of sterol metabolism, SREBP2, is a highly conserved transcription factor and difficult to target. But findings by others in solid tumors have brought RORγ into focus as a new known driver of cholesterol metabolism, that is upstream and directly regulates SREBP2 [159]. RORγ is a DNA-binding transcription factor and a member of the nuclear receptor family (reviewed by [193]). Recently, a new inhibitor of RORγ, named XY018, has enabled the efficient blockade of the cholesterol metabolism without activation of the negative feedback and promoted anti-tumor effects [198]. Using XY018 in this work, inhibition of RORγ induced leukemic cell death of CRISPR/Cas9 *t(4;11)* cells, while healthy control cells were significantly less sensitive to the inhibitor. Interestingly, effective targeting of RORγ by XY018 resulted in a much stronger inhibition of cholesterol pathway-related genes than treatment with the direct SREBP2 inhibitor FS. It can be concluded that for anti-leukemic therapy, direct inhibition of RORγ and thus indirect inhibition of the transcriptional action of SREBP2 is a more promising therapeutic approach than direct inhibition by FS or HMGCR inhibition by ATV, which also leads to unknown toxicity [202].

The initial results of RORγ inhibition were promising and the thesis should therefore focus on characterizing the nuclear receptor in relation to leukemic cholesterol metabolism. The role of RORγ will be discussed in the next section.

5.3 RORγ in the context of *t(4;11)* leukemia

Results to date have shown that targeted inhibition of the NR RORγ induces promising anti-leukemic effects without affecting healthy cells of the hematopoietic system. RORγ belongs to the superfamily of structurally conserved ligand-regulated NRs and is one of the most studied members of this subfamily. RORγ and its isoform RORγt have been shown to display distinct tissue-specific expression patterns (reviewed by [193]). On the one hand, RORγt is involved in the differentiation of regulatory T (Treg) or Th17 lineages and binds to Th17 differentiation-associated gene loci [249]. In addition, RORγt has been shown to regulate IL-17 expression of γδ T cells and to contribute to the development of secondary lymphoid organs in mice [250, 251]. Clinical research on the other isoform, RORγ, came into focus when Wang and colleagues presented a meta-analysis of NR gene expression profiling showing high levels of RORγ expression in tumors of CRPC cells [198]. Finally, RORγ has been shown to play a

prominent role in enhancing androgen receptor function by activating androgen receptor gene expression [198]. By stimulating genes involved in metabolism, cancer stemness and proliferation, RORγ has also been identified as an important driver of TNBC, pancreatic adenocarcinoma, and small cell lung cancer [159, 200, 252]. In our experiments, we aimed to detect intranuclear RORγ protein expression by flow cytometry and expression in whole cell lysates by Western blot using a monoclonal antibody that reacts with both isoforms. CRISPR/Cas9 *t(4;11)* and *t(4;11)* cell lines showed both a high total protein expression from whole cell lysates and a high percentage of cells expressing intranuclear RORγ. Finally, both healthy stem cells and PBMCs were shown to express the protein at some level. This suggests that it is not the basal RORγ expression, whether intranuclear or cytoplasmic, that is responsible for the different responses to the RORγ antagonist, but rather a different mechanism. This possibility is discussed below.

RORγt ligands have been identified as selective modulators of RORs, and a number of antagonists/inverse agonists have been developed and are in clinical trials to modulate immune cells for the treatment of autoimmune diseases (reviewed by [253]). Interestingly, various RORγ-targeting small molecules have been shown to have different context-specific activities in modulating RORγ and RORγ function ([201], reviewed by [160]).
Genetic kd of RORγ and antagonist treatment have increased apoptosis and decreased proliferation and cell survival, while xenograft experiments have shown a significant inhibition of CRPC tumor growth and metastasis by antagonist treatment [198]. In TNBC, RORγ antagonists were highly effective in inducing tumor regression and blocking metastasis in this cancer subtype [159]. Using the most potent RORγ antagonist, XY018, RORγ inhibition induced leukemic cell death, apoptosis, and significant cell cycle arrest in CRISPR/Cas9 *t(4;11)* cells. Cell cycle analysis revealed a significant reduction in S-phase, where DNA replication occurs in preparation for cell division, in the CRISPR/Cas9 *t(4;11)* and *t(4;11)* cell lines. Furthermore, the frequency of post-synthetic or pre-mitotic and mitosis-associated G2/M-positive *t(4;11)* cells was significantly reduced with increasing inhibitor concentration. The reduced proliferative capacity was also demonstrated by the viability assay using alamarBlue reagent. Further analysis showed a significant increase in the number of early and late apoptotic cells in the *t(4;11)* population after seven days of XY018 treatment. During the early stages of apoptosis, cytochrome c is often released from the mitochondria into the cytoplasm, leading to caspase activation and ultimately to degradation of apoptotic cells [214]. An intrinsic activation of the apoptotic pathway with mitochondrial involvement can be suggested, as shown by cytochrome c release assay and mitochondrial activation of genes and pseudogenes in the RNA-Seq. Pharmacological inhibition of RORγ also resulted in the induction of caspase 3 and caspase 7-induced apoptosis in TNBC cells and prostate cancer xenografts, supporting these findings [159, 198]. Interestingly, cytochrome c release decreased at the highest inhibitor

concentration, which can be explained by the effect of *t(4;11)* cells entering the state of late apoptosis/secondary necrosis [254]. In the absence of effective cytolysis (e.g. clearance by macrophages) and as a result of caspase targeting of mitochondria, cells undergo autolytic disintegration [254], explaining the observed phenotype in RORγ-targeted *t(4;11)* cells.
Since healthy cells also require cholesterol for their proliferation and especially immature cells have a high SREBP2 and RORγ expression, we investigated the sensitivity of CD34+ HSPCs to RORγ inhibition. While *t(4;11)* cells underwent apoptosis and cell cycle arrest, CD34+ HSPCs were nearly resistant under the same conditions. This was further confirmed by another control with CD34+ cells cultured for three weeks under myeloid conditions (CD34-), which have lower levels of SREBP2. Consistent with the level of SREBP2, these cells were even less sensitive to RORγ inhibition, demonstrating SREBP2 dependence [202]. In addition, Wang *et al.* could have demonstrated that intraperitoneal injection of up to 20 mg/kg XY018 5 times per week significantly inhibited tumor growth in CRPC xenograft models without affecting body weight, vital organ weight, and behavioral changes such as feeding and water intake [198]. Of course, dosing and application type in a leukemia model would need to be individualized, but the results provide a potential therapeutic window for translating our data into an *in vivo* and later clinical setting. It is also noteworthy that we observed a higher sensitivity of *t(4;11)* cell lines compared to a non-*KMT2A*r cell line, highlighting the specificity of the pathway studied and the importance of defining specific subgroups of patients who may benefit from the therapy [202].
The number of studies describing RORγ as a potent transcriptional activator in some solid cancer cells has steadily increased in recent years [159, 198-201, 252, 255, 256]. In the present study, it was possible to identify another cancer subtype, this time in hematopoietic cells with a *t(4;11)* translocation, in which RORγ appears to act as an active driver of oncogenic leukemia progression. It should be noted that this statement could be supported by data showing similar results in *t(4;11)* leukemia using a genetic RORγ kd or knockout [159, 198, 199]. This approach was also investigated, but conventional methods using siRNA pools, shRNA, and CRISPR/Cas9 failed to downregulate RORγ (data not shown). One reason for this may be the relatively low basal *RORC* mRNA expression (data also not shown), suggesting that in the case of RORγ, mRNA and protein expression are not concordant. However, an advantage of our results is that pharmacological inhibition leads to a better translation to the patient situation, as we focus on endogenous RORγ inhibition.

In this study, we compared the gene expression profiles by RNA-Seq before and after RORγ inhibition. The strongest upregulation was observed after RORγ inhibition in *t(4;11)* cells on cholesterol efflux genes (*ABCA1*, *ABCG1*), confirming the role of RORγ as a repressor to silence LXR downstream genes [202]. These results are consistent with results in prostate cancer cells, where RORγ has been shown to repress the expression of cholesterol efflux

genes under pro-tumor conditions [199]. Data on the role of ABCA1 in oncogenic metabolism are very heterogeneous; some studies have identified the cholesterol efflux transporter with high expression in solid tumors [138, 139], and silencing resulted in increased apoptosis in melanoma and HL-60 AML cells [144, 145]. Other groups have suggested a tumor suppressor role [140-142]. Data from our own research group also showed a significant increase in ABC transporter mRNA expression following inhibition of cell growth in the *t(4;11)* model by targeting methionine adenosyltransferase 2A (MAT2A) [257]. Therefore, it is likely that ABC transporters and their role in mediating cholesterol efflux play a key role in the survival and proliferation of *t(4;11)* cells. In summary, the data from this study indicate that ABCA1 in *t(4;11)* cells, as in healthy cholesterol metabolism, has the role of maintaining intracellular cholesterol levels constant [121]. Since SREBP2 kd resulted in decreased expression and RORγ inhibition led to increased *ABCA1* mRNA expression, it can be confirmed that RORγ controls cholesterol levels in a highly coordinated manner in *t(4;11)* cells [199]. In addition, IPA identified RORγ as an activator of the SREBP2-mediated gene program in *t(4;11)* cells, which was confirmed at the protein and intracellular cholesterol levels. Thereby, XY018 reduced cholesterol biosynthetic enzymes (HMGCR, HMGCS, SQLE) and cholesterol uptake by LDLR. Analysis of the RT-qPCR results also showed that CD34+ and SKM-1 cells, which exhibited no effect on their proliferative capacity at the concentrations used, predominantly showed no significant changes in the mRNA expression of the cholesterol synthesis and import genes [202].

In addition to our data, Cai *et al.* demonstrated a strong interaction of RORγ with SREBP2, resulting in an exaggerated stimulation of cholesterol homeostasis in TNBC [159]. Specific binding has been demonstrated by finding N-terminal SREBP2 in immunoprecipitates of RORγ and synergistic transactivation of the *MVK* gene in cells co-transfected with RORγ and N-SREBP2. The transcriptional co-activity was suggested to be mediated by the recruitment of the histone acetyltransferase p300, and RORγ antagonists strongly reduced the occupancy of the p300-written H3K27ac mark at the chromatin regions of cholesterol synthesis genes. The data were supported by ChIP-Seq experiments showing that RORγ significantly reduced genome-wide SREBP2 binding without altering its protein expression ([159], reviewed by [160]). These observations are similar to the data from this work, in which the effects of RORγ inhibition primarily affected intracellular cholesterol biosynthesis and cholesterol export. No further data are known about a possible interaction between RORγ and SREBP2 in cells of the hematopoietic system or in leukemia cells. It is known that wild-type KMT2A protein associates with CBP/p300 through the TAD presumably promoted by the co-presence of transcription factors such as CREB and MYB [34-36]. During hematopoietic cell differentiation, CBP/p300 recruitment is tightly regulated and progressively repressed [258]. In contrast, in *KMT2A*r leukemias, there is a form of CBP/p300 recruitment that mimics the active form of KMT2A and places H3K27ac marks on target genes such as *HOXA9* and *MYC* [259]. Another study demonstrated a KMT2A fusion with the CBP/p300 interacting AFX protein [260]. However, no

such direct interaction has been observed in *t(4;11)* leukemia (reviewed by [261]). Nevertheless, AFF1 has been shown to form higher complexes with several interacting proteins, resulting in both SEC and AEP and subsequent recruitment of DOT1L [50, 262]. Interestingly, experiments with breast cancer cells have shown a collaboration of DOT1L with MYC and p300 complexes [263]. Based on the results of previous studies, such an interaction would also be possible in *t(4;11)* leukemia cells. But it is more likely that the KMT2A-AFF1 fusion-induced H3K79me chromatin landscape increases the binding of CREB, which in turn promotes the recruitment of CBP/p300. In this regard, Gilan and colleagues have shown a loss of H3K79me marks and p300 binding at gene targets following DOT1L inhibition [264]. Subsequent experiments using KMT2A-AFF1 siRNA have also reduced DOT1L recruitment and subsequently CBP/p300-mediated acetylation [265]. Furthermore, the reciprocal AFF1-KMT2A protein still retains the TAD and its CBP/p300 recruiting capacity. Combining these data with the results of the present study and the results in TNBC [159], a hypothetical model can be created at the molecular level that suggests the overarching role of an SREBP2-RORγ interaction with respect to KMT2A-AFF1 fusions (**Figure 42**).

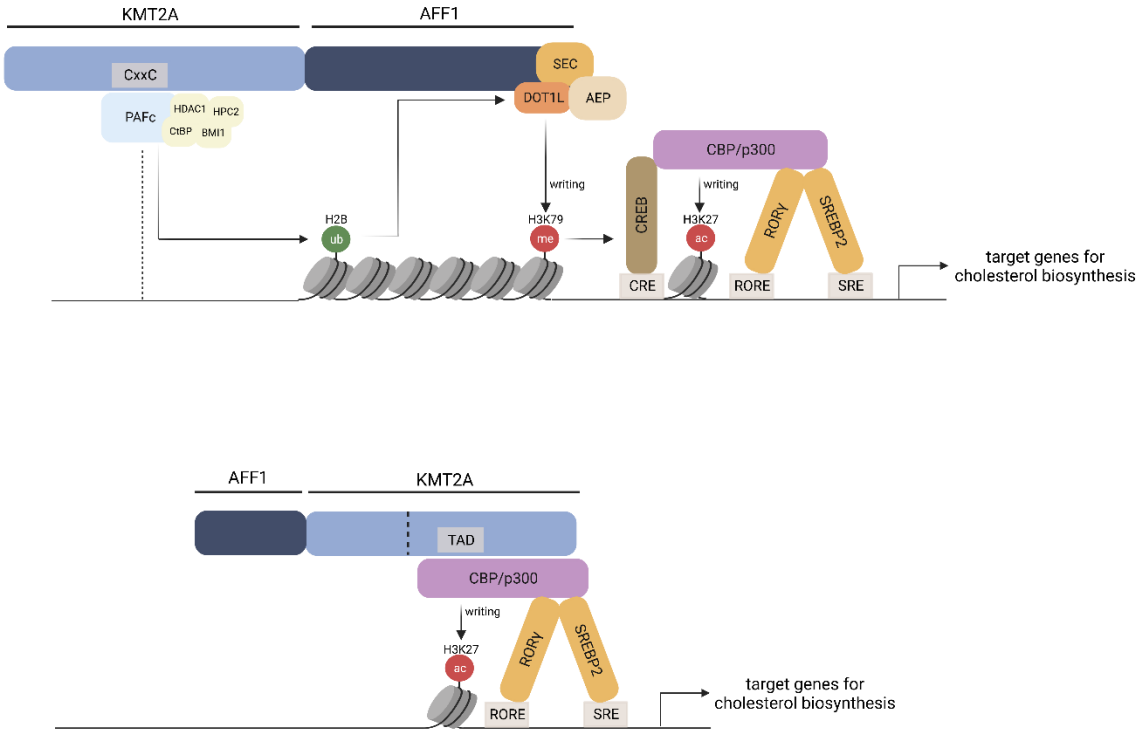

Figure 42: Hypothetical model of the overarching role of an SREBP2-RORγ interaction with respect to KMT2A-AFF1 fusion proteins.

The conceivable feedforward regulation in *t(4;11)* cells regarding SREBP2 and RORγ is shown. The figure displays initial considerations for both the KMT2A-AFF1 protein (top) and the AFF1-KMT2A protein (bottom) based on the findings of multiple research groups ([159, 259, 262, 264, 265], reviewed by [160]). CBP/p300 may be involved in both protein complexes, as it forms higher complexes with SREBP2 and RORγ. These considerations can serve as starting point for further experiments. Figure generated with BioRender.

In this model, the occurrence of a *t(4;11)* translocation favors the abnormal recruitment of CBP/p300 through the physiological function of the reciprocal AFF1-KMT2A fusion protein and additionally through the oncogenic effect of KMT2A-AFF1 via various transcription elongation complexes. This in turn stimulates the methyltransferase DOT1L and leads to H3K79me hypermethylation of hematopoietic developmental regulatory genes, resulting in a more permissive chromatin environment for CREB binding. Ultimately, this may lead to the stabilization of RORγ and SREBP2 via CBP/p300 in the nucleus and contribute to abnormal cholesterol synthesis in *t(4;11)* leukemia. How *KMT2A*r leukemias lead to increased SREBP2-mediated cholesterol metabolism can only be speculated at this time. Further experiments with both the KMT2A-AFF1 and AFF1-KMT2A may shed more light on this issue. Finally, although it is reasonable to assume that RORγ and SREBP2 interact via CBP/p300 in *t(4;11)* cells similarly to TNBC, many questions remain unanswered. Cai *et al.* showed that pharmacological inhibition of RORγ significantly reduced p300 occupancy in relation to SREBP2. As a subsequent cascade, XY018 treatment also reduced the histone mark H3K27ac in chromatin regions and the promoter occupancy of RNAP II, especially its transcription initiation-associated CTD-ser 5 phosphorylated form [159]. Based on the current state of knowledge, it cannot be conclusively determined whether the anti-leukemic effects induced by XY018 are due to the disruption of an SREBP2-RORγ interaction in relation to p300. Additional chromatin immunoprecipitation and ChIP-Seq experiments would be helpful to investigate this possibility in *t(4;11)* leukemia.

As chemotherapy is the standard treatment for patients with acute leukemia [5, 6], the interactions of such agents on the cholesterol metabolism have been investigated. It has been shown that elevated cholesterol levels are associated with resistance to common induction chemotherapies such as daunorubicin and cytarabine [180]. Interestingly, the anti-leukemic effect of decitabine has been reported to be mechanistically linked to the inhibition of cholesterol metabolism [266], and cholesterol-lowering drugs have induced cytotoxic effects in AML stem cells [173, 267]. Furthermore, AML cell lines respond to chemotherapeutics by increasing their intracellular cholesterol levels, and in turn, primary AML cell samples could be sensitized to cytarabine by mevastatin [173, 180]. However, in our setting the *t(4;11)* cells did not respond to chemotherapy exposure with an upregulated cholesterol target gene expression. Nevertheless, in a combinatorial treatment experiment with cytarabine and XY018, we found a beneficial outcome by additive effects on reduced *t(4;11)* cell viability. Even more interesting is our observation that inhibition of RORγ in combination with ATV, a widely used and generally well tolerated agent in cardiovascular disease, significantly reduced *SREBF2* gene expression. At the same time, the statin-induced feedback response was completely abolished, resulting in a potent anti-leukemia synergism. Our findings may be further supported

by studies in solid cancer cells, which have shown nearly identical results regarding the synergistic effect of combining XY018 and statins *in vivo* [159, 199]. Although no *in vivo* experiments were performed in our study, which may limit the conclusions drawn here, the patient-like CRISPR/Cas9 *t(4;11)* model contributes to a more comprehensive view of the association between cancer and the cholesterol pathway as a general targeting mechanism for rapidly growing tumor cells [202].

Based on the above assumptions of a possible interaction of the KMT2A-AFF1 protein complex with SREBP2 and RORγ via the recruitment of DOT1L and histone acetylases, RORγ inhibition in combination with the CBP/p300 inhibitor C646 [259, 268] and with DOT1L inhibitors [82] would also be a very interesting approach.

5.4 Evaluation of the CRISPR/Cas9 *t(4;11)* leukemia model compared to other *KMT2A*r models and its clinical relevance

Since the CRISPR/Cas9 *t(4;11)* leukemia model served as the basis for most of the experiments used to generate the results of this work, the classification of this model in comparison to other cell models will now be examined in more detail. As previously discussed in the introduction to this thesis (see **Section 1.2.4**), the leukemia model developed by the Schneidawind group has notable advantages over previously published models. Nevertheless, the model has some limitations that could be addressed by further protocol optimization.

Several studies have demonstrated that the BM niche provides direct and indirect support to neoplastic and leukemic cells during the development of hematologic malignancies, including *KMT2A*r leukemia. Tumorigenic characteristics include the release of survival-promoting factors, competition for niche space with healthy HSPCs, stroma reprogramming, and physical protection from chemotherapy (reviewed by [269, 270]). Unfortunately, these factors cannot be accurately modeled in cultures containing only *KMT2A*r leukemia cells. Mesenchymal stromal cells (MSCs) constitute a structural element of the BM niche and have an adherent growing character *in vitro* with fibroblast-like morphology. They can be isolated from human BM samples [93, 271-273] or have been established as stromal cell lines. The extension of the CRISPR/Cas9 *KMT2A*r leukemia model by co-culturing of leukemia cells with MSCs will result in experiments that more closely resemble the physiological situation in patients. Furthermore, it is worth noting that *t(4;11)* leukemias typically present a lymphatic phenotype in most affected patients [13]. However, the use of the CRISPR/Cas9 model in the original setting only allows for testing of myeloid differentiation. In the context of B-ALL, besides the cytokine milieu, MSCs may play a crucial role in defining a leukemia-supportive microenvironment [274]. Changing the cultivation conditions would enable testing for both *KMT2A*r AML and ALL. In this regard, Richardson and colleagues have developed a detailed protocol for the *in vitro* differentiation of human pluripotent stem cells into the B-lineage using OP9 and MS-5 co-culture systems [275]. Two other research groups have previously developed model systems to test pro-B-ALL with

t(4;11) chromosomal translocations from CD34+ HSPCs at various developmental stages [93, 94]. Our research group is currently working on establishing a CRISPR/Cas9 model for pro-B-ALL using CD34+ HSPCs derived from huBM and huCB as well. **Figure 43** illustrates the possible procedure with specific adjustments to the cytokine composition and concentration, as well as the use of MS-5 cells [93, 94]. Additional studies could involve transplanting of *t(4;11)* leukemia cells into immunodeficient mice to assess the impact of RORγ inhibition and any potential toxicity *in vivo*. With regard to the cholesterol metabolism in *t(4;11)* leukemia, the results obtained here can be used as a basis for further studies of this type in subsequent models.

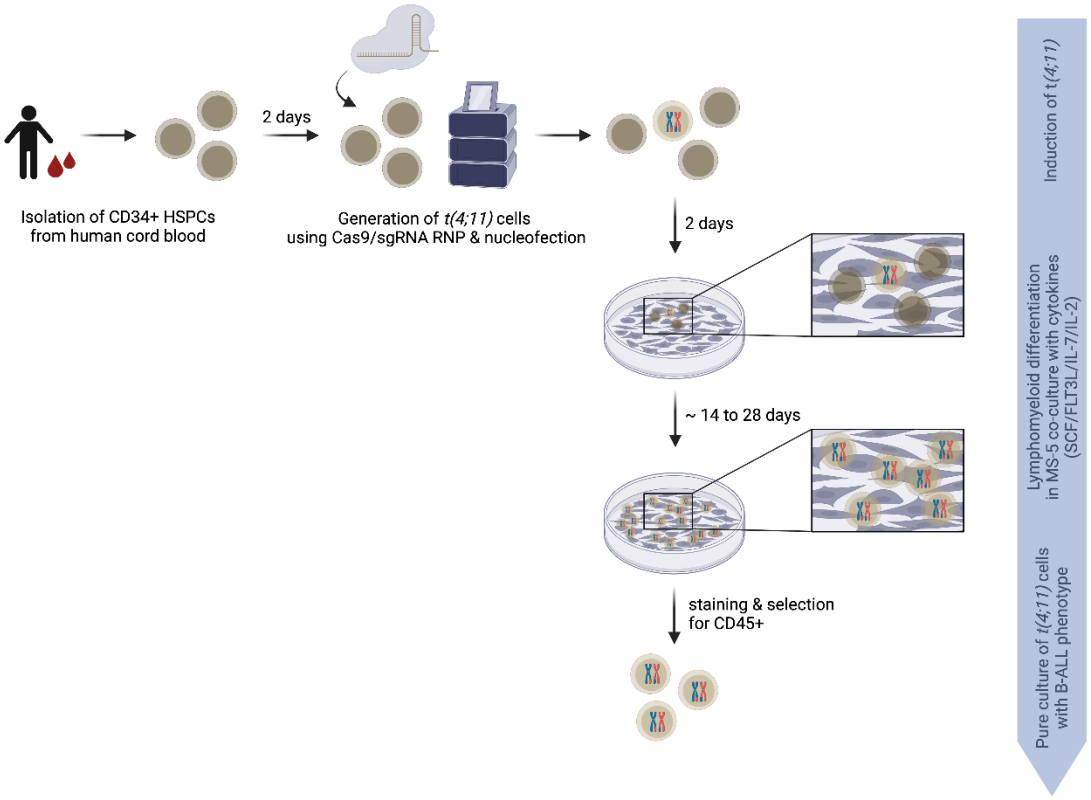

Figure 43: Schematic representation of the CRISPR/Cas9 *t(4;11)* leukemia model for B-ALL phenotype.

CD34+ HSPCs from huCB are cultured and nucleofected with an RNP complex consisting of Cas9 protein and sgRNAs targeting *KMT2A* and *AFF1* [82]. To increase the proliferation of B lymphocytes *in vitro*, the cells are cultured in the presence of MS-5 cells and exposed to a specific cytokine environment. After two to four weeks, an increase in the absolute number of CD45+ CD19+ cells is expected, which can be used as a model system for the further characterization of *t(4;11)* B-ALL. Protocol adapted from [93, 94]. Figure generated with BioRender.

6 Conclusion and outlook

In this study, we found that cholesterol metabolism is significantly upregulated in leukemia cells harboring a *t(4;11)* chromosomal translocation. Furthermore, we identified the RORγ-SREBP2 axis as a promising target for new treatment options for *t(4;11)* leukemia patients to promote anti-leukemic effects. Inhibition of RORγ by an antagonist resulted in a change in intracellular cholesterol metabolism, specifically decreased cholesterol synthesis and uptake, and increased cholesterol export mediated by SREBP2. In addition, the anti-leukemic effects of RORγ inhibition were significantly enhanced by combining it with statins and chemotherapy. Thus, limitations regarding the negative statin-induced feedback can be circumvented and therapeutic efficacy can be enhanced to eventually overcome the poor prognosis of *KMT2A*r leukemia patients [202].

However, there are still questions that need to be addressed in future studies. First, it is still unclear to what extent a *t(4;11)* chromosomal translocation leads to increased leukemic cholesterol metabolism at the molecular level. It is likely that the structural changes associated with a KMT2A-AFF1 fusion lead to increased interaction with the *SREBF2* gene and thus to its activation [229]. The results of our study indicate a superordinate role of the nuclear receptor RORγ. It has a specific influence on the SREBP2-controlled cholesterol metabolism and thus on the growth capacity and consequently on the oncogenic character of *t(4;11)* leukemia cells. Similar to the transcriptional co-activity of the two proteins in TNBC [159], this could also occur in *t(4;11)* leukemias by recruiting CBP/p300 (**Figure 42**). However, we cannot conclude which binding partners of the KMT2A-AFF1 complex are involved leading to a hyper-stimulated cholesterol synthesis. Further experiments using co-immunoprecipitation could provide valuable insights into whether an interaction between SREBP2 and RORγ occurs in *t(4;11)* cells, possibly similar to TNBC, also involving CBP/p300. Treating *t(4;11)* cells with XY018 followed by ChIP-Seq to identify binding sites at promoters of cholesterol biosynthesis genes and examining H3K27ac signaling at these loci would also provide important information on transcriptional activity. In addition, to investigate the direct or indirect involvement of RORγ in the regulation of cholesterol biosynthesis genes in *t(4;11)* cells, a luciferase reporter gene assay would provide valuable information. By cloning the promoter regions of e.g. *HMGCR* in front of the luciferase gene, subsequent transfection of the leukemia cells and treatment with the RORγ antagonist, any changes in luciferase activity could be measured and would provide more information on the involvement of RORγ in cholesterol metabolism.

Second, the focus of our work was mainly on KMT2A-AFF1 fusions with myeloid expression type. Although the results with different cell lines, including the ALL cell line RS4;11, suggest that the conclusions regarding cholesterol metabolism are relevant for both AML and ALL patients, no definitive statements can be made. Therefore, it would be beneficial to extend our *KMT2A*r leukemia model to include a lymphatic phenotype (**Figure 43**). In this respect, an adaptation of the existing CRISPR/Cas9 *t(4;11)* leukemia model with regard to co-cultivation

with MS-5 cells and adjustment of the cytokine concentration would be conceivable. This extended model would make it possible to directly compare AML and ALL cells from one and the same cord blood donor with regard to cholesterol metabolism and other transcriptional pathways.

For all the above purposes, additional experiments with animal models would be beneficial. Once a pure, stably growing culture of *t(4;11)* cells is achieved, these cells could be transplanted into immunocompromised NSG mice. Since NSG mice have already shown a preference for lymphoid differentiation [276], the extended *t(4;11)* model would be of crucial importance, as engraftment of *t(4;11)* cells with a lymphoid phenotype is conceivable. Thus, further investigation is possible to elucidate the pathophysiological role of KMT2A cleavage in relation to RORγ and SREBP2 activity *in vivo*, as well as to gain a better understanding of the potential outcomes of RORγ-targeting therapies.

7 Appendix

Supplementary Table 1: List of patient data sets included in the analysis of gent2 database (*http://gent2.appex.kr*).

Modified from Erkner *et al.* [202].

GSE6401	GSE5820	GSE9476
GSE6477	GSE5788	GSE9874
GSE1133	GSE14286	GSE10631
GSE4475	GSE13996	GSE5580
GSE635	E-MEXP-120	GSE6740
GSE1427	E-MEXP-313	GSE1751
GSE12995	E-TABM-117	GSE2779
GSE6477	E-TABM-125	GSE1010
GSE10255	GSE13591	GSE7893
GSE635	GSE15777	GSE5967
GSE3912	GSE14317	GSE7429
GSE1466	GSE11907	GSE1124
GSE4119	GSE6477	GSE1140
GSE6365	GSE1133	GSE5808
GSE11038	GSE11582	GSE7148
GSE2113	GSE8650	GSE12845
GSE4698	GSE9006	GSE14577
GSE5122	GSE6269	E-AFMX-5
GSE6691	GSE7638	GSE13591
GSE9476	GSE3365	GSE15777
GSE10631	GSE6613	GSE14317
GSE13280	GSE1466	
GSE8970	GSE6236	

Supplementary Table 2: Top downregulated most differentially expressed genes (DEGs) of *t(4;11)* cells treated with XY018 compared to DMSO control (ranked to p_{adj}, genes related to cholesterol metabolism are written in bold).

Modified from Erkner *et al.* [202].

log2FoldChange	p_{value}	p_{adj}	Gene
-1,39798318	4,6588E-31	1,3495E-27	***LDLR***
-2,05193556	1,2451E-29	2,7051E-26	***MSMO1***
-1,75211645	3,6002E-29	6,2571E-26	***SQLE***
-1,46674822	4,2897E-26	6,2129E-23	***TMEM97***
-1,5583479	1,0874E-23	1,35E-20	***FDFT1***
-1,86429591	1,8723E-22	2,0338E-19	***HMGCS1***
-2,06090219	2,606E-22	2,5162E-19	*S100A8*
-1,20751037	8,2093E-22	7,1339E-19	*FADS1*
-1,74153799	1,8133E-19	1,3131E-16	***HMGCR***
-1,28663364	5,4494E-19	3,6427E-16	***SC5D***
-0,90347558	9,3291E-17	5,4046E-14	***SREBF2***
-2,44405671	6,4579E-16	3,5075E-13	***DHCR7***
-1,97176976	1,284E-15	6,5637E-13	***DHCR24***
-1,42200338	1,6756E-15	8,0893E-13	***MVK***
-1,84462906	5,012E-14	2,1777E-11	*PNPLA3*

-0,92476183	1,4276E-12	5,9074E-10	***SCD***
-0,950253	2,3924E-11	9,4501E-09	***EBP***
-1,66355796	1,6312E-10	5,6699E-08	***STARD4***
-1,35743249	1,5106E-09	2,9835E-07	*TGFBI*
-1,27329827	1,562E-09	3,0163E-07	*FADS2*
-0,82879812	1,7598E-09	3,3245E-07	*KCNE3*
-1,19879354	2,5328E-09	4,683E-07	*SLC25A1*
-0,69450329	5,9628E-09	1,0575E-06	***AACS***
-1,96341157	8,8532E-09	1,5085E-06	*NFE2*
-1,80482334	1,2048E-07	1,9036E-05	*F13A1*
-0,7931399	1,7237E-07	2,6279E-05	*PLAC8*
-1,59331917	1,9734E-07	2,9567E-05	*LRG1*
-0,83919034	2,8223E-07	4,1569E-05	*NLRC4*
-0,96318157	3,8031E-07	5,4179E-05	*MMAB*
-0,88095377	4,2589E-07	5,9693E-05	*TUBA1A*
-0,47379277	1,2395E-06	0,0001561	*PPDPF*
-1,18993573	1,7311E-06	0,00021188	***INSIG1***
-2,03950448	1,8232E-06	0,00022005	*S100A9*
-1,16204274	2,3817E-06	0,00028352	***MVD***
-0,47944467	2,7106E-06	0,00030993	*ACTG1*
-0,55222706	3,3288E-06	0,00036616	*NCF4*
-0,91268133	3,6508E-06	0,00039656	*ATF5*
-0,67369716	3,7169E-06	0,00039763	*S100A6*
-0,48965061	4,0326E-06	0,00041718	*ITGB2*
-0,58011046	4,685E-06	0,00046796	*RHOU*
-0,47006398	5,7401E-06	0,00056683	*RNASET2*
-0,44420597	5,9116E-06	0,00057721	*ANP32B*
-0,9256395	6,3872E-06	0,00060994	*PRKAR2B*
-1,44666071	6,9435E-06	0,0006488	*SERPINF1*
-0,52455652	6,9173E-06	0,0006488	*H4C3*
-0,75876605	7,0752E-06	0,00065408	*MIR223HG*
-0,4820088	7,7408E-06	0,00068641	*GPI*
-0,42442134	8,1877E-06	0,0007187	*PGD*
-0,73689431	8,3177E-06	0,00072281	*EPB41L4A-AS1*
-0,62211004	8,494E-06	0,00073082	*MXD1*
-0,793365077	1,45502E-05	0,001227581	*C1orf162*
-0,96268822	1,69448E-05	0,001389155	*ARRDC3*
-0,414918232	1,69068E-05	0,001389155	*PGK1*
-1,124896562	1,71714E-05	0,001394574	*RPH3AL-AS1*
-0,618388526	1,83444E-05	0,001474611	*TNFSF13B*
-0,489899328	1,84963E-05	0,001474611	*NXPE3*
-0,462406004	1,97207E-05	0,001557935	*FOSL2*
-1,018729307	2,12641E-05	0,001664732	*CCR2*
-0,438675963	2,28405E-05	0,001772175	*IFITM2*
-0,518436246	2,329E-05	0,001791059	*FCGR2B*
-0,724302412	2,60277E-05	0,001984038	*SIGLEC14*
-1,131643966	3,338E-05	0,00250062	***ERG28***
-0,422926118	3,67371E-05	0,002705471	*APLP2*

-0,818912996	3,88463E-05	0,002836761	***NSDHL***
-1,79523157	4,87517E-05	0,003362316	*BPI*
-1,173908309	4,9991E-05	0,003393919	*PLB1*
-0,877158433	5,47186E-05	0,003576247	*FCGR2C*
-0,822778131	5,40149E-05	0,003576247	*SULT1A1*
-0,757391802	5,42288E-05	0,003576247	*QPRT*
-0,755358735	5,31698E-05	0,003576247	*GBE1*
-0,475748218	5,56259E-05	0,003607378	*TOMM7*
-0,491279499	6,05905E-05	0,003871554	*OSCAR*
-1,575050414	6,233E-05	0,003953631	***IDI1***
-0,527480159	6,84539E-05	0,004256196	*TKT*
-0,40418795	6,90591E-05	0,004256196	*OIP5-AS1*
-0,386074837	6,90547E-05	0,004256196	*PGAM1*
-0,976629126	7,26158E-05	0,004412806	*MLXIPL*
-0,560976996	7,97027E-05	0,004776662	*LDHA*
-0,728816854	8,10051E-05	0,00482147	*CSF3R*
-0,384222814	8,17959E-05	0,004835416	*SEC11A*
-0,476961156	0,000100347	0,005852431	*IRF2BPL*
-0,826530535	0,000112452	0,006471553	*CYTOR*
-0,571972292	0,000117277	0,006704839	*ROGDI*
-0,943068168	0,000118798	0,006747428	*NDRG1*
-0,493524511	0,000123355	0,006915816	*NUDT16L1*
-0,553944386	0,00013357	0,007346354	*MTHFR*
-0,641025003	0,000136634	0,007467586	
-0,446712943	0,000138646	0,007530191	*CKS1B*
-0,884878565	0,000166814	0,008732622	***HSD17B7***
-0,716045839	0,000180235	0,009267714	*SLC46A3*
-0,763450473	0,000182253	0,00931634	*AIF1*

Supplementary Table 3: Top upregulated DEGs of *t(4;11)* cells treated with XY018 compared to DMSO control (ranked to p_{adj}, genes related to cholesterol metabolism are written in bold).

Modified from Erkner *et al.* [202].

log2FoldChange	p_{value}	p_{adj}	Gene
3,30006868	2,8072E-53	2,4394E-49	***ABCA1***
4,06725785	1,281E-41	5,5661E-38	***ABCG1***
1,29150457	9,1069E-20	7,1945E-17	*MTCO1P40*
1,0108047	4,1568E-18	2,5802E-15	*MTCO1P12*
1,06043552	8,9642E-15	4,1E-12	*MT-TS1*
0,95208639	6,1209E-11	2,3126E-08	*MT-TN*
0,72032363	6,4643E-11	2,3406E-08	*CERT1*
0,80813702	3,4736E-10	9,1449E-08	*NEAT1*
0,8393719	3,9066E-10	9,1449E-08	***RNF145***
1,21572517	4,1271E-10	9,1449E-08	*RNA5S15*
1,21572517	4,1271E-10	9,1449E-08	*RNA5S16*
1,21646942	4,5251E-10	9,1449E-08	*RNA5S1*
1,21646942	4,5251E-10	9,1449E-08	*RNA5S2*

1,21646942	4,5251E-10	9,1449E-08	*RNA5S3*
1,21646942	4,5251E-10	9,1449E-08	*RNA5S4*
1,21646942	4,5251E-10	9,1449E-08	*RNA5S5*
1,21646942	4,5251E-10	9,1449E-08	*RNA5S6*
1,21646942	4,5251E-10	9,1449E-08	*RNA5S7*
1,21646942	4,5251E-10	9,1449E-08	*RNA5S8*
1,21646942	4,5251E-10	9,1449E-08	*RNA5S10*
1,21646942	4,5251E-10	9,1449E-08	*RNA5S11*
1,21646942	4,5251E-10	9,1449E-08	*RNA5S12*
1,21646942	4,5251E-10	9,1449E-08	*RNA5S13*
1,21646942	4,5251E-10	9,1449E-08	*RNA5S14*
1,21646942	4,5251E-10	9,1449E-08	*RNA5S17*
0,81066124	2,6556E-09	4,8077E-07	*MYLIP*
1,22933232	7,2657E-09	1,2628E-06	*SELL*
0,53964992	1,3445E-08	2,2469E-06	*MT-RNR2*
0,71189136	3,4257E-08	5,6169E-06	*MTRNR2L3*
0,63072599	4,2151E-08	6,7832E-06	*ASAH1*
0,86496297	1,36E-07	2,1105E-05	*STS*
0,76161511	3,7661E-07	5,4179E-05	*LPCAT1*
1,31660903	4,4429E-07	6,1283E-05	*TNS1*
0,89599323	4,7169E-07	6,4047E-05	*LGALS3*
0,78045386	6,4065E-07	8,565E-05	*BTD*
0,63753322	7,3714E-07	9,7057E-05	*MT-CO1*
1,40769834	1,0893E-06	0,00014129	*MTSS1*
1,86662953	1,1258E-06	0,00014388	*TFRC*
0,751778	1,3913E-06	0,00017272	*WASF1*
1,25233252	2,578E-06	0,00030274	*PPP1R27*
0,55096739	2,6488E-06	0,00030691	*FNIP1*
0,57712323	2,9904E-06	0,00033748	*CALU*
0,7510253	3,1456E-06	0,00035045	*MTRNR2L6*
0,47155898	3,7978E-06	0,00039763	*MBNL1*
0,6374291	3,7933E-06	0,00039763	*MTCO2P12*
0,62351577	4,1386E-06	0,00042311	*PAN3*
1,03114317	4,2599E-06	0,00043044	*ANKRD28*
0,62871492	6,2548E-06	0,00060393	*PLIN2*
0,55020699	7,4048E-06	0,00067651	*CAPG*
0,62401754	7,4736E-06	0,00067651	*MTND6P3*
0,846842188	7,56878E-06	0,000678069	*MT-TA*
0,59976656	1,36119E-05	0,001159681	*MT-CO2*
0,599036062	1,56736E-05	0,001309653	*BIVM*
0,690712647	2,63293E-05	0,001989576	*MT-ATP6*
0,552166641	3,45145E-05	0,002563514	*STX3*
0,71712826	4,06946E-05	0,002946969	*PDGFC*
0,424042485	4,12856E-05	0,00296506	*ARL8B*
0,683881766	4,53325E-05	0,00322901	*HIVEP1*
0,650294432	4,65663E-05	0,003289928	*RASAL2*
0,460905904	4,7024E-05	0,00329547	*GOLGA4*
0,795066295	4,80608E-05	0,003341185	*CAMK1D*

0,451649367	4,95394E-05	0,003389745	*SLC39A7*
0,45801416	5,47343E-05	0,003576247	*NFE2L2*
1,161504218	5,92441E-05	0,003813566	*ENPP2*
0,79346386	6,46046E-05	0,004068218	*CAMSAP2*
0,655460926	6,96471E-05	0,004262209	*CREB3*
0,416373308	7,56131E-05	0,004563038	*NFATC1*
0,493968222	9,83416E-05	0,00577425	*MT-CYB*
0,796859354	0,000104879	0,006076002	*SCFD2*
0,894045185	0,000123163	0,006915816	*RELB*
0,751611775	0,000126436	0,007043137	*LTB*
0,871842151	0,000128625	0,007119415	*PITPNC1*
0,542707442	0,00014164	0,007645066	*CYFIP1*
0,454989576	0,000147423	0,007908063	*TUT4*
0,428542553	0,000148585	0,007921486	*MTRNR2L12*
0,433367252	0,000162	0,00858403	*MTRNR2L8*
0,507853617	0,000165467	0,008714601	*MT-ATP8*
0,70112291	0,000173349	0,009020354	*PDGFA*
0,77727253	0,000177238	0,009167847	*MEMO1*
0,402211614	0,000183497	0,009325064	*MT-RNR1*
0,647116533	0,000191639	0,009636629	*MGLL*
0,411439242	0,00024883	0,012356178	*FLT3*
0,3973053	0,000322054	0,015722739	*CELF2*
0,551264808	0,000324142	0,015736278	*MTATP8P1*
0,643229014	0,000340186	0,016332692	*MT-TE*
0,414123891	0,000347673	0,016600442	*GLS*
0,472233097	0,000375523	0,017587591	*LILRB1*
0,560446115	0,000428578	0,019810335	*MTMR10*
0,462685044	0,000476325	0,021446979	*TTC3P1*
0,930307405	0,000485154	0,021731889	*UBASH3B*
0,728938509	0,000501737	0,022245377	*ENAH*
0,811988275	0,000513991	0,022673002	*RHOBTB1*
0,728026224	0,000520637	0,02273535	*LINC00641*
0,310211963	0,000555654	0,024143169	*WDR43*
0,375114513	0,000572553	0,024631105	*LCORL*
0,975532998	0,000584851	0,025036251	*IGSF6*
0,437282794	0,000590116	0,025137805	*RALGDS*
0,349147973	0,000679143	0,028373817	*ALG5*

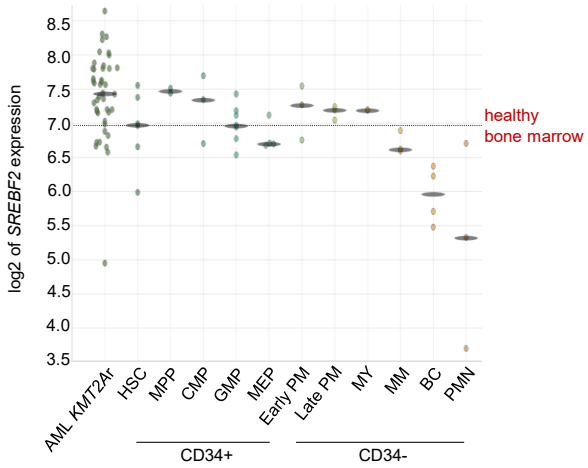

Supplementary Figure 1: *SREBF2* expression in AML *KMT2A*r cells of leukemia patients and healthy cells at different cell differentiation stages of healthy individuals.

HSC (hematopoietic stem cell), MPP (multipotential progenitors), CMP (common myeloid progenitors), GMP (granulocyte monocyte progenitors), MEP (megakaryocyte-erythroid progenitors), early PM (early promyelocyte), late PM (late promyelocyte), MY (myelocyte), MM (metamyelocytes), BC (band cell), PMN (polymorphonuclear cells). Data obtained from GSE13159, *https://servers.binf.ku.dk/bloodspot/,* accessed 05/2023.

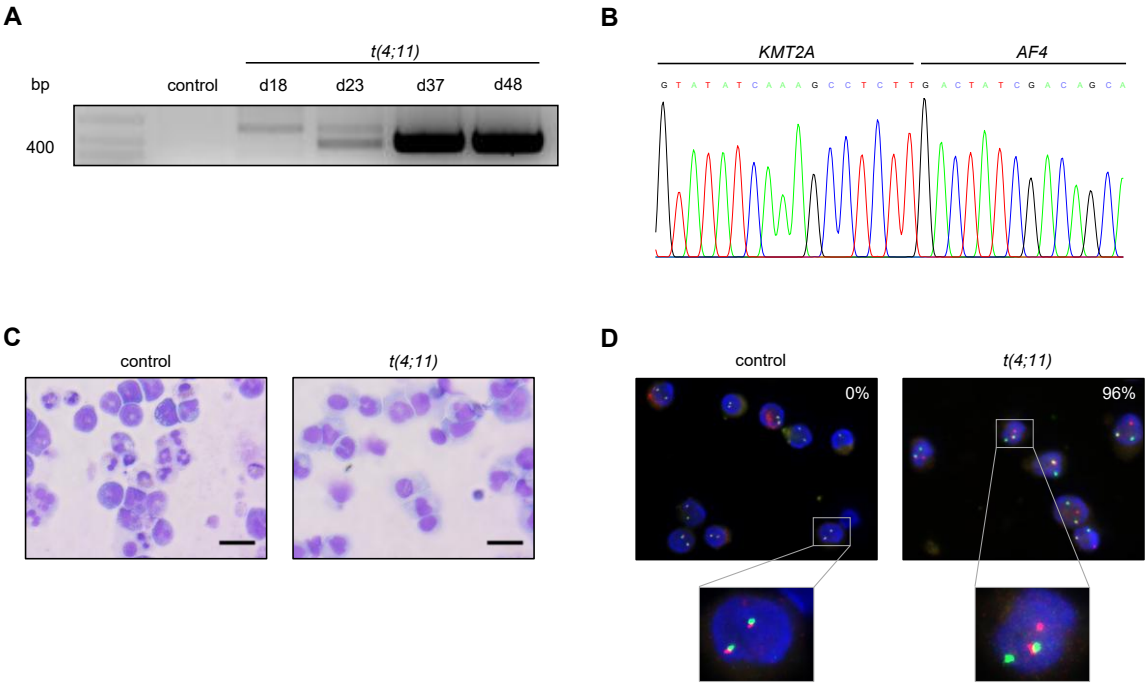

Supplementary Figure 2: Generation of CRISPR/Cas9 *t(4;11)* cells.

CD34+ HSPCs were isolated and nucleofected with RNPs consisting of Cas9 protein and sgRNAs targeting the *KMT2A* and *AFF1* genes. **(A)** Representative translocation fusion products were detected in genomic DNA by PCR at different time points. Cells nucleofected without RNP served as control. **(B)** After successful detection of fusion products, DNA was isolated and sequenced by Sanger sequencing.

The sequences were aligned with reference sequences of human *KMT2A* and *AF4*. **(C)** For further characterization, cell morphology and differentiation pattern were analyzed by Pappenheim staining. Shown are representative images of CRISPR/Cas9 *t(4;11)* cells and control cells nucleofected without RNP and cultured over the same time period. Images of *t(4;11)* cells show a homogenous culture of blasts, while control cells already show a mature differentiation pattern. Scale bars represent 20 µm. **(D)** Verification and determination of the percentage of translocated cells by FISH analysis using a *KMT2A* dual colour break-apart probe. FISH was performed between day 60 and day 100 after nucleofection. Shown are representative images of *t(4;11)* and control cells. In the case of a positive translocation, the green and red fluorescence signals were separated. The percentage of cells positive for the translocation was determined by examining 100 cells per sample.

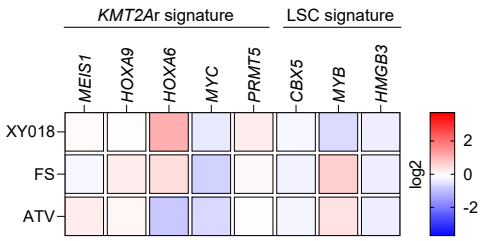

Supplementary Figure 3: *KMT2A*r and LSC gene signature of CRISPR/Cas9 *t(4;11)* cells treated with cholesterol-modulating agents.

Heat map display of fold changes (in log2) in *KMT2A*r- and LSC-related genes in CRISPR/Cas9 *t(4;11)* cells treated with 15 µM of XY018, FS or ATV for seven days. The expression of indicated genes was measured by RT-qPCR for which DMSO-treated cells were set as 1. Each square represents the mean of three independent donors (n=3) ± SD.

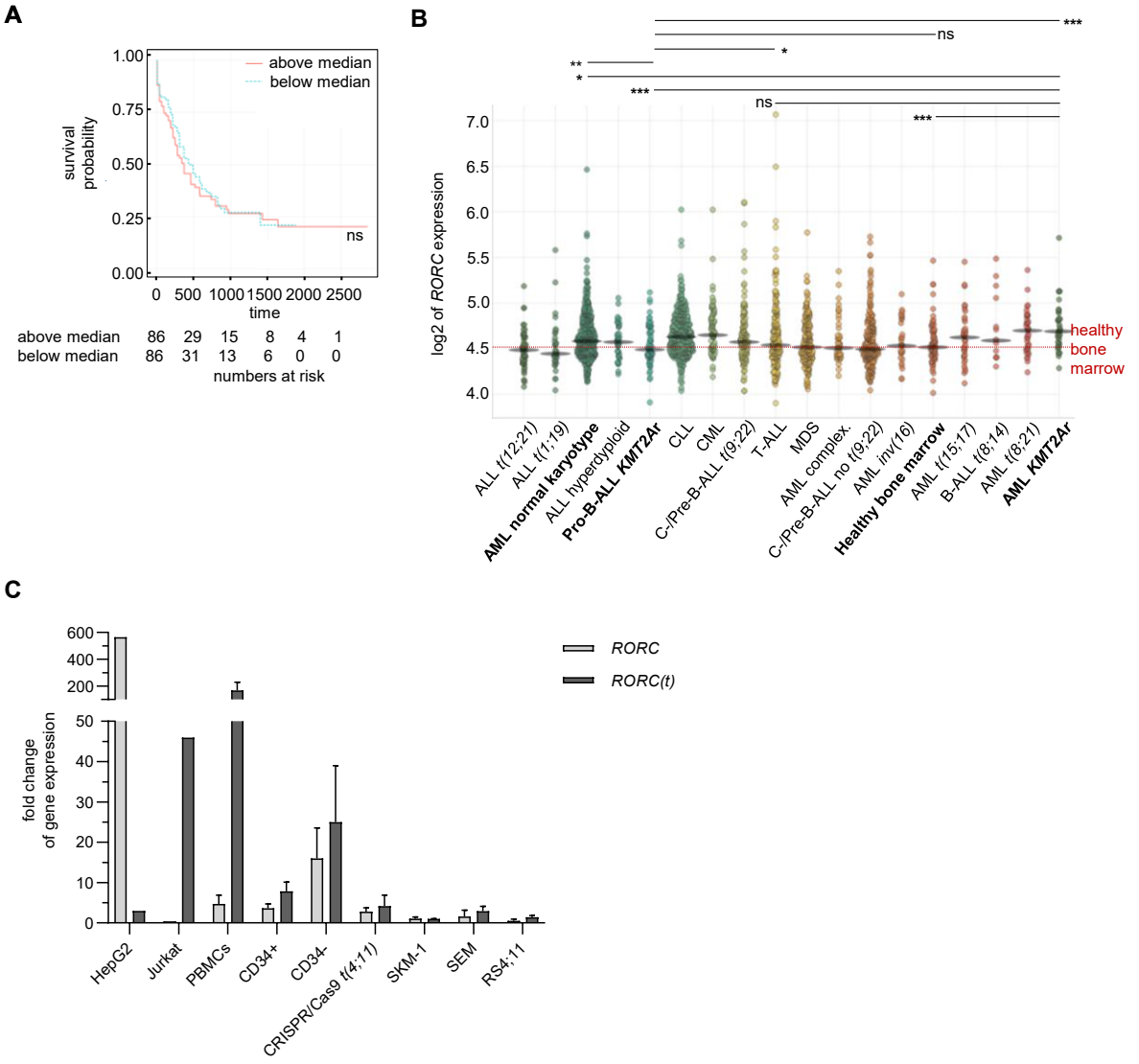

Supplementary Figure 4: Validation of *RORC* level in different types of leukemia.

(A) Using data from AML patients from The Cancer Genome Atlas (*https://tcga-data.nci.nih.gov/tcga*), the overall survival of AML patients, divided into *RORC*^{low} (blue line) and *RORC*^{high} group (red line) according to the median value of *RORC*, were compared with Kaplan-Meier analysis (data obtained from *https://servers.binf.ku.dk/bloodspot/*). Student's *t* test. ns=not significant. **(B)** *RORC* expression (in log2) in healthy and leukemic patient samples (GSE13159, data obtained from *https://servers.binf.ku.dk/bloodspot/,* accessed 05/2023). Student's *t* test. **p*<0.05. ***p*<0.01. ****p*<0.001. ns=not significant. **(C)** RT-qPCR analysis of *RORC* and *RORC(t)* gene expression in different cell types. For primer testing, HepG2 (for *RORC*) and Jurkat cells (for *RORC(t)*) were used as positive control. SKM-1 cells were set at 1. Bars show the mean of three independent donors (n=3) ± SD for primary cells and independent experiments (n=3) for cell lines. Modified from Erkner *et al.* [202].

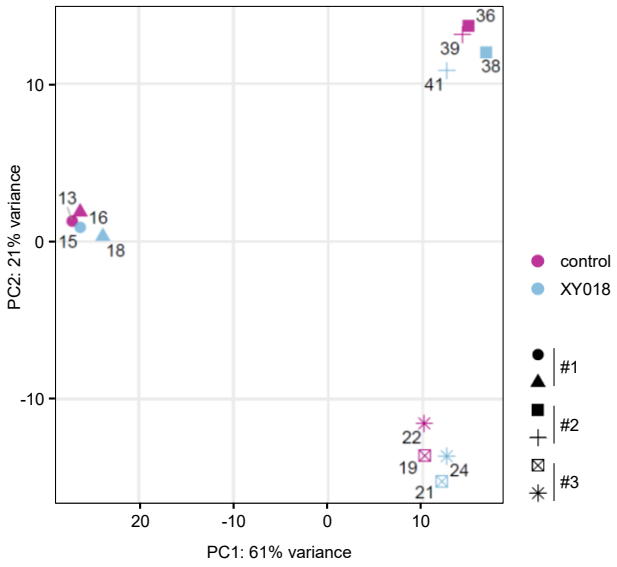

Supplementary Figure 5: RNA-Seq data sample overview.

Plot of principal component (PC) analysis of gene expression variation in the 12 sequenced samples. CRISPR/Cas9 *t(4;11)* cells were treated with DMSO (control, purple) or 15 µM XY018 (blue) for seven days. For RNA-Seq, three independent donors (n=3) in biological duplicates were used. # describes independent donors.

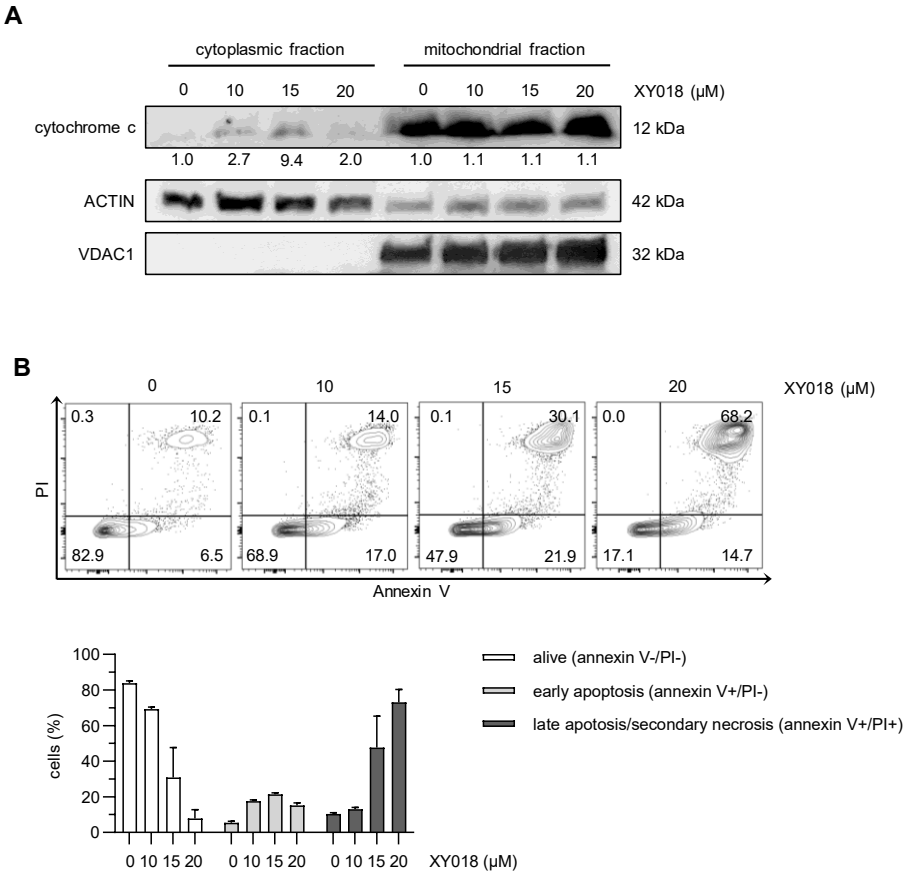

Supplementary Figure 6: XY018 induces cytochrome c release from mitochondria during apoptosis.

(A) Representative Western blot analysis of cytochrome c in CRISPR/Cas9 *t(4;11)* cells treated with indicated concentrations of XY018 or DMSO (0 µM) for seven days. For each sample, 20 µg of cytosolic and mitochondrial proteins were used. Anti-GAPDH was used as cytosol fraction loading control and anti-VDAC1 as mitochondrial fraction loading control. **(B)** Representative dot plots and pooled data showing living (Annexin V-, PI-), early apoptotic (Annexin V+, PI-) and late apoptotic cells (Annexin V+, PI+). CRISPR/Cas9 *t(4;11)* cells were treated as described in (A) and histograms show the mean of three independent donors (n=3) ± SD.

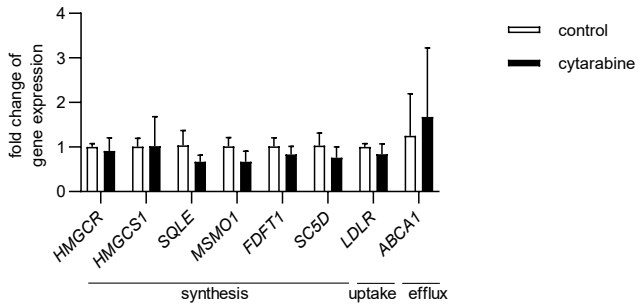

Supplementary Figure 7: Cholesterol target gene expression of CRISPR/Cas9 *t(4;11)* cells treated with cytarabine.

CRISPR/Cas9 *t(4;11)* cells were treated with 5nM cytarabine or the respective control (PBS) for seven days and analyzed with RT-qPCR. Bars represent the mean of three independent donors (n=3) ± SD.

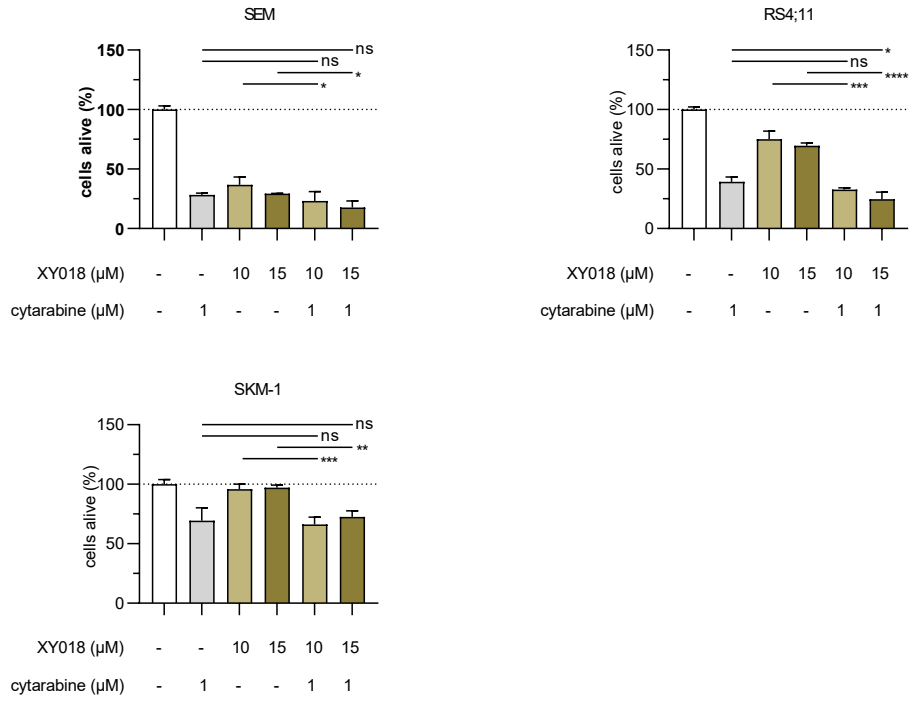

Supplementary Figure 8: Combinatorial treatment effect of XY018 and cytarabine in cell lines.

t(4;11) cell lines (SEM, RS4;11 and MV4-11) and SKM-1 cells were treated with 10 µM or 15 µM XY018 alone or in combination with 1 µM cytarabine for 48 hours. Bars represent the mean of three independent experiments (n=3) ± SD. One-way ANOVA. ***p*<0.01. ****p*<0.001. *****p*<0.0001. ns=not significant. Modified from Erkner *et al.* [202].

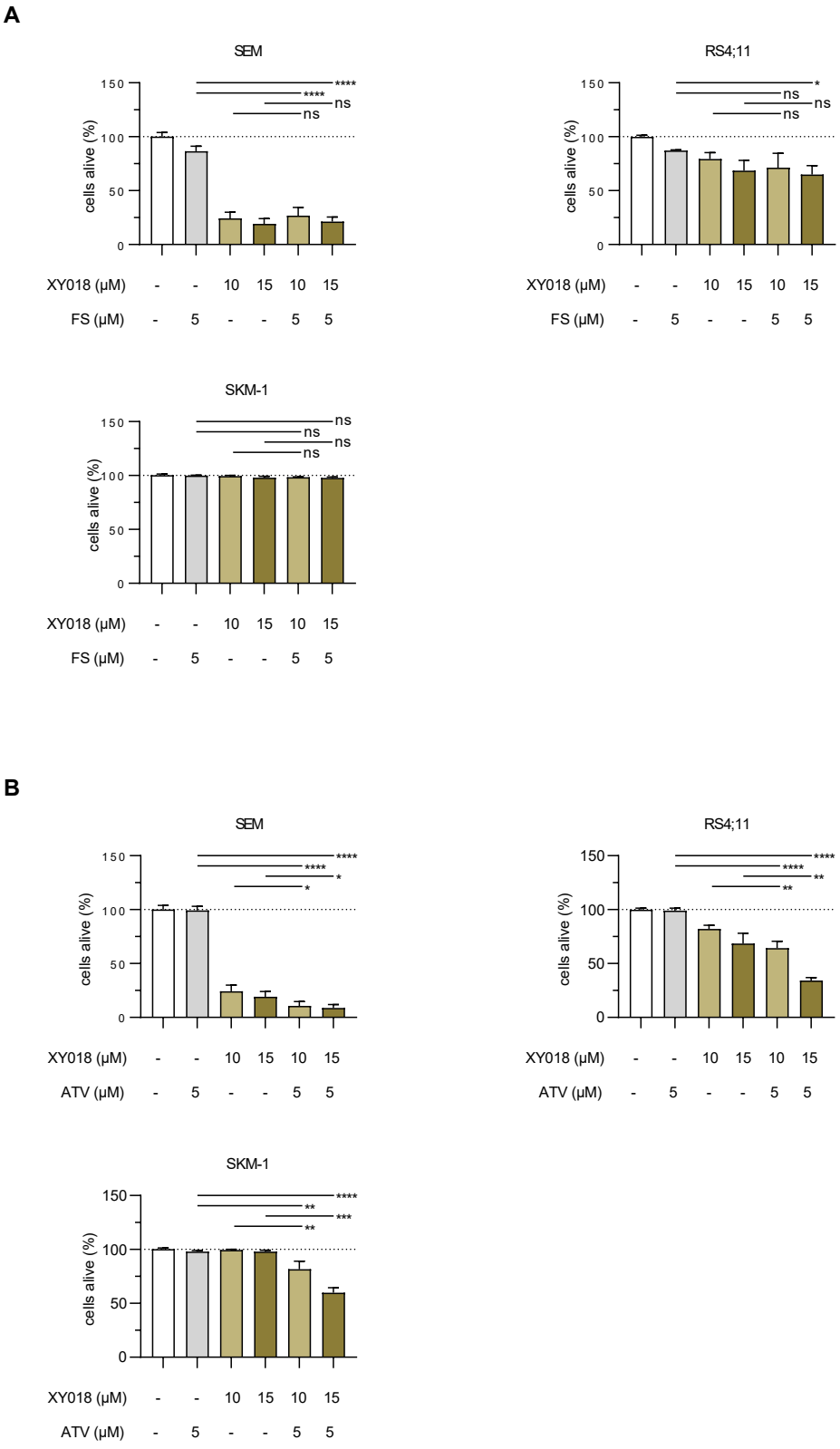

Supplementary Figure 9: Combinatorial treatment effect of XY018 and cholesterol-modulating agents in cell lines.

t(4;11) cell lines (SEM, RS4;11 and MV4-11) and SKM-1 cells were treated with 10 µM or 15 µM XY018 alone or in combination with 5 µM FS **(A)** or 5 µM ATV **(B)** for 48 hours. Bars represent the mean of three independent experiments (n=3) ± SD. One-way ANOVA. ***p*<0.01. ****p*<0.001. *****p*<0.0001. ns=not significant. Modified from Erkner *et al.* [202].

8 References

1. Till, J.E. and E.A. McCulloch, *Hemopoietic stem cell differentiation.* Biochim Biophys Acta, 1980. **605**(4): p. 431-59.
2. Notta, F., et al., *Isolation of single human hematopoietic stem cells capable of long-term multilineage engraftment.* Science, 2011. **333**(6039): p. 218-21.
3. Eaves, C.J., *Hematopoietic stem cells: concepts, definitions, and the new reality.* Blood, 2015. **125**(17): p. 2605-13.
4. Zhang, Y., et al., *Hematopoietic Hierarchy - An Updated Roadmap.* Trends Cell Biol, 2018. **28**(12): p. 976-986.
5. Gökbuget, N., et al., *Leitlinie Akute Lymphatische Leukämie (ALL) der Fachgesellschaften DGHO, OeGHO, SGMO, SGH+SSH.* www.onkopedia.com, 2022.
6. Röllig, C., et al., *Leilinie Akute Myeloische Leukämie (AML) der Fachgesellschaften DGHO, OeGHO, SGMO, SGH+SSH.* www.onkopedia.com, 2023.
7. Arber, D.A., et al., *The 2016 revision to the World Health Organization classification of myeloid neoplasms and acute leukemia.* Blood, 2016. **127**(20): p. 2391-405.
8. Khoury, J.D., et al., *The 5th edition of the World Health Organization Classification of Haematolymphoid Tumours: Myeloid and Histiocytic/Dendritic Neoplasms.* Leukemia, 2022. **36**(7): p. 1703-1719.
9. Alaggio, R., et al., *The 5th edition of the World Health Organization Classification of Haematolymphoid Tumours: Lymphoid Neoplasms.* Leukemia, 2022. **36**(7): p. 1720-1748.
10. Kreuzer, K.A., et al., *Leilinie Hämatologische Diagnostik der Fachgesellschaften DGHO, OeGHO, SGMO, SGH+SSH.* www.onkopedia.com, 2022.
11. Harris, N.L., et al., *The World Health Organization classification of neoplastic diseases of the hematopoietic and lymphoid tissues. Report of the Clinical Advisory Committee meeting, Airlie House, Virginia, November, 1997.* Ann Oncol, 1999. **10**(12): p. 1419-32.
12. Meyer, C., et al., *New insights to the MLL recombinome of acute leukemias.* Leukemia, 2009. **23**(8): p. 1490-9.
13. Meyer, C., et al., *The KMT2A recombinome of acute leukemias in 2023.* Leukemia, 2023. **37**(5): p. 988-1005.
14. Marschalek, R., *Systematic Classification of Mixed-Lineage Leukemia Fusion Partners Predicts Additional Cancer Pathways.* Ann Lab Med, 2016. **36**(2): p. 85-100.
15. Sherbenou, D.W. and B.J. Druker, *Applying the discovery of the Philadelphia chromosome.* J Clin Invest, 2007. **117**(8): p. 2067-74.
16. Komorowski, L., et al., *Philadelphia Chromosome-Positive Leukemia in the Lymphoid Lineage-Similarities and Differences with the Myeloid Lineage and Specific Vulnerabilities.* Int J Mol Sci, 2020. **21**(16).
17. Andersson, A.K., et al., *The landscape of somatic mutations in infant MLL-rearranged acute lymphoblastic leukemias.* Nat Genet, 2015. **47**(4): p. 330-7.
18. Tkachuk, D.C., S. Kohler, and M.L. Cleary, *Involvement of a homolog of Drosophila trithorax by 11q23 chromosomal translocations in acute leukemias.* Cell, 1992. **71**(4): p. 691-700.
19. Djabali, M., et al., *A trithorax-like gene is interrupted by chromosome 11q23 translocations in acute leukaemias.* Nat Genet, 1992. **2**(2): p. 113-8.
20. Hsieh, J.J., et al., *Proteolytic cleavage of MLL generates a complex of N- and C-terminal fragments that confers protein stability and subnuclear localization.* Mol Cell Biol, 2003. **23**(1): p. 186-94.
21. Hsieh, J.J., E.H. Cheng, and S.J. Korsmeyer, *Taspase1: a threonine aspartase required for cleavage of MLL and proper HOX gene expression.* Cell, 2003. **115**(3): p. 293-303.
22. Yokoyama, A. and M.L. Cleary, *Menin critically links MLL proteins with LEDGF on cancer-associated target genes.* Cancer Cell, 2008. **14**(1): p. 36-46.
23. Caslini, C., et al., *Interaction of MLL amino terminal sequences with menin is required for transformation.* Cancer Res, 2007. **67**(15): p. 7275-83.
24. Wang, H., et al., *Structure of H3K36-methylated nucleosome-PWWP complex reveals multivalent cross-gyre binding.* Nat Struct Mol Biol, 2020. **27**(1): p. 8-13.

25. Birke, M., et al., *The MT domain of the proto-oncoprotein MLL binds to CpG-containing DNA and discriminates against methylation.* Nucleic Acids Res, 2002. **30**(4): p. 958-65.
26. Muntean, A.G., et al., *The PAF complex synergizes with MLL fusion proteins at HOX loci to promote leukemogenesis.* Cancer Cell, 2010. **17**(6): p. 609-21.
27. McGinty, R.K., et al., *Chemically ubiquitylated histone H2B stimulates hDot1L-mediated intranucleosomal methylation.* Nature, 2008. **453**(7196): p. 812-6.
28. Xia, Z.B., et al., *MLL repression domain interacts with histone deacetylases, the polycomb group proteins HPC2 and BMI-1, and the corepressor C-terminal-binding protein.* Proc Natl Acad Sci U S A, 2003. **100**(14): p. 8342-7.
29. Chang, P.Y., et al., *Binding of the MLL PHD3 finger to histone H3K4me3 is required for MLL-dependent gene transcription.* J Mol Biol, 2010. **400**(2): p. 137-44.
30. Fair, K., et al., *Protein interactions of the MLL PHD fingers modulate MLL target gene regulation in human cells.* Mol Cell Biol, 2001. **21**(10): p. 3589-97.
31. Wysocka, J., et al., *WDR5 associates with histone H3 methylated at K4 and is essential for H3 K4 methylation and vertebrate development.* Cell, 2005. **121**(6): p. 859-72.
32. Steward, M.M., et al., *Molecular regulation of H3K4 trimethylation by ASH2L, a shared subunit of MLL complexes.* Nat Struct Mol Biol, 2006. **13**(9): p. 852-4.
33. Milne, T.A., et al., *MLL targets SET domain methyltransferase activity to Hox gene promoters.* Mol Cell, 2002. **10**(5): p. 1107-17.
34. Ernst, P., et al., *MLL and CREB bind cooperatively to the nuclear coactivator CREB-binding protein.* Mol Cell Biol, 2001. **21**(7): p. 2249-58.
35. Dou, Y., et al., *Physical association and coordinate function of the H3 K4 methyltransferase MLL1 and the H4 K16 acetyltransferase MOF.* Cell, 2005. **121**(6): p. 873-85.
36. Weinert, B.T., et al., *Time-Resolved Analysis Reveals Rapid Dynamics and Broad Scope of the CBP/p300 Acetylome.* Cell, 2018. **174**(1): p. 231-244 e12.
37. Yu, B.D., et al., *Altered Hox expression and segmental identity in Mll-mutant mice.* Nature, 1995. **378**(6556): p. 505-8.
38. Butler, L.H., et al., *The HRX proto-oncogene product is widely expressed in human tissues and localizes to nuclear structures.* Blood, 1997. **89**(9): p. 3361-70.
39. Ernst, P., et al., *Definitive hematopoiesis requires the mixed-lineage leukemia gene.* Dev Cell, 2004. **6**(3): p. 437-43.
40. Ernst, P., et al., *An Mll-dependent Hox program drives hematopoietic progenitor expansion.* Curr Biol, 2004. **14**(22): p. 2063-9.
41. Look, A.T., *Oncogenic transcription factors in the human acute leukemias.* Science, 1997. **278**(5340): p. 1059-64.
42. Tyagi, S., et al., *E2F activation of S phase promoters via association with HCF-1 and the MLL family of histone H3K4 methyltransferases.* Mol Cell, 2007. **27**(1): p. 107-19.
43. Liu, H., E.H. Cheng, and J.J. Hsieh, *Bimodal degradation of MLL by SCFSkp2 and APCCdc20 assures cell cycle execution: a critical regulatory circuit lost in leukemogenic MLL fusions*. Genes Dev, 2007. **21**(19): p. 2385-98.
44. Reichel, M., et al., *Rapid isolation of chromosomal breakpoints from patients with t(4;11) acute lymphoblastic leukemia: implications for basic and clinical research.* Cancer Res, 1999. **59**(14): p. 3357-62.
45. Fugmann, S.D., et al., *The RAG proteins and V(D)J recombination: complexes, ends, and transposition.* Annu Rev Immunol, 2000. **18**: p. 495-527.
46. Reichel, M., et al., *Fine structure of translocation breakpoints in leukemic blasts with chromosomal translocation t(4;11): the DNA damage-repair model of translocation.* Oncogene, 1998. **17**(23): p. 3035-44.
47. Gillert, E., et al., *A DNA damage repair mechanism is involved in the origin of chromosomal translocations t(4;11) in primary leukemic cells.* Oncogene, 1999. **18**(33): p. 4663-71.
48. Nilson, I., et al., *Exon/intron structure of the human ALL-1 (MLL) gene involved in translocations to chromosomal region 11q23 and acute leukaemias.* Br J Haematol, 1996. **93**(4): p. 966-72.

49. Nilson, I., et al., *Exon/intron structure of the human AF-4 gene, a member of the AF-4/LAF-4/FMR-2 gene family coding for a nuclear protein with structural alterations in acute leukaemia.* Br J Haematol, 1997. **98**(1): p. 157-69.
50. Okuda, H., et al., *Cooperative gene activation by AF4 and DOT1L drives MLL-rearranged leukemia.* J Clin Invest, 2017. **127**(5): p. 1918-1931.
51. Krivtsov, A.V., et al., *Transformation from committed progenitor to leukaemia stem cell initiated by MLL-AF9.* Nature, 2006. **442**(7104): p. 818-22.
52. Chang, M.J., et al., *Histone H3 lysine 79 methyltransferase Dot1 is required for immortalization by MLL oncogenes.* Cancer Res, 2010. **70**(24): p. 10234-42.
53. Bitoun, E., P.L. Oliver, and K.E. Davies, *The mixed-lineage leukemia fusion partner AF4 stimulates RNA polymerase II transcriptional elongation and mediates coordinated chromatin remodeling.* Hum Mol Genet, 2007. **16**(1): p. 92-106.
54. Okada, Y., et al., *hDOT1L links histone methylation to leukemogenesis.* Cell, 2005. **121**(2): p. 167-78.
55. Krivtsov, A.V., et al., *H3K79 methylation profiles define murine and human MLL-AF4 leukemias.* Cancer Cell, 2008. **14**(5): p. 355-68.
56. Ayton, P.M. and M.L. Cleary, *Transformation of myeloid progenitors by MLL oncoproteins is dependent on Hoxa7 and Hoxa9.* Genes Dev, 2003. **17**(18): p. 2298-307.
57. Rowley, J.D., *The der(11) chromosome contains the critical breakpoint junction in the 4;11, 9;11, and 11;19 translocations in acute leukemia.* Genes Chromosomes Cancer, 1992. **5**(3): p. 264-6.
58. Kowarz, E., et al., *Complex MLL rearrangements in t(4;11) leukemia patients with absent AF4.MLL fusion allele.* Leukemia, 2007. **21**(6): p. 1232-8.
59. Bursen, A., et al., *The AF4.MLL fusion protein is capable of inducing ALL in mice without requirement of MLL.AF4.* Blood, 2010. **115**(17): p. 3570-9.
60. Gaussmann, A., et al., *Combined effects of the two reciprocal t(4;11) fusion proteins MLL.AF4 and AF4.MLL confer resistance to apoptosis, cell cycling capacity and growth transformation.* Oncogene, 2007. **26**(23): p. 3352-63.
61. Dohner, H., et al., *Diagnosis and management of AML in adults: 2022 recommendations from an international expert panel on behalf of the ELN.* Blood, 2022. **140**(12): p. 1345-1377.
62. Creutzig, U., M. Dworzak, and D. Reinhardt, *L11 Akute Myeloische Leukämie -AML- im Kindes- und Jugendalter.* www.awmf.org, 2019.
63. Escherich, G., and M. Schrappe, *Akute lymphoblastische Leukämie -ALL- im Kindesalter.* www.awmf.org, 2021.
64. Pieters, R., et al., *Outcome of Infants Younger Than 1 Year With Acute Lymphoblastic Leukemia Treated With the Interfant-06 Protocol: Results From an International Phase III Randomized Study.* J Clin Oncol, 2019. **37**(25): p. 2246-2256.
65. Brown, P., R. Pieters, and A. Biondi, *How I treat infant leukemia.* Blood, 2019. **133**(3): p. 205-214.
66. Tomizawa, D., et al., *A risk-stratified therapy for infants with acute lymphoblastic leukemia: a report from the JPLSG MLL-10 trial.* Blood, 2020. **136**(16): p. 1813-1823.
67. Balducci, E., et al., *Lineage switch from B acute lymphoblastic leukemia to acute monocytic leukemia with persistent t(4;11)(q21;q23) and cytogenetic evolution under CD19-targeted therapy.* Ann Hematol, 2017. **96**(9): p. 1579-1581.
68. Gardner, R., et al., *Acquisition of a CD19-negative myeloid phenotype allows immune escape of MLL-rearranged B-ALL from CD19 CAR-T-cell therapy.* Blood, 2016. **127**(20): p. 2406-10.
69. Winters, A.C. and K.M. Bernt, *MLL-Rearranged Leukemias-An Update on Science and Clinical Approaches.* Front Pediatr, 2017. **5**: p. 4.
70. Rice, S. and A. Roy, *MLL-rearranged infant leukaemia: A 'thorn in the side' of a remarkable success story.* Biochim Biophys Acta Gene Regul Mech, 2020. **1863**(8): p. 194564.
71. Ryningen, A., C. Stapnes, and O. Bruserud, *Clonogenic acute myelogenous leukemia cells are heterogeneous with regard to regulation of differentiation and effect of epigenetic pharmacological targeting.* Leuk Res, 2007. **31**(9): p. 1303-13.

72. Bruserud, O., et al., *New strategies in the treatment of acute myelogenous leukemia (AML): in vitro culture of aml cells--the present use in experimental studies and the possible importance for future therapeutic approaches.* Stem Cells, 2001. **19**(1): p. 1-11.
73. Mayani, H., E. Flores-Figueroa, and A. Chavez-Gonzalez, *In vitro biology of human myeloid leukemia.* Leuk Res, 2009. **33**(5): p. 624-37.
74. Cucchi, D.G.J., et al., *Ex vivo cultures and drug testing of primary acute myeloid leukemia samples: Current techniques and implications for experimental design and outcome.* Drug Resist Updat, 2020. **53**: p. 100730.
75. Bruserud, O., et al., *In vitro culture of human acute lymphoblastic leukemia (ALL) cells in serum-free media; a comparison of native ALL blasts, ALL cell lines and virus-transformed B cell lines.* Leuk Res, 2003. **27**(5): p. 455-64.
76. Rucker, F.G., et al., *Molecular profiling reveals myeloid leukemia cell lines to be faithful model systems characterized by distinct genomic aberrations.* Leukemia, 2006. **20**(6): p. 994-1001.
77. Kasai, F., et al., *Changes of heterogeneous cell populations in the Ishikawa cell line during long-term culture: Proposal for an in vitro clonal evolution model of tumor cells.* Genomics, 2016. **107**(6): p. 259-66.
78. Antonelli, A., et al., *Establishing human leukemia xenograft mouse models by implanting human bone marrow-like scaffold-based niches.* Blood, 2016. **128**(25): p. 2949-2959.
79. Drynan, L.F., et al., *Mll fusions generated by Cre-loxP-mediated de novo translocations can induce lineage reassignment in tumorigenesis.* EMBO J, 2005. **24**(17): p. 3136-46.
80. Wachter, K., E. Kowarz, and R. Marschalek, *Functional characterisation of different MLL fusion proteins by using inducible Sleeping Beauty vectors.* Cancer Lett, 2014. **352**(2): p. 196-202.
81. Horton, S.J., et al., *MLL-AF9-mediated immortalization of human hematopoietic cells along different lineages changes during ontogeny.* Leukemia, 2013. **27**(5): p. 1116-26.
82. Secker, K.A., et al., *Inhibition of DOT1L and PRMT5 promote synergistic anti-tumor activity in a human MLL leukemia model induced by CRISPR/Cas9.* Oncogene, 2019. **38**(46): p. 7181-7195.
83. Breese, E.H., et al., *Use of Genome Engineering to Create Patient Specific MLL Translocations in Primary Human Hematopoietic Stem and Progenitor Cells.* PLoS One, 2015. **10**(9): p. e0136644.
84. Schneidawind, C., et al., *MLL leukemia induction by t(9;11) chromosomal translocation in human hematopoietic stem cells using genome editing.* Blood Adv, 2018. **2**(8): p. 832-845.
85. Buechele, C., et al., *MLL leukemia induction by genome editing of human CD34+ hematopoietic cells.* Blood, 2015. **126**(14): p. 1683-94.
86. Jeong, J., et al., *High-efficiency CRISPR induction of t(9;11) chromosomal translocations and acute leukemias in human blood stem cells.* Blood Adv, 2019. **3**(19): p. 2825-2835.
87. Gundry, M.C., et al., *Highly Efficient Genome Editing of Murine and Human Hematopoietic Progenitor Cells by CRISPR/Cas9.* Cell Rep, 2016. **17**(5): p. 1453-1461.
88. Brüstl, S., *Impact of the MLL Breakpoint on Leukaemogenesis in a CRISPR/Cas9-Generated Model of MLL-Rearranged Leukaemia.* Master's Thesis of the University of Tübingen, 2021.
89. Strissel, P.L., et al., *DNA structural properties of AF9 are similar to MLL and could act as recombination hot spots resulting in MLL/AF9 translocations and leukemogenesis.* Hum Mol Genet, 2000. **9**(11): p. 1671-9.
90. Fitzel, R., et al., *Targeting MYC in combination with epigenetic regulators induces synergistic anti-leukemic effects in MLLr leukemia and simultaneously improves immunity.* Neoplasia, 2023. **41**: p. 100902.
91. Secker, K.A., et al., *Only Hematopoietic Stem and Progenitor Cells from Cord Blood Are Susceptible to Malignant Transformation by MLL-AF4 Translocations.* Cancers (Basel), 2020. **12**(6).

92. Sarrou, E., et al., *CRISPR Gene Editing of Murine Blood Stem and Progenitor Cells Induces MLL-AF9 Chromosomal Translocation and MLL-AF9 Leukaemogenesis.* Int J Mol Sci, 2020. **21**(12).
93. Rice, S., et al., *A human fetal liver-derived infant MLL-AF4 acute lymphoblastic leukemia model reveals a distinct fetal gene expression program.* Nat Commun, 2021. **12**(1): p. 6905.
94. Bueno, C., et al., *A human genome editing-based MLL::AF4 B-cell ALL model recapitulates key cellular and molecular leukemogenic features.* Blood, 2023.
95. Schoop, V., et al., *Cellular cholesterol and how to find it.* Biochim Biophys Acta Mol Cell Biol Lipids, 2021. **1866**(9): p. 158989.
96. Xia, W., et al., *The role of cholesterol metabolism in tumor therapy, from bench to bed.* Front Pharmacol, 2023. **14**: p. 928821.
97. Hua, X., et al., *Structure of the human gene encoding sterol regulatory element binding protein-1 (SREBF1) and localization of SREBF1 and SREBF2 to chromosomes 17p11.2 and 22q13.* Genomics, 1995. **25**(3): p. 667-73.
98. Brown, M.S. and J.L. Goldstein, *The SREBP pathway: regulation of cholesterol metabolism by proteolysis of a membrane-bound transcription factor.* Cell, 1997. **89**(3): p. 331-40.
99. Radhakrishnan, A., et al., *Switch-like control of SREBP-2 transport triggered by small changes in ER cholesterol: a delicate balance.* Cell Metab, 2008. **8**(6): p. 512-21.
100. Yang, T., et al., *Crucial step in cholesterol homeostasis: sterols promote binding of SCAP to INSIG-1, a membrane protein that facilitates retention of SREBPs in ER.* Cell, 2002. **110**(4): p. 489-500.
101. Horton, J.D., et al., *Combined analysis of oligonucleotide microarray data from transgenic and knockout mice identifies direct SREBP target genes.* Proc Natl Acad Sci U S A, 2003. **100**(21): p. 12027-32.
102. Prinz, W.A., A. Toulmay, and T. Balla, *The functional universe of membrane contact sites.* Nat Rev Mol Cell Biol, 2020. **21**(1): p. 7-24.
103. Chang, T.Y., et al., *Cholesterol sensing, trafficking, and esterification.* Annu Rev Cell Dev Biol, 2006. **22**: p. 129-57.
104. Sever, N., et al., *Accelerated degradation of HMG CoA reductase mediated by binding of insig-1 to its sterol-sensing domain.* Mol Cell, 2003. **11**(1): p. 25-33.
105. Lehmann, J.M., et al., *Activation of the nuclear receptor LXR by oxysterols defines a new hormone response pathway.* J Biol Chem, 1997. **272**(6): p. 3137-40.
106. Peet, D.J., et al., *Cholesterol and bile acid metabolism are impaired in mice lacking the nuclear oxysterol receptor LXR alpha.* Cell, 1998. **93**(5): p. 693-704.
107. Song, C., et al., *Ubiquitous receptor: structures, immunocytochemical localization, and modulation of gene activation by receptors for retinoic acids and thyroid hormones.* Ann N Y Acad Sci, 1995. **761**: p. 38-49.
108. Willy, P.J., et al., *LXR, a nuclear receptor that defines a distinct retinoid response pathway.* Genes Dev, 1995. **9**(9): p. 1033-45.
109. Apfel, R., et al., *A novel orphan receptor specific for a subset of thyroid hormone-responsive elements and its interaction with the retinoid/thyroid hormone receptor subfamily.* Mol Cell Biol, 1994. **14**(10): p. 7025-35.
110. Bookout, A.L., et al., *Anatomical profiling of nuclear receptor expression reveals a hierarchical transcriptional network.* Cell, 2006. **126**(4): p. 789-99.
111. Kaneko, E., et al., *Induction of intestinal ATP-binding cassette transporters by a phytosterol-derived liver X receptor agonist.* J Biol Chem, 2003. **278**(38): p. 36091-8.
112. Groen, A.K., et al., *The ins and outs of reverse cholesterol transport.* Ann Med, 2004. **36**(2): p. 135-45.
113. Lynen, F., *Acetyl coenzyme A and the fatty acid cycle.* Harvey Lect, 1952. **48**: p. 210-44.
114. Bloch, K., *The biological synthesis of cholesterol.* Science, 1965. **150**(3692): p. 19-28.
115. Goldstein, J.L. and M.S. Brown, *Regulation of the mevalonate pathway.* Nature, 1990. **343**(6257): p. 425-30.
116. Bishop, A.L. and A. Hall, *Rho GTPases and their effector proteins.* Biochem J, 2000. **348 Pt 2**(Pt 2): p. 241-55.

117. Goldstein, J.L. and M.S. Brown, *Binding and degradation of low density lipoproteins by cultured human fibroblasts. Comparison of cells from a normal subject and from a patient with homozygous familial hypercholesterolemia.* J Biol Chem, 1974. **249**(16): p. 5153-62.
118. Anderson, R.G., M.S. Brown, and J.L. Goldstein, *Role of the coated endocytic vesicle in the uptake of receptor-bound low density lipoprotein in human fibroblasts.* Cell, 1977. **10**(3): p. 351-64.
119. Fielding, P.E., et al., *A two-step mechanism for free cholesterol and phospholipid efflux from human vascular cells to apolipoprotein A-1.* Biochemistry, 2000. **39**(46): p. 14113-20.
120. Wang, N., et al., *Specific binding of ApoA-I, enhanced cholesterol efflux, and altered plasma membrane morphology in cells expressing ABC1.* J Biol Chem, 2000. **275**(42): p. 33053-8.
121. Fredenrich, A. and P. Bayer, *Reverse cholesterol transport, high density lipoproteins and HDL cholesterol: recent data.* Diabetes Metab, 2003. **29**(3): p. 201-5.
122. Fitzgerald, M.L., Z. Mujawar, and N. Tamehiro, *ABC transporters, atherosclerosis and inflammation.* Atherosclerosis, 2010. **211**(2): p. 361-70.
123. Gomes, A.L., et al., *Hypercholesterolemia promotes bone marrow cell mobilization by perturbing the SDF-1:CXCR4 axis.* Blood, 2010. **115**(19): p. 3886-94.
124. Cimato, T.R., et al., *LDL cholesterol modulates human CD34+ HSPCs through effects on proliferation and the IL-17 G-CSF axis.* PLoS One, 2013. **8**(8): p. e73861.
125. Crysandt, M., et al., *Hypercholesterolemia and its association with enhanced stem cell mobilization and harvest after high-dose cyclophosphamide+G-CSF.* Bone Marrow Transplant, 2011. **46**(11): p. 1426-9.
126. Yvan-Charvet, L., et al., *ATP-binding cassette transporters and HDL suppress hematopoietic stem cell proliferation.* Science, 2010. **328**(5986): p. 1689-93.
127. Westerterp, M., et al., *Regulation of hematopoietic stem and progenitor cell mobilization by cholesterol efflux pathways.* Cell Stem Cell, 2012. **11**(2): p. 195-206.
128. Hanahan, D. and R.A. Weinberg, *Hallmarks of cancer: the next generation.* Cell, 2011. **144**(5): p. 646-74.
129. Allott, E.H., et al., *Serum lipid profile and risk of prostate cancer recurrence: Results from the SEARCH database.* Cancer Epidemiol Biomarkers Prev, 2014. **23**(11): p. 2349-56.
130. Qin, W.H., et al., *High Serum Levels of Cholesterol Increase Antitumor Functions of Nature Killer Cells and Reduce Growth of Liver Tumors in Mice.* Gastroenterology, 2020. **158**(6): p. 1713-1727.
131. Murdock, D.J., et al., *Serum cholesterol and the risk of developing hormonally driven cancers: A narrative review.* Cancer Med, 2023. **12**(6): p. 6722-6767.
132. Kitahara, C.M., et al., *Total cholesterol and cancer risk in a large prospective study in Korea.* J Clin Oncol, 2011. **29**(12): p. 1592-8.
133. Wu, Q., et al., *27-Hydroxycholesterol promotes cell-autonomous, ER-positive breast cancer growth.* Cell Rep, 2013. **5**(3): p. 637-45.
134. Nelson, E.R., et al., *27-Hydroxycholesterol links hypercholesterolemia and breast cancer pathophysiology.* Science, 2013. **342**(6162): p. 1094-8.
135. Freed-Pastor, W.A., et al., *Mutant p53 disrupts mammary tissue architecture via the mevalonate pathway.* Cell, 2012. **148**(1-2): p. 244-58.
136. Casalou, C., et al., *Cholesterol regulates VEGFR-1 (FLT-1) expression and signaling in acute leukemia cells.* Mol Cancer Res, 2011. **9**(2): p. 215-24.
137. Usman, H., et al., *Leukemia cells display lower levels of intracellular cholesterol irrespective of the exogenous cholesterol availability.* Clin Chim Acta, 2016. **457**: p. 12-7.
138. Schimanski, S., et al., *Expression of the lipid transporters ABCA3 and ABCA1 is diminished in human breast cancer tissue.* Horm Metab Res, 2010. **42**(2): p. 102-9.
139. Smith, B. and H. Land, *Anticancer activity of the cholesterol exporter ABCA1 gene.* Cell Rep, 2012. **2**(3): p. 580-90.

140. Scoles, D.R., et al., *Liver X receptor agonist inhibits proliferation of ovarian carcinoma cells stimulated by oxidized low density lipoprotein.* Gynecol Oncol, 2010. **116**(1): p. 109-16.
141. Gabitova, L., et al., *Endogenous Sterol Metabolites Regulate Growth of EGFR/KRAS-Dependent Tumors via LXR.* Cell Rep, 2015. **12**(11): p. 1927-38.
142. McDonnell, D.P., C.Y. Chang, and E.R. Nelson, *The estrogen receptor as a mediator of the pathological actions of cholesterol in breast cancer.* Climacteric, 2014. **17 Suppl 2**(0 2): p. 60-5.
143. Pan, H., et al., *Expression of LXR-beta, ABCA1 and ABCG1 in human triple-negative breast cancer tissues.* Oncol Rep, 2019. **42**(5): p. 1869-1877.
144. Bachmeier, B.E., et al., *Overexpression of the ATP binding cassette gene ABCA1 determines resistance to Curcumin in M14 melanoma cells.* Mol Cancer, 2009. **8**: p. 129.
145. Kachalaki, S., et al., *Reversal of chemoresistance with small interference RNA (siRNA) in etoposide resistant acute myeloid leukemia cells (HL-60).* Biomed Pharmacother, 2015. **75**: p. 100-4.
146. Garcia-Bermudez, J., et al., *Squalene accumulation in cholesterol auxotrophic lymphomas prevents oxidative cell death.* Nature, 2019. **567**(7746): p. 118-122.
147. Huang, J., et al., *Tumor-Induced Hyperlipidemia Contributes to Tumor Growth.* Cell Rep, 2016. **15**(2): p. 336-48.
148. Gallagher, E.J., et al., *Elevated tumor LDLR expression accelerates LDL cholesterol-mediated breast cancer growth in mouse models of hyperlipidemia.* Oncogene, 2017. **36**(46): p. 6462-6471.
149. Stopsack, K.H., et al., *Cholesterol uptake and regulation in high-grade and lethal prostate cancers.* Carcinogenesis, 2017. **38**(8): p. 806-811.
150. Ehmsen, S., et al., *Increased Cholesterol Biosynthesis Is a Key Characteristic of Breast Cancer Stem Cells Influencing Patient Outcome.* Cell Rep, 2019. **27**(13): p. 3927-3938 e6.
151. Kuzu, O.F., M.A. Noory, and G.P. Robertson, *The Role of Cholesterol in Cancer.* Cancer Res, 2016. **76**(8): p. 2063-70.
152. Ettinger, S.L., et al., *Dysregulation of sterol response element-binding proteins and downstream effectors in prostate cancer during progression to androgen independence.* Cancer Res, 2004. **64**(6): p. 2212-21.
153. Li, X., et al., *SREBP-2 promotes stem cell-like properties and metastasis by transcriptional activation of c-Myc in prostate cancer.* Oncotarget, 2016. **7**(11): p. 12869-84.
154. Jie, Z., et al., *SREBP-2 aggravates breast cancer associated osteolysis by promoting osteoclastogenesis and breast cancer metastasis.* Biochim Biophys Acta Mol Basis Dis, 2019. **1865**(1): p. 115-125.
155. Armengol, S., et al., *SREBP-2-driven transcriptional activation of human SND1 oncogene.* Oncotarget, 2017. **8**(64): p. 108181-108194.
156. Moon, S.H., et al., *p53 Represses the Mevalonate Pathway to Mediate Tumor Suppression.* Cell, 2019. **176**(3): p. 564-580 e19.
157. Zhong, C., et al., *SREBP2 is upregulated in esophageal squamous cell carcinoma and co-operates with c-Myc to regulate HMGCR expression.* Mol Med Rep, 2019. **20**(4): p. 3003-3010.
158. Giandomenico, V., et al., *Coactivator-dependent acetylation stabilizes members of the SREBP family of transcription factors.* Mol Cell Biol, 2003. **23**(7): p. 2587-99.
159. Cai, D., et al., *RORgamma is a targetable master regulator of cholesterol biosynthesis in a cancer subtype.* Nat Commun, 2019. **10**(1): p. 4621.
160. Zou, H., et al., *RORgamma is a context-specific master regulator of cholesterol biosynthesis and an emerging therapeutic target in cancer and autoimmune diseases.* Biochem Pharmacol, 2022. **196**: p. 114725.
161. Istvan, E.S. and J. Deisenhofer, *Structural mechanism for statin inhibition of HMG-CoA reductase.* Science, 2001. **292**(5519): p. 1160-4.
162. Weide, K.V.D., *The use of statins in acute myeloid leukemia.* Thesis of the University of Groningen, 2011.

163. Sirtori, C.R., *The pharmacology of statins.* Pharmacol Res, 2014. **88**: p. 3-11.
164. Schachter, M., *Chemical, pharmacokinetic and pharmacodynamic properties of statins: an update.* Fundam Clin Pharmacol, 2005. **19**(1): p. 117-25.
165. Ricci, G., et al., *Statins: Pharmacokinetics, Pharmacodynamics and Cost-Effectiveness Analysis.* Curr Vasc Pharmacol, 2019. **17**(3): p. 213-221.
166. Thibault, A., et al., *Phase I study of lovastatin, an inhibitor of the mevalonate pathway, in patients with cancer.* Clin Cancer Res, 1996. **2**(3): p. 483-91.
167. Tilija Pun, N. and C.H. Jeong, *Statin as a Potential Chemotherapeutic Agent: Current Updates as a Monotherapy, Combination Therapy, and Treatment for Anti-Cancer Drug Resistance.* Pharmaceuticals (Basel), 2021. **14**(5).
168. Pandyra, A., et al., *Immediate utility of two approved agents to target both the metabolic mevalonate pathway and its restorative feedback loop.* Cancer Res, 2014. **74**(17): p. 4772-82.
169. Clendening, J.W., et al., *Exploiting the mevalonate pathway to distinguish statin-sensitive multiple myeloma.* Blood, 2010. **115**(23): p. 4787-97.
170. Lee, J.S., et al., *Statins enhance efficacy of venetoclax in blood cancers.* Sci Transl Med, 2018. **10**(445).
171. de Jonge-Peeters, S.D., et al., *Variability in responsiveness to lovastatin of the primitive CD34+ AML subfraction compared to normal CD34+ cells.* Ann Hematol, 2009. **88**(6): p. 573-80.
172. van der Weide, K., et al., *Combining simvastatin with the farnesyltransferase inhibitor tipifarnib results in an enhanced cytotoxic effect in a subset of primary CD34+ acute myeloid leukemia samples.* Clin Cancer Res, 2009. **15**(9): p. 3076-83.
173. Li, H.Y., et al., *Cholesterol-modulating agents kill acute myeloid leukemia cells and sensitize them to therapeutics by blocking adaptive cholesterol responses.* Blood, 2003. **101**(9): p. 3628-34.
174. Sheen, C., et al., *Statins are active in acute lymphoblastic leukaemia (ALL): a therapy that may treat ALL and prevent avascular necrosis.* Br J Haematol, 2011. **155**(3): p. 403-7.
175. Infante, E., S.J. Heasman, and A.J. Ridley, *Statins inhibit T-acute lymphoblastic leukemia cell adhesion and migration through Rap1b.* J Leukoc Biol, 2011. **89**(4): p. 577-86.
176. Zolnierczyk, J.D., et al., *Promising anti-leukemic activity of atorvastatin.* Oncol Rep, 2013. **29**(5): p. 2065-71.
177. Chapman-Shimshoni, D., et al., *Simvastatin induces apoptosis of B-CLL cells by activation of mitochondrial caspase 9.* Exp Hematol, 2003. **31**(9): p. 779-83.
178. Ellis, M., et al., *The anti-leukemic and lipid lowering effects of imatinib are not hindered by statins in CML: a retrospective clinical study and in vitro assessment of lipid-genes transcription.* Leuk Lymphoma, 2017. **58**(5): p. 1172-1177.
179. Jang, H.J., et al., *Statins Enhance the Molecular Response in Chronic Myeloid Leukemia when Combined with Tyrosine Kinase Inhibitors.* Cancers (Basel), 2021. **13**(21).
180. Banker, D.E., et al., *Cholesterol synthesis and import contribute to protective cholesterol increments in acute myeloid leukemia cells.* Blood, 2004. **104**(6): p. 1816-24.
181. Kornblau, S.M., et al., *Blockade of adaptive defensive changes in cholesterol uptake and synthesis in AML by the addition of pravastatin to idarubicin + high-dose Ara-C: a phase 1 study.* Blood, 2007. **109**(7): p. 2999-3006.
182. Advani, A.S., et al., *SWOG S0910: a phase 2 trial of clofarabine/cytarabine/epratuzumab for relapsed/refractory acute lymphocytic leukaemia.* Br J Haematol, 2014. **165**(4): p. 504-9.
183. Advani, A.S., et al., *Report of the relapsed/refractory cohort of SWOG S0919: A phase 2 study of idarubicin and cytarabine in combination with pravastatin for acute myelogenous leukemia (AML).* Leuk Res, 2018. **67**: p. 17-20.
184. Bjarnadottir, O., et al., *Targeting HMG-CoA reductase with statins in a window-of-opportunity breast cancer trial.* Breast Cancer Res Treat, 2013. **138**(2): p. 499-508.

185. Bjarnadottir, O., et al., *Global Transcriptional Changes Following Statin Treatment in Breast Cancer.* Clin Cancer Res, 2015. **21**(15): p. 3402-11.
186. Kimbung, S., et al., *High expression of cholesterol biosynthesis genes is associated with resistance to statin treatment and inferior survival in breast cancer.* Oncotarget, 2016. **7**(37): p. 59640-59651.
187. Wang, M.S., et al., *PPARalpha agonist fenofibrate relieves acquired resistance to gefitinib in non-small cell lung cancer by promoting apoptosis via PPARalpha/AMPK/AKT/FoxO1 pathway.* Acta Pharmacol Sin, 2022. **43**(1): p. 167-176.
188. Bemlih, S., M.D. Poirier, and A. El Andaloussi, *Acyl-coenzyme A: cholesterol acyltransferase inhibitor Avasimibe affect survival and proliferation of glioma tumor cell lines.* Cancer Biol Ther, 2010. **9**(12): p. 1025-32.
189. Kamisuki, S., et al., *A small molecule that blocks fat synthesis by inhibiting the activation of SREBP.* Chem Biol, 2009. **16**(8): p. 882-92.
190. Li, X., et al., *Fatostatin displays high antitumor activity in prostate cancer by blocking SREBP-regulated metabolic pathways and androgen receptor signaling.* Mol Cancer Ther, 2014. **13**(4): p. 855-66.
191. Yao, L., S. Chen, and W. Li, *Fatostatin inhibits the development of endometrial carcinoma in endometrial carcinoma cells and a xenograft model by targeting lipid metabolism.* Arch Biochem Biophys, 2020. **684**: p. 108327.
192. Gao, S., et al., *Fatostatin suppresses growth and enhances apoptosis by blocking SREBP-regulated metabolic pathways in endometrial carcinoma.* Oncol Rep, 2018. **39**(4): p. 1919-1929.
193. Jetten, A.M., *Retinoid-related orphan receptors (RORs): critical roles in development, immunity, circadian rhythm, and cellular metabolism.* Nucl Recept Signal, 2009. **7**: p. e003.
194. Xiao, S., et al., *Small-molecule RORgammat antagonists inhibit T helper 17 cell transcriptional network by divergent mechanisms.* Immunity, 2014. **40**(4): p. 477-89.
195. Chang, M.R., et al., *Pharmacologic repression of retinoic acid receptor-related orphan nuclear receptor gamma is therapeutic in the collagen-induced arthritis experimental model.* Arthritis Rheumatol, 2014. **66**(3): p. 579-88.
196. Rutz, S., et al., *Post-translational regulation of RORgammat-A therapeutic target for the modulation of interleukin-17-mediated responses in autoimmune diseases.* Cytokine Growth Factor Rev, 2016. **30**: p. 1-17.
197. Zhang, X., et al., *Simvastatin inhibits IL-17 secretion by targeting multiple IL-17-regulatory cytokines and by inhibiting the expression of IL-17 transcription factor RORC in CD4+ lymphocytes.* J Immunol, 2008. **180**(10): p. 6988-96.
198. Wang, J., et al., *Corrigendum: ROR-gamma drives androgen receptor expression and represents a therapeutic target in castration-resistant prostate cancer.* Nat Med, 2016. **22**(6): p. 692.
199. Yang, N., et al., *Deregulation of Cholesterol Homeostasis by a Nuclear Hormone Receptor Crosstalk in Advanced Prostate Cancer.* Cancers (Basel), 2022. **14**(13).
200. Lytle, N.K., et al., *A Multiscale Map of the Stem Cell State in Pancreatic Adenocarcinoma.* Cell, 2019. **177**(3): p. 572-586 e22.
201. Zou, H., et al., *Nuclear receptor RORgamma inverse agonists/antagonists display tissue- and gene-context selectivity through distinct activities in altering chromatin accessibility and master regulator SREBP2 occupancy.* Pharmacol Res, 2022. **182**: p. 106324.
202. Erkner, E., et al., *The RORɣ/SREBP2 pathway is a master regulator of cholesterol metabolism and serves as potential therapeutic target in t(4;11) leukemia.* Oncogene, 2024. **43**(4): p. 281-293.
203. Boyum, A., *Isolation of mononuclear cells and granulocytes from human blood. Isolation of monuclear cells by one centrifugation, and of granulocytes by combining centrifugation and sedimentation at 1 g.* Scand J Clin Lab Invest Suppl, 1968. **97**: p. 77-89.
204. van der Burg, M., et al., *Rapid and sensitive detection of all types of MLL gene translocations with a single FISH probe set.* Leukemia, 1999. **13**(12): p. 2107-13.

205. Reichel, M., et al., *Biased distribution of chromosomal breakpoints involving the MLL gene in infants versus children and adults with t(4;11) ALL.* Oncogene, 2001. **20**(23): p. 2900-7.
206. Bligh, E.G. and W.J. Dyer, *A rapid method of total lipid extraction and purification.* Can J Biochem Physiol, 1959. **37**(8): p. 911-7.
207. Moreno-Mateos, M.A., et al., *CRISPRscan: designing highly efficient sgRNAs for CRISPR-Cas9 targeting in vivo.* Nat Methods, 2015. **12**(10): p. 982-8.
208. Ma, F., et al., *A comparison between whole transcript and 3' RNA sequencing methods using Kapa and Lexogen library preparation methods.* BMC Genomics, 2019. **20**(1): p. 9.
209. Lexogen. *QuantSeq 3‘ mRNA-Seq Integrated Data Analysis Pipelines on BlueBee® Genomics Platform*. 2012.
210. Dobin, A., et al., *STAR: ultrafast universal RNA-seq aligner.* Bioinformatics, 2013. **29**(1): p. 15-21.
211. Love, M.I., W. Huber, and S. Anders, *Moderated estimation of fold change and dispersion for RNA-seq data with DESeq2.* Genome Biol, 2014. **15**(12): p. 550.
212. Edelmann, S., et al., *Blood transcriptome analysis suggests an indirect molecular association of early life adversities and adult social anxiety disorder by immune-related signal transduction.* Front Psychiatry, 2023. **14**: p. 1125553.
213. Lowry, O.H., et al., *Protein measurement with the Folin phenol reagent.* J Biol Chem, 1951. **193**(1): p. 265-75.
214. Chandra, D., J.W. Liu, and D.G. Tang, *Early mitochondrial activation and cytochrome c up-regulation during apoptosis.* J Biol Chem, 2002. **277**(52): p. 50842-54.
215. Chou, T.C., *Drug combination studies and their synergy quantification using the Chou-Talalay method.* Cancer Res, 2010. **70**(2): p. 440-6.
216. Loewe, S., *The problem of synergism and antagonism of combined drugs.* Arzneimittelforschung, 1953. **3**(6): p. 285-90.
217. Passegue, E., et al., *Normal and leukemic hematopoiesis: are leukemias a stem cell disorder or a reacquisition of stem cell characteristics?* Proc Natl Acad Sci U S A, 2003. **100 Suppl 1**(Suppl 1): p. 11842-9.
218. Schnerch, D., et al., *Cell cycle control in acute myeloid leukemia.* Am J Cancer Res, 2012. **2**(5): p. 508-28.
219. Barbalata, C.I., et al., *Statins in risk-reduction and treatment of cancer.* World J Clin Oncol, 2020. **11**(8): p. 573-588.
220. McIver, L.A. and M.S. Siddique, *Atorvastatin*, in *StatPearls*. 2023: Treasure Island (FL).
221. Somervaille, T.C., et al., *Hierarchical maintenance of MLL myeloid leukemia stem cells employs a transcriptional program shared with embryonic rather than adult stem cells.* Cell Stem Cell, 2009. **4**(2): p. 129-40.
222. Xia, Z., et al., *Blocking protein geranylgeranylation is essential for lovastatin-induced apoptosis of human acute myeloid leukemia cells.* Leukemia, 2001. **15**(9): p. 1398-407.
223. Wong, W.W., et al., *Determinants of sensitivity to lovastatin-induced apoptosis in multiple myeloma.* Mol Cancer Ther, 2007. **6**(6): p. 1886-97.
224. Alhmoud, J.F., et al., *DNA Damage/Repair Management in Cancers.* Cancers (Basel), 2020. **12**(4).
225. Nakayama, G.R., et al., *Assessment of the Alamar Blue assay for cellular growth and viability in vitro.* J Immunol Methods, 1997. **204**(2): p. 205-8.
226. Vitols, S., et al., *Multilevel regulation of low-density lipoprotein receptor and 3-hydroxy-3-methylglutaryl coenzyme A reductase gene expression in normal and leukemic cells.* Blood, 1994. **84**(8): p. 2689-98.
227. Vitols, S., et al., *Uptake of low density lipoproteins by human leukemic cells in vivo: relation to plasma lipoprotein levels and possible relevance for selective chemotherapy.* Proc Natl Acad Sci U S A, 1990. **87**(7): p. 2598-602.
228. Krivtsov, A.V. and S.A. Armstrong, *MLL translocations, histone modifications and leukaemia stem-cell development.* Nat Rev Cancer, 2007. **7**(11): p. 823-33.
229. Harman, J.R., et al., *A KMT2A-AFF1 gene regulatory network highlights the role of core transcription factors and reveals the regulatory logic of key downstream target genes.* Genome Res, 2021. **31**(7): p. 1159-73.

230. Oliner, J.D., et al., *SREBP transcriptional activity is mediated through an interaction with the CREB-binding protein.* Genes Dev, 1996. **10**(22): p. 2903-11.
231. Marschalek, R., *The reciprocal world of MLL fusions: A personal view.* Biochim Biophys Acta Gene Regul Mech, 2020. **1863**(7): p. 194547.
232. Klock, J.C. and J.K. Pieprzyk, *Cholesterol, phospholipids, and fatty acids of normal immature neutrophils: comparison with acute myeloblastic leukemia cells and normal neutrophils.* J Lipid Res, 1979. **20**(7): p. 908-11.
233. Tatidis, L., et al., *Cholesterol catabolism in patients with acute myelogenous leukemia and hypocholesterolemia: suppressed levels of a circulating marker for bile acid synthesis.* Cancer Lett, 2001. **170**(2): p. 169-75.
234. Vitols, S., et al., *Hypocholesterolaemia in malignancy due to elevated low-density-lipoprotein-receptor activity in tumour cells: evidence from studies in patients with leukaemia.* Lancet, 1985. **2**(8465): p. 1150-4.
235. Pugliese, L., et al., *Severe hypocholesterolaemia is often neglected in haematological malignancies.* Eur J Cancer, 2010. **46**(9): p. 1735-43.
236. Dong, L., et al., *Leukaemogenic effects of Ptpn11 activating mutations in the stem cell microenvironment.* Nature, 2016. **539**(7628): p. 304-308.
237. Lehner, K.M., et al., *Bone Marrow Microenvironment-Induced Chemoprotection in KMT2A Rearranged Pediatric AML Is Overcome by Azacitidine-Panobinostat Combination.* Cancers (Basel), 2023. **15**(12).
238. Sidhu, I., S.P. Barwe, and A. Gopalakrishnapillai, *The extracellular matrix: A key player in the pathogenesis of hematologic malignancies.* Blood Rev, 2021. **48**: p. 100787.
239. Menter, T. and A. Tzankov, *Tumor Microenvironment in Acute Myeloid Leukemia: Adjusting Niches.* Front Immunol, 2022. **13**: p. 811144.
240. Moore, C.B., et al., *Short hairpin RNA (shRNA): design, delivery, and assessment of gene knockdown.* Methods Mol Biol, 2010. **629**: p. 141-58.
241. Shao, W., C.E. Machamer, and P.J. Espenshade, *Fatostatin blocks ER exit of SCAP but inhibits cell growth in a SCAP-independent manner.* J Lipid Res, 2016. **57**(8): p. 1564-73.
242. Brovkovych, V., et al., *Fatostatin induces pro- and anti-apoptotic lipid accumulation in breast cancer.* Oncogenesis, 2018. **7**(8): p. 66.
243. Wen, Y.A., et al., *Downregulation of SREBP inhibits tumor growth and initiation by altering cellular metabolism in colon cancer.* Cell Death Dis, 2018. **9**(3): p. 265.
244. Klimke, K., *Rx-Trendbericht: Lipidsenker – ein Update.* Zentralinstitut für die kassenärztliche Versorgung in Deutschland, 2019.
245. Alizadeh, J., et al., *Mevalonate Cascade Inhibition by Simvastatin Induces the Intrinsic Apoptosis Pathway via Depletion of Isoprenoids in Tumor Cells.* Sci Rep, 2017. **7**: p. 44841.
246. Shojaei, S., et al., *Simvastatin increases temozolomide-induced cell death by targeting the fusion of autophagosomes and lysosomes.* FEBS J, 2020. **287**(5): p. 1005-1034.
247. Taylor-Harding, B., et al., *Fluvastatin and cisplatin demonstrate synergistic cytotoxicity in epithelial ovarian cancer cells.* Gynecol Oncol, 2010. **119**(3): p. 549-56.
248. Dirks, A.J. and K.M. Jones, *Statin-induced apoptosis and skeletal myopathy.* Am J Physiol Cell Physiol, 2006. **291**(6): p. C1208-12.
249. Yang, X.O., et al., *T helper 17 lineage differentiation is programmed by orphan nuclear receptors ROR alpha and ROR gamma.* Immunity, 2008. **28**(1): p. 29-39.
250. Ivanov, II, et al., *The orphan nuclear receptor RORgammat directs the differentiation program of proinflammatory IL-17+ T helper cells.* Cell, 2006. **126**(6): p. 1121-33.
251. Sun, Z., et al., *Requirement for RORgamma in thymocyte survival and lymphoid organ development.* Science, 2000. **288**(5475): p. 2369-73.
252. Chen, J., et al., *Therapeutic targeting RORgamma with natural product N-hydroxyapiosporamide for small cell lung cancer by reprogramming neuroendocrine fate.* Pharmacol Res, 2022. **178**: p. 106160.
253. Capone, A. and E. Volpe, *Transcriptional Regulators of T Helper 17 Cell Differentiation in Health and Autoimmune Diseases.* Front Immunol, 2020. **11**: p. 348.
254. Silva, M.T., *Secondary necrosis: the natural outcome of the complete apoptotic program.* FEBS Lett, 2010. **584**(22): p. 4491-9.

255. Wang, Y., et al., *Therapeutic Targeting of MDR1 Expression by RORgamma Antagonists Resensitizes Cross-Resistant CRPC to Taxane via Coordinated Induction of Cell Death Programs.* Mol Cancer Ther, 2020. **19**(2): p. 364-374.
256. Wang, Y.N., et al., *Targeting the cholesterol-RORalpha/gamma axis inhibits colorectal cancer progression through degrading c-myc.* Oncogene, 2022. **41**(49): p. 5266-5278.
257. Secker, K.A., et al., *MAT2A as Key Regulator and Therapeutic Target in MLLr Leukemogenesis.* Cancers (Basel), 2020. **12**(5).
258. Jude, C.D., et al., *Unique and independent roles for MLL in adult hematopoietic stem cells and progenitors.* Cell Stem Cell, 2007. **1**(3): p. 324-37.
259. Miyamoto, R., et al., *Activation of CpG-Rich Promoters Mediated by MLL Drives MOZ-Rearranged Leukemia.* Cell Rep, 2020. **32**(13): p. 108200.
260. So, C.W. and M.L. Cleary, *MLL-AFX requires the transcriptional effector domains of AFX to transform myeloid progenitors and transdominantly interfere with forkhead protein function.* Mol Cell Biol, 2002. **22**(18): p. 6542-52.
261. Yokoyama, A., *[The mechanism of MLL-rearranged leukemogenesis and its targeted therapies].* Rinsho Ketsueki, 2021. **62**(8): p. 988-997.
262. Yokoyama, A., et al., *A higher-order complex containing AF4 and ENL family proteins with P-TEFb facilitates oncogenic and physiologic MLL-dependent transcription.* Cancer Cell, 2010. **17**(2): p. 198-212.
263. Cho, M.H., et al., *DOT1L cooperates with the c-Myc-p300 complex to epigenetically derepress CDH1 transcription factors in breast cancer progression.* Nat Commun, 2015. **6**: p. 7821.
264. Gilan, O., et al., *Functional interdependence of BRD4 and DOT1L in MLL leukemia.* Nat Struct Mol Biol, 2016. **23**(7): p. 673-81.
265. Godfrey, L., et al., *MLL-AF4 binds directly to a BCL-2 specific enhancer and modulates H3K27 acetylation.* Exp Hematol, 2017. **47**: p. 64-75.
266. Zhang, F., X. Dai, and Y. Wang, *5-Aza-2'-deoxycytidine induced growth inhibition of leukemia cells through modulating endogenous cholesterol biosynthesis.* Mol Cell Proteomics, 2012. **11**(7): p. M111 016915.
267. Hartwell, K.A., et al., *Niche-based screening identifies small-molecule inhibitors of leukemia stem cells.* Nat Chem Biol, 2013. **9**(12): p. 840-848.
268. Bowers, E.M., et al., *Virtual ligand screening of the p300/CBP histone acetyltransferase: identification of a selective small molecule inhibitor.* Chem Biol, 2010. **17**(5): p. 471-82.
269. Mendez-Ferrer, S., et al., *Bone marrow niches in haematological malignancies.* Nat Rev Cancer, 2020. **20**(5): p. 285-298.
270. Witkowski, M.T., S. Kousteni, and I. Aifantis, *Mapping and targeting of the leukemic microenvironment.* J Exp Med, 2020. **217**(2).
271. Manabe, A., et al., *Bone marrow-derived stromal cells prevent apoptotic cell death in B-lineage acute lymphoblastic leukemia.* Blood, 1992. **79**(9): p. 2370-7.
272. Perucca, S., et al., *Mesenchymal stromal cells (MSCs) induce ex vivo proliferation and erythroid commitment of cord blood haematopoietic stem cells (CB-CD34+ cells).* PLoS One, 2017. **12**(2): p. e0172430.
273. Sison, E.A., et al., *MLL-rearranged acute lymphoblastic leukaemia stem cell interactions with bone marrow stroma promote survival and therapeutic resistance that can be overcome with CXCR4 antagonism.* Br J Haematol, 2013. **160**(6): p. 785-97.
274. Kihira, K., et al., *Close interaction with bone marrow mesenchymal stromal cells induces the development of cancer stem cell-like immunophenotype in B cell precursor acute lymphoblastic leukemia cells.* Int J Hematol, 2020. **112**(6): p. 795-806.
275. Richardson, S.E., et al., *In vitro differentiation of human pluripotent stem cells into the B lineage using OP9-MS5 co-culture.* STAR Protoc, 2021. **2**(2): p. 100420.
276. Martinov, T., et al., *Building the Next Generation of Humanized Hemato-Lymphoid System Mice.* Front Immunol, 2021. **12**: p. 643852.

9 Publications and conference presentations

9.1 Publications

Benz T., Larghero P., Meyer C., Müller M., Brüggmann D., Hentrich A.E., **Erkner E.**, Fitzel R., Louwen F., Schneidawind C., Marschalek R. CRISPR/Cas9-mediated induction of *KMT2A*-rearrangements in cell line and Umbilical Cord Blood Hematopoietic Stem and Progenitor Cells. STAR Protoc, 2024 Dec, 17;6(1):103481.
Contribution: I contributed to troubleshoot the methodology for generating CRISPR-Cas9-induced KMT2A-r chromosomal translocations.

Fischer J., **Erkner E.**, Radszuweit P., Hentrich T., Schulze-Hentrich J., Fitzel R., Korkmaz F., Keppeler H., Lengerke C., Schneidawind D., Schneidawind C. Only infant MLL rearranged leukemia is susceptible to an inhibition of PLK-1 by volasertib. Int J Mol Sci, 2024 Nov, 27;25(23):12760.
Contribution: I contributed to the design of the project.

Schumacher M., Beer S., Moraes Ribeiro E., Korkmaz F., Keppeler H., Fitzel R., **Erkner E.**, Radszuweit P., Lengerke C., Schneidawind C., Hoefert S., Mauz P.S., Schneidawind D. Treatment response of advanced HNSCC towards immune checkpoint inhibition is associated with an activated effector memory T cell phenotype. Front Oncol, 2024 Mar, 14:1333640.
Contribution: I contributed to the performance of experiments.

Erkner E., Hentrich T., Schairer R., Fitzel R., Secker-Grob K.A., Jeong J., Keppeler H., Korkmaz F., Schulze-Hentrich J.M., Lengerke C., Schneidawind D., Schneidawind C. The RORγ/SREBP2 pathway is a master regulator of cholesterol metabolism and serves as potential therapeutic target in t(4;11) leukemia. Oncogene, 2024 Jan, 43(4):281-293.
Contribution: I designed the project, planned and performed experiments, analyzed and interpreted data, prepared figures and tables, and wrote the manuscript.

Fischer J., **Erkner E.**, Fitzel R., Radszuweit P., Keppeler H., Korkmaz F., Roti G., Lengerke C., Schneidawind D., Schneidawind C. Uncovering NOTCH1 as a Promising Target in the Treatment of MLL-Rearranged Leukemia. Int J Mol Sci, 2023 Sep, 24(19):14466.
Contribution: I contributed to the design of the project, planning of experiments, and analysis of data.

Fitzel R., Secker-Grob K.A., Keppeler H., Korkmaz F., Schairer R., **Erkner E.**, Schneidawind D., Lengerke C., Hentrich T., Schulze-Hentrich J.M., Schneidawind C. Targeting MYC in

combination with epigenetic regulators induces synergistic anti-leukemic effects in MLLr leukemia and simultaneously improves immunity. Neoplasia, 2023 Jul, 41:100902.
Contribution: I contributed to the performance of experiments and analysis of data.

Tindall C.A.*, **Erkner E.***, Stichel J., Beck-Sickinger A.G., Hoffmann A., Weiner S., Heiker J.T. Cleavage of the vaspin N-terminus releases cell-penetrating peptides that affect early stages of adipogenesis and inhibit lipolysis in mature adipocytes. Adipocyte, 2021 Dec, 10(1):216-231. *Contributed equally.
Contribution: I contributed to the design of the project, planning and performance of experiments, analysis and interpretation of data, and preparation of figures.

9.2 Conference presentations

“The Rorɣ/SREBP2 Pathway Is a Master Regulator of Cholesterol Metabolism and Serves As Potential Therapeutic Target in *T(4;11)* Leukemia”, *64th ASH Annual Meeting and Exposition*, New Orleans, 12/2022 (Poster presentation).

“Targeting SREBP2 promotes anti-leukemic effects by altering dysregulated cholesterol metabolism in *t(4;11)* leukemia”, *Jahrestagung der Deutschen Gesellschaft für Hämatologie und Onkologie*, Wien, 10/2022 (Lecture).

“Targeting Dysregulated Cholesterol Metabolism As Potential Treatment Strategy of *MLL*-rearranged Leukemia *t(4;11)* Leads to Reduction of Leukemic Activity”, *63rd ASH Annual Meeting and Exposition*, Atlanta, 12/2021 (Poster presentation & winner of the *ASH Abstract Achievement Award*).

„Targeting dysregulated cholesterol metabolism in *MLL*-rearranged leukemia diminishes leukemia activity“, *Jahrestagung der Deutschen Gesellschaft für Hämatologie und Onkologie*, Berlin, 10/2021 (Lecture).

„Screening und Assessment von Mangelernährung im Krankenhaus – Prävalenz bei Kolon- und Rektumkarzinompatienten in einem Darmzentrum Deutschlands“, *Ernährung 2018*, Kassel, 06/2018 (Poster presentation)

10 Acknowledgement

First and foremost, I would like to thank PD Dr. Corina Schneidawind for the opportunity to work on this exciting project. Thank you, Corina, for providing the framework conditions, your trust, and the individual supervision of my dissertation. Furthermore, thank you for always having an open ear for scientific discussions and for giving me the opportunity to participate in some really exciting conferences beyond my dissertation.

Special thanks go to Prof. Dr. Thilo Stehle for his kindly agreement to act as a reviewer for this thesis and for his valuable final comments.
I would like to thank Prof. Dr. Gabriele Dodt and Prof. Dr. Dirk Schwarzer for their willingness to act as examiners for this dissertation.

I would like to take this opportunity to extend a very special thank you to all the parents and children who donate umbilical cord blood for research and make a vital contribution to making this research possible. My thanks also go to all our cooperation partners for the great scientific exchange and support. Many thanks to the kind staff of the Neonatology Department for providing the umbilical cord blood, the Pathology Department with Barbara Mankel for the FISH analyses, Dr. Thomas Hentrich for the evaluation of the RNA Seq results, and the FACS Core Facility for the support with the flow cytometric analyses.

Another big thank you goes to all the groups of the Inner Medicine II and KKE Translational Immunology. Many thanks to my colleagues in the AG Lengerke, AG Munz, AG Skokowa, AG Haraszti and AG Salih for their professional expertise, the friendly exchange of ideas, the numerous opportunities to help each other, and the fun conversations.

I would also like to thank all the lab members of the AG Schneidawind in Tübingen, who have always made my everyday life sweeter. Thanks to Dominik, Rahel, Pia, Rebekka, Jacqueline, Fulya, Hilde, Emma, Sara, Kathy, Anton and Max for our valuable exchange and the great working atmosphere. Additionally, a huge thank you to my wonderful colleagues in the office. Dear Rahel, Pia, Lya, Jacqueline, Rebekka - I have very special memories of our fun lunch breaks, sports sessions, joint conferences, camel walks, secretly slipping a certain piece of paper, little jokes, and the mental support with you. I hope you know that you all made a big contribution to my unforgettable time in Tübingen.

Nicht zuletzt danke ich meiner unschlagbaren Familie, meinen Freunden, die längst auch zur Familie geworden sind, und meinem unerschütterlichen Verlobten. Wo mir die Worte fehlen, lasse ich Bruce Springsteen sprechen - „Darlin' I'm countin' on a miracle. To come through." - Ihr seid mein Wunder und ich verdanke euch so viel.